

Elucidating the Role of Pattern Recognition Receptors in Understanding, Treating, and Targeting Cancer

Veronica Marie Scaia

Dissertation submitted to the faculty of the Virginia Polytechnic Institute and State University in partial fulfillment of the requirements for the degree of

Doctor of Philosophy
in
Translational Biology, Medicine, and Health

Irving C. Allen, PhD, Chair
Richey M. Davis, PhD
Nikolaos G. Dervisis, DVM, PhD
Kenneth J. Oestreich, PhD
Eva M. Schmelz, PhD

March 15, 2019
Blacksburg, Virginia

Keywords: NLRP1, colon cancer, pyroptosis, breast cancer, TLR4, nanoparticles

This work is licensed under the Creative Commons Attribution 4.0 International License. To view a copy of this license, visit <http://creativecommons.org/licenses/by/4.0/>.



Elucidating the Role of Pattern Recognition Receptors in Understanding, Treating, and Targeting Cancer

Veronica Marie Ringel-Scaia

ABSTRACT

Pattern Recognition Receptors (PRRs) are a group of evolutionarily conserved and germline-encoded cellular receptors of the innate immune system that are responsible for recognizing and responding to the entirety of the pathogens a host encounters. The ingenuity of the innate immune system is that with a comparatively miniscule pool of receptors, these receptors are capable of responding to a diverse and large array of pathogens and damage signals. Two highly relevant subsets of PRRs include nucleotide binding domain leucine rich repeat containing (NOD-like) receptors (NLRs) and Toll-like receptors (TLRs). Both NLRs and TLRs have been implicated in several diseases, including autoimmune disorders, inflammatory conditions, and cancer. Mice lacking a specific NLR, NLRP1, are more susceptible to chemically induced colitis and colitis-associated tumorigenesis. We investigated whether the absence of NLRP1 in the gastrointestinal tract influenced the composition of the microbiome, and whether it was responsible for the predisposition of these animals to colitis-associated cancer. By carefully controlling for non-genotype influences, we found that in fact maternal and housing factors were greater predictors over genotype of gut flora composition. This study concluded with a clearer understanding of NLRP1. We next investigated the effectiveness of a novel tumor ablation therapy, termed High-Frequency Irreversible Electroporation (H-FIRE) in a murine model of triple negative breast cancer. The chosen 4T1 model closely mimics aggressive human metastatic triple negative breast cancer, and metastasizes to the same organs. After ablation of the primary mammary tumor, we saw significant improvements in disease burden and metastases, both of which were accompanied by PRR activation within the tumor microenvironment, implicating PRRs in the successful treatment outcome following H-FIRE ablation. Lastly, we generated novel CRISPR-Cas9 plasmids to genetically manipulate the *Tlr4* gene of wild type C57Bl/6 mice in order to recapitulate the LPS-hyporesponsive TLR4 protein of C3H/HeJ mice. This proof-of-concept study successfully demonstrated that PRRs can be targets for gene editing purposes, and that nanoparticle delivery leads to enhanced and improved delivery. Collectively, this work attempts to better appreciate the role of PRRs in understanding, treating, and targeting cancer.

Elucidating the Role of Pattern Recognition Receptors in Understanding, Treating, and Targeting Cancer

Veronica Marie Ringel-Scaia

GENERAL AUDIENCE ABSTRACT

The work presented here focuses on the role of the immune system in the progression of cancer. Put simply, the properly functioning immune system of a healthy individual should recognize and eliminate mutated or cancerous cells prior to the development of a tumor, thereby implying that the progression to a tumor is due to some dysfunction of the immune system. The immune system is made up of two arms: the innate and adaptive. A key difference between the innate and adaptive immune systems is that upon an infection, the adaptive response is slow and specific while the innate response is rapid and broad. Pattern Recognition Receptors (PRRs) are a group of cellular receptors of the innate immune system that are responsible for recognizing and responding to the entirety of the pathogens a host encounters. The ingenuity of the innate immune system is that with a comparatively miniscule pool of receptors, these receptors are capable of responding to a diverse and large array of pathogens. Two highly relevant PRR families are nucleotide binding domain leucine rich repeat containing (NOD-like) receptors (NLRs) and Toll-like receptors (TLRs). Both NLRs and TLRs have been implicated in several diseases, including autoimmune disorders, inflammatory conditions, and cancer.

In this work, we investigated whether the absence of an NLR protein influenced the composition of the microbes that reside within the gastrointestinal tract, and whether this absence was responsible for the predisposition of these animals to colitis-associated cancer. By carefully controlling for all additional influences, we found that in our mice, the other animals with which they shared a cage were more influential on the microbes within the gut, rather than the NLR deficiency. We next investigated a novel tumor ablation therapy in an animal model of breast cancer, which closely mimics human metastatic triple negative breast cancer and metastasizes to the same organs. After treatment of the mammary tumor, we saw significant improvements in disease burden and metastases, both of which were accompanied by PRR activation. Lastly, we manipulated a TLR gene in mice to demonstrate that PRRs can be targeted for therapeutic gene editing. Collectively, this work provides evidence that PRRs are a highly useful tool for improving our understanding of cancer.

We have been through more in the past ten years than most families have to face in a lifetime, and yet we came out stronger.

Because of this, I dedicate this dissertation to my incredible family.

Particularly my parents, Paul and Ginny Ringel, who deserve more credit than I am able to adequately express – without your unconditional love and encouragement, none of this would be possible.

The honorary title of this dissertation is “Cancer Sucks.”

Acknowledgements

None of the work presented here would be possible without the support from several people. I'd like to extend my sincerest thanks to my advisor Dr. Coy Allen, who took a chance on me when I first rotated in his lab, and decided to offer me a spot despite the fact that I almost poisoned everyone with TRIzol, contaminated all my cells, and couldn't touch a mouse without screaming. Five years later, although I am (almost) entirely to blame for the rule "no humor in the Allen lab," I am leaving the lab fully trained and ready for my next challenge. You set me up for success from the very beginning, Dr. Allen, and for that I am truly grateful. I would also like to thank each of my graduate committee members, Dr. Richey Davis, Dr. Nik Dervisis, Dr. Ken Oestreich, and Dr. Eva Schmelz for their thoughtful discussions and suggestions regarding my work. Our interactions helped me approach my problems from all possible angles and made me a better scientist.

To my lab mates, both former and current, each of you has been vital for my growth and development as a scientist during our shared time in the lab. We are a team, and have always had this mentality, working towards both individual and group accomplishments. Thank you for all that you've done to lead to my and our success. Thank you to lab manager Bettina Heid for her willingness to share her knowledge and teach me crucial laboratory techniques. Special thanks to my first lab mates, Dr. Sheryl Coutermarsh-Ott, Dr. Kristin Eden, Dr. Dan Rothschild, and Dr. Dylan McDaniel, for learning alongside me and sharing your expertise, suggestions, and friendship. We will *always* get to say we ~~survived~~ earned our PhDs together, and that's a bond that will not soon be forgotten. To the more recent lab members, Rebecca, Alissa, Holly, and Margaret, and to all of the undergraduate students I worked with either directly or indirectly, thank you for allowing me to become a better collaborator and teacher during our time working together. And to all the other grad students that became close friends, particularly Dr. Nithya Ramalingam and Dr. Michael Edwards, thank you for always being willing to procrastinate with (and/or because of) me (sorry) and talk things out – both scientific and otherwise.

Lastly, I cannot overstate my gratitude for my family for always providing unwavering encouragement and love throughout my time in graduate school. Brooke and Harrison, I probably could not have survived without our numerous group chats (and all the dog pictures). You two are the best siblings a big sister could ask for...but don't let that go to your heads. Mommy and Daddy, I couldn't possibly say it adequately or enough, but here's an attempt: thank you for everything – raising me to never doubt myself, providing constant love, always believing in me, and being the best parents and support team. To my loving husband, who is the only person on the planet who can possibly calm me down from one of my frantic spirals: Vincent Scaia, I will be forever grateful for you and your endless patience, love, and support – we did it, let's go home.

Table of Contents

Attribution	vii
Chapter One: Introduction: Pattern Recognition Receptors and Cancer.....	1
Chapter Two: The Goldilocks Conundrum: NLR Inflammasome Modulation of Gastrointestinal Inflammation during Inflammatory Bowel Disease.....	13
Chapter Three: Maternal Influence and Murine Housing Confound Impact of NLRP1 Inflammasome on Microbiome.....	88
Chapter Four: High-Frequency Irreversible Electroporation (H-FIRE) is an Effective Tumor Ablation Strategy that Induces Immunologic Cell Death and Promotes Systemic Anti-Tumor Immunity.....	132
Chapter Five: The Role of Nanotechnology in Detection and Treatment in Gastrointestinal Cancers.....	183
Chapter Six: Fabrication and Characterization of PLGA Nanoparticles Encapsulating Large CRISPR-Cas9 Plasmid.....	221
Chapter Seven: Discussion and Conclusions.....	264
Appendix A: Complete List of Published Works.....	275

Attribution

In chapter one, the figure presented is from a published review in which I share co-first authorship with Dr. Daniel E. Rothschild and Dr. Dylan K. McDaniel. I designed and made the figure and wrote the legend that is included.

In chapter three, I share first-authorship with Dr. Yufeng Qin. My role was in the design of the experimentation and the handling, maintenance, and genotyping of the animals. I collected the feces and extracted DNA which was then sent to Yufeng, which he used to generate the 16s libraries. We both interpreted the data and wrote conclusions, and participated in the writing and revising of the text.

In chapter six, I share first-authorship with Dr. Ami Jo. My role was to plan, conduct, and analyze all of the cell studies. I was also responsible for designing, constructing, and purifying the CRISPR plasmid, which Ami encapsulated in a nanoparticle. We both interpreted the data and wrote conclusions, and participated in the writing and revising of the text.

Chapter One

Introduction: Pattern Recognition Receptors and Cancer

Veronica M. Ringel-Scaia

Cancer is a diverse and variable collection of diseases. In order to maximize and optimize targeting and treating cancer, we must truly understand it, a challenging and noble undertaking. Due to the heterogeneity of cancer, there are several ways to approach cancer research, each with unique advantages. The work presented here focuses on the role of the immune system in the progression of cancer. Put simply, the properly functioning immune system of a healthy individual should recognize and eliminate mutated or cancerous cells prior to the development of a tumor, thereby implying that the progression to a tumor is due to some dysfunction of the immune system. This concept of “immunological surveillance” was first proposed over 50 years ago,¹ and has since been accepted as a defining factor of cancer.² The critical role of the innate immune system in the development of and predisposition to, as well as the prevention of and treatment for cancer are the overarching themes of this work.

The two arms of the immune system, innate and adaptive, are distinct yet intimately connected. The faster acting and “first line of defense” innate immune system is responsible for reacting to the initial onslaught to the system in a broad and rapid manner. Conversely, the adaptive, or acquired, immune system is classified by slower onset, highly specific response to fight off an infection, and as the name indicates is “acquired” following exposure to specific pathogens. Briefly, specialized cells of the innate immune system phagocytose, or digest, the

invading pathogen and present unique antigens associated with the pathogen to cells of the adaptive immune system, leading to the activation and proliferation of lymphocytes specifically targeting the antigen. Counterpart to the elegant precision of adaptive immune responses, the innate immune system relies on a handful of receptors and cell types to recognize all the potential invading pathogens that may come into contact with the host. By some estimates, there exist over one trillion unique microbial species;³ the ingenuity of the innate immune system lies in the ability of a comparatively small pool of cell types and receptors to respond to such a diverse array of pathogens.

Pattern Recognition Receptors (PRRs) are a broad class of germline-encoded cellular receptors of the innate immune system that are responsible for sensing features of pathogens.⁴ PRRs can be divided into families based on protein domain composition: Toll-like receptors (TLRs), C-type lectin receptor (CLRs), nucleotide-binding oligomerization domain leucine-rich repeat containing (NOD-like) receptors (NLRs), Rig-I-like receptors (RLRs), and AIM2-like receptors (ALRs).⁴ These five families can be further sub-divided into either membrane-bound or intracellular receptors. As depicted in **Figure 1**, TLRs and CLRs are membrane-bound, while NLRs, RLRs, and ALRs reside in the cytosol.⁵ The domains of several of these PRRs are evolutionarily conserved across a multitude of species, from cnidarians to mammals.⁶ Upon recognition of either a pathogen-associated molecular pattern (PAMP) or damage-associated molecular pattern (DAMP) by a PRR, the primary outcome is the activation of potent cellular responses to eliminate the pathogen. PRR activation can lead to transcription of pro-inflammatory cytokines and chemokines as well as interferons,^{4,5} depicted in **Figure 1** converging on the NF- κ B pathway. Non-transcriptional consequences of PRR activation include

induction of phagocytosis, autophagy, cell death, and cytokine processing, and ultimately the activation of the adaptive immune system.

A delicate balance exists whereby the immune system must both protect the host from external pathogens and insults, while simultaneously maintaining discipline to suppress overzealous responses.⁷ Nowhere in the human body does this balancing act provide more context than in the gastrointestinal system. Under normal conditions, PRRs within the gut are responsible for both directly and indirectly maintaining immune system homeostasis. There are over 24 distinct NLRs and NLR-like proteins in humans, which can be divided into three primary sub-groups: inflammasome-forming NLRs, regulatory NLRs, and reproductive NLRs. The inflammasome is a multi-protein complex responsible for the cleavage and activation of the potent pro-inflammatory cytokines, IL-1 β and IL-18, as well as a unique form of cell death called pyroptosis.⁸ Among their many vital roles, inflammasome-forming NLRs function to sustain proper intestinal epithelial cell regeneration and repair, cell death, and a well-balanced inflammatory microenvironment. Inflammatory Bowel Disease (IBD) is associated with excessive gastrointestinal inflammation, dysregulation of immune tolerance, and damage to the epithelial cell barrier within the gastrointestinal tract. Chapter two provides an extensive review of the role of NLR inflammasomes in IBD, highlighting the precarious balancing act of maintaining homeostasis, which we referred to as “The Goldilocks Conundrum.” The evidence indicates that NLR inflammasomes have both protective and detrimental effects in gastrointestinal health and disease, with both increased and decreased NLR inflammasome activity having equally detrimental effects on the progression of IBD and associated gut tumorigenesis.

The coexistence of microbes in the gastrointestinal tract, despite the near-constant potential for translocation to and subsequent inflammation of the mucosa, is one of the most prominent examples of innate immune tolerance. Evidence has strongly suggested that a function of NLR family members in the gastrointestinal system is likely associated with their recognition of the host microbiome and their modulation of a balanced host immune response following loss of epithelial cell barrier integrity^{9,10}. Not only are NLR-deficient animals more susceptible to chemically-induced colitis and colitis associated tumorigenesis, but cohousing wild type animals with these mice is sufficient to partially transfer susceptibility¹¹⁻¹⁶, so it makes sense that the next logical step was to investigate the microbiomes of different NLR-deficient mice. The dysbiotic microbiome of *Nlrp6*^{-/-} mice was first reported in 2011, represented by overabundance of *Prevotellaceae* and reduction in *Lactobacillus*⁹. Shortly thereafter, mechanistic studies reported that the abundance of *Prevotellaceae* was directly due to an attenuation of goblet cell mucin production¹⁷. Within the NLR field, it became accepted that a significant role of NLRP6 was regulation of the intestinal microbiome, and assumptions were made that the increased susceptibility to colitis and colitis-associated tumorigenesis was due, at least in part, to the dysbiotic microbiome in these animals. We sought to investigate the microbiome composition of mice lacking NLRP1, propelled by the hypothesis that the driving factor for the increased sensitivity of *Nlrp1*^{-/-} animals to colitis would closely mimic that of *Nlrp6*^{-/-} animals. As detailed in chapter three, we found that by carefully controlling for all potential influences, maternal and housing strategy were higher predictors of microbial compositions rather than genotype. Interestingly, the role of NLRP6 in regulating the microbiome has recently been called into question by two studies that also suggest maternal and caging are greater predictors of the microbial composition rather than genotype^{18,19}. The work presented in chapter three moves the

NLR field forward by providing strong evidence that littermates should always be used in future studies evaluating NLRs in the context of gastrointestinal inflammation and microbiome interactions.

As previously mentioned, pyroptosis is a possible outcome of inflammasome activation. Pyroptosis is a type of programmed cell death that is caspase-1 or caspase-11/4/5 dependent, and is lytic in nature, characterized by cell swelling, loss of membrane integrity, and release of cellular contents^{8,20}. As the Greek origin of the name indicates (“pyro” meaning fire), pyroptosis is an inflammatory form of cell death. Within the tumor ablation field, the consensus is that the ablation must induce “immunogenic cell death” in order to elicit a robust systemic anti-tumor immune response²¹. Following murine mammary tumor ablation with high-frequency irreversible electroporation (H-FIRE), we observed not only consistent ablation of the primary tumor, but additional reductions in metastatic lesions in the lung and metastatic colonies in circulation. Chapter four of this work describes the immune response following H-FIRE ablation. The goal of chapter four is to provide evidence that the so-called “immunogenic cell death” of the tumor ablation field is mechanistically consistent with pyroptosis. A clearer understanding of the type of cell death following tumor ablation is instrumental in progressing the field forward and achieving not only better tumor ablation, but also better systemic immune responses.

Due to their utility, an interesting point to consider is whether it might be possible to manipulate PRRs to achieve therapeutic advantage. Since first being utilized for highly precise genome engineering, the Clustered Regularly Interspaced Short Palindromic Repeats (CRISPR)-Cas9 system has revolutionized targeted genome editing²². The precision and relative ease of design of CRISPR-Cas9 gene editing technology effectively allows for genome engineering on a significantly grander scale than ever before possible. Single nucleotide polymorphisms (SNPs) in

TLR genes have been linked to a variety of infectious diseases and cancers (reviewed in ²³). A single point mutation in the third exon of the *Tlr4* gene of C3H/HeJ mice substitutes a histidine for a proline residue in the Tlr4 protein, which causes these mice to have a marked hyporesponsive phenotype to LPS^{24,25}. By engineering a CRISPR construct to target the LPS locus of the murine *Tlr4* gene, we attempted to mutate wild type C57Bl/6 *Tlr4* to resemble that of the C3H/HeJ LPS-hyporesponsive defective Tlr4 protein, as outlined in chapter six. One significant problem with utilizing CRISPR-Cas9 is delivery of the large DNA construct to the tissue of interest. To circumvent this, we encapsulated our CRISPR-Cas9 plasmid in PLGA nanoparticle. The utility of nanoparticle delivery in gastrointestinal cancers is outlined in chapter five.

Collectively, all of the projects presented here represent an innate immune perspective on cancer, and aim to elucidate the role PRRs play in understanding, treating, and targeting cancer.

References

- 1 Burnet, M. Cancer: a biological approach. III. Viruses associated with neoplastic conditions. IV. Practical applications. *Br Med J* **1**, 841-847 (1957).
- 2 Hanahan, D. & Weinberg, R. A. Hallmarks of cancer: the next generation. *Cell* **144**, 646-674, doi:10.1016/j.cell.2011.02.013 (2011).
- 3 Locey, K. J. & Lennon, J. T. Scaling laws predict global microbial diversity. *Proc Natl Acad Sci U S A* **113**, 5970-5975, doi:10.1073/pnas.1521291113 (2016).
- 4 Brubaker, S. W., Bonham, K. S., Zanoni, I. & Kagan, J. C. Innate immune pattern recognition: a cell biological perspective. *Annu Rev Immunol* **33**, 257-290, doi:10.1146/annurev-immunol-032414-112240 (2015).
- 5 Rothschild, D. E., McDaniel, D. K., Ringel-Scaia, V. M. & Allen, I. C. Modulating inflammation through the negative regulation of NF-kappaB signaling. *J Leukoc Biol*, doi:10.1002/JLB.3MIR0817-346RRR (2018).
- 6 Zhang, Q., Zmasek, C. M. & Godzik, A. Domain architecture evolution of pattern-recognition receptors. *Immunogenetics* **62**, 263-272, doi:10.1007/s00251-010-0428-1 (2010).
- 7 Davis, B. K. *et al.* Emerging significance of NLRs in inflammatory bowel disease. *Inflamm Bowel Dis* **20**, 2412-2432, doi:10.1097/MIB.000000000000151 (2014).
- 8 Platnich, J. M. & Muruve, D. A. NOD-like receptors and inflammasomes: A review of their canonical and non-canonical signaling pathways. *Arch Biochem Biophys*, doi:10.1016/j.abb.2019.02.008 (2019).

- 9 Elinav, E. *et al.* NLRP6 inflammasome regulates colonic microbial ecology and risk for colitis. *Cell* **145**, 745-757, doi:10.1016/j.cell.2011.04.022 (2011).
- 10 Zaki, M. H., Lamkanfi, M. & Kanneganti, T. D. The Nlrp3 inflammasome: contributions to intestinal homeostasis. *Trends Immunol* **32**, 171-179, doi:10.1016/j.it.2011.02.002 (2011).
- 11 Chen, G. Y., Liu, M., Wang, F., Bertin, J. & Nunez, G. A functional role for Nlrp6 in intestinal inflammation and tumorigenesis. *J Immunol* **186**, 7187-7194, doi:10.4049/jimmunol.1100412 (2011).
- 12 Hu, B. *et al.* Inflammation-induced tumorigenesis in the colon is regulated by caspase-1 and NLRC4. *Proc Natl Acad Sci U S A* **107**, 21635-21640, doi:10.1073/pnas.1016814108 (2010).
- 13 Hu, B. *et al.* Microbiota-induced activation of epithelial IL-6 signaling links inflammasome-driven inflammation with transmissible cancer. *Proc Natl Acad Sci U S A* **110**, 9862-9867, doi:10.1073/pnas.1307575110 (2013).
- 14 Zaki, M. H. *et al.* The NLRP3 inflammasome protects against loss of epithelial integrity and mortality during experimental colitis. *Immunity* **32**, 379-391, doi:10.1016/j.immuni.2010.03.003 (2010).
- 15 Allen, I. C. *et al.* The NLRP3 inflammasome functions as a negative regulator of tumorigenesis during colitis-associated cancer. *J Exp Med* **207**, 1045-1056, doi:10.1084/jem.20100050 (2010).

- 16 Williams, T. M. *et al.* The NLRP1 inflammasome attenuates colitis and colitis-associated tumorigenesis. *J Immunol* **194**, 3369-3380, doi:10.4049/jimmunol.1402098 (2015).
- 17 Wlodarska, M. *et al.* NLRP6 inflammasome orchestrates the colonic host-microbial interface by regulating goblet cell mucus secretion. *Cell* **156**, 1045-1059, doi:10.1016/j.cell.2014.01.026 (2014).
- 18 Mamantopoulos, M. *et al.* Nlrp6- and ASC-Dependent Inflammasomes Do Not Shape the Commensal Gut Microbiota Composition. *Immunity* **47**, 339-348 e334, doi:10.1016/j.immuni.2017.07.011 (2017).
- 19 Lemire, P. *et al.* The NLR Protein NLRP6 Does Not Impact Gut Microbiota Composition. *Cell Rep* **21**, 3653-3661, doi:10.1016/j.celrep.2017.12.026 (2017).
- 20 Shi, J., Gao, W. & Shao, F. Pyroptosis: Gasdermin-Mediated Programmed Necrotic Cell Death. *Trends Biochem Sci* **42**, 245-254, doi:10.1016/j.tibs.2016.10.004 (2017).
- 21 Galluzzi, L., Buque, A., Kepp, O., Zitvogel, L. & Kroemer, G. Immunogenic cell death in cancer and infectious disease. *Nat Rev Immunol* **17**, 97-111, doi:10.1038/nri.2016.107 (2017).
- 22 Cong, L. *et al.* Multiplex genome engineering using CRISPR/Cas systems. *Science* **339**, 819-823, doi:10.1126/science.1231143 (2013).
- 23 Trejo-de la, O. A., Hernandez-Sancen, P. & Maldonado-Bernal, C. Relevance of single-nucleotide polymorphisms in human TLR genes to infectious and inflammatory diseases and cancer. *Genes Immun* **15**, 199-209, doi:10.1038/gene.2014.10 (2014).

- 24 Hoshino, K. *et al.* Cutting edge: Toll-like receptor 4 (TLR4)-deficient mice are hyporesponsive to lipopolysaccharide: evidence for TLR4 as the Lps gene product. *J Immunol* **162**, 3749-3752 (1999).
- 25 Poltorak, A. *et al.* Defective LPS signaling in C3H/HeJ and C57BL/10ScCr mice: mutations in Tlr4 gene. *Science* **282**, 2085-2088 (1998).

Figure 1: Convergence of pattern recognition receptor families on NF- κ B signaling

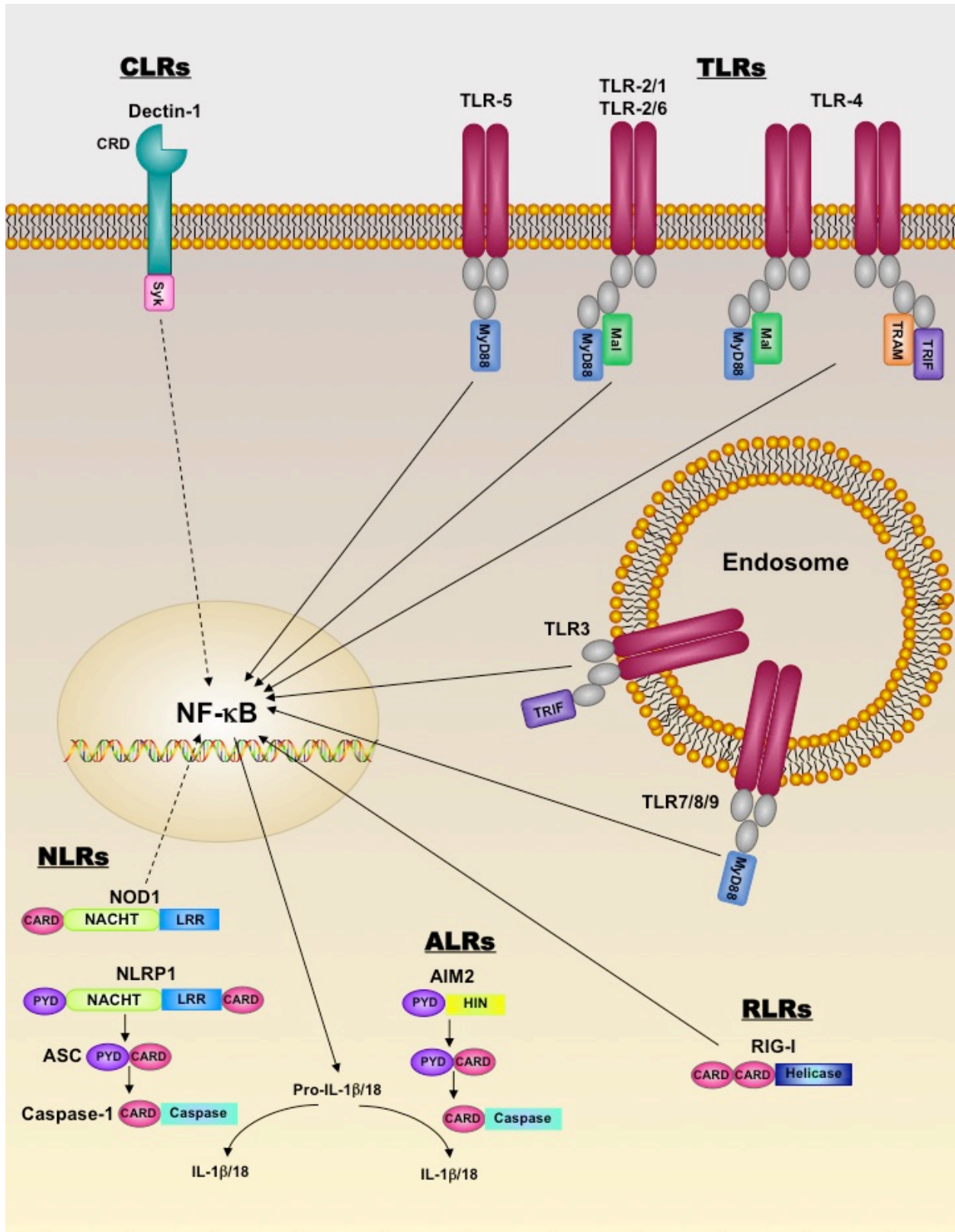


Figure 1: Convergence of pattern recognition receptor families on NF- κ B signaling. The PRR families include membrane associated C-type lectin receptors (CLRs) and Toll-like receptors (TLRs), and the cytosolic receptors Nod-like receptors (NLRs), AIM2-like receptors (ALRs), and RIG-I-like receptors (RLRs); which all play a role in NF- κ B signaling. CLRS, such as Dectin-1, recruit the adaptor Syk to their cytoplasmic domain upon binding a ligand at the carbohydrate recognition domain (CRD). Upon ligand binding, TLRs hetero- or homo-dimerize, resulting in a conformational change in the receptor that leads to the recruitment of adaptor molecules MyD88, Mal, TRIF, and/or TRAM to their TIR domain. RLRs, such as RIG-I, have two N-terminal caspase-recruitment-domain (CARD) domains and recruit mitochondria anti-viral signaling (MAVS) via CARD-CARD interaction to activate NF- κ B signaling upon recognition of RNA viruses. The NLRs are comprised of a central NACHT domain, LRR, and either CARD or PYD, or both in the case of NLRP1; ALRs such as AIM2 also possess a PYD. NLRs including NOD1 indirectly stimulate NF- κ B, but the predominant role of NLRs and ALRs in NF- κ B signaling is processing the output pro-IL-1 β and pro-IL-18 into mature IL-1 β and IL-18 by the multiprotein complex known as the inflammasome, which is dependent on the adaptors ASC and Caspase-1.

Figure reprinted from Journal of Leukocyte Biology, DE Rothschild, DK McDaniel, VM Ringel-Scaia, IC Allen, "Modulating Inflammation through the Negative Regulation of NF- κ B Signaling," pp. 1131-1150, (2018), with permission from John Wiley and Sons, under license number 4533690006969. Full citation: DE Rothschild, DK McDaniel*, VM Ringel-Scaia*, IC Allen. (2018). Modulating Inflammation through the Negative Regulation of NF- κ B Signaling. Journal of Leukocyte Biology. 2018;103:1131-1150. PMID: 29389019.*

Chapter Two

The Goldilocks Conundrum: NLR Inflammasome Modulation of Gastrointestinal Inflammation during Inflammatory Bowel Disease

Veronica M. Ringel-Scaia, Dylan K. McDaniel, and Irving C. Allen

Reprinted from Critical Reviews™ in Immunology, Volume 34, VM Ringel-Scaia, DK McDaniel, IC Allen, "The Goldilocks Conundrum: NLR Inflammasome Modulation of Gastrointestinal Inflammation during Inflammatory Bowel Disease," pp. 283-314, (2016), with permission from Begell House, Inc. Full citation: VM Ringel-Scaia, DK McDaniel, IC Allen. (2016). The Goldilocks Conundrum: NLR Inflammasome Modulation of Gastrointestinal Inflammation during Inflammatory Bowel Disease. Critical Reviews in Immunology. 2016;36(4):283-314. PMID: 28322135. DOI: 10.1615/CritRevImmunol.2017019158.

Running Title: NLR Modulation of IBD and cancer

ABSTRACT:

Recent advances have revealed significant insight into Inflammatory Bowel Disease (IBD) pathobiology. Ulcerative colitis and Crohn's disease, the chronic relapsing clinical manifestations of IBD, are complex disorders with genetic and environmental influences. These

diseases are associated with the dysregulation of immune tolerance, excessive inflammation, and damage to the epithelial cell barrier. Increasing evidence indicates that pattern recognition receptors, including Toll-like Receptors (TLRs) and nucleotide-binding domain and leucine-rich repeat-containing proteins (NLRs), function to maintain immune system homeostasis, modulate the gastrointestinal microbiome, and promote proper intestinal epithelial cell regeneration and repair. New insights have revealed that NLR family members are essential components in maintaining this immune system homeostasis. To date, the vast majority of studies associated with NLRs have focused on family members that form a multi-protein signaling platform, termed the inflammasome. These signaling complexes are responsible for the cleavage and activation of the potent pleiotropic cytokines, IL-1 β and IL-18, and facilitate a unique form of cell death defined as pyroptosis. In this review, we summarize the current paradigms associated with NLR inflammasome maintenance of immune system homeostasis in the gastrointestinal system. New concepts related to canonical and non-canonical inflammasome signaling, and the implications of classical and alternative inflammasomes in IBD pathogenesis are also reviewed.

KEYWORDS: microbiome; immune system; colon; pattern recognition receptor; Nod-like receptor; cancer

ABBREVIATIONS:

GI	Gastrointestinal
IBD	Inflammatory Bowel Disease
UC	Ulcerative Colitis
CD	Crohn's disease

TLR	Toll-like Receptor
NLR	Nucleotide-binding domain and leucine-rich repeat-containing proteins
PRR	Pattern Recognition Receptor
RLR	RIG-I-like Helicase Receptor
CLR	C-type lectin receptor
PAMP	Pathogen associated molecular pattern
DAMP	Damage associated molecular pattern
ROS	Reactive oxygen species
CARD	Caspase activating and recruitment domain
ASC	Apoptosis-associated speck-like protein containing a CARD
AIM2	Absent in melanoma 2
NAIP	NLR family, apoptosis inhibitory protein
GSDMD	gasdermin D
AOM	Azoxymethane
DSS	Dextran sulfate sodium
PARP	Poly(ADP-ribose) polymerase
TMS1	Target of methylation-inducing silencing 1
ICE	IL-1 β cleaving enzyme
LPS	Lipopolysaccharide
CIAS1	Cold induced auto-inflammatory syndrome 1
SNP	Single nucleotide polymorphism
AMP	Anti-microbial peptide
LeTx	Lethal Toxin
MDP	Muramyl dipeptide
GWAS	Genome wide association studies
GBP	Guanylate-binding proteins
NBD	Nucleotide binding domain
LRR	Leucine-rich repeat
FIIND	Function to find domain
CARD	Caspase activating and recruitment domain
CRC	Colorectal cancer
senGC	Sentinel goblet cell

I. INTRODUCTION

In the gastrointestinal (GI) tract, there is a delicate alliance between the immune system and microbiota. When optimally balanced, this alliance facilitates host immunity against pathogens, drives tolerance towards innocuous antigens, and protects the host against a diverse range of autoimmune and inflammatory disorders.¹ Indeed, we now appreciate that any shift in this balance towards either a more aggressive or attenuated host immune response targeting elements of the microflora can have dramatic and often unpredictable consequences in disease pathogenesis. Inflammatory bowel disease (IBD) is one of the most common diseases associated with aberrant inflammation in the GI tract. IBD is a complex disorder with genetic, immune system, microbiome and environmental influences that can be sub-divided into two distinct forms, ulcerative colitis (UC) and Crohn's disease (CD) (**Fig. 1**). Both of these disorders are associated with dysregulated inflammation either restricted to the colon or throughout the gastrointestinal tract, respectively. The loss of immune system homeostasis in the gut is a hallmark feature of IBD and is commonly found associated with dysbiosis.

Immune system homeostasis in the GI tract is maintained by pattern recognition receptors (PRRs). In the context of IBD, the prevailing literature has focused on the role of Toll-like receptor (TLR), nucleotide-binding domain and leucine-rich repeat containing (NLR), RIG-I-like Helicase Receptors (RLR), and C-type lectin receptors (CLR) family members.^{2,3} These PRR families sense highly conserved pathogen associated molecular patterns (PAMPs) and damage associated molecular patterns (DAMPs) and modulate the ensuing innate immune response following microbial exposure, damage, and cellular stress. The biological signaling cascades associated with each of these PRRs can have significant effects on IBD pathogenesis beyond the direct modulation of inflammation, including the regulation of cell proliferation and death, tissue

repair and remodeling, and the production of potent signaling molecules, such as reactive oxygen species (ROS), in the gut.⁴ To maintain immune system homeostasis in the GI tract, PRR activation is required to be robust and sufficient to facilitate the host immune response against pathogens and damage, while also being sufficiently constrained and permissive to promote a healthy gut microflora and avoid prolonged activation. Persistent stimulation and chronic dysregulation of PRR signaling in the GI tract is associated with significant collateral damage and a shift in the microbiome towards dysbiosis, which can contribute to chronic inflammation, autoimmunity, and cancer.² Thus, we have previously described this phenomenon as a “Goldilocks conundrum”, where PRR expression, activation, and repression must be constantly maintained in balance to promote immune system homeostasis.^{2,5}

Over the last few years, we have witnessed a significant expansion in the number of reports associated with the contribution of NLR family members in IBD pathobiology.² These studies have shed new insight on the complex mechanisms modulated by NLRs in the GI tract. In large part, the interest in exploring the role of NLRs in IBD stems from human genetic association studies that have linked single nucleotide polymorphisms (SNPs) in several NLR family members with either UC or CD.⁶ The most well-known of these mutations are in NOD2 and are associated with CD pathogenesis in patient sub-populations.⁷ However, beyond NOD2, genome-wide association studies (GWAS) have identified a number of other risk alleles in NLR genes associated with IBD, including mutations in NOD1 and NLRP3 and dysregulated expression of a variety of NLR genes have recently been found in IBD patient populations.² Beyond these mutation and gene expression findings, mechanistic and functional insight in human subjects is currently lacking. The overwhelming majority of data pertaining to NLR function in IBD has been derived from mouse models.

There are over 24 distinct NLR and NLR-like proteins in humans, of which only about half have been well characterized.⁸⁻¹⁰ These initial characterization studies have revealed that the NLR family members can be divided into 3 primary sub-groups: inflammasome forming NLRs, regulatory NLRs, and reproductive NLRs.¹¹ Of these sub-groups, the vast majority of studies have focused on identifying and characterizing the inflammasome forming NLRs. NLR inflammasomes are macromolecular platforms that sense cytosolic PAMPs and DAMPs, resulting in the maturation of pro-IL-1 β and pro-IL-18 into their bioactive cytokines (**Fig. 2**).¹² In addition to IL-1 β and IL-18 maturation, inflammasome activation can also result in a unique form of inflammatory cell death, termed pyroptosis or pyronecrosis.¹³⁻¹⁸ The core unit of the inflammasome is composed of a specific NLR(s); the apoptosis-associated speck-like protein containing a caspase activating and recruitment domain (CARD) (ASC; encoded by the gene *PYCARD*); and a specific caspase (typically Caspase-1). NLRP1, NLRP3, NLRP6, NLRC4, and the functionally related protein Absent in melanoma 2 (AIM2) have been clearly shown to form inflammasome complexes; whereas, NLRC5, NLRP7, NLRP12, and NAIP co-factors are less defined, but also appear to contribute or directly function through inflammasome formation under cell type-, species-, stimuli-, and/or temporal-specific mechanisms.¹⁹⁻²⁶ These NLR and NLR-like proteins sense specific PAMPs and/or DAMPs and form a specific NLR inflammasome following recognition and activation.⁹ In general, the mechanisms and signals associated with NLR activation are currently unclear. However, two mechanisms have been proposed: direct ligand binding or indirect milieu sensing.² Evidence supporting both mechanisms is prominent in the literature. For example, AIM2 directly binds dsDNA and NAIP5 directly binds to flagellin fragments.^{20,27-29} Conversely, NLRP3 does not appear to directly bind any specific PAMP or DAMP associated ligand/s, acting instead through indirect milieu sensing.

NLRP3 has been suggested to sense changes in the intracellular environment and/or disruptions in the cytosol associated with pathogen infection, cellular damage, and stress.¹⁹ These changes include K⁺ efflux, generation of mitochondrial ROS, lysosomal damage, and/or cathepsin B release.¹⁹

Despite extensive study, there are still a significant number of unsolved mysteries in NLR biology.³⁰ In the context of IBD, the clinical relevance of NLR inflammasome function is still unclear, cell type specific effects have yet to be extensively characterized, and the role of NLRs outside of direct host-microbe sensing remains largely unexplored. Likewise, the seemingly conflicting data from an exponentially increasing number of mouse studies has generated a highly complex and often misinterpreted mechanistic overview of NLR biology in the gut. In this review, we summarize our current understanding of the emerging concepts associated with NLR inflammasome formation and maintenance of immune system homeostasis in the GI tract. We discuss new and emerging concepts in NLR inflammasome biology, provide an overview of the current mouse model literature, discuss insights pertaining to human IBD pathobiology, and attempt to reconcile divergent mouse model findings.

II. NLR INFLAMMASOMES

A. The Canonical Inflammasome

The previous paradigm in innate immunology and the PRR field was that inflammasome organization and signaling proceeds through a relatively simple, linear process. In the “classical” inflammasome formation model, the cell requires “Signal 1” for transcriptional priming (**Fig. 2**). In essence, the stimulation of TLRs results in increased transcription and translation of pro-IL-

1 β . Similarly, this process also results in increased pro-IL-18; however, pro-IL-18 is constitutively expressed in a variety of cell types and increases following TLR stimulation.³¹ These pro-form cytokines are maintained in the cytosol in their immature states until inflammasome formation occurs to drive post-translational processing and cleavage into the mature cytokines. In the classical model, the adaptor protein ASC (encoded by the *PYCARD* gene) links the NLR sensor to caspase-1 to form the basic inflammasome sub-unit. ASC includes a pyrin domain and a CARD.³² The ASC protein interacts with NLR family members through pyrin-pyrin interactions, which trigger the formation of a large multimer of dimers termed the ASC speck.³² Following speck formation, monomers of pro-caspase-1 are recruited and form CARD-CARD interactions with ASC. This interaction induces the self-cleavage of pro-caspase-1 and results in the formation of a heterotetrameric, active caspase-1. Both pro-IL-1 β and pro-IL-18 are proteolytic targets of caspase-1, and are thus cleaved when caspase-1 becomes activated. Several inflammasome forming NLR proteins contain CARD domains, such as NLRC4, and can thus activate caspase-1 without ASC.³³ However, IL-1 β and IL-18 generation is significantly enhanced with ASC speck formation and various co-factors are typically involved in pattern recognition to assist NLRC4 with signaling.³³ Following cleavage and activation, IL-1 β and IL-18 require a “Signal 2”, which typically includes exogenous ATP, to facilitate release from the cell (**Fig 2**).

This classical overview of NLR inflammasome formation and function has been predominately based on studies conducted utilizing knockout mouse models and human cell lines. However, it has long been realized that significant differences exist between human and mouse processing and secretion of IL-1 β /IL-18 and pyroptosis. For example, human cells typically do not require the exogenous ATP associated with Signal 2 for IL-1 β and IL-18 release

following PAMP stimulation; whereas, this is essential for mouse cells. Adding a level of complexity to this observation, ATP is only needed in the context of PAMP stimulation, as most pathogens are capable of initiating complex signaling cascades and generated sufficient levels of Signal 2 to promote cytokine release without exogenous stimulation. Likewise, whole pathogen exposure also negates the need for Signal 1, as the PAMPs and DAMPs associated with the infection also serve as the transcriptional priming step. Recently, the mechanism associated with the differences between mouse and human cells has come to light. It is now recognized that inflammasome formation can occur through either the “classical” pathway or a newly described “alternative” pathway (**Table 1**).³⁴ Specifically, classical inflammasome formation, as defined in mouse monocytes/macrophages, requires Signal 1 (transcriptional priming) and Signal 2 (ATP); whereas, inflammasome signaling in human cells can proceed without the dual signals and can also occur independently of exogenous ATP, pyroptosome formation, and pyroptosis (**Table 1**). This “alternative” inflammasome activation was defined in the context of the NLRP3 inflammasome following LPS exposure.³⁴ Mechanistically, the alternative inflammasome signals through a TLR4-TRIF-RIPK1-FADD-Caspase 8 cascade, all up-stream of NLRP3 activation in humans.³⁴ While more mechanistic insight is certainly needed to better define this mechanism, it is now clear that inflammasome formation and function are much more complex than initially thought and a multitude of questions pertaining to this alternative inflammasome remain unanswered. For example, it is unclear if there is cell type specificity for classical and alternative inflammasome formation. The vast majority of studies have characterized and defined inflammasome function in monocyte/macrophage populations, but significantly less is known beyond these leukocyte populations. It is also unclear as to whether or not this is a stimuli specific or an NLR specific effect. The alternative inflammasome was defined following LPS

exposure and in the context of NLRP3 activation. It is unclear if this applies to other PAMPs/stimuli or additional NLR inflammasomes. Finally, it is also unclear if these differences are species specific. NLR family members are highly conserved and it is unclear if the alternative inflammasome functions in other mammals or even in other cell types in humans and mice. This question was partially addressed in the study that defined the alternative inflammasome, whereby, this mechanism was observed in both human and pig monocytes.³⁴

In addition to direct inflammasome formation, some NLRs also require co-factors for inflammasome formation. These co-factors function to assist with signal recognition or to stabilize the activated NLR. The best-characterized co-factors are the NLR family, apoptosis inhibitory protein (NAIP) proteins. These co-factors have been characterized in mouse models associated with NLRC4 inflammasome formation and signaling. Because NLRC4 has a CARD protein, rather than a pyrin domain, the exact mechanism underlying inflammasome formation remains a bit unclear. However, recent findings have revealed that NLRC4 forms complexes with NAIP proteins to facilitate signaling. In this model, the NAIP proteins directly recognize the respective PAMPs through receptor-ligand interactions and subsequently complex NLRC4 to facilitate inflammasome formation. In mice, NAIP1 detects the type III secretion system needle, NAIP2 senses the type III secretion system rod protein, while NAIP5 and NAIP6 detect flagellin, prior to interactions with NLRC4.^{21,35,36} However, only a single NAIP orthologue has been identified in the human genome and it functions similar to the murine NAIP1 protein to sense the type III secretion system needle.³⁶ Thus, the mechanism used by NLRC4 in human cells to sense flagellin is still unclear, but does not appear to utilize the same NAIP5/NAIP6 mechanism described in mice.

Pyroptosis, a unique form of inflammatory cell death that is also associated with inflammasome formation, is similar to apoptosis in that both rely on the activation of specific repertoires of caspases to trigger programmed cell death. Apoptosis relies on a set of initiator caspases (caspase-2, -8, -9, -10) that respond to apoptotic signals and cleave effector caspases (caspase-3, -6, -7). These effector caspases proceed to cleave target proteins to drive apoptotic cell death. Conversely, pyroptosis is defined by the activation of a sub-set of inflammatory caspases (caspase-1, -4, -5, -11), which encode both the initiator and effector functions to orchestrate cleavage of target proteins and modulate cell death pathways. Pyroptosis is defined by the following unique characteristics: (1) the activation of an inflammatory caspase; (2) pore formation in the plasma membrane; (3) low levels of DNA damage and an intact nucleus; and (4) poly(ADP-ribose) polymerase (PARP) activity is not required.³⁷ Pyroptosis and inflammation are intimately linked in host-pathogen responses. Indeed, pyroptosis is an efficient mechanism to restrict pathogens by destroying their protective, intracellular niche within infected cells.³⁷

The mechanistic link between caspase signaling and pyroptosis has recently been found to involve gasdermin D (GSDMD).³⁸⁻⁴⁰ The critical role of GSDMD in inflammasome signaling hinges on caspase cleavage and activation of GSDMD from the “pro” full-length protein of 53 kDa to the active 30 kDa N-terminal fragment.⁴⁰ Interestingly, GSDMD proteolytic cleavage can be mediated via caspase-1,⁴⁰ as well as by caspase-11 in mouse cells or caspase-4 in human cells.³⁹ This potentially indicates some diversity as to the role of GSDMD in canonical or noncanonical inflammasome function. Functionally, cleaved GSDMD was found to selectively bind to plasma membranes containing lipids, such as the mitochondrial and bacterial lipid cardiolipin, and phosphatidylinositol phosphates that are located on the inner leaflet of the mammalian cell membrane.³⁸ The result of this binding is the formation of oligomeric pores that

kill mammalian cells, which is restricted to the activated cell and does not kill bystander cells.³⁸ GSDMD was also shown to directly kill bacteria, but because active GSDMD binds selectively to phospholipids that are restricted to the inner leaflet of mammalian cell membranes, it remains unclear whether the antibacterial function of GSDMD is limited to killing bacteria that escaped the phagosome.³⁸

B. ASC and Caspase-1 in IBD Pathogenesis

ASC is considered an essential adaptor protein for inflammasome function due to its critical role as a “bridge” between NLRs containing PYD domains and pro-caspase-1 and significantly enhances the activity of NLRs containing CARD domains.^{19,32} Indeed, ASC is a major player in multiple inflammatory diseases and implicated in several autoimmune diseases associated with inflammasome dysfunction.⁴¹ Because of ASC’s central role in inflammasome formation, *Asc*^{-/-} mice are commonly used in murine models to investigate inflammasome function, as deletion of ASC results in the ablation of all inflammasome function. In murine models of chemically induced colitis with dextran sulfate sodium (DSS), the absence of ASC has been consistently shown to have a more severe phenotype than other individual NLR knockout genotypes,⁴²⁻⁴⁷ implying that loss of all inflammasomes is more detrimental to IBD pathogenesis than the loss of any individual sensor. In general, these studies all demonstrate that *Asc*^{-/-} mice present with more severe clinical features associated with colitis progression, including increased mortality, weight loss, loose stool, dehydration, and decreased colon length. Histopathologically, mice lacking ASC have increased colon inflammation and significant defects in the epithelial cell barrier. These barrier defects have been shown to be associated with increased levels of serum endotoxin, indicating enhanced permeability and bacteria translocation in the *Asc*^{-/-} mice.⁴⁴

Colitis sensitivity in the *Asc*^{-/-} mice is correlated with ablated levels of IL-1 β and IL-18, due to the loss of inflammasome function.⁴²⁻⁴⁷ Together, these data reveal that NLR inflammasomes function to attenuate gastrointestinal inflammation during experimental colitis.

Patients with IBD have a significantly increased risk of developing a distinct form of cancer, defined as colitis-associated cancer.⁴⁸ One of the distinct advantages of DSS based experimental colitis models is the ability to robustly study not only gastrointestinal inflammation, but also colitis-associated cancer. In these models, mice are exposed to the mutagen azoxymethane (AOM) prior to DSS driven inflammation.⁴⁹ AOM induces mutations in intestinal epithelial cells, which leads to a well-defined pathological progression to colorectal cancer, typically adenocarcinoma, in genetically susceptible mouse genotypes. This process is significantly enhanced when DSS is used to drive inflammation and a wound healing response in the epithelial cells. Increasing evidence has linked ASC and cancer progression. Indeed, prior to the discovery of the inflammasome and ASC speck formation, ASC was originally defined as target of methylation-inducing silencing 1 (TMS1) and was shown to be silenced through methylation in human breast and gastric cancers.^{50,51} Prior to what we now define as pyroptosis, these early studies suggested that ASC silencing was associated with reduced apoptosis and increased cancer severity.^{50,51} Subsequently, ASC expression has also been shown to be reduced in several cancers including melanoma, colorectal cancer, lung cancer, and oral squamous cell carcinoma.⁵²⁻⁵⁵ Thus, the majority of studies evaluating the *Asc*^{-/-} mice in the DSS models also included assessments of inflammation driven tumorigenesis using the AOM+DSS model. Consistent with the experimental colitis findings, mice lacking ASC also demonstrate significantly increased tumor formation, with some studies identifying large macroscopic polyps and significantly enhanced morbidity and mortality in the *Asc*^{-/-} mice as early as 30 days after

AOM treatment.⁴² This indicates that tumor formation occurs approximately twice as rapidly and much more aggressively in the *Asc*^{-/-} mice compared to wild type animals.⁴² Taken together, it seems that the *Asc*^{-/-} mouse model data is consistent with the *ASC* expression and silencing findings in human patient populations, which correlate decreased expression with increased cancer pathogenesis.

The findings associated with *ASC* were originally unexpected as the *Asc*^{-/-} mice were postulated to have reduced inflammation and tumorigenesis due to the loss of pro-inflammatory IL-1 β and IL-18 signaling. Thus, parallel studies were also conducted evaluating caspase-1. Caspase-1, formally known as IL-1 β cleaving enzyme (ICE), is considered the archetypal member of the inflammatory caspases. In mammals, this family of inflammatory caspases includes caspase-1, caspase-4, caspase-5, caspase-11 and caspase-12.⁵⁶ Some differences in these caspases are observed between mice and humans. For example, in most humans, caspase-12 is mutated and encodes for a nonfunctional protein.⁸ In addition, caspase-11 is found in mice, while caspases-4 and 5 are found in humans and are considered to be the human homologs of caspase-11.⁸ Interestingly, all of the inflammatory caspases, including caspase-1, contain an N-terminal CARD, which is responsible for binding *ASC* in the formation of the canonical inflammasome.^{12,56} Like *ASC*, caspase-1 was originally considered essential for the function of all inflammasomes and critical for the cleavage of pro-IL-1 β and pro-IL-18 into their mature forms.^{12,57-59} Due to its overwhelming role in many inflammatory processes, including inflammasome formation, caspase-1 is the most fully characterized of the inflammatory caspases.⁸ As mentioned previously, caspase-1 activation is triggered by the oligomerization of NLRs via their NACHT domains and the subsequent interaction with *ASC*.⁸ When these molecules are in close proximity, the autocatalytic activity of caspase-1 is initiated, leading to its

activation.⁶⁰ It should be noted that compared to other caspases, such as caspase-3 and caspase-7, caspase-1 has a restricted substrate repertoire.⁶¹ However, caspase-1 has been shown to be involved in a variety of “inflammation-independent” functions, such as cell death, glucose homeostasis, and triglyceride metabolism.⁶²⁻⁶⁴ Regardless, most of these other functions of caspase-1 are speculated to be dependent on caspase-1 activation via inflammasome formation.⁶²

As with ASC, due to the importance of caspase-1 to IL-1 β and IL-18 processing and inflammasome formation, several mouse studies have evaluated the role of caspase-1 in experimental colitis models.^{42,47,65} One of the earliest of these by Siegmund et al. (2001) utilized *Casp1*^{-/-} mice in acute and chronic models of DSS colitis. Counter to the findings associated with the *Asc*^{-/-} mice, this study found decreased weight loss, diarrhea score, and bleeding score in mice lacking caspase-1 put through both acute and chronic DSS models.⁶⁵ However, more recent studies have consistently shown that loss of *Casp1*^{-/-} results in worsened disease progression in similar mouse models.^{42,47,66,67} In each of these current studies, mice lacking caspase-1 displayed significantly increased morbidity and mortality, weight loss, rectal bleeding, and other pathological features of disease progression. Likewise, each of these studies correlated increased disease progression with ablation of IL-1 β and/or IL-18.^{42,47,66,67} Together, the consensus data is consistent with the findings for ASC and further supports a protective role for the NLR inflammasome in IBD pathobiology. Due to its protective role in IBD pathogenesis, caspase-1 has also gained attention in the context of colitis-associated cancer. Recent studies using the AOM-DSS model have shown that mice lacking *Casp1* display increased tumor load and tumor frequency compared to wild type mice.⁶⁸ Interestingly, in the same study, it was found that there was no difference in inflammation between wild type and *Casp1*^{-/-} mice.⁶⁸ This finding is in

contrast to the studies mentioned earlier, in which *Casp1*^{-/-} mice showed increased levels of inflammation and tumorigenesis compared to wild type mice.^{42,47,66,67}

While the DSS model is an excellent choice to evaluate inflammation driven tumorigenesis, one common critique is that DSS fails to accurately model many clinical and physiological features associated with human IBD. Thus, many investigators utilize spontaneous colitis models to complement DSS findings. For example, the most common approach used to study spontaneous colitis utilizes mice on an IL-10 defective background. Surprisingly, studies utilizing *Il-10*^{-/-} mice are relatively rare in the inflammasome field compared to DSS. In one of the few studies to evaluate caspase-1 in the *Il-10*^{-/-} colitis model, inhibition of either IL-1 receptor signaling or caspase-1 using chemical antagonists suppressed IL-1 β and IL-17 production from inflamed colon explants significantly ameliorated the development of spontaneous colitis.⁶⁹ These data are consistent with another recent spontaneous colitis and colitis-associated cancer model utilizing IEC *Clgalt*^{-/-} mice.⁷⁰ Core 1- and core 3-derived mucin-type O-linked oligosaccharides (O-glycans) are major components of the mucus layer in the gut.⁷⁰ When this mechanism is disrupted in the gut in mice lacking core 1-derived O-glycans (IEC *Clgalt*^{-/-}), the animals develop spontaneous colitis, followed by the appearance of invasive carcinomas as the mice age.⁷⁰ This spontaneous inflammation-driven tumorigenesis is likely highly dependent on the host microbiota, which is able to have increased interactions with the intestinal epithelial cells and translocate more readily due to the decreased integrity of the mucosal barrier.⁷⁰ Similar to the observations in the *Il-10*^{-/-} model, when these IEC *Clgalt*^{-/-} mice were crossed with mice deficient in *Casp-1*, the resultant animals showed significantly reduced development of colitis-associated tumorigenesis compared to IEC *Clgalt*^{-/-} mice.⁷⁰

In the DSS and spontaneous colitis studies, it is clear that caspase-1 deletion dramatically alters the phenotype. However, it is currently unclear if caspase-1 protects against or augments IBD and colitis-associated cancer progression. Likewise, it is unclear if this is associated with model differences, stimuli, temporal, or cell-type specific differences. Adding a level of complexity to these studies, it should be noted that, to our knowledge, the majority of commercially available *Casp1*^{-/-} mice used in prior experimental colitis and IL-1 β /IL-18 studies are actually *Casp1*^{-/-} and *Casp11*^{-/-} double knockout animals, due to the nested nature of the *Casp1* and *Casp11* genes.⁷¹ Thus, it is difficult to reconcile the individual contributions of caspase-1 to disease pathogenesis, without also considering the possible effects of caspase-11 deletion. Since all three of the described models have significant microbiome contributions, it is also highly likely that differences in the gut flora could significantly impact the phenotypes observed in each of these models.

C. The Noncanonical Inflammasome

NLR inflammasome activation an essential pillar of innate immunity and maintains immune system homeostasis in the gut. However, in addition to the “canonical” inflammasome, which includes classical and alternative activation and relies on caspase-1, a “non-canonical” inflammasome has also been characterized and is associated with caspase-4/-5 in humans and caspase-11 in mice (**Fig. 1; Table 1**).⁷¹ These caspases are broadly expressed in both hematopoietic and non-hematopoietic derived cells.^{16,45,71} Caspase-11 has been found to significantly modulate the host immune response following exposure to *Escherichia coli*, *Citrobacter rodentium*, and *Vibrio cholera*.^{39,71} It appears that caspase-11 and the human paralogs caspase-4 and caspase-5 function through directly binding cytosolic LPS and lipid A

from gram negative bacteria.⁷² This binding has been suggested to be highly specific and occurs through the CARD domains.⁷² Once binding occurs, the caspases oligomerize and become activated.⁷² Subsequent findings have revealed that caspase-11 functions as an essential initiator of other caspases during acute pathological conditions,⁷³ such as sepsis, endotoxic shock, and acute bacterial infection. Indeed, it appears that the non-canonical inflammasome also plays a dominant role during acute inflammation, whereby activation of caspase-11 results in IL-1 β and IL-18 cleavage through a canonical inflammasome-dependent mechanism.⁷¹ Beyond IL-1 β and IL-18 processing, the non-canonical inflammasome also plays a potent role in pyroptosis. However, non-canonical inflammasome associated pyroptosis appears to proceed through a canonical inflammasome independent mechanism,⁷¹ which has yet to be well characterized. As mentioned above in the caspase-1 discussion, the majority of commercially available *Casp1*^{-/-} mice are actually *Casp1*^{-/-} and *Casp11*^{-/-} double knockout animals.⁷¹ Subsequent studies using the *Casp11*^{-/-} targeted mice have revealed that caspase-11 functions in a variety of biological mechanisms once thought to be solely dependent on caspase-1 and has also revealed several caspase-1 independent functions.^{71,74,75}

The overwhelming majority of studies characterizing caspase-11, -4, -5 have focused on acute bacteria exposure models and sepsis.^{73,76,77} Thus, it is unclear if other PAMPs beyond LPS and Lipid A signals associated with gram negative bacteria can initiate non-canonical inflammasome formation. Interestingly, recent work by our team and others, has revealed that non-canonical inflammasome signaling may extend well beyond the currently identified mechanisms associated with cytosolic LPS recognition. Specifically, our research has recently revealed that caspase-11 modulates inflammation during *Toxoplasma gondii* infection.⁷⁸ Using *Casp11*^{-/-} mice, our results revealed that non-canonical inflammasome signaling significantly

impacts neuro-inflammation and cyst burden during the chronic phases of disease.⁷⁸ While the mechanism underlying these findings are still unclear, these data suggest a role of caspase-11 in the sensing and response to a currently unidentified molecular pattern associated with this eukaryotic parasite or implicate that non-canonical inflammasome signaling is functioning in response to intracellular changes driven by the parasite.⁷⁸ Thus, it is highly likely that future studies will continue to expand the role of non-canonical inflammasome function and signaling.

D. Noncanonical Inflammasome Associated Caspases in IBD

The majority of previous research regarding caspases and IBD has focused on caspase-1. However, there has been significant increase in studies investigating caspase-11 and the non-canonical inflammasome in the pathogenesis of IBD due to the recent revelation that the *Casp1*^{-/-} mice used previously in many IBD studies are truly *Casp1*^{-/-}/*Casp11*^{-/-} double knockout mice. Similar to the prior caspase-1 studies, caspase-11 has also been shown to attenuate gastrointestinal inflammation during experimental colitis in mice.⁴⁵ Specifically, *Casp11*^{-/-} mice in an acute DSS study had increased morbidity, mortality, and clinical parameters associated with disease severity.⁴⁵ Furthermore, *Casp11*^{-/-} mice displayed increased inflammation and epithelial cell damage in the colon compared to wild type animals.⁴⁵ However, unlike *Asc*^{-/-} and *Casp1*^{-/-}/*Casp11*^{-/-} mice, the *Casp11*^{-/-} animals showed attenuated IL-1 β and IL-18 levels in colon culture supernatants, rather than full ablation, and that reconstitution of these cytokines in these mice attenuated experimental colitis pathogenesis.⁴⁵ Unlike the *Asc*^{-/-} and *Casp1*^{-/-}/*Casp11*^{-/-} mice, the protective influence of caspase-11 appears to be restricted to acute experimental colitis, as deletion of caspase-11 only had a minor impact in chronic DSS and AOM+DSS models.⁴⁵ These data are consistent with hypothesis that caspase-11 functions prevalently during severe

damage and inflammation, rather than during chronic or minor insults. Consistent with these findings, a second study also found that *Casp11*^{-/-} mice were more susceptible to DSS induced experimental colitis.⁷⁹ Interestingly, *Casp11*^{-/-} mice were found to be highly susceptible to acute DSS, independent of microbiome shifts.⁷⁹ The microbiome of *Casp11*^{-/-} mice contained a reduced abundance of *Prevotellacea* compared to wild type animals. However, cohousing *Casp11*^{-/-} and wild type mice equilibrated *Prevotellacea* and *Bacteroides* contents, but the mice lacking caspase-11 still displayed the same increased severity phenotype.⁷⁹

In humans, the caspase-11 orthologues caspase-4 and caspase-5 have recently been shown to be significantly upregulated in both CD and UC patient samples.⁸⁰ This study revealed that *caspase-4* expression is higher in non-inflamed ileum and colon tissues from IBD patients, suggesting that caspase-4 may be a candidate for a biomarker of disease.⁸⁰ In contrast, both caspase-1 and -5 expression was significantly higher in inflamed colonic, not ileal, tissue, suggesting their involvement with colitis, rather than ileitis.⁸⁰ Taken together, these data indicate that caspases-4 and -5 are involved in intestinal inflammation observed during IBD. This study also evaluated colorectal cancer tissue, and found the same trend of increased caspase-4 and -5 expression with some correlation to cancer stage.⁸⁰ Indeed, it has been hypothesized that caspase-5 mutations may be linked with gastrointestinal cancers that have a microsatellite mutator phenotype.⁸¹ However, despite some trends associated with progression of disease, there are currently no significant functional or mechanistic studies in humans directly linking these caspases and non-canonical inflammasome signaling with mechanisms underlying IBD or colorectal cancer pathogenesis.

III. INFLAMMASOME FORMING NLRS IN IBD AND COLITIS ASSOCIATED CANCER

A. NLRP3

NLRP3 (also known as cryopyrin and NALP3) is the most well-characterized NLR and is known for sensing a diverse array of signals.^{2,19} In humans it is encoded by the *NLRP3* gene, sometime referred to as the cold induced auto-inflammatory syndrome 1 (CIAS1) gene and is best characterized in leukocytes.⁸² While the exact mechanism of NLRP3 activation is still a mystery, there are currently at least three prevailing models that attempt to address this cryptic process. In the first model, NLRP3 inflammasome formation involves the ligation of extracellular ATP via pore formation associated with the ATP channel P2X7. Once this channel is formed, K^+ can then exit the cell and subsequently recruit pannexin 1, allowing PAMPs to enter the cytosol (**Fig. 3**).² In the second model, NLRP3 activation involves the phagocytosis of particulates, such as asbestos and monosodium urate crystals, leading to a phenomenon known as “frustrated phagocytosis”.² Thus, lysosomal instability occurs and leads to the release of cathepsin B into the cytosol.^{2,83,84} In the third model, NLRP3 inflammasome formation occurs following the generation and subsequent recognition of ROS.² In each of these models, NLRP3 functions through an indirect sensing mechanism to drive inflammasome formation. Thus, regardless of which mechanism is more accurate or widespread, this indirect strategy allows NLRP3 to sense broad changes in the intracellular environment and respond to a diverse range of pathogens and/or damage to drive the host innate immune response.

Recent studies have shown that NLRP3 attenuates disease progression during experimental colitis similar to the recent findings regarding ASC and Caspase-1.^{42,47,85}

Specifically, mice deficient in *Nlrp3* show increased morbidity, mortality, and have higher levels of inflammation in their gastrointestinal tract in acute DSS models.^{42,47,85} Interestingly, *Nlrp3*^{-/-} mice show a more subtle disease during the recurring or chronic model of experimental colitis, compared to mice deficient in other inflammasome components (*Casp1*^{-/-} and *Asc*^{-/-}), although mice lacking *Nlrp3* were still shown to have worse disease than wild type mice.⁴² As with ASC and caspase-1, NLRP3 functions to attenuate colitis progression through the modulation of IL-1 β and IL-18.^{66,86} Specifically, lower levels of IL-1 β can significantly impact T cell differentiation, leading to increased intestinal inflammation.⁸⁶ Likewise, decreased levels of IL-18 result in defective epithelial cell regeneration and repair, which contribute to increased barrier dysfunction in the *Nlrp3*^{-/-} mice.⁴⁷ Together, the altered T cell differentiation and reduced barrier function results in increased bacterial translocation and inflammation in the gut.

Similar to its role in IBD pathogenesis, NLRP3 has been shown to play a protective role in mouse models of colitis-associated tumorigenesis, whereby loss of *Nlrp3* leads to significantly worsened disease progression in AOM+DSS models.^{42,47} Specifically, *Nlrp3*^{-/-} mice showed higher mortality, morbidity and significantly truncated colons during this model of inflammation driven tumorigenesis.⁴² Importantly, *Nlrp3*^{-/-} mice show significantly higher tumor burdens compared to wild type mice receiving the same treatment, indicating that NLRP3 indeed plays an important role in attenuating colitis-associated cancer.^{42,47} Mechanistically, the enhanced tumorigenesis seen in the *Nlrp3*^{-/-} mice appears to be associated with dysregulated IL-18 production.⁴⁷ While both IL-1 β and IL-18 levels are significantly attenuated in *Nlrp3*^{-/-} mice, IL-18 appears to play a more vital role in maintaining gastrointestinal homeostasis. Specifically, the levels of IL-18 were found to be much lower in colon homogenates from *Nlrp3*^{-/-} mice compared to wild type mice treated with AOM+DSS, while the levels of other important inflammatory

cytokines (IL-6, IL-12 and TNF) were found to be unchanged.^{42,66} As mentioned earlier, IL-18 has been shown to play an important role in promoting epithelial cell regeneration and repair during experimental colitis using DSS.^{47,67} However, it also inhibits hyperplasia and proliferation during the AOM+DSS model.⁶⁶ Thus, IL-18 plays multiple roles through the epithelial cell compartment that can significantly impact both IBD and cancer.

The role of NLRP3 in IBD and colitis-associated cancer has also been evaluated in human disease, mostly through the investigation of meta-analysis of polymorphisms and disease risk. In humans, 60 SNPs have been identified in the NLRP3 gene.⁸² One of the most prevalent of these is *NLRP3* rs35829419, which is a gain-of-function mutation that is heavily associated with human inflammatory diseases, such as rheumatoid arthritis, celiac disease, and CD.⁸² In a recent meta-analysis study, it was also found that this SNP was closely associated with protection against UC and colorectal cancer (CRC).⁸² In colorectal cancer, this protection is hypothesized to come from the increased interaction with caspase-1 leading to inflammasome activation and subsequent cell death.⁸² In the case of IBD, it was suggested that the rs35829419 polymorphism interacts with the rs2043211 polymorphism in the *CARD8* gene that encodes a human inflammasome adaptor protein (CARD8; TUCAN).⁸² Specifically this *CARD8* polymorphism creates a truncated CARD8 protein, which reduces inflammasome activation and thus attenuated IBD pathology.⁸² The finding that a gain-in-function mutation in *Nlrp3* is protective during IBD and colorectal cancer is in agreement with the animal studies that show loss of function or deletion enhance disease progression.

B. NLRP6

The NLRP6 inflammasome was first identified in 2002, where initial *in vitro* studies reported the co-localization of NLRP6 with ASC, and that NLRP6 and ASC co-expression resulted in production of IL-1 β .⁸⁷ NLRP6 has since been found widely expressed in immune cells such as neutrophils, dendritic cells, macrophages, and T-cells, but is also highly expressed in epithelial cells, particularly those in the duodenum, ileum, and by myofibroblasts within the stem-cell niche of the colon.⁸⁸ Therefore, NLRP6 and its role in regulating inflammation in the gut has been a topic of considerable interest. Similar to NLRP3, *Nlrp6*^{-/-} mice are significantly more susceptible to intestinal inflammation and tumorigenesis compared to wild type animals when subjected to DSS induced experimental colitis.^{89,90} *Nlrp6*^{-/-} mice exhibit significantly increased inflammation and fail to properly repair damaged epithelium as efficiently as their wild type counterparts.^{89,90} The combination of increased inflammation and inefficient repair results in increased epithelial cell proliferation, ultimately promoting both spontaneous intestinal hyperplasia and exacerbation of colon tumorigenesis in the DSS model.^{89,90} As with the other inflammasome deficient animals, *Nlrp6*^{-/-} mice were also found to have reduced IL-1 β and IL-18 levels. Subsequent studies, utilizing *Il-1 β* ^{-/-} and *Il-18*^{-/-} mice, adoptive transfer, and co-housing studies revealed that the sensitivity of the *Nlrp6*^{-/-} mice was associated with epithelial cell derived IL-18.^{46,88-90} However, monocyte derived NLRP6 also appears to play a role in reducing susceptibility to experimental colitis.⁹¹ Adoptive transfer of wild type Ly6C^{hi} monocytes into *Nlrp6*^{-/-} mice was sufficient to protect the mice during acute colitis through a mechanism associated with IL-18 dependent TNF production.⁹¹

Mechanistically, the protective nature of NLRP6 during experimental colitis is highly correlated with the gut flora, as the microbiome of *Nlrp6*^{-/-} animals is significantly different compared to that of wild type mice (**Fig. 4**).⁹⁰ Specifically, the *Nlrp6*^{-/-} mice were characterized

by an expansion of the Bacteroidetes, Prevotellaceae, and TM7 phyla.⁹⁰ This altered microbiome, and subsequent disease susceptibility, of *Nlrp6*^{-/-} mice was transmissible to wild type animals when cohoused, with no preference or dependence on age as both animals cohoused early in postnatal life, as well as, during adulthood demonstrated the exacerbated DSS colitis phenotype.⁹⁰ The absence of NLRP6 results in decreased mucus production due to impaired mucin granule exocytosis and Muc2 secretion and subsequent impaired mucus layer formation throughout the GI tract.⁴⁶ This defective mucus layer results in mice that are more susceptible to enteric infections (**Fig. 4**).⁴⁶ Similar to *Nlrp6*^{-/-} animals, this phenotype was also seen in *Asc*^{-/-} and *Casp-1*^{-/-}/*Casp-11*^{-/-} mice.⁴⁶ In fact, a so-called “sentinel” goblet cell (senGC) at the base of the colonic crypt was recently discovered that is responsible for nonspecific endocytosis of any bacteria that penetrates the inner mucus layer.⁹² Evidence suggests that senGCs are able to activate the NLRP6 inflammasome following endocytosis of TLR ligands, in turn leading to MyD88 Nox/Duos reactive oxygen species synthesis. This initiates calcium ion signaling to drive secretion of Muc2 mucin from the senGC generating intercellular gap junction signaling, inducing Muc2 secretion from responsive and adjacent goblet cells.⁹² This in turn expels bacteria from the opening of the crypt that penetrated the inner mucus layer, protecting both the lower crypt and intestinal stem cells.⁹² The absence of NLRP6 and the subsequent impaired mucus layer creates a permissive niche for *Prevotelloceae* to exploit, resulting in these bacteria colonizing areas of the crypt where they would normally be excluded. This increased colonization results in chronic inflammation in the colon, driven by other PRRs that likely compensate for the loss of NLRP6. Likewise, this shift in the host microbiome associated with the loss of NLRP6 results in dramatic changes in microbiota-modulated metabolites. For example, the microbiota-associated metabolites taurine, histamine, and spermine co-modulate

NLRP6 inflammasome signaling and can significantly impact IL-18 production and anti-microbial peptide (AMP) profiles.⁹³ The AMP distortion appears to be another critical component of the mechanism associated with NLRP6 deficiency as restoration of the AMP axis with Ang4 is able to restore microbial diversity in the absence of IL-18 production.⁹³

Beyond experimental colitis and colitis associated tumorigenesis, *Nlrp6*^{-/-} mice are also more susceptible to infection with enteric pathogens compared to their wild type counterparts. For example, *Nlrp6*^{-/-} mice that were subjected to infection with *Citrobacter rodentium*, which is often used as a model of altering the microbial community, were unable to clear the bacteria effectively compared to wild type mice exposed to the same dosage.⁴⁶ Taken together, it is clear that the relationship between NLRP6 and the control of microbial composition via mucus and AMP production has strong implications to the pathophysiology of a variety of diseases and pathogens associated with inflammation of the gut. Additional studies are warranted to better define stimuli, cell-type and temporal specific mechanisms associated with NLRP6 inflammasome activity and function in the gut and beyond.

C. NLRP1

NLRP1 was the first inflammasome to be identified.¹² The NLRP1 inflammasome is activated following exposure to either anthrax Lethal Toxin (LeTx) or *Toxoplasma gondii* in rodents and muramyl dipeptide (MDP) in humans.⁹⁴⁻⁹⁹ Consistent with the host specific differences, the protein structure of NLRP1 is species specific. Human NLRP1 contains both an N-terminal PYRIN domain and a CARD domain; whereas, mouse NLRP1 only contains a CARD domain.² At the genomic level, rodents encode three different paralogs of *Nlrp1*, which are all poorly characterized.⁹⁵ Currently, it appears that NLRP1A plays a role in regulating

hematopoiesis, NLRP1B is involved with sensing *Bacillus anthracis* LeTx, and NLRP1C is predicted to be a pseudogene.^{95,96,100} Because of the CARD domain, NLRP1 can bypass the requirement for ASC during inflammasome formation similar to NLRC4 (**Fig. 5**). However, as with NLRC4, ASC significantly enhances inflammasome formation and modulates the formation of this signaling platform optimizing caspase-1 activation.⁹⁴

Until recently, the multiple paralogs of *Nlrp1* in the mouse had confounded efforts to generate a NLRP1 deficient animal. However, two independent groups have now generated targeted *Nlrp1abc*^{-/-} and *Nlrp1b*^{-/-} mice.^{96,100} Although the extent of the literature on the involvement of NLRP1 in gastrointestinal inflammation in both human and mouse studies is currently limited, the availability of these novel mouse lines now allows for robust assessment of murine NLRP1 function. To date, only a single study has evaluated NLRP1 in the experimental colitis model. Similar to the other inflammasome forming NLRs, the *Nlrp1b*^{-/-} mice were found to have significantly more weight loss compared to their wild type counterparts, in both the acute DSS model and the chronic DSS model of relapsing remitting disease.⁴⁴ As with the other NLRs, NLRP1 deficient mice also demonstrated increased inflammation and attenuated IL-1 β and IL-18 production.⁴⁴ Interestingly, reconstitution of the *Nlrp1b*^{-/-} mice with either recombinant IL-1 β or IL-18 partially restored protection in the acute DSS model and inhibition with either anti-IL-1 β or anti-IL-18 in wild type mice resulted in increased sensitivity.⁴⁴ Thus, it appears that NLRP1 attenuation of disease pathogenesis is, at least in part, associated with the production of both IL-1 β and IL-18. When evaluated in the AOM+DSS model of colitis associated tumorigenesis, the absence of NLRP1 resulted in increased tumor burden and size compared to wild type mice.⁴⁴ Consistent with its dominant epithelial cell expression pattern, the protection associated with NLRP1 did not appear to be dependent on the hematopoietic compartment, as

Nlrp1^{-/-} wild type chimeras did not show improvement in the DSS induced colitis model.⁴⁴ Similar to the findings for NLRP6, the microbiome in the *Nlrp1*^{-/-} mice appears to strongly modulate the progression of experimental colitis as antibiotic treatment and co-housing studies significantly impacted colitis pathogenesis.⁴⁴ It is still unclear which aspects of the host microbiome are influencing colitis and cancer progression in the *Nlrp1b*^{-/-} mice. However, as with NLRP6, future studies will further define this phenotype and provide additional mechanistic insight.

In humans, *NLRP1* mutations have been linked to a range of autoimmune and autoinflammatory disorders, including vitiligo, celiac disease, Rheumatoid Arthritis, systemic lupus erythematosus, and type I diabetes.¹⁰¹⁻¹⁰⁶ GWAS identified CD susceptibility mutations in NLRP1 associated with co-occurring extra-intestinal manifestations in skin, although the data was in a small sample size.⁶ Additionally, polymorphisms in NLRP1 were associated with increased responsiveness to IBD steroid therapeutics in a study of pediatric IBD patients.¹⁰⁷ Beyond GWAS and SNP evaluations, NLRP1 expression levels have also been shown to be significantly altered during IBD. Retrospective pooled data from three distinct studies demonstrated that *NLRP1* expression was significantly increased in colon biopsies from patients with active ulcerative colitis compared to specimens from healthy patients.⁴⁴ Conversely, when investigating the expression of *NLRP1* from eight separate studies of patients that evaluated colon biopsies from tumors versus adjacent tissue or biopsies/tissue from colon cancer patients compared with healthy controls, *NLRP1* was significantly down regulated.⁴⁴ These cancer findings are consistent with a second retrospective study analyzing the expression patterns of several different NLRs in a cohort of colorectal cancer patients that also found NLRP1

significantly downregulated relative to healthy controls.¹⁰⁸ Thus, it appears that NLRP1 expression in humans is significantly altered in the colon in a disease specific manner.

Interestingly, polymorphisms in the regulatory NLR NOD2 are the best-characterized mutations associated with IBD in select human sub-populations. Likewise, both NOD2 and NLRP1 have been shown to recognize MDP in humans and NOD2 has been previously shown to be necessary for NLRP1 inflammasome function.^{94,109,110} While the exact mechanism is still unclear, it is likely that NOD2, which has 2 CARD domains, functions to stabilize NLRP1 or act as a co-factor to augment NLRP1 inflammasome formation. This later scenario would be reminiscent of the mechanism similar to that described for the NAIP co-factors in the NLRC4 inflammasome. It is interesting to speculate that mutations in either NOD2 or NLRP1 could significantly impact the function of one or both of these proteins and potentially impact IBD progression in human patients.

D. NLRC4

NLRC4, also known as IPAF, is unique compared to the other inflammasome forming NLRs mentioned, in that it is capable of acting in concert with NAIP proteins, which provide ligand specificity.^{21,36} The NLRC4 inflammasome senses flagella, as well as, gram negative bacteria that use type III or IV secretion systems (**Fig. 6**).²⁴ The ligand bound NAIP protein releases the auto-inhibited NLRC4 to allow the NLRC4-NAIP-ligand multimeric complex, ASC, and caspase-1 to form the subsequent inflammasome.^{2,24} As mentioned previously, there are multiple differences between the single human NAIP and the multiple murine NAIP proteins.²⁴ In addition to utilizing the NAIP co-factors, the CARD domain of NLRC4 is likely also able to directly associate with the CARD domain of caspase-1, complicating the understanding of the

role of ASC in NLRC4 inflammasome formation.² In response to *Shigella flexneri*, ASC appears to be required for optimal caspase-1 activation and IL-1 β production, while ASC is not required for NLRC4- inflammasome formation in response to *Pseudomonas aeruginosa* or caspase-1–dependent cell death in response to *Shigella*.¹¹¹⁻¹¹³ Additionally, NLRC4 is unique compared to other NLRs in that inflammasome formation is not dependent on potassium efflux, which could be due to direct interactions of bacterial PAMPs and NAIP proteins.¹¹⁴

Beyond the complexities associated with the NLRC4 inflammasome, the role of NLRC4 in IBD is also quite convoluted. Originally, when NLRC4 was evaluated in DSS models using *Nlrc4*^{-/-} mice, no significant differences were observed between the *Nlrc4*^{-/-} and wild type animals in clinical, histopathological, or immunological features of experimental colitis or colitis associated tumorigenesis progression.⁴² However, subsequent studies found that NLRC4 did not appear to alter the progression of experimental colitis induced by blocking IL-10 using anti-IL-10R monoclonal antibody treatments, but did appear to have a role in DSS induced disease.¹¹⁵ Here, loss of NLRC4 was associated with increased disease severity due to increased epithelial cell barrier damage.¹¹⁵ In a third study, *Nlrc4*^{-/-} mice developed increased epithelial cell damage and inflammation in the DSS and AOM+DSS models, similar to the other inflammasome forming NLRs discussed above.⁶⁸ While these data may appear discrepant, we can speculate that they can be reconciled by considering potential differences in the microbiome populations present in these different animals. It is highly likely that the loss of NLRC4 created permissive niches in these animals that were exploited by different populations of microflora. Unfortunately, these studies were conducted prior to the routine assessments of the microbiome in the NLR field. Thus, future studies targeting the microbiome may better define the mechanisms underlying these different phenotypes.

One must also consider the NAIP proteins when discussing the NLRC4 inflammasome. In mice there are 6 NAIP paralogs (*Naip1-6*), four of which are functional and 2 are non-coding.¹¹⁶ To thoroughly explore the contribution of the NAIPs in IBD, mice were generated with a targeted deletion of all 6 paralogs (*Naip1-6^{ΔΔ}*). These mice were subjected to AOM+DSS models of colitis associated tumorigenesis and were found to significantly protect against cancer progression. The *Naip1-6^{ΔΔ}* mice demonstrated a significant increase in colorectal tumors in an epithelial-intrinsic manner.¹¹⁶ Interestingly, the increased tumorigenesis was not associated with exacerbated inflammation, rather NAIP1-6 appear to protect the animals through the modulation of apoptosis and maintenance of proliferation.¹¹⁶ These findings were confirmed using AOM only treatments, which is an inflammation independent model.¹¹⁶ The *Naip1-6^{ΔΔ}* mice displayed STAT3 hyper-activation and p53 defects that were not observed in the *Nlrc4^{-/-}* animals.¹¹⁶ Together, these data suggest that the NAIPs attenuate tumor initiation and progression through facilitating the death and removal of damaged epithelial cells. This appears to occur through an NLRC4 inflammasome-independent mechanism. More work is certainly needed to translate the findings from these mouse models to humans, where only NAIP1 is encoded in the genome. Likewise, while much more difficult to address, additional studies are warranted to better resolve which NAIP paralogs may be responsible for the observed phenotypes.

E. AIM2 (PYHIN family member)

In addition to the NLRs, other proteins have been shown to form inflammasomes. The best characterized of these proteins is AIM2 (absent in melanoma 2). AIM2 is a unique member of the HIN200 protein family, and is capable of interacting with ASC through its PYRIN domain to form an “NLR-like” inflammasome.^{27,28} AIM2 is a sensor of double stranded DNA, and is

best characterized for its ability to instigate inflammasome formation following the recognition of pathogen associated DNA.^{27,28} Some of the earliest studies evaluating the AIM2 inflammasome characterized its role in host-pathogen interactions following infection with *Francisella tularensis* and *Listeria monocytogenes*.^{28,117,118} Notably, AIM2 is also able to sense host-derived DNA in the cytoplasm, which has strong implications for a variety of autoimmune diseases and cancer.^{119,120} Of particular relevance to this current review, one of the earliest findings associated with AIM2 relates to its role in CRC.¹²⁰ AIM2 is often found inactivated in melanoma, breast cancer, mammary tumors, gastric cancer, and CRC. Restoration of AIM2 in a colon cancer cell line was found to suppress proliferation and drive G2/M cell cycle arrest.¹²⁰ Beyond CRC, the presence of anti-nuclear and double stranded DNA antibodies has been linked with decreased efficacy of anti-TNF therapies and adverse outcomes in patients with both CD and UC.^{121,122} Indeed, one of these more common adverse outcomes in IBD patients is an increased frequency of a lupus-like syndrome that has been suggested to be associated with these elevated autoantibodies.^{121,122} Due to its role in lupus and sensing host DNA,¹²³ it is certainly possible that AIM2 may also play a role in this IBD associated lupus-like syndrome.

In addition to indirect effects on IBD progression, recent findings have revealed a more direct role for AIM2 in modulating intestinal homeostasis and inflammation (**Fig. 7**). Consistent with the data from human cell lines, AIM2 deficient mice have been shown to be highly sensitive to colonic tumor development.^{124,125} The loss of AIM2 resulted in increased intestinal stem cell proliferation that was associated with aberrant Wnt signaling.¹²⁴ Unlike the other NLRs, colon histopathology from *Aim2*^{-/-} mice revealed increased crypt dysplasia and hyperplasia compared to wild type animals, despite any differences with regard to inflammatory immune infiltrates in the colon.¹²⁵ Likewise, the increased tumorigenesis observed in the AIM2 deficient mice was

independent of IL-1 β and IL-18.^{124,125} However, similar to the NLRs, the cancer progression was significantly enhanced by the dysbiotic microbiome.¹²⁴ The mechanism linking AIM2 and tumorigenesis appears to be, in part, associated with direct regulation of both Wnt signaling and the Akt pathway.^{124,125} While these prior two studies indicated that AIM2 function in tumorigenesis is independent of inflammation, it should be noted that the dysbiosis noted in the AIM2 deficient mice was found to result in higher experimental colitis susceptibility in subsequent studies.¹²⁶ Specifically, *Aim2*^{-/-} mice were found to have higher colonic levels of *Escherichia coli*.¹²⁶ In this study, *Aim2*^{-/-} mice were found to be sensitive to acute DSS in this single study and reconstitution with IL-18 was found to reduce experimental colitis progression.¹²⁶ Similar to these findings, a more recent study using a *Salmonella typhimurium* colitis/acute infection model also found that AIM2 functions to protect against experimental colitis progression.¹²⁷ The mechanism identified suggests that AIM2 functions to promote tight junction formation through AKT activation, which would be consistent with the IL-18 and AKT results previously reported.¹²⁵⁻¹²⁷

III. THE EFFECTS OF THE INFLAMMASOME ON THE HOST MICROBIOME

The relationship between aberrant inflammasome signaling and dysbiosis in the gut associated with IBD is a common theme that has recently emerged. Gut commensal bacteria function to protect the host from pathogenic bacteria by occupying and competing for biological niches. In order for the bacteria to exist and flourish in the gut, the immune system must create a permissive environment. The increasingly expanding interest in the contribution of the microbiome in health and disease is accompanied by an existing void as to mechanistic insights

as to how microbiome components could be exerting such effects. Any breakdown in intestinal epithelial barrier function can lead to the translocation of microbial flora, and subsequent recognition by NLRs. A compelling hypothesis implicating NLRs in the role of maintaining homeostasis between the resident commensal microbial community and the host is that NLRs keep the unique microbial components in check. With a loss or depletion of mucosal barrier protection, as is so often observed in IBD and CAC patients,^{128,129} bacteria from the microbiome are able to come into contact with the epithelium and occupy niches within the gut where they would normally be excluded. In healthy populations, the translocation of the microbiome to the epithelium is sensed by inflammasome-forming NLRs. However, with a decreased NLR repertoire, as seen in both IBD and CAC populations, the host immune response is sub-optimal and creates microenvironments where bacteria are likely to hyper-proliferate. Ultimately, this results in a loss of flora diversity and potentially leads to an increase in harmful commensal or pathogenic bacteria in the gut. This shift in the microbiome has far reaching effects, including significant changes in the metabolomic profile of the host, which can have dramatic effects on IBD and beyond.

IV. THE GOLDILOCKS CONUNDRUM

Immune system homeostasis in the gut is a delicate balancing act. The immune system must maintain a significant level of vigilance to protect the host from harmful pathogens and environmental insults, while simultaneously suppressing overzealous inflammation in response to the probiotic and commensal flora present in the microbiome. PRRs are essential components of this process and are maintained at a critical threshold to enable a rapid response if needed, but

insufficient to drive widespread gastrointestinal inflammation.¹³⁰ NLR family members are integral PRRs in the gut and play vital roles, both directly and indirectly, in maintaining immune system homeostasis. Under normal conditions, inflammasome forming NLRs in cells associated with the mucosal barrier and leukocytes function to maintain proper intestinal epithelial cell regeneration and repair, cell death, and a well-balanced inflammatory microenvironment. However, the loss of NLR signaling, as observed in knockout mouse models, results in increased inflammation, enhanced IBD pathogenesis, and augments the progression colitis associated cancer (**Fig. 8**). In general, the consensus data suggests that this is true for all of the NLR family members, co-factors, adaptor proteins, and caspases. In fact, in our hands, we typically observe robust gastrointestinal inflammation and colon tumorigenesis in mice lacking the common adaptor protein ASC or caspase-1/-11. However, while disease progression is still significantly increased over the wild type animals, the loss of any individual NLR typically results in an attenuated phenotype compared to animals with completely defective inflammasomes. Suggesting that some NLR inflammasomes function through redundant mechanisms in the gut to protect the host during IBD.

At first glance, the increased IBD progression in inflammasome deficient mice appears to be counterintuitive. One would predict, as most research groups originally did, that loss of NLR inflammasome function would result in reduced IL-1 β and IL-18 levels and attenuated disease pathogenesis. However, both of these robust pro-inflammatory cytokines have significant roles beyond simply driving inflammation. For example, IL-18 is also critically important in epithelial cell regeneration and repair.¹³¹ Thus, in the context of IBD, the loss of IL-18, the subsequent increase in damage to the epithelial cell layer, and increase in microbial translocation across the barrier, actually promotes more robust inflammation driven by other compensatory PRRs outside

of the NLR family (i.e. TLRs). Likewise, the loss of specific NLRs create permissive niches for the colonization of commensal and pathogenic components of the host microbiome,^{46,90,93} and has been summarized in **Table 2**. In essence, without specific NLR recognition, some microbes can take advantage of the sub-optimal immune response and colonize areas of the gastrointestinal tract where they are typically excluded. Ultimately, this can result in significant shifts in the local microbial microenvironment and changes in the metabolomic profile associated with the change in flora. In sum, this too results in increased inflammation, IBD pathogenesis and tumorigenesis. Conversely, if NLR inflammasome signaling is enhanced and not properly resolved, as observed following pathogen infection or chronic damage to the epithelial cell barrier, then overzealous inflammation can also occur (**Fig. 8**). This heightened level of inflammation is directly associated with increased cytokine signaling and leukocyte activation. The robust pro-inflammatory microenvironment promotes increased epithelial cell proliferation and inflammation driven colon tumorigenesis. Likewise, enhanced IL-1 β signaling can significantly impact Th cell differentiation through enhancing the effects of lineage-specifying cytokines.¹³² In the presence of specific cytokine milieu, IL-1 β can significantly impact the differentiation of Th cells into specific Th1, Th2, or Th17 sub-populations.¹³² Together, the functional studies associated with NLR inflammasome maintenance of immune system homeostasis has revealed a highly complex network of both protective and detrimental roles in gastrointestinal health and disease. It is now clear that skewing NLR activation either towards reduced activity (i.e. to cold) or enhanced activity (i.e. to hot) have equally detrimental effects on IBD progression and associated tumorigenesis in the gut (**Fig. 8**).

V. CONCLUSIONS

Significant progress has been made over the last decade defining the contribution of NLR family members in IBD pathobiology. Early studies focused on inflammasome forming NLRs as potential therapeutic targets for CD and UC. These early studies postulated that if a specific NLR could be linked to IBD pathogenesis and successfully targeted, inflammation could be strategically attenuated with minimal detrimental effects. However, it became quickly evident that deletion of any NLR inflammasome components resulted in unpredictable gastrointestinal phenotypes in IBD models. These unexpected findings have fueled numerous and exciting new avenues of research associated with NLR function in gastrointestinal health and disease. Indeed, we now realize that NLR inflammasome function in the gut is significantly more complex than originally thought. A key challenge in future studies will be translating these highly complex findings from mouse models to human patients.

As with any rapidly moving area of research, there are many published studies in the NLR field that appear to offer seemingly contradictory findings. This is especially true in the context of the IBD models described in this review. In our opinion, we believe that these apparent discrepancies can be best reconciled by considering the impact and interaction between the various parameters that drive IBD pathogenesis. Many of the earlier studies associated with NLR inflammasomes exclusively focused on genetics and immune system dysfunction. However, as we stated in the introduction, IBD is a disease that is also characterized by microbiome and environmental factors that are not well understood. It is now clear that NLRs can dramatically modulate the host microbiome and the absence of an individual inflammasome results in dramatic shifts in the gastrointestinal flora that can significantly alter disease progression. The niches that are created in the absence of an NLR inflammasome are open to

exploitation by both commensal microbes already present in the host and microbes present in the specific environment unique to each individual vivarium. It is certainly clear that future studies must account not only for genetics and immune system function, but also the microbiome and specific environmental conditions present at the site of testing. Beyond microbiome compositional analysis, it will also be critical to gain greater insight into the functional differences associated with specific microbiome and metabolomics profiles that are directly associated with NLR inflammasome function.

Further understanding of the mechanisms associated with NLR inflammasome function, regulation, and effects on the host microbiome will provide significant insight into IBD pathobiology and pathogenesis. It is our hope that a better understanding of these highly interesting PRRs will lead to novel therapeutic strategies that will ultimately aid in the diagnosis, management, and treatment of IBD.

VI. ACKNOWLEDGEMENTS

This work was supported in part through the National Institutes of Health, NIDDK (K01DK092355; R03DK105975); the Virginia Tech Translational Biology, Medicine, and Health Program; and the VA-MD Regional College of Veterinary Medicine (CVM-IRC). The content is solely the responsibility of the authors and does not necessarily represent the official views of the National Institutes of Health. Figures were generated with the assistance of VisiScience software.

VII. REFERENCES

1. Belkaid Y, Hand TW. Role of the microbiota in immunity and inflammation. *Cell*. 2014;157(1):121-41.
2. Davis BK, Philipson C, Hontecillas R, Eden K, Bassaganya-Riera J, Allen IC. Emerging significance of NLRs in inflammatory bowel disease. *Inflamm Bowel Dis*. 2014;20(12):2412-32.
3. Walsh D, McCarthy J, O'Driscoll C, Melgar S. Pattern recognition receptors--molecular orchestrators of inflammation in inflammatory bowel disease. *Cytokine Growth Factor Rev*. 2013;24(2):91-104.
4. Kutikhin AG, Yuzhalin AE. Inherited variation in pattern recognition receptors and cancer: dangerous liaisons? *Cancer Manag Res*. 2012;4:31-8.
5. Allen IC. Non-Inflammasome Forming NLRs in Inflammation and Tumorigenesis. *Front Immunol*. 2014;5:169.
6. Cummings JR, Cooney RM, Clarke G, Beckly J, Geremia A, Pathan S, Hancock L, Guo C, Cardon LR, Jewell DP. The genetics of NOD-like receptors in Crohn's disease. *Tissue Antigens*. 2010;76(1):48-56.
7. Hugot JP. CARD15/NOD2 mutations in Crohn's disease. *Ann N Y Acad Sci*. 2006;1072:9-18.
8. Schroder K, Tschopp J. The inflammasomes. *Cell*. 2010;140(6):821-32.
9. Ting JP, Williams KL. The CATERPILLER family: an ancient family of immune/apoptotic proteins. *Clin Immunol*. 2005;115(1):33-7.
10. Ting JP, Willingham SB, Bergstralh DT. NLRs at the intersection of cell death and immunity. *Nat Rev Immunol*. 2008;8(5):372-9.

11. Kufer TA, Sansonetti PJ. NLR functions beyond pathogen recognition. *Nat Immunol.* 2011;12(2):121-8.
12. Martinon F, Burns K, Tschopp J. The inflammasome: a molecular platform triggering activation of inflammatory caspases and processing of proIL-beta. *Mol Cell.* 2002;10(2):417-26.
13. Fernandes-Alnemri T, Wu J, Yu JW, Datta P, Miller B, Jankowski W, Rosenberg S, Zhang J, Alnemri ES. The pyroptosome: a supramolecular assembly of ASC dimers mediating inflammatory cell death via caspase-1 activation. *Cell Death Differ.* 2007;14(9):1590-604.
14. Cookson BT, Brennan MA. Pro-inflammatory programmed cell death. *Trends Microbiol.* 2001;9(3):113-4.
15. Fink SL, Cookson BT. Caspase-1-dependent pore formation during pyroptosis leads to osmotic lysis of infected host macrophages. *Cell Microbiol.* 2006;8(11):1812-25.
16. Fink SL, Cookson BT. Pyroptosis and host cell death responses during *Salmonella* infection. *Cell Microbiol.* 2007;9(11):2562-70.
17. Vanden Berghe T, Linkermann A, Jouan-Lanhouet S, Walczak H, Vandenabeele P. Regulated necrosis: the expanding network of non-apoptotic cell death pathways. *Nat Rev Mol Cell Biol.* 2014;15(2):135-47.
18. Willingham SB, Bergstralh DT, O'Connor W, Morrison AC, Taxman DJ, Duncan JA, Barnoy S, Venkatesan MM, Flavell RA, Deshmukh M, Hoffman HM, Ting JP. Microbial pathogen-induced necrotic cell death mediated by the inflammasome components CIAS1/cryopyrin/NLRP3 and ASC. *Cell Host Microbe.* 2007;2(3):147-59.

19. Davis BK, Wen H, Ting JP. The inflammasome NLRs in immunity, inflammation, and associated diseases. *Annu Rev Immunol.* 2011;29:707-35.
20. Halff EF, Diebolder CA, Versteeg M, Schouten A, Brondijk TH, Huizinga EG. Formation and structure of a NAIP5-NLRC4 inflammasome induced by direct interactions with conserved N- and C-terminal regions of flagellin. *J Biol Chem.* 2012;287(46):38460-72.
21. Kofoed EM, Vance RE. Innate immune recognition of bacterial ligands by NAIPs determines inflammasome specificity. *Nature.* 2011;477(7366):592-5.
22. Lightfield KL, Persson J, Trinidad NJ, Brubaker SW, Kofoed EM, Sauer JD, Dunipace EA, Warren SE, Miao EA, Vance RE. Differential requirements for NAIP5 in activation of the NLRC4 inflammasome. *Infect Immun.* 2011;79(4):1606-14.
23. Triantafilou K, Hughes TR, Triantafilou M, Morgan BP. The complement membrane attack complex triggers intracellular Ca²⁺ fluxes leading to NLRP3 inflammasome activation. *J Cell Sci.* 2013;126(Pt 13):2903-13.
24. von Moltke J, Ayres JS, Kofoed EM, Chavarria-Smith J, Vance RE. Recognition of bacteria by inflammasomes. *Annu Rev Immunol.* 2013;31:73-106.
25. Khare S, Dorfleutner A, Bryan NB, Yun C, Radian AD, de Almeida L, Rojanasakul Y, Stehlik C. An NLRP7-containing inflammasome mediates recognition of microbial lipopeptides in human macrophages. *Immunity.* 2012;36(3):464-76.
26. Vladimer GI, Weng D, Paquette SW, Vanaja SK, Rathinam VA, Aune MH, Conlon JE, Burbage JJ, Proulx MK, Liu Q, Reed G, Meccas JC, Iwakura Y, Bertin J, Goguen JD, Fitzgerald KA, Lien E. The NLRP12 inflammasome recognizes *Yersinia pestis*. *Immunity.* 2012;37(1):96-107.

27. Hornung V, Ablasser A, Charrel-Dennis M, Bauernfeind F, Horvath G, Caffrey DR, Latz E, Fitzgerald KA. AIM2 recognizes cytosolic dsDNA and forms a caspase-1-activating inflammasome with ASC. *Nature*. 2009;458(7237):514-8.
28. Fernandes-Alnemri T, Yu JW, Datta P, Wu J, Alnemri ES. AIM2 activates the inflammasome and cell death in response to cytoplasmic DNA. *Nature*. 2009;458(7237):509-13.
29. Burckstummer T, Baumann C, Bluml S, Dixit E, Durnberger G, Jahn H, Planyavsky M, Bilban M, Colinge J, Bennett KL, Superti-Furga G. An orthogonal proteomic-genomic screen identifies AIM2 as a cytoplasmic DNA sensor for the inflammasome. *Nat Immunol*. 2009;10(3):266-72.
30. Lupfer C, Kanneganti TD. Unsolved Mysteries in NLR Biology. *Front Immunol*. 2013;4:285.
31. Garlanda C, Dinarello CA, Mantovani A. The interleukin-1 family: back to the future. *Immunity*. 2013;39(6):1003-18.
32. Compan V, Martin-Sanchez F, Baroja-Mazo A, Lopez-Castejon G, Gomez AI, Verkhratsky A, Brough D, Pelegrin P. Apoptosis-associated speck-like protein containing a CARD forms specks but does not activate caspase-1 in the absence of NLRP3 during macrophage swelling. *J Immunol*. 2015;194(3):1261-73.
33. Latz E, Xiao TS, Stutz A. Activation and regulation of the inflammasomes. *Nat Rev Immunol*. 2013;13(6):397-411.
34. Gaidt MM, Ebert TS, Chauhan D, Schmidt T, Schmid-Burgk JL, Rapino F, Robertson AA, Cooper MA, Graf T, Hornung V. Human Monocytes Engage an Alternative Inflammasome Pathway. *Immunity*. 2016;44(4):833-46.

35. Zhao Y, Shi J, Shi X, Wang Y, Wang F, Shao F. Genetic functions of the NAIP family of inflammasome receptors for bacterial ligands in mice. *J Exp Med*. 2016;213(5):647-56.
36. Zhao Y, Yang J, Shi J, Gong YN, Lu Q, Xu H, Liu L, Shao F. The NLRC4 inflammasome receptors for bacterial flagellin and type III secretion apparatus. *Nature*. 2011;477(7366):596-600.
37. Jorgensen I, Miao EA. Pyroptotic cell death defends against intracellular pathogens. *Immunol Rev*. 2015;265(1):130-42.
38. Liu X, Zhang Z, Ruan J, Pan Y, Magupalli VG, Wu H, Lieberman J. Inflammasome-activated gasdermin D causes pyroptosis by forming membrane pores. *Nature*. 2016;535(7610):153-8.
39. Kayagaki N, Stowe IB, Lee BL, O'Rourke K, Anderson K, Warming S, Cuellar T, Haley B, Roose-Girma M, Phung QT, Liu PS, Lill JR, Li H, Wu J, Kummerfeld S, Zhang J, Lee WP, Snipas SJ, Salvesen GS, Morris LX, Fitzgerald L, Zhang Y, Bertram EM, Goodnow CC, Dixit VM. Caspase-11 cleaves gasdermin D for non-canonical inflammasome signalling. *Nature*. 2015;526(7575):666-71.
40. He WT, Wan H, Hu L, Chen P, Wang X, Huang Z, Yang ZH, Zhong CQ, Han J. Gasdermin D is an executor of pyroptosis and required for interleukin-1beta secretion. *Cell Res*. 2015;25(12):1285-98.
41. Yang CA, Chiang BL. Inflammasomes and human autoimmunity: A comprehensive review. *J Autoimmun*. 2015;61:1-8.
42. Allen IC, TeKippe EM, Woodford RM, Uronis JM, Holl EK, Rogers AB, Herfarth HH, Jobin C, Ting JP. The NLRP3 inflammasome functions as a negative regulator of tumorigenesis during colitis-associated cancer. *J Exp Med*. 2010;207(5):1045-56.

43. Bauer C, Duewell P, Mayer C, Lehr HA, Fitzgerald KA, Dauer M, Tschopp J, Endres S, Latz E, Schnurr M. Colitis induced in mice with dextran sulfate sodium (DSS) is mediated by the NLRP3 inflammasome. *Gut*. 2010;59(9):1192-9.
44. Williams TM, Leeth RA, Rothschild DE, Coutermarsh-Ott SL, McDaniel DK, Simmons AE, Heid B, Cecere TE, Allen IC. The NLRP1 inflammasome attenuates colitis and colitis-associated tumorigenesis. *J Immunol*. 2015;194(7):3369-80.
45. Williams TM, Leeth RA, Rothschild DE, McDaniel DK, Coutermarsh-Ott SL, Simmons AE, Kable KH, Heid B, Allen IC. Caspase-11 attenuates gastrointestinal inflammation and experimental colitis pathogenesis. *Am J Physiol Gastrointest Liver Physiol*. 2015;308(2):G139-50.
46. Wlodarska M, Thaïss CA, Nowarski R, Henao-Mejia J, Zhang JP, Brown EM, Frankel G, Levy M, Katz MN, Philbrick WM, Elinav E, Finlay BB, Flavell RA. NLRP6 inflammasome orchestrates the colonic host-microbial interface by regulating goblet cell mucus secretion. *Cell*. 2014;156(5):1045-59.
47. Zaki MH, Boyd KL, Vogel P, Kastan MB, Lamkanfi M, Kanneganti TD. The NLRP3 inflammasome protects against loss of epithelial integrity and mortality during experimental colitis. *Immunity*. 2010;32(3):379-91.
48. Danese S, Malesci A, Vetrano S. Colitis-associated cancer: the dark side of inflammatory bowel disease. *Gut*. 2011;60(12):1609-10.
49. Wirtz S, Neufert C, Weigmann B, Neurath MF. Chemically induced mouse models of intestinal inflammation. *Nat Protoc*. 2007;2(3):541-6.

50. Conway KE, McConnell BB, Bowring CE, Donald CD, Warren ST, Vertino PM. TMS1, a novel proapoptotic caspase recruitment domain protein, is a target of methylation-induced gene silencing in human breast cancers. *Cancer Res.* 2000;60(22):6236-42.
51. Moriai R, Tsuji N, Kobayashi D, Yagihashi A, Namiki Y, Takahashi H, Watanabe N. A proapoptotic caspase recruitment domain protein gene, TMS1, is hypermethylated in human breast and gastric cancers. *Anticancer Res.* 2002;22(6C):4163-8.
52. Guan X, Sagara J, Yokoyama T, Koganehira Y, Oguchi M, Saida T, Taniguchi S. ASC/TMS1, a caspase-1 activating adaptor, is downregulated by aberrant methylation in human melanoma. *Int J Cancer.* 2003;107(2):202-8.
53. Machida EO, Brock MV, Hooker CM, Nakayama J, Ishida A, Amano J, Picchi MA, Belinsky SA, Herman JG, Taniguchi S, Baylin SB. Hypermethylation of ASC/TMS1 is a sputum marker for late-stage lung cancer. *Cancer Res.* 2006;66(12):6210-8.
54. Shimane T, Kobayashi H, Takeoka M, Kitazawa M, Matsumura T, Hida S, Xiao T, Koike T, Taniguchi S, Kurita H. Clinical significance of apoptosis-associated speck-like protein containing a caspase recruitment domain in oral squamous cell carcinoma. *Oral Surg Oral Med Oral Pathol Oral Radiol.* 2013;115(6):799-809.
55. Yokoyama T, Sagara J, Guan X, Masumoto J, Takeoka M, Komiyama Y, Miyata K, Higuchi K, Taniguchi S. Methylation of ASC/TMS1, a proapoptotic gene responsible for activating procaspase-1, in human colorectal cancer. *Cancer Lett.* 2003;202(1):101-8.
56. Martinon F, Tschopp J. Inflammatory caspases: linking an intracellular innate immune system to autoinflammatory diseases. *Cell.* 2004;117(5):561-74.
57. Thornberry NA, Bull HG, Calaycay JR, Chapman KT, Howard AD, Kostura MJ, Miller DK, Molineaux SM, Weidner JR, Aunins J, Ellistone KO, Ayala JM, Casano FJ, Chin J,

- Ding GJ-F, Egger LA, Gaffney EP, Limjuco G, Palyha OC, Raju SM, Rolando AM, Salley JP, Yamin T-T, Lee TD, Shively JE, Maccross M, Mumford RA, Schmidt JA, Tocci MJ. A novel heterodimeric cysteine protease is required for interleukin-1 beta processing in monocytes. *Nature*. 1992;356(6372):768-74.
58. Kuida K, Lippke JA, Ku G, Harding MW, Livingston DJ, Su MS, Flavell RA. Altered cytokine export and apoptosis in mice deficient in interleukin-1 beta converting enzyme. *Science*. 1995;267(5206):2000-3.
59. Li P, Allen H, Banerjee S, Franklin S, Herzog L, Johnston C, McDowell J, Paskind M, Rodman L, Salfeld J, Towne E, Tracey D, Wardwell S, Wei F-Y, Wong W, Kamen R, Seshadri T. Mice deficient in IL-1 beta-converting enzyme are defective in production of mature IL-1 beta and resistant to endotoxic shock. *Cell*. 1995;80(3):401-11.
60. Ciraci C, Sutterwala FS. Inhibitors of apoptosis proteins and IL-1beta: a tangled relationship. *Immunity*. 2012;36(2):155-7.
61. Walsh JG, Logue SE, Luthi AU, Martin SJ. Caspase-1 promiscuity is counterbalanced by rapid inactivation of processed enzyme. *J Biol Chem*. 2011;286(37):32513-24.
62. Kotas ME, Jurczak MJ, Annicelli C, Gillum MP, Cline GW, Shulman GI, Medzhitov R. Role of caspase-1 in regulation of triglyceride metabolism. *Proc Natl Acad Sci U S A*. 2013;110(12):4810-5.
63. Wen H, Gris D, Lei Y, Jha S, Zhang L, Huang MT, Brickey WJ, Ting JP. Fatty acid-induced NLRP3-ASC inflammasome activation interferes with insulin signaling. *Nat Immunol*. 2011;12(5):408-15.
64. Denes A, Lopez-Castejon G, Brough D. Caspase-1: is IL-1 just the tip of the ICEberg? *Cell Death Dis*. 2012;3:e338.

65. Siegmund B, Lehr HA, Fantuzzi G, Dinarello CA. IL-1 beta -converting enzyme (caspase-1) in intestinal inflammation. *Proc Natl Acad Sci U S A*. 2001;98(23):13249-54.
66. Zaki MH, Vogel P, Body-Malapel M, Lamkanfi M, Kanneganti TD. IL-18 production downstream of the Nlrp3 inflammasome confers protection against colorectal tumor formation. *J Immunol*. 2010;185(8):4912-20.
67. Dupaul-Chicoine J, Yeretssian G, Doiron K, Bergstrom KS, McIntire CR, LeBlanc PM, Meunier C, Turbide C, Gros P, Beauchemin N, Vallance BA, Saleh M. Control of intestinal homeostasis, colitis, and colitis-associated colorectal cancer by the inflammatory caspases. *Immunity*. 2010;32(3):367-78.
68. Hu B, Elinav E, Huber S, Booth CJ, Strowig T, Jin C, Eisenbarth SC, Flavell RA. Inflammation-induced tumorigenesis in the colon is regulated by caspase-1 and NLRC4. *Proc Natl Acad Sci U S A*. 2010;107(50):21635-40.
69. Zhang J, Fu S, Sun S, Li Z, Guo B. Inflammasome activation has an important role in the development of spontaneous colitis. *Mucosal Immunol*. 2014;7(5):1139-50.
70. Bergstrom K, Liu X, Zhao Y, Gao N, Wu Q, Song K, Cui Y, Li Y, McDaniel JM, McGee S, Chen W, Huycke MM, Houchen CW, Zenewicz LA, West CM, Chen H, Braun J, Fu J, Xia L. Defective Intestinal Mucin-Type O-Glycosylation Causes Spontaneous Colitis-Associated Cancer in Mice. *Gastroenterology*. 2016;151(1):152-64 e11.
71. Kayagaki N, Warming S, Lamkanfi M, Vande Walle L, Louie S, Dong J, Newton K, Qu Y, Liu J, Heldens S, Zhang J, Lee WP, Roose-Girma M, Dixit VM. Non-canonical inflammasome activation targets caspase-11. *Nature*. 2011;479(7371):117-21.
72. Kayagaki N, Wong MT, Stowe IB, Ramani SR, Gonzalez LC, Akashi-Takamura S, Miyake K, Zhang J, Lee WP, Muszynski A, Forsberg LS, Carlson RW, Dixit VM.

- Noncanonical inflammasome activation by intracellular LPS independent of TLR4. *Science*. 2013;341(6151):1246-9.
73. Napier BA, Brubaker SW, Sweeney TE, Monette P, Rothmeier GH, Gertsvolf NA, Puschnik A, Carette JE, Khatri P, Monack DM. Complement pathway amplifies caspase-11-dependent cell death and endotoxin-induced sepsis severity. *J Exp Med*. 2016;213(11):2365-82.
 74. Caution K, Gavrilin MA, Tazi M, Kanneganti A, Layman D, Hoque S, Krause K, Amer AO. Caspase-11 and caspase-1 differentially modulate actin polymerization via RhoA and Slingshot proteins to promote bacterial clearance. *Sci Rep*. 2015;5:18479.
 75. Broz P, Ruby T, Belhocine K, Bouley DM, Kayagaki N, Dixit VM, Monack DM. Caspase-11 increases susceptibility to *Salmonella* infection in the absence of caspase-1. *Nature*. 2012;490(7419):288-91.
 76. Hotchkiss RS, Osmon SB, Chang KC, Wagner TH, Coopersmith CM, Karl IE. Accelerated lymphocyte death in sepsis occurs by both the death receptor and mitochondrial pathways. *J Immunol*. 2005;174(8):5110-8.
 77. Aziz M, Jacob A, Wang P. Revisiting caspases in sepsis. *Cell Death Dis*. 2014;5:e1526.
 78. Coutermarsh-Ott SL, Doran JT, Campbell C, Williams TM, Lindsay DS, Allen IC. Caspase-11 Modulates Inflammation and Attenuates *Toxoplasma gondii* Pathogenesis. *Mediators Inflamm*. 2016;2016:9848263.
 79. Demon D, Kuchmiy A, Fossoul A, Zhu Q, Kanneganti TD, Lamkanfi M. Caspase-11 is expressed in the colonic mucosa and protects against dextran sodium sulfate-induced colitis. *Mucosal Immunol*. 2014;7(6):1480-91.

80. Flood B, Oficjalska K, Laukens D, Fay J, O'Grady A, Caiazza F, Heetun Z, Mills KH, Sheahan K, Ryan EJ, Doherty GA, Kay E, Creagh EM. Altered expression of caspases-4 and -5 during inflammatory bowel disease and colorectal cancer: Diagnostic and therapeutic potential. *Clin Exp Immunol.* 2015;181(1):39-50.
81. Schwartz S, Jr., Yamamoto H, Navarro M, Maestro M, Reventos J, Perucho M. Frameshift mutations at mononucleotide repeats in caspase-5 and other target genes in endometrial and gastrointestinal cancer of the microsatellite mutator phenotype. *Cancer Res.* 1999;59(12):2995-3002.
82. Zhang Z, Zhang R. Epigenetics in autoimmune diseases: Pathogenesis and prospects for therapy. *Autoimmun Rev.* 2015;14(10):854-63.
83. Halle A, Hornung V, Petzold GC, Stewart CR, Monks BG, Reinheckel T, Fitzgerald KA, Latz E, Moore KJ, Golenbock DT. The NALP3 inflammasome is involved in the innate immune response to amyloid-beta. *Nat Immunol.* 2008;9(8):857-65.
84. Hornung V, Bauernfeind F, Halle A, Samstad EO, Kono H, Rock KL, Fitzgerald KA, Latz E. Silica crystals and aluminum salts activate the NALP3 inflammasome through phagosomal destabilization. *Nat Immunol.* 2008;9(8):847-56.
85. Hirota SA, Ng J, Lueng A, Khajah M, Parhar K, Li Y, Lam V, Potentier MS, Ng K, Bawa M, McCafferty DM, Rioux KP, Ghosh S, Xavier RJ, Colgan SP, Tschopp J, Muruve D, MacDonald JA, Beck PL. NLRP3 inflammasome plays a key role in the regulation of intestinal homeostasis. *Inflamm Bowel Dis.* 2011;17(6):1359-72.
86. Coccia M, Harrison OJ, Schiering C, Asquith MJ, Becher B, Powrie F, Maloy KJ. IL-1beta mediates chronic intestinal inflammation by promoting the accumulation of IL-17A

- secreting innate lymphoid cells and CD4(+) Th17 cells. *J Exp Med*. 2012;209(9):1595-609.
87. Grenier JM, Wang L, Manji GA, Huang WJ, Al-Garawi A, Kelly R, Carlson A, Merriam S, Lora JM, Briskin M, DiStefano PS, Bertin J. Functional screening of five PYPAF family members identifies PYPAF5 as a novel regulator of NF-kappaB and caspase-1. *FEBS Lett*. 2002;530(1-3):73-8.
88. Normand S, Delanoye-Crespin A, Bressenot A, Huot L, Grandjean T, Peyrin-Biroulet L, Lemoine Y, Hot D, Chamailard M. Nod-like receptor pyrin domain-containing protein 6 (NLRP6) controls epithelial self-renewal and colorectal carcinogenesis upon injury. *Proceedings of the National Academy of Sciences of the United States of America*. 2011;108(23):9601-6.
89. Chen GY, Liu M, Wang F, Bertin J, Nunez G. A functional role for Nlrp6 in intestinal inflammation and tumorigenesis. *J Immunol*. 2011;186(12):7187-94.
90. Elinav E, Strowig T, Kau AL, Henao-Mejia J, Thaiss CA, Booth CJ, Peaper DR, Bertin J, Eisenbarth SC, Gordon JI, Flavell RA. NLRP6 inflammasome regulates colonic microbial ecology and risk for colitis. *Cell*. 2011;145(5):745-57.
91. Seregin SS, Golovchenko N, Schaf B, Chen J, Eaton KA, Chen GY. NLRP6 function in inflammatory monocytes reduces susceptibility to chemically induced intestinal injury. *Mucosal Immunol*. 2016.
92. Birchenough GM, Nystrom EE, Johansson ME, Hansson GC. A sentinel goblet cell guards the colonic crypt by triggering Nlrp6-dependent Muc2 secretion. *Science*. 2016;352(6293):1535-42.

93. Levy M, Thaïss CA, Zeevi D, Dohnalova L, Zilberman-Schapira G, Mahdi JA, David E, Savidor A, Korem T, Herzig Y, Pevsner-Fischer M, Shapiro H, Christ A, Harmelin A, Halpern Z, Latz E, Flavell RA, Amit I, Segal E, Elinav E. Microbiota-Modulated Metabolites Shape the Intestinal Microenvironment by Regulating NLRP6 Inflammasome Signaling. *Cell*. 2015;163(6):1428-43.
94. Faustin B, Lartigue L, Bruey JM, Luciano F, Sergienko E, Bailly-Maitre B, Volkmann N, Hanein D, Rouiller I, Reed JC. Reconstituted NALP1 inflammasome reveals two-step mechanism of caspase-1 activation. *Mol Cell*. 2007;25(5):713-24.
95. Boyden ED, Dietrich WF. Nalp1b controls mouse macrophage susceptibility to anthrax lethal toxin. *Nat Genet*. 2006;38(2):240-4.
96. Kovarova M, Hesker PR, Jania L, Nguyen M, Snouwaert JN, Xiang Z, Lommatzsch SE, Huang MT, Ting JP, Koller BH. NLRP1-dependent pyroptosis leads to acute lung injury and morbidity in mice. *J Immunol*. 2012;189(4):2006-16.
97. Witola WH, Mui E, Hargrave A, Liu S, Hypolite M, Montpetit A, Cavailles P, Bisanz C, Cesbron-Delauw MF, Fournie GJ, McLeod R. NALP1 influences susceptibility to human congenital toxoplasmosis, proinflammatory cytokine response, and fate of *Toxoplasma gondii*-infected monocytic cells. *Infect Immun*. 2011;79(2):756-66.
98. Cirelli KM, Gorfu G, Hassan MA, Printz M, Crown D, Leppla SH, Grigg ME, Saeij JP, Moayeri M. Inflammasome sensor NLRP1 controls rat macrophage susceptibility to *Toxoplasma gondii*. *PLoS Pathog*. 2014;10(3):e1003927.
99. Ewald SE, Chavarria-Smith J, Boothroyd JC. NLRP1 is an inflammasome sensor for *Toxoplasma gondii*. *Infect Immun*. 2014;82(1):460-8.

100. Masters SL, Gerlic M, Metcalf D, Preston S, Pellegrini M, O'Donnell JA, McArthur K, Baldwin TM, Chevrier S, Nowell CJ, Cengia LH, Henley KJ, Collinge JE, Kastner DL, Feigenbaum L, Hilton DJ, Alexander WS, Kile BT, Croker BA. NLRP1 inflammasome activation induces pyroptosis of hematopoietic progenitor cells. *Immunity*. 2012;37(6):1009-23.
101. Jin Y, Mailloux CM, Gowan K, Riccardi SL, LaBerge G, Bennett DC, Fain PR, Spritz RA. NALP1 in vitiligo-associated multiple autoimmune disease. *N Engl J Med*. 2007;356(12):1216-25.
102. Levandowski CB, Mailloux CM, Ferrara TM, Gowan K, Ben S, Jin Y, McFann KK, Holland PJ, Fain PR, Dinarello CA, Spritz RA. NLRP1 haplotypes associated with vitiligo and autoimmunity increase interleukin-1beta processing via the NLRP1 inflammasome. *Proc Natl Acad Sci U S A*. 2013;110(8):2952-6.
103. Pontillo A, Vendramin A, Catamo E, Fabris A, Crovella S. The missense variation Q705K in CIAS1/NALP3/NLRP3 gene and an NLRP1 haplotype are associated with celiac disease. *Am J Gastroenterol*. 2011;106(3):539-44.
104. Sui J, Li H, Fang Y, Liu Y, Li M, Zhong B, Yang F, Zou Q, Wu Y. NLRP1 gene polymorphism influences gene transcription and is a risk factor for rheumatoid arthritis in han chinese. *Arthritis Rheum*. 2012;64(3):647-54.
105. Pontillo A, Girardelli M, Kamada AJ, Pancotto JA, Donadi EA, Crovella S, Sandrin-Garcia P. Polimorphisms in inflammasome genes are involved in the predisposition to systemic lupus erythematosus. *Autoimmunity*. 2012;45(4):271-8.
106. Magitta NF, Boe Wolff AS, Johansson S, Skinningsrud B, Lie BA, Myhr KM, Undlien DE, Joner G, Njolstad PR, Kvien TK, Forre O, Knappskog PM, Husebye ES. A coding

- polymorphism in NALP1 confers risk for autoimmune Addison's disease and type 1 diabetes. *Genes Immun.* 2009;10(2):120-4.
107. De Iudicibus S, Stocco G, Martelossi S, Londero M, Ebner E, Pontillo A, Lionetti P, Barabino A, Bartoli F, Ventura A, Decorti G. Genetic predictors of glucocorticoid response in pediatric patients with inflammatory bowel diseases. *J Clin Gastroenterol.* 2011;45(1):e1-7.
 108. Liu R, Truax AD, Chen L, Hu P, Li Z, Chen J, Song C, Chen L, Ting JP. Expression profile of innate immune receptors, NLRs and AIM2, in human colorectal cancer: correlation with cancer stages and inflammasome components. *Oncotarget.* 2015;6(32):33456-69.
 109. Hsu LC, Ali SR, McGillivray S, Tseng PH, Mariathasan S, Humke EW, Eckmann L, Powell JJ, Nizet V, Dixit VM, Karin M. A NOD2-NALP1 complex mediates caspase-1-dependent IL-1beta secretion in response to *Bacillus anthracis* infection and muramyl dipeptide. *Proc Natl Acad Sci U S A.* 2008;105(22):7803-8.
 110. Ferwerda G, Kramer M, de Jong D, Piccini A, Joosten LA, Devesaginer I, Girardin SE, Adema GJ, van der Meer JW, Kullberg BJ, Rubartelli A, Netea MG. Engagement of NOD2 has a dual effect on proIL-1beta mRNA transcription and secretion of bioactive IL-1beta. *Eur J Immunol.* 2008;38(1):184-91.
 111. Sutterwala FS, Mijares LA, Li L, Ogura Y, Kazmierczak BI, Flavell RA. Immune recognition of *Pseudomonas aeruginosa* mediated by the IPAF/NLRC4 inflammasome. *J Exp Med.* 2007;204(13):3235-45.
 112. Suzuki T, Franchi L, Toma C, Ashida H, Ogawa M, Yoshikawa Y, Mimuro H, Inohara N, Sasakawa C, Nunez G. Differential regulation of caspase-1 activation, pyroptosis, and

- autophagy via Ipaf and ASC in Shigella-infected macrophages. *PLoS Pathog.* 2007;3(8):e111.
113. Suzuki T, Nunez G. A role for Nod-like receptors in autophagy induced by Shigella infection. *Autophagy.* 2008;4(1):73-5.
114. Petrilli V, Papin S, Dostert C, Mayor A, Martinon F, Tschopp J. Activation of the NALP3 inflammasome is triggered by low intracellular potassium concentration. *Cell Death Differ.* 2007;14(9):1583-9.
115. Carvalho FA, Nalbantoglu I, Aitken JD, Uchiyama R, Su Y, Doho GH, Vijay-Kumar M, Gewirtz AT. Cytosolic flagellin receptor NLRC4 protects mice against mucosal and systemic challenges. *Mucosal Immunol.* 2012;5(3):288-98.
116. Allam R, Maillard MH, Tardivel A, Chennupati V, Bega H, Yu CW, Velin D, Schneider P, Maslowski KM. Epithelial NAIPs protect against colonic tumorigenesis. *J Exp Med.* 2015;212(3):369-83.
117. Fernandes-Alnemri T, Yu JW, Juliana C, Solorzano L, Kang S, Wu J, Datta P, McCormick M, Huang L, McDermott E, Eisenlohr L, Landel CP, Alnemri ES. The AIM2 inflammasome is critical for innate immunity to Francisella tularensis. *Nat Immunol.* 2010;11(5):385-93.
118. Rathinam VA, Jiang Z, Waggoner SN, Sharma S, Cole LE, Waggoner L, Vanaja SK, Monks BG, Ganesan S, Latz E, Hornung V, Vogel SN, Szomolanyi-Tsuda E, Fitzgerald KA. The AIM2 inflammasome is essential for host defense against cytosolic bacteria and DNA viruses. *Nat Immunol.* 2010;11(5):395-402.

119. Panchanathan R, Duan X, Arumugam M, Shen H, Liu H, Choubey D. Cell type and gender-dependent differential regulation of the p202 and Aim2 proteins: implications for the regulation of innate immune responses in SLE. *Mol Immunol.* 2011;49(1-2):273-80.
120. Patsos G, Germann A, Gebert J, Dihlmann S. Restoration of absent in melanoma 2 (AIM2) induces G2/M cell cycle arrest and promotes invasion of colorectal cancer cells. *Int J Cancer.* 2010;126(8):1838-49.
121. Beigel F, Schnitzler F, Paul Laubender R, Pfennig S, Weidinger M, Goke B, Seiderer J, Ochsenkuhn T, Brand S. Formation of antinuclear and double-strand DNA antibodies and frequency of lupus-like syndrome in anti-TNF-alpha antibody-treated patients with inflammatory bowel disease. *Inflamm Bowel Dis.* 2011;17(1):91-8.
122. Kiss LS, Lovasz BD, Golovics PA, Vegh Z, Farkas K, Molnar T, Palatka K, Papp M, Mohas A, Szilagyi BK, Fekete SA, Mandel M, Lakatos PL. Levels of anti-double-stranded DNA but not antinuclear antibodies are associated with treatment efficacy and adverse outcomes in Crohn's disease patients treated with anti-TNFalpha. *J Gastrointest Liver Dis.* 2013;22(2):135-40.
123. Panchanathan R, Duan X, Shen H, Rathinam VA, Erickson LD, Fitzgerald KA, Choubey D. Aim2 deficiency stimulates the expression of IFN-inducible Ifi202, a lupus susceptibility murine gene within the Nba2 autoimmune susceptibility locus. *J Immunol.* 2010;185(12):7385-93.
124. Man SM, Zhu Q, Zhu L, Liu Z, Karki R, Malik A, Sharma D, Li L, Malireddi RK, Gurung P, Neale G, Olsen SR, Carter RA, McGoldrick DJ, Wu G, Finkelstein D, Vogel P, Gilbertson RJ, Kanneganti TD. Critical Role for the DNA Sensor AIM2 in Stem Cell Proliferation and Cancer. *Cell.* 2015;162(1):45-58.

125. Wilson JE, Petrucelli AS, Chen L, Koblansky AA, Truax AD, Oyama Y, Rogers AB, Brickey WJ, Wang Y, Schneider M, Muhlbauer M, Chou WC, Barker BR, Jobin C, Allbritton NL, Ramsden DA, Davis BK, Ting JP. Inflammasome-independent role of AIM2 in suppressing colon tumorigenesis via DNA-PK and Akt. *Nat Med.* 2015;21(8):906-13.
126. Hu S, Peng L, Kwak YT, Tekippe EM, Pasare C, Malter JS, Hooper LV, Zaki MH. The DNA Sensor AIM2 Maintains Intestinal Homeostasis via Regulation of Epithelial Antimicrobial Host Defense. *Cell Rep.* 2015;13(9):1922-36.
127. Hu GQ, Song PX, Li N, Chen W, Lei QQ, Yu SX, Zhang XJ, Du CT, Deng XM, Han WY, Yang YJ. AIM2 contributes to the maintenance of intestinal integrity via Akt and protects against *Salmonella* mucosal infection. *Mucosal Immunol.* 2016;9(5):1330-9.
128. Png CW, Linden SK, Gilshenan KS, Zoetendal EG, McSweeney CS, Sly LI, McGuckin MA, Florin TH. Mucolytic bacteria with increased prevalence in IBD mucosa augment in vitro utilization of mucin by other bacteria. *Am J Gastroenterol.* 2010;105(11):2420-8.
129. Chen GY, Stappenbeck TS. Mucus, it is not just a static barrier. *Sci Signal.* 2014;7(323):11.
130. Asquith M, Powrie F. An innately dangerous balancing act: intestinal homeostasis, inflammation, and colitis-associated cancer. *J Exp Med.* 2010;207(8):1573-7.
131. Zambetti LP, Laudisi F, Licandro G, Ricciardi-Castagnoli P, Mortellaro A. The rhapsody of NLRPs: master players of inflammation...and a lot more. *Immunol Res.* 2012;53(1-3):78-90.

132. Hebel K, Rudolph M, Kosak B, Chang HD, Butzmann J, Brunner-Weinzierl MC. IL-1beta and TGF-beta act antagonistically in induction and differentially in propagation of human proinflammatory precursor CD4+ T cells. *J Immunol.* 2011;187(11):5627-35.
133. Koch KN, Muller A. *Helicobacter pylori* activates the TLR2/NLRP3/caspase-1/IL-18 axis to induce regulatory T-cells, establish persistent infection and promote tolerance to allergens. *Gut Microbes.* 2015;6(6):382-7.
134. Engler DB, Leonardi I, Hartung ML, Kyburz A, Spath S, Becher B, Rogler G, Muller A. *Helicobacter pylori*-specific protection against inflammatory bowel disease requires the NLRP3 inflammasome and IL-18. *Inflamm Bowel Dis.* 2015;21(4):854-61.
135. Ng J, Hirota SA, Gross O, Li Y, Ulke-Lemee A, Potentier MS, Schenck LP, Vilaysane A, Seamone ME, Feng H, Armstrong GD, Tschopp J, Macdonald JA, Muruve DA, Beck PL. *Clostridium difficile* toxin-induced inflammation and intestinal injury are mediated by the inflammasome. *Gastroenterology.* 2010;139(2):542-52.
136. Lee HM, Yuk JM, Kim KH, Jang J, Kang G, Park JB, Son JW, Jo EK. *Mycobacterium abscessus* activates the NLRP3 inflammasome via Dectin-1-Syk and p62/SQSTM1. *Immunol Cell Biol.* 2012;90(6):601-10.
137. Mishra BB, Moura-Alves P, Sonawane A, Hacohen N, Griffiths G, Moita LF, Anes E. *Mycobacterium tuberculosis* protein ESAT-6 is a potent activator of the NLRP3/ASC inflammasome. *Cell Microbiol.* 2010;12(8):1046-63.
138. Wong KW, Jacobs WR, Jr. Critical role for NLRP3 in necrotic death triggered by *Mycobacterium tuberculosis*. *Cell Microbiol.* 2011;13(9):1371-84.
139. Seo SU, Kamada N, Munoz-Planillo R, Kim YG, Kim D, Koizumi Y, Hasegawa M, Himpfl SD, Browne HP, Lawley TD, Mobley HL, Inohara N, Nunez G. Distinct

- Commensals Induce Interleukin-1beta via NLRP3 Inflammasome in Inflammatory Monocytes to Promote Intestinal Inflammation in Response to Injury. *Immunity*. 2015;42(4):744-55.
140. Chen KW, Gross CJ, Sotomayor FV, Stacey KJ, Tschopp J, Sweet MJ, Schroder K. The neutrophil NLRC4 inflammasome selectively promotes IL-1beta maturation without pyroptosis during acute Salmonella challenge. *Cell Rep*. 2014;8(2):570-82.
141. Qu Y, Misaghi S, Newton K, Maltzman A, Izrael-Tomasevic A, Arnott D, Dixit VM. NLRP3 recruitment by NLRC4 during Salmonella infection. *J Exp Med*. 2016;213(6):877-85.
142. Nordlander S, Pott J, Maloy KJ. NLRC4 expression in intestinal epithelial cells mediates protection against an enteric pathogen. *Mucosal Immunol*. 2014;7(4):775-85.

VIII. FIGURES AND LEGENDS

Figure 1: Inflammatory Bowel Disease Pathogenesis

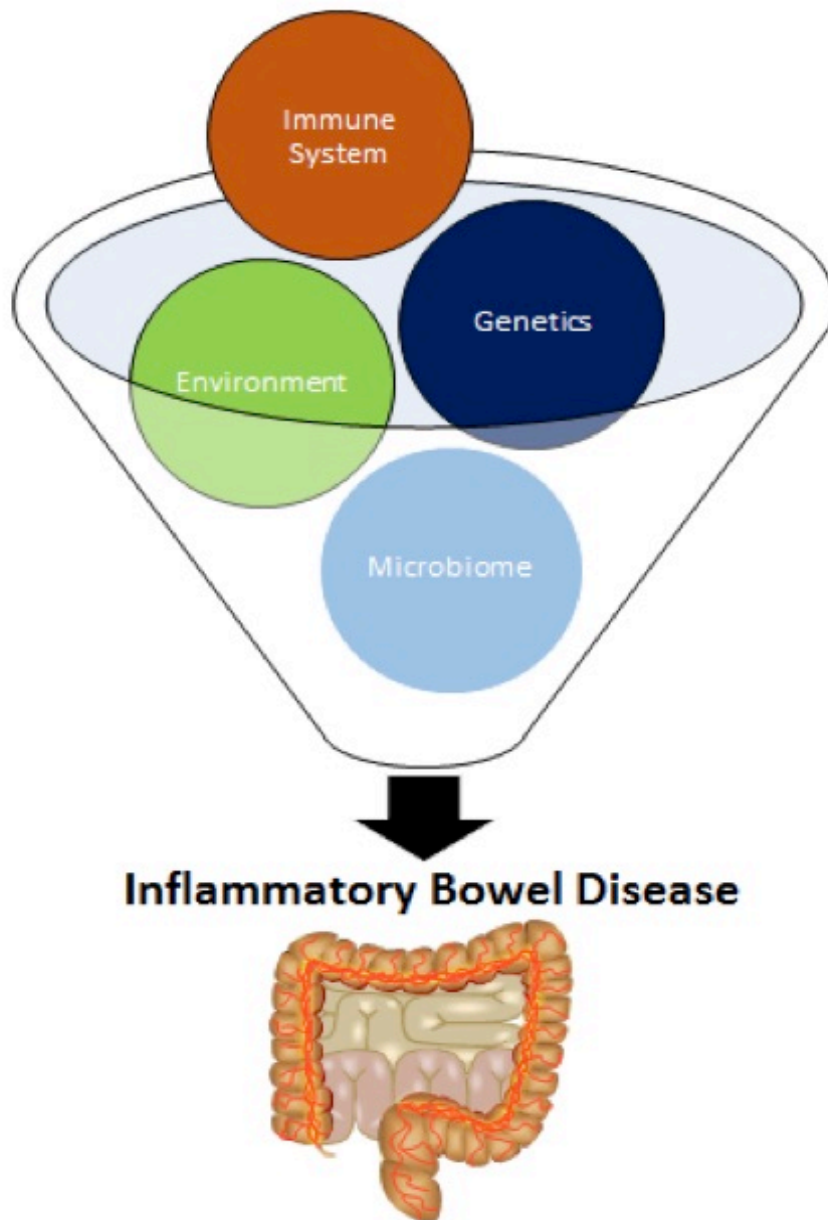


Figure 1: Inflammatory Bowel Disease Pathogenesis. Crohn's disease (CD) and ulcerative colitis (UC) are complex disorders, which are driven by poorly understood genetic and environmental influences. These disorders are strongly associated with dysfunctional and

overzealous immune system signaling in the gastrointestinal tract. It is also clear that dysbiosis and perhaps even mild-to-moderate changes in specific host microbiome populations can dramatically influence IBD progression and prognosis. Each of these mechanisms function in synergy to drive IBD pathobiology.

Figure 2: The Canonical and Non-Canonical Inflammasome

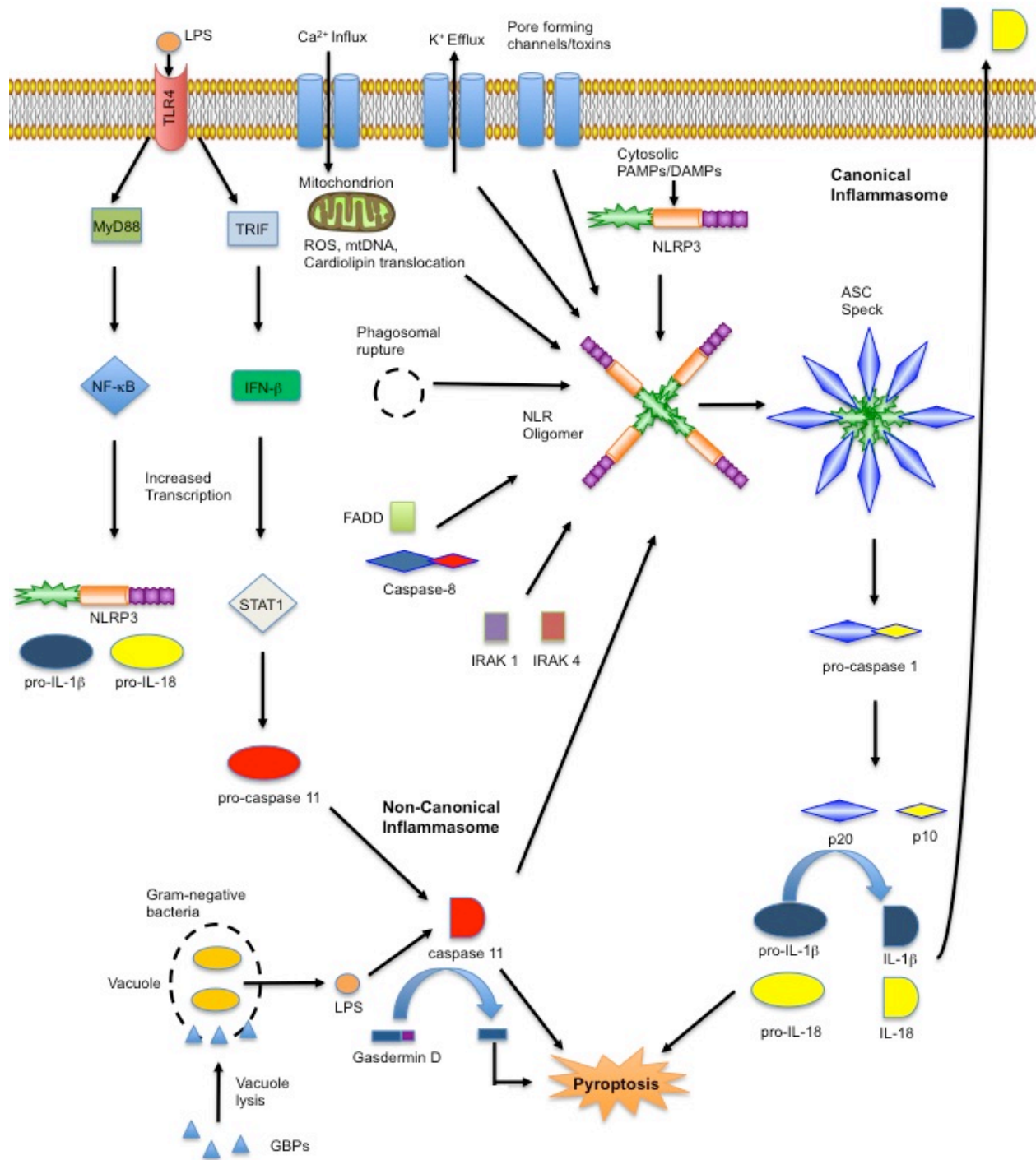


Figure 2: The Canonical and Non-Canonical Inflammasome. The activation of the canonical NLR inflammasome requires priming, typically via activation of a Toll-like receptor (TLR).

Following ligation of the TLR, MyD88 is recruited and subsequently leads to the activation of NF- κ B signaling. Activated NF- κ B promotes the transcription of pro-IL-1 β and pro-IL-18. There are many proposed mechanisms for the activation of the NLR inflammasome once priming has occurred. These include: direct PAMP sensing, K⁺ efflux, pore forming channels and toxins, Ca²⁺ influx, reactive oxygen species from the mitochondria, mitochondrial DNA, cardiolipin translocation, FADD, caspase-8 and rupture of phagosomes. Upon activation from one of the mechanisms listed above, the NLR, ASC and caspase-1 come together to form the core unit of the inflammasome. This assembly leads to the cleavage of pro-IL-1 β and pro-IL-18 into their mature forms and the induction of the pro-inflammatory form of cell death defined as pyroptosis. In non-canonical inflammasome activation, type I interferon is stimulated via the TLR-TRIF mediated pathway, which drives STAT1 activation and leads to the induction of caspase-11 expression. Gram-negative bacteria in the cytosol that escape vacuoles release their LPS inside the cell. This mechanism requires rupture of the vacuoles via interferon-inducible guanylate-binding proteins (GBPs). The binding of cytosolic LPS to caspase-11 induces its activation leading to pyroptosis and potentially feedback into the canonical inflammasome pathway. Gasdermin D functions as a substrate for caspase-11 and the cleavage of gasdermin D is part of the driving force for the non-canonical inflammasome mediated activation of pyroptosis, IL-1 β maturation, and also functions to regulate epithelial cell proliferation.

Figure 3: NLR Inflammasomes in Inflammatory Bowel Disease and Tumorigenesis

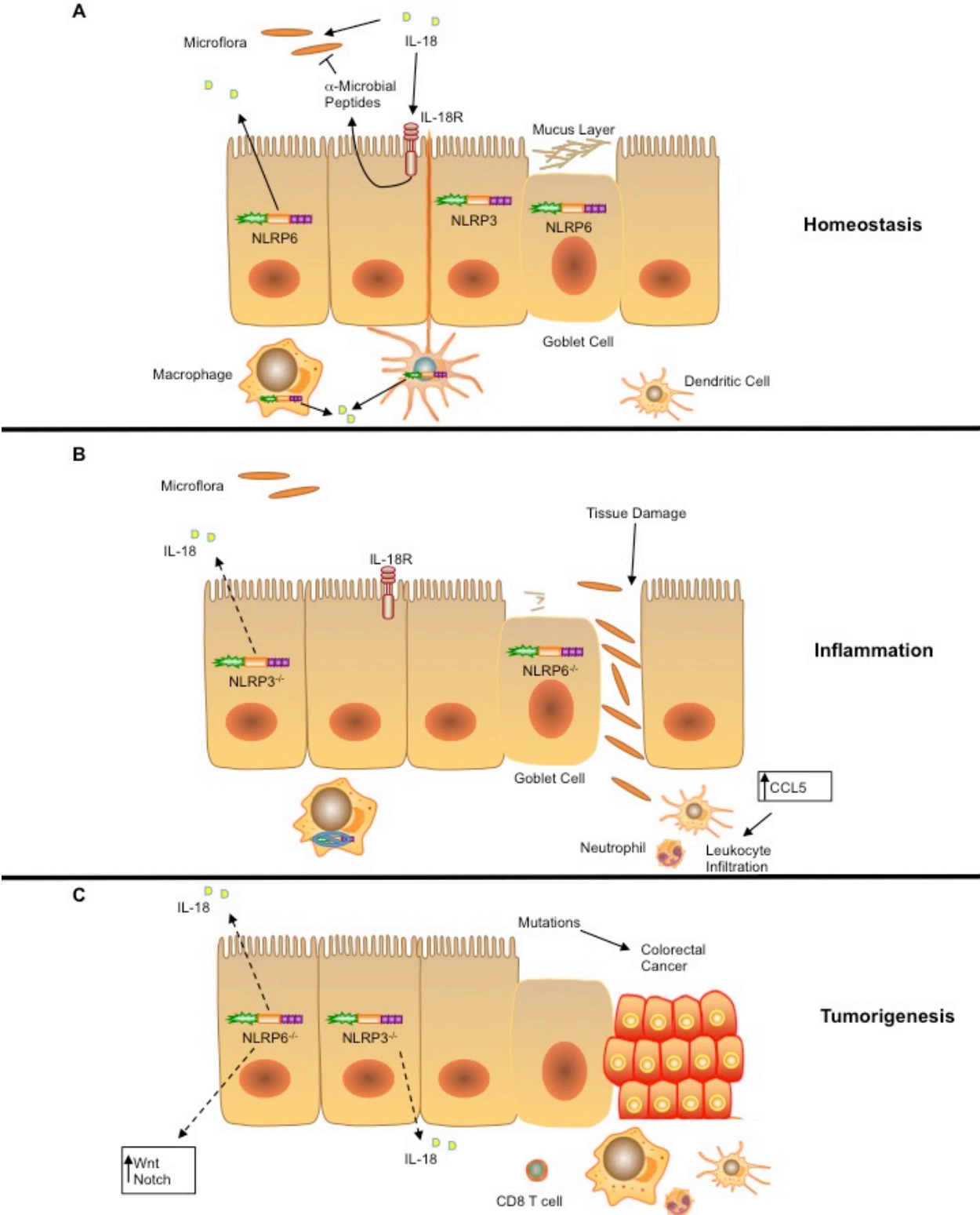


Figure 3: NLR Inflammasomes in Inflammatory Bowel Disease and Tumorigenesis. A)

NLRP3 and NLRP6 in epithelial cells maintain the secretion of IL-1 β and IL-18 to maintain immune system homeostasis in the gut. One major role of IL-18 is to maintain intestinal epithelial cell homeostasis through controlling proper proliferation and tissue repair. In addition, IL-18 is also responsible for the secretion of peptides for anti-microbial defense. Goblet cells also express NLRP6, which is responsible for the secretion of mucus into the lumen. This results in increased protection against harmful commensal microbes and pathogens. **B)** Damage to the epithelial cell barrier drives acute inflammation. When either NLRP3 or NLRP6 are absent, IL-18 generation is attenuated. This leads to dysbiosis and the expansion of bacteria into niches where they are typically excluded. In mice lacking NLRP6, CCL5 is upregulated, resulting in an increase in leukocyte recruitment and infiltration. Without IL-18, there is a lack of epithelial cell repair, crypt proliferation and secretion of anti-microbial peptides. In addition, the lack of NLRP6 leads to a decreased mucus production, which allows microbes from the lumen to gain better access to the epithelial cell barrier, increased bacterial translocation, and increased inflammation. **C)** Chronic inflammation of the colon is commonly associated with tumorigenesis and is often referred to colitis-associated cancer in human patients. It has been shown that mice lacking NLRP3 and NLRP6 have decreased production of IL-18 when put through a model for colitis associated cancer. Inflammasome formation has been shown to significantly impact Wnt, Notch, and AKT signaling, which are all highly associated with tumorigenesis and likely impact this aspect of IBD.

Figure 4: NLRP6 in Inflammatory Bowel Disease

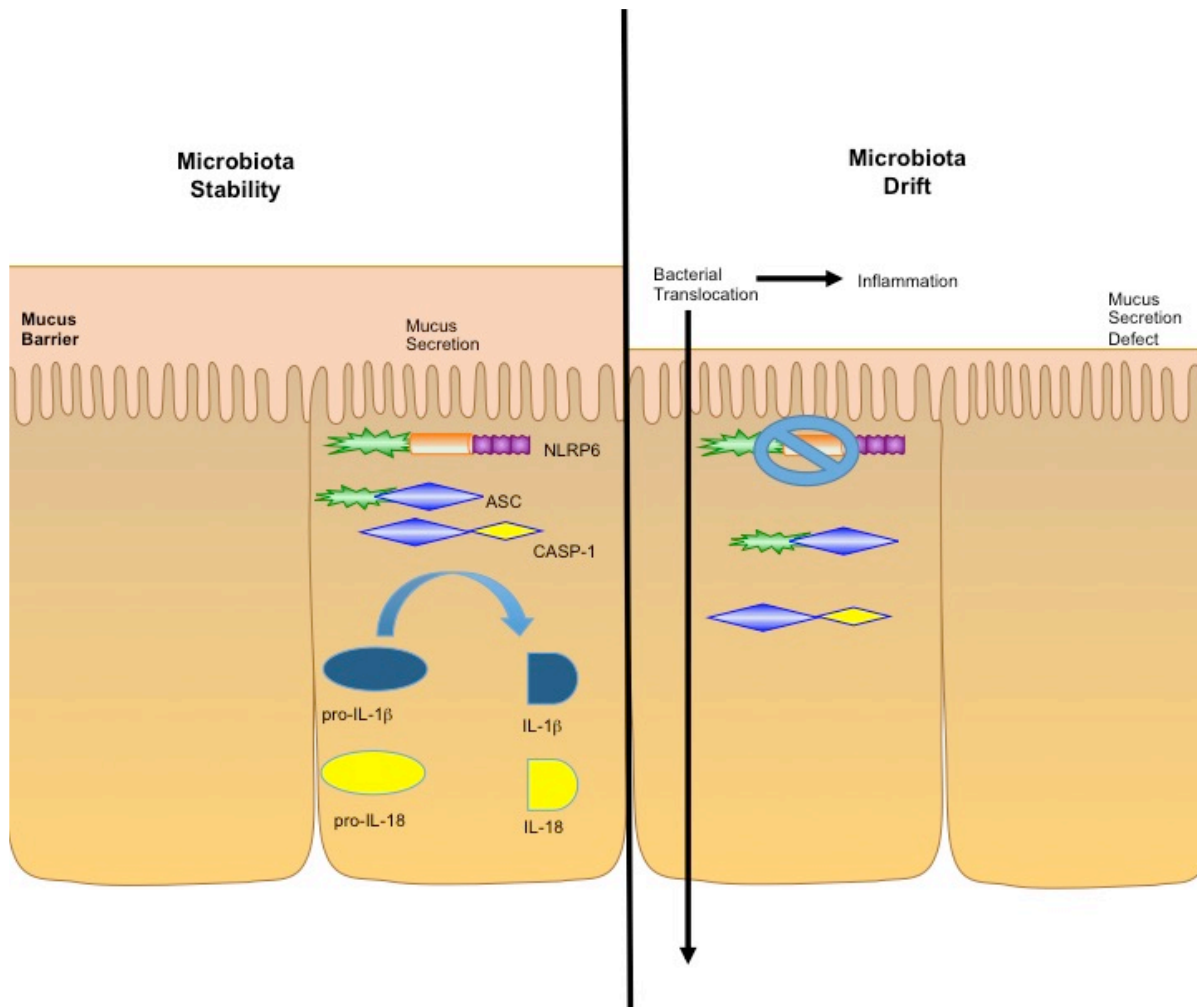


Figure 4: NLRP6 in Inflammatory Bowel Disease. When NLRP6 is present and active, it is heavily involved in the maintenance and regulation of the homeostasis of the gut via its production of mature IL-18. This includes the maintenance of intestinal epithelial cell proliferation, repair of injury, and secretion of the protective mucus layer. All of these functions play a role in maintaining the balance of pathogenic and commensal flora. However, in the absence of NLRP6, IL-1 β and IL-18 production is decreased, leading to dysfunctional mucus secretion and sub-optimal host responses to specific components of the microbiome. This

ultimately results in a disruption in the balance of pathogenic and commensal bacteria, leading to bacterial translocation and inflammation.

Figure 5: Domain Structure and Activation of NLRP1

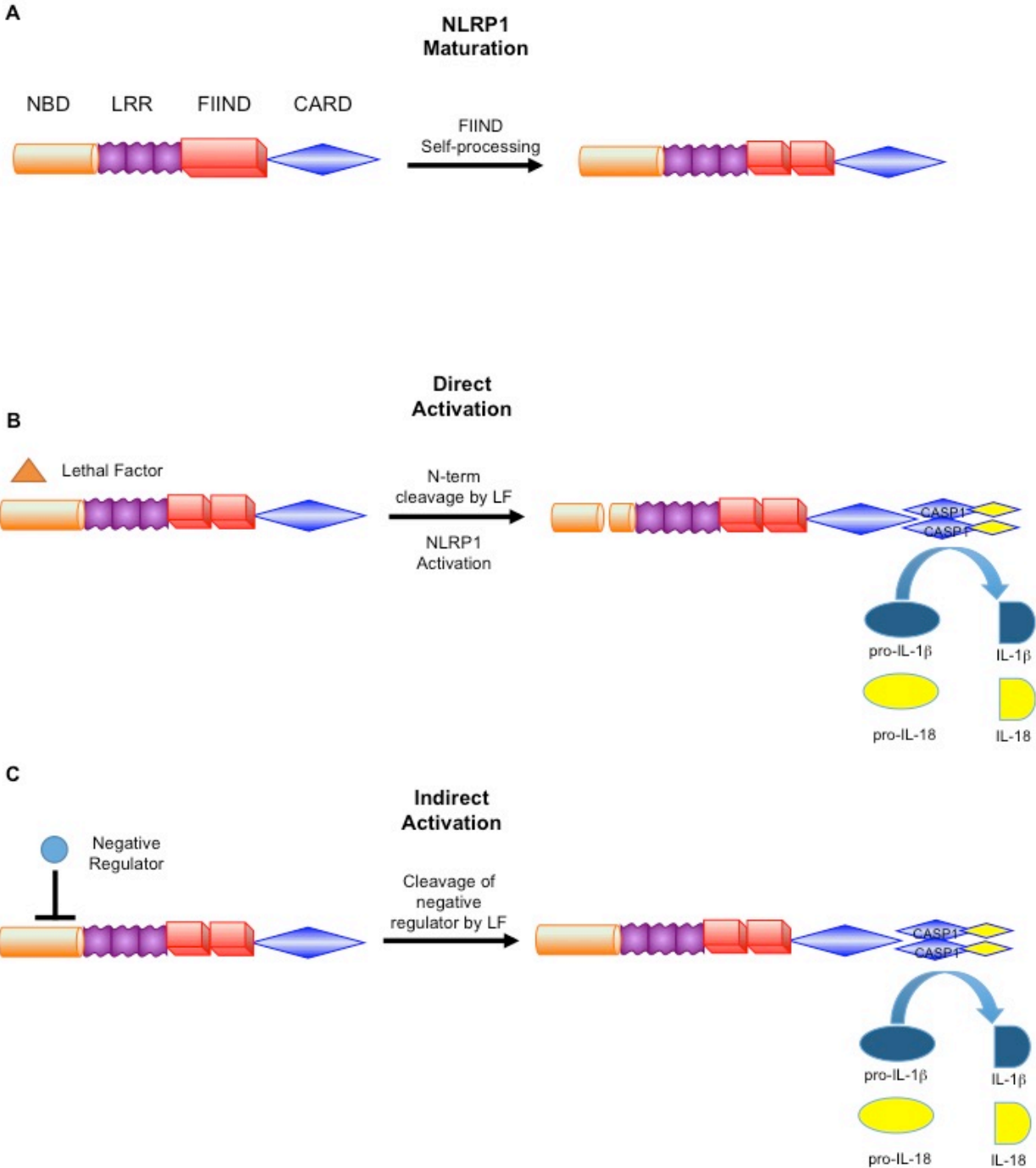


Figure 5: Domain Structure and Activation of NLRP1. Murine NLRP1 contains a nucleotide binding domain (NBD), leucine-rich repeat (LRR) domain, function to find domain (FIIND), and

caspase activating and recruitment domain (CARD). **A)** In mice, NLRP1 has been shown to sense Anthrax lethal toxin (LeTx). Initially NLRP1 is unprocessed and considered to be in its immature form. However, the FIIND domain is able to cleave itself to create the mature form of NLRP1, which is then considered to be responsive to LeTx. NLRP1 can then undergo one of two pathways associated with activation. **B)** The first is the Direct Activation Pathway. This pathway involves the cleavage of the N-terminal of NLRP1 via LeTx. This cleavage event activates NLRP1 and allows it to dimerize with caspase-1, leading to cleavage of pro-IL-1 β and pro-IL-18 into their mature forms. **C)** The second pathway for LeTx -mediated NLRP1 activation is the Indirect Activation Pathway. This pathway involves the cleavage of a negative regulator of NLRP1 by LeTx. Once the negative regulator has been removed, NLRP1 becomes activated leading to caspase-1 recruitment/activation and maturation of IL-1 β and IL-18. Because murine NLRP1 contains a CARD domain, it is possible the NLRP1 utilizes co-factors and other CARD containing proteins to augment signaling. However, additional mechanistic insight is necessary to better define NLRP1 activation and signaling triggers beyond LeTx.

Figure 6: Activation of NLRC4

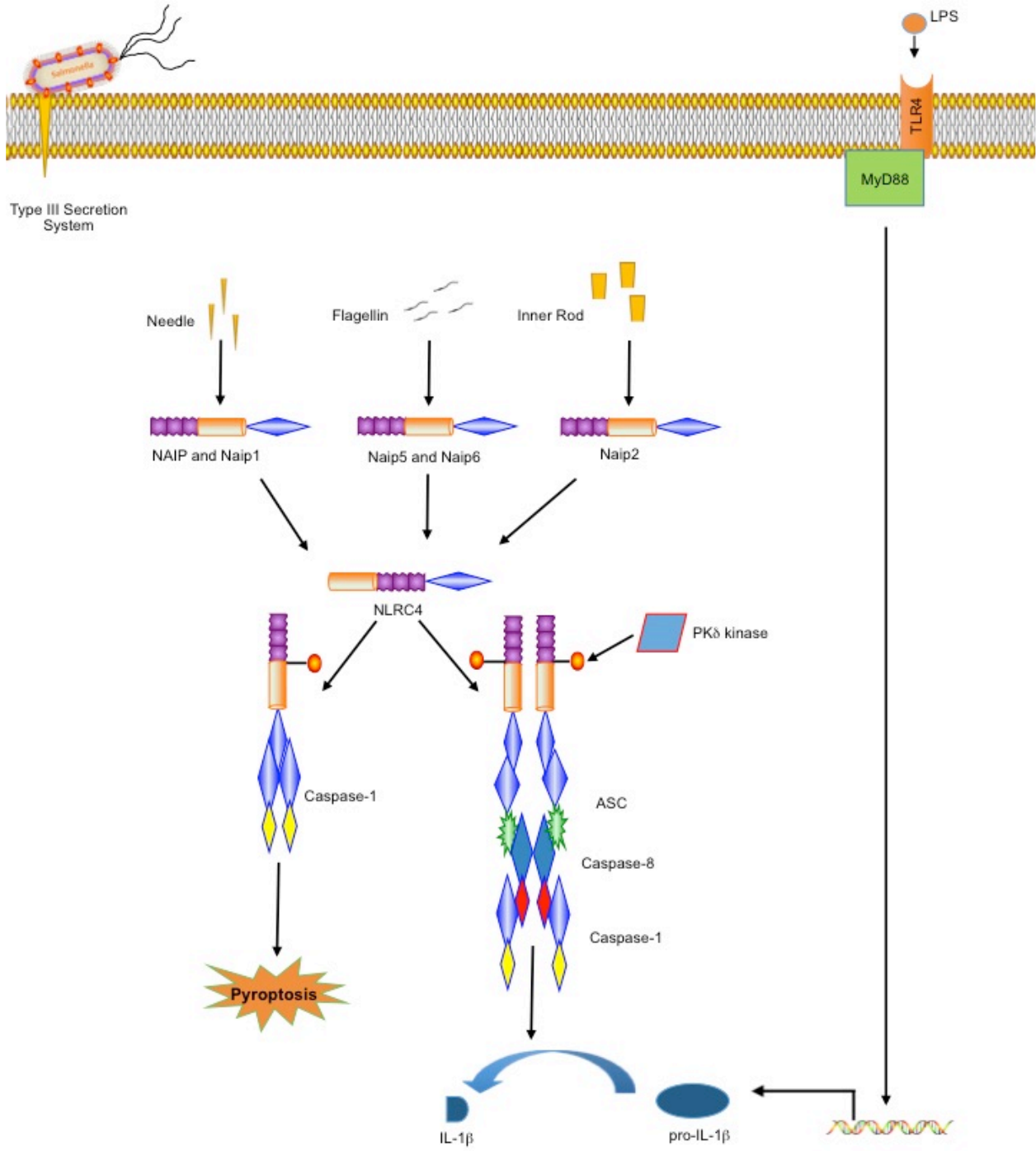


Figure 6: Activation of NLRC4. Some bacteria utilize the type III secretion system, such as *Salmonella typhimurium*, to insert its pathogenic components into the cell. Once inside the cell, these components are detected by NAIPs, which serve as co-factors and provide specificity for the activation of NLRC4. Once NLRC4 is activated, ASC is recruited along with caspase-8 and caspase-1, which together form the NLRC4 inflammasome. The formation of this inflammasome activates caspase-1, which then cleaves pro-IL-1 β and pro-IL-18 into their mature forms. The formation of the NLRC4 inflammasome is also responsible for pyroptosis via a caspase-1 dependent, but ASC independent mechanism. It has also been speculated that PK δ kinase is also involved in the activation of NLRC4, although it may not be a necessary component.

Figure 7: The AIM2 Inflammasome

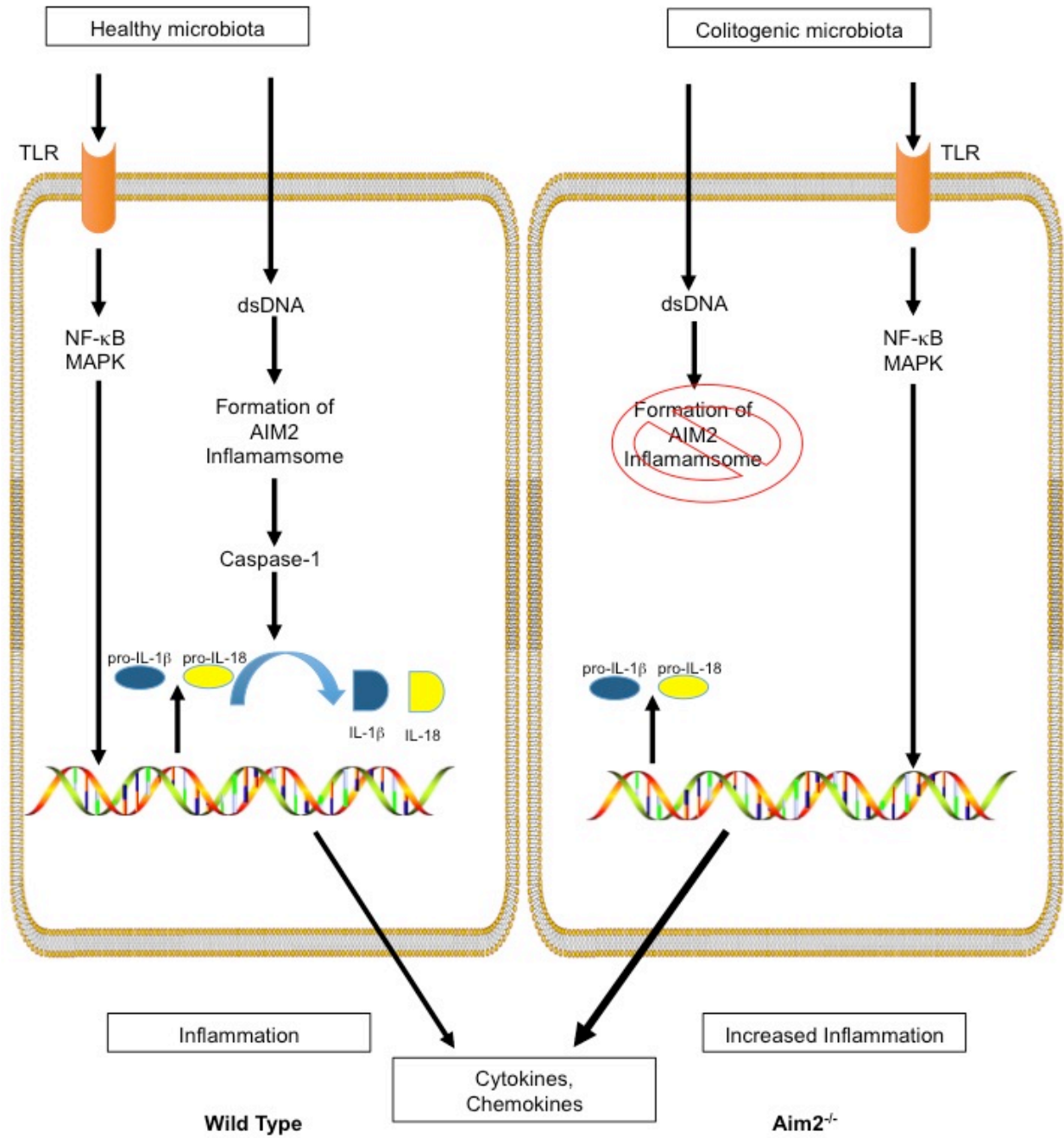


Figure 7: The AIM2 Inflammasome. Upon sensing of dsDNA, AIM2 forms an inflammasome resulting in caspase-1 activation and the subsequent cleavage of IL-1 β and IL-18. AIM2 has also

been shown to modulate signaling through the Wnt and AKT signaling cascades, which have significant implications associated with gastrointestinal inflammation and tumorigenesis. Dysbiosis is a significant contributing factor associated with AIM2 inflammasome function.

Figure 8: The Goldilocks Conundrum

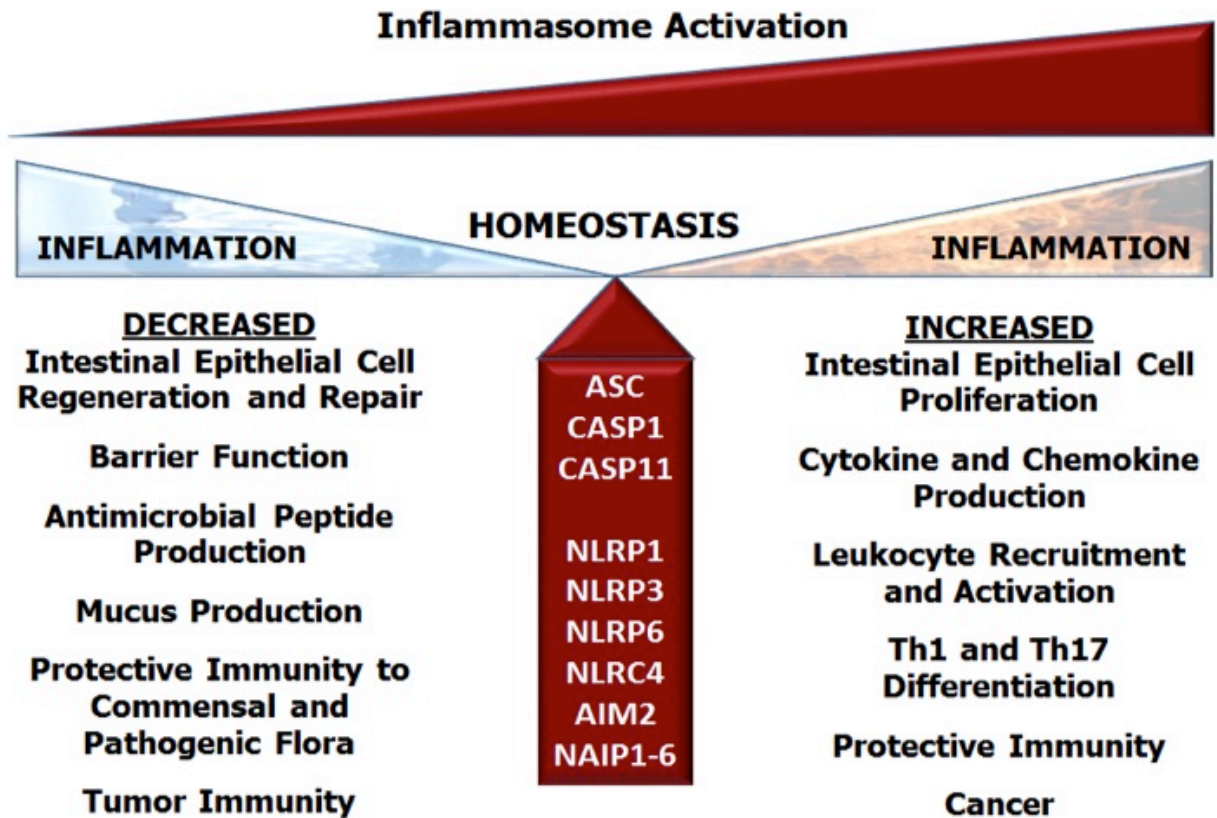


Figure 8: The Goldilocks Conundrum. In the gut, NLRs function to maintain immune system homeostasis by modulating inflammatory signaling pathways, either directly or indirectly. These pathways are balanced at a critical threshold throughout the gastrointestinal system. If NLR signaling is disrupted, then inflammation and disease pathogenesis can be increased due to reduced barrier function, the formation and expansion of permissive niches for pathogenic microbes, and reduced tumor surveillance. Conversely, if NLR signaling is increased and not properly resolved, then the overzealous inflammation can result in significant collateral damage to the epithelial cell barrier, promote epithelial cell proliferation, augment leukocyte activation, and drive IBD pathogenesis.

Table 1: Inflammasome Terminology

TERMINOLOGY	DEFINING FEATURE	SPECIES
Canonical Inflammasome	Caspase-1 Dependent	human/mouse
Non-Canonical Inflammasome	Caspase-4/-5/-11 Dependent	human(Casp-4/-5); mouse (Casp-11)
Classical Inflammasome	Signal 1; Signal 2; Requires ATP	mouse/human (cell type/stimuli specific?)
Alternative Inflammasome	Utilizes TRIF, RIPK1, FADD, and Casp8; ATP not required for IL- 1 β Release; only defined in macrophages	human (cell type/stimuli specific?)

Table 2. Microbiome Effects on NLR Modulation of IBD and CAC

NLR	Bacteria	References
NLRP3	<i>Helicobacter pylori</i>	133,134
	<i>Clostridium</i>	85,135
	<i>Mycobacterium</i>	136-138
	<i>Collinsella</i>	85
	<i>Subdoligranulum</i>	85
	<i>Enterobacteriaceae</i>	139
	<i>Ralstonia</i>	85
NLRP6	<i>Prevotellaceae</i>	90
	<i>Helicobacter hepaticus</i>	90
NLRP1	Unknown Microbiome Component	44
NLRC4	<i>Salmonella</i>	140,141
	<i>Citrobacter rodentium</i>	142
	<i>Shigella flexneri</i>	111-113

Chapter Three

Maternal Influence and Murine Housing Confound Impact of NLRP1

Inflammasome on Microbiome Composition

Veronica M. Ringel-Scaia, Yufeng Qin, Cassidy A. Thomas, Kathleen E. Huie, Dylan K. McDaniel, Kristin Eden, Paul A. Wade, and Irving C. Allen

Reprinted from Journal of Innate Immunity, VM Ringel-Scaia, Y Qin, CA Thomas, KE Huie, DK McDaniel, K Eden, PA Wade, IC Allen, “Maternal Influence and Murine Housing Confound Impact of NLRP1 Inflammasome on Microbiome,” pp. 1-16, (2019), with permission from S Karger AG, under license number 4534231396189. Full citation: VM Ringel-Scaia, Y Qin*, CA Thomas, KE Huie, DK McDaniel, K Eden, PA Wade, IC Allen. (2019). Maternal Influence and Murine Housing Confound Impact of NLRP1 Inflammasome on Microbiome. Journal of Innate Immunity. 2019 Feb 13:1-16. PMID: 30759441.*

KEYWORDS: Nod-like receptor; microbiome; inflammatory bowel disease; experimental colitis; colitis associated cancer; short chain fatty acid; ASC; dysbiosis

ABSTRACT:

The NLRP1 inflammasome attenuates inflammatory bowel disease (IBD) progression and colitis associated tumorigenesis. A possible mechanism postulates the lack of the NLRP1

inflammasome creates permissive niches in the gut for pathogenic bacteria to flourish, causing dysbiosis and increased IBD susceptibility. To evaluate this hypothesis, we characterized the gut microbiome of wild type, *Nlrp1b*^{-/-}, and *Asc*^{-/-} mice under naïve conditions by sequencing the V3 region of 16s rRNA gene. For both genetically modified mouse lines, the microbiome composition reflected overrepresentation of bacteria associated with dysbiosis relative to wild type animals. Measurement of short and medium chain fatty acids by mass spectrometry further revealed significant differences between genotypes. However, prior to concluding that the NLRP1 inflammasome plays a role in regulating the composition of the microbiome, we evaluated two additional strategies for cohousing wild type and *Nlrp1b*^{-/-} mice; breeding homozygous parents and cohousing at weaning, and breeding from heterozygous parents and cohousing littermates. We found that maternal influence was the greater predictor of microbiome composition rather than genotype. With the rise in microbiome research across disciplines, our study should be viewed as a cautionary example that illustrates the importance of careful breeding and housing strategies when evaluating host-microbiome interactions.

INTRODUCTION

Nearly 4 million people worldwide suffer from inflammatory bowel disease (IBD). IBD is characterized by chronic and relapsing inflammation in the gastrointestinal (GI) tract and has two primary clinical manifestations, either ulcerative colitis (UC) or Crohn's disease (CD). Beyond the direct role of dysregulated inflammation on IBD progression, the loss of immune system homeostasis in the GI tract during IBD is also associated with an increased risk of developing a unique form of colorectal cancer, termed colitis associated cancer, in patient populations [1]. Although the direct cause of IBD remains unclear, it has increasingly become evident that the microbiome plays a role in the development, progression, and/or risk of disease. Indeed, several studies have noted that patients with IBD possess dysbiotic microbiomes relative to healthy controls [2-7]. During CD and UC, the protective epithelium of the GI tract becomes damaged and uncontrolled host microbiome translocation from the lumen drives inflammation. Thus, the composition of the host microbiome can dramatically influence the resultant immune response and disease progression.

Nucleotide-binding domain and leucine-rich repeat-containing (NLR) proteins are a group of intracellular pattern recognition receptors (PRRs) responsible for sensing a variety of pathogen associated molecular patterns (PAMPs) and damage associated molecular patterns (DAMPs). In the GI tract, NLR family members are essential mediators of inflammation during IBD and maintain immune system homeostasis [8]. There are 22 distinct NLR and NLR-like proteins identified in humans and several murine paralogs, many of which have yet to be fully characterized. One sub-group of NLRs has been found to form multi-protein complexes, defined as inflammasomes, that function to activate IL-1 β and IL-18. Inflammasome formation is also associated with a unique form of inflammatory cell death, termed pyroptosis. Upon stimulation

with a specific PAMP or DAMP, a given NLR senses a specific pattern and oligomerizes, activating Apoptotic Speck protein containing a CARD (Pycard; ASC), which results in the cleavage and activation of pro-caspase-1 to its mature form. Activated caspase-1 cleaves pro-IL-1 β and pro-IL-18 into their respective active cytokines that are subsequently released from the cell.

Several NLR family members possess structural motifs that allow them to function as intracellular sensors and participate in inflammasome formation. In the context of IBD, NLRP1, NLRP3, NLRC4, and NLRP6 are well-characterized inflammasome forming NLRs that significantly modulate the progression of experimental colitis and/or colitis associated tumorigenesis in mouse models [9-14]. Likewise, the inflammasome adaptor protein ASC and the relevant caspases, caspase-1 and caspase-11, also modulate inflammation in the gut during IBD and cancer [9-11, 15, 16]. In general, the majority of studies evaluating NLR inflammasomes have found that loss of any specific NLR or inflammasome component results in increased GI inflammation, epithelial cell barrier disruption, and inflammation driven tumorigenesis. Inflammasome formation has been suggested to maintain immune system homeostasis in the gut and attenuate IBD progression through a variety of mechanisms including promoting epithelial cell regeneration and repair, facilitating T-cell differentiation, and controlling cell death [8, 17]. This evidence has strongly suggested that a function of NLR family members in the gut is likely associated with their recognition of pathogenic and commensal members of the host microbiome and their modulation of a balanced host immune response following loss of epithelial cell barrier integrity [18, 19].

Our research team previously demonstrated that NLRP1 attenuates IBD and colitis associated tumorigenesis progression [9]. Notably, we also saw evidence of increased expression

of *NLRP1* in human subjects with active ulcerative colitis relative to healthy controls [9]. Beyond IBD, polymorphisms in the *NLRP1* gene have been associated with several autoimmune disorders including vitiligo, celiac disease, rheumatoid arthritis, systemic lupus erythematosus, and type I diabetes [8]. It is clear that NLRP1 plays an important role in modulating inflammatory diseases, but the direct mechanism/s is not yet defined. Using *Nlrp1b*^{-/-} and *Asc*^{-/-} mice in the DSS model, we found that animals lacking components of the NLRP1 inflammasome demonstrated significantly increased morbidity, colon inflammation, and tumorigenesis compared to wild type littermate control animals. These observations were correlated with reduced levels of IL-1 β and IL-18 [9]. Of specific relevance to the current work, antibiotic administration and co-housing studies between *Nlrp1b*^{-/-}, *Asc*^{-/-}, and wild type animals suggested that sensitivity to DSS was strongly associated with each animal's microbiome [9]. However, beyond these broad antibiotic and co-housing observations, the compositions of the microbiome in these animals have not been characterized. It was our belief that NLRP1 might be responsible for sensing a specific bacteria or bacterial component that is associated with the microbiome, and that by identifying the baseline bacterial constituents, we might be able to conclude that the NLRP1 inflammasome attenuates IBD and colitis associated tumorigenesis by limiting the growth of this, as yet to be identified, bacteria or PAMP.

Our initial hypothesis predicted that the loss of any individual NLR inflammasome would establish permissive niches in the gut and lead to significant dysbiosis in the host microbiome that drives dysregulated inflammation in the GI tract. Here, we evaluate this hypothesis in animals lacking components of the NLRP1 inflammasome. Our data indicates that the microbiome profiles for singly housed *Nlrp1b*^{-/-}, *Asc*^{-/-}, and wild type mice are distinct prior to any exacerbation via chemically induced colitis and are highly dysbiotic. Microbiome dysbiosis

in the *Nlrp1b*^{-/-} and *Asc*^{-/-} mice are associated with significant changes in the metabolic profile, including short chain fatty acid (SCFA) and medium chain fatty acid (MCFA) metabolism measured via mass spectrometry (GC/MS). Thus, suggesting a functional link between the dysbiotic host microbiome and susceptibility to IBD in the context of NLRP1 inflammasome deficient mice.

However, before accepting this conclusion, we further evaluated the impact of different breeding and housing strategies on our findings. These additional studies were based on recent reports associated with NLRP6, which is an inflammasome forming NLR that is widely accepted as having a direct influence on inflammation in the gut by regulating the intestinal microbial content [12, 15, 18, 20]. Two individual teams concluded that NLRP6 does not influence the microbiome, but instead observed that maternal influence was the greater predictor of gut microbiome content [21, 22]. In both cases, cohousing littermates from heterozygous parents ameliorated any significant differences in microbiome bacteria composition. Armed with this information, we evaluated two different methods of cohousing *Nlrp1b*^{-/-} and wild type mice to determine if these findings held true for NLRP1. Similar to the previous findings with NLRP6, our data demonstrates that maternal influence and housing, rather than genetic factors are responsible for the differences observed in the microbiome composition.

MATERIALS AND METHODS

Experimental Animals

The characterization and generation of *Nlrp1b*^{-/-} and *Asc*^{-/-} mice has previously been described [23, 24]. All experiments were conducted in accordance with NIH Guide for the Care

and Use of Laboratory Animals and following the protocol approved by the Virginia Tech IACUC. Wild type, *Nlrp1b*^{-/-}, and *Asc*^{-/-} mice were housed under standard SPF conditions in vivarium space at the Virginia Maryland College of Veterinary Medicine. These facilities are American Association for Laboratory Animal Care (AALAC) accredited and the SPF status of our colony is routinely verified using standard best practices. The list of excluded and included agents in our vivarium is described in **Table S1**. The singly housed animals used in these studies were maintained as independent homozygous colonies, while the littermates were derived from heterozygous breeder pairs generated by crossing our independent homozygous mice within our vivarium and housed in the same physical location (room and rack). All experiments were conducted with 6-17 week old mice that were maintained on the C57Bl/6J background.

For cohousing studies, pups born from singly housed wild type and singly housed *Nlrp1b*^{-/-} breeder pairs (Matched-Co-Housed) and pups born from heterozygote *Nlrp1b*^{+/-} breeder pairs (Littermate-Co-Housed) were weaned and cohoused at 1:1 ratios for four weeks prior to assessments. Cohoused wild type and knockout mice were given autoclaved water with ampicillin (1mg/ml), streptomycin (5mg/ml) and vancomycin (0.25mg/ml) daily for two weeks to normalize their respective microbiomes. At 12 weeks of age (Matched-Co-Housed) or 7 weeks of age (Littermate-Co-Housed), the animals were sacrificed and colonic contents were collected. All studies were controlled with gender and age-matched WT animals that were maintained under SPF conditions and received 2018 chow (LabDiet) and water *ad libitum*.

Fecal Harvest

Tools were washed and autoclaved prior to harvest. Mice were euthanized, and separate sets of tools were designated and used for each genotype for necropsy in a biological safety

cabinet. Colonic contents were collected and samples were immediately placed on dry ice. Fecal bacterial DNA was isolated using the QIAamp DNA Stool Mini Kit following the manufacturer's instructions for isolation of DNA from stool for pathogen detection (Qiagen, Germany).

16S rRNA Gene Sequencing and Data Analysis

To amplify the V3 region of the bacterial 16S rRNA gene for sequencing, two rounds of PCR reactions were used. Primers used in the first round PCR have the overhang sequences with Illumina adapters. Forward Primer: TCGTCGGCAGCGTCAGATGTGTATAAGAGACAGCC AGACTCCTACGGGAGGCAG; Reverse Primer: GTCTCGTGGGCTCGGAGATGTGTATA AGAGACAGCGTATTACCGCGGCTGCTG. The PCR conditions were 98°C for 3 min; 15 cycles of 98°C for 30 s; and 62°C for 30 s, 72°C for 30 s. The second round of PCR was used to add the index to the amplicons for sequencing. PCR conditions were 95°C for 3 min; 8 cycles of 95°C for 30s; and 55°C for 30 s, 72°C for 30 s. Sequencing was performed on the MiSeq platform in multiplex. Although no single hypervariable region can distinguish every individual bacteria, the V3 region was chosen because previous literature has found that it contains maximum nucleotide heterogeneity and discriminatory power [25]. Analysis of sequencing data was conducted using mothur [26]. Briefly, mothur was used to group or assign 16S rRNA sequences into OTUs using 97% similarity. Classifications were determined by comparing sequences to the Greengene database (gg_13_8_99). Classified OTUs were used to determine the relative abundance of bacterial phyla and family in each sample. To adjust for differences in sequencing depth, all samples were normalized to the same number in the following analysis. Principal coordinates analysis was used to assess community similarity among all samples and

Bray Curtis distances between the communities were displayed in a two-dimensional space [27]. Lefse (<https://huttenhower.sph.harvard.edu/galaxy/>) was used to compare the differential bacterial abundance with default settings [28].

Short Chain Fatty Acid and Medium Chain Fatty Acid Detection

Fecal samples were harvested as described above. Samples were weighed, and sterile molecular grade water (Sigma-Aldrich) was added to each. Samples were placed on a tilt table for 4 hours at room temperature, vortexed once every hour to break up remaining stool pellets, and allowed to settle. For analysis, 900 μ l of liquid was removed and 10 μ l of 85% phosphoric acid was added to each vial. Volatile Fatty Acid (VFA) analysis was carried out using an Agilent 6890 Gas Chromatograph (Wilmington, DE) equipped with a split injector, a flame-ionization detector and Chemstation software for data analysis. VFA separation was performed using a Nukol™ fused silica 15 m x 0.53 mm capillary column with 0.5 μ m film thickness. Helium was used as the carrier gas at a flow rate of 15 ml/min with a split ratio of 2:1. The oven temperature was maintained at 80°C for 3 minutes and then increased to 140°C at a rate of 6°C per minute and held for 1 minute. Injector temperature was 200°C and the detector temperature was 250°C. VFAs are expressed as mg/L of individual species (C2-C7 fatty acids), and then divided by weight of total feces collected in grams to a final mg/L/g feces.

Statistical Analysis

Data were analyzed using GraphPad Prism, version 6 (San Diego, CA). We utilized a Student's two-tailed t test for comparisons between two experimental groups. Multiple comparisons were conducted using one-way and two-way ANOVA where appropriate followed

by Mann-Whitney or Tukey post-test for multiple pairwise examinations. Correlation was also computed using GraphPad Prism. Changes were identified as statistically significant if p was less than 0.05. Mean values were reported together with the standard error of the mean (SEM) or standard deviation (SD), as appropriate. Statistical analyses for α -diversity and β -diversity were compared by non-parametric Mann-Whitney U tests and non-parametric multidimensional ANOVA. Distance-based redundancy analysis determined the contribution of different variables to microbiota profile variations.

Data Availability

The datasets used and/or analyzed during the current study have been made public on NCBI's GenBank comprehensive database.

RESULTS

Singly housed mice lacking the pan-inflammasome adaptor ASC have a distinct gut microbiome population

Mice lacking the pan-inflammasome adaptor protein ASC are highly sensitive to experimental colitis and demonstrate significantly increased inflammation driven colon tumorigenesis [9-11, 15, 29]. Surprisingly, there are few comprehensive studies evaluating the microbiome composition in the *Asc*^{-/-} mice under naïve conditions and of those that have been conducted, there is currently conflicting data regarding the role of ASC in shaping the commensal gut microbiota composition [18, 21]. Here, we sought to evaluate the contribution of ASC and NLR inflammasome signaling on the composition of the gut microbiome in our

vivarium, under non-pathologic and specific pathogen free (SPF) housing conditions. Mice were necropsied and stool was collected directly from the colons of 9 *Asc*^{-/-} and 10 wild type animals, without scraping but by removing each pellet with sterile forceps. Thus, it is likely that mucosal-adherent bacteria were under-represented in the samples. Through 16S sequencing, we observed significant, genotype-associated changes in microbial ecology between these separately housed knockout animals and wild type (**Figure 1A-E**). Although we did not investigate the difference in observed species between the genotypes, the Shannon's diversity index of the gut microbiome was significantly decreased in *Asc*^{-/-} mice relative to wild type (**Figure 1A-B**). We next determined the β -diversity to assess the differences in diversity among fecal specimens from the *Asc*^{-/-} and wild type mice (**Figure 1B**). Principal coordinate analysis (PCoA) of Bray-Curtis distances illustrated that although cage and housing was a relevant factor, the main separation of the fecal communities was determined by mouse genotype (**Figure 1C**). Phylum level analysis indicated that the fecal microbial community composition is dominated by Bacteroidetes, Firmicutes, Proteobacteria, and Unclassified Bacteria (**Figure 1D, Table S2**). Despite inter-individual differences, relative abundance was significantly higher for Proteobacteria and lower for Unclassified Bacteria in *Asc*^{-/-} mice (**Figure 1E**). Together, these findings suggest that *Asc*^{-/-} mice have a unique gut microbiome composition that is different compared to the wild type animals in the absence of an applied stressor.

We next sought to evaluate the specific taxonomic variations in the gut microbiomes from *Asc*^{-/-} and wild type mice. We used Linear Discriminant Analysis effect size (LEfSe) to classify specific bacteria that were differentially represented in the *Asc*^{-/-} and wild type microbiomes [28] (**Figure 2A**). The wild type mice had a higher abundance of bacteria from *Odoribacter*, *Turicibacter*, *Bifidobacterium*, *Pseudomonas*, and *Anaeroplasma* genera, with

respective LDA scores (log10) greater than 2 under all-against-all strategy (**Figure 2A and B**). Conversely, *Asc*^{-/-} mice had a higher abundance of *Bacteroides*, *Parabacteroides*, *Rikenella*, AF12, *Helicobacter*, *Prevotella*, *Mucispirillum*, and *Flexispira* genera with respective LDA scores greater than 2 (**Figure 2A and B**). These findings are relatively consistent with those originally reported by Elinav *et al.*, including the findings of increased *Prevotella* [18]. This is not surprising, as the experimental conditions for this assessment most closely match those of Elinav *et al.*, rather than assessments of ex-germfree animals evaluated by Mamantopoulos *et al.* [21]. Combined, these data suggest that in mice lacking the pan-inflammasome adaptor protein ASC, there is an outgrowth of bacteria that could be implicated in a dysbiotic microbiome. This interpretation would be consistent with the previously reported increased sensitivity of these mice to models of experimental colitis and colitis associated cancer [18, 29].

The NLRP1 inflammasome appears to be critical for maintaining a healthy colonic microbial ecosystem

As with other PRRs, the inflammasome forming NLRs are highly conserved and evolutionarily designed to sense specific PAMPs associated with bacteria from the same order, family, and/or genus. Thus, we postulated that loss of inflammasome signaling would result in the expansion of very specific bacteria populations in the gut microbiome. In essence, bacteria typically sensed by a specific NLR would be able to more readily expand into permissive niches in the absence of inflammasome signaling that would normally drive the host innate immune system to limit the expansion of commensal or pathogenic elements of the gut microbiota. Our data associated with microbiome changes in the *Asc*^{-/-} mice support this hypothesis and suggest

that NLR inflammasomes may be important in maintaining GI homeostasis via modulation of the composition of the microbiome.

It has been postulated that the NLRP3 and NLRP6 inflammasomes regulate immune system homeostasis in the gut, in part through modulating specific bacteria populations in the host microbiome. While the mechanisms associated with the function of these NLRs in modulating the host microbiome is currently an area of intense research, it is reasonable to conclude that these microbiome differences are associated, either directly or indirectly, with the increased pathogenesis of experimental colitis in the *Nlrp3*^{-/-} and *Nlrp6*^{-/-} mice [11, 15, 18-20]. As previously stated, similar to NLRP3 and NLRP6, mice lacking NLRP1 also demonstrate significantly increased progression of experimental colitis and colitis associated cancer [9]. However, virtually nothing is known about the microbiome composition of *Nlrp1b*^{-/-} animals. Thus, based on the similarity of the phenotypes observed in animals lacking a functional NLRP1 inflammasome with *Nlrp3*^{-/-} and *Nlrp6*^{-/-} animals, we next sought to evaluate the microbiome composition in the *Nlrp1b*^{-/-} mice. As described above for the *Asc*^{-/-} studies, stool was collected directly from the colons of 10 *Nlrp1b*^{-/-} and 10 wild type mice, and the V3 region of 16s rRNA was sequenced. Due to the fact that two different cohorts of wild type mice were used for the *Asc*^{-/-} and *Nlrp1b*^{-/-} versus wild type comparisons, we compared the two groups (**Figure S1, Table S4**). Despite variations in PCoA between the four groups, the wild type group compared with *Asc*^{-/-} (WT1) and the wild type group compared with *Nlrp1b*^{-/-} (WT2) clustered together, indicating that genotype contributed to the composition of the microbiome for the two wild type groups (**Figure S1B**). We did not observe a significant difference in alpha diversity between wild type and *Nlrp1b*^{-/-} mice (**Figure 3A-B**). However, PCoA of Bray-Curtis distances revealed significant separation of microbial communities based on genotype (**Figure 3C**). Likewise,

phylum level analysis indicated that relative abundance of Proteobacteria was significantly higher in *Nlrp1b*^{-/-} mice (**Figure 3D-E, Table S3**). Together, these data suggest that *Nlrp1b*^{-/-} mice have a gut microbiome composition that is unique compared to the wild type animals.

While NLRP1 was one of the first NLRs identified, it is one of the least characterized. For example, it is still unclear what microbial associated molecular patterns or signals are recognized by NLRP1, especially in the context of GI health and disease. To date, NLRP1 has only been shown to recognize anthrax lethal toxin (LeTx) and *Toxoplasma gondii* [30, 31]. Neither of which are likely associated with either experimental colitis or cancer pathogenesis in the *Nlrp1b*^{-/-} mice. Thus, it is unclear what specific microbial families and genera may flourish in the gut microbiome in the absence of NLRP1. To evaluate the microbial ecosystem in greater detail, we utilized LEfSe to identify and classify specific bacteria in the microbiomes from singly housed and separated *Nlrp1b*^{-/-} and wild type mice (**Figure 4A and B**). In wild type mice, a higher abundance of bacteria from the *Bacteroides*, *Oribacterium*, *Allobaculum*, and *Barnesiella* genera were observed, while in the *Nlrp1b*^{-/-} mice, we observed increased representation from bacteria associated with *Helicobacter*, *Parabacteroides*, *Clostridium*, *Odoribacter*, *Turicibacter*, and *Mucispirillum* genera with respective LDA scores greater than 2 (**Figure 4A and B**). Indeed, many of these bacteria genera were also consistently increased in the *Asc*^{-/-} mice (**Figure 2**). Interestingly, the abundance of several of the genera in the microbiomes in the *Nlrp1b*^{-/-} mice are associated with more commensal and pathogenic species known to be associated with inflammation and cancer in the GI tract, including *H. pylori* [32], *H. hepaticus* [33], *M. schaedleri* [34], and *C. difficile* [35]. It is tempting to speculate that the previously reported increased sensitivity of these knockout animals in models of experimental colitis and colitis associated tumorigenesis could be due to changes in their microbiome composition [9].

Alterations in the gastrointestinal microbiome in NLRP1 inflammasome deficient mice results in significant shifts in the metabolic profile

Changes in the composition of the gut microbiome can have dramatic effects on biochemistry and metabolism in the GI tract. Thus, we next sought to evaluate the functional consequences of the changes in the microbial ecosystems in the *Asc^{-/-}* and *Nlrp1b^{-/-}* mice. To assess metabolic changes associated with bacteria metabolism in the gut, we quantified fecal levels of SCFA and MCFA using mass spectrometry (GC/MS) (**Figure 5**). SCFAs are a necessary waste product, required to balance redox equivalent production in the anaerobic environment of the gut [36]. SCFAs are saturated aliphatic organic acids that consist of one to five carbons, of which acetate (C2), propionate (C3), and butyrate (C4) are the most abundant ($\geq 90 - 95\%$) in the gut and are associated with carbohydrate fermentation [37]. We found significant differences in SCFA levels in the feces from *Nlrp1b^{-/-}* and *Asc^{-/-}* mice compared to the wild type animals (**Figure 5A-B, 5G**). Specifically, *Nlrp1b^{-/-}* mice had significantly increased levels of acetate (5978.6 mg/L/g feces) compared to the wild type animals (2642.9 mg/L/g feces) (**Figure 5A**). Similarly, *Asc^{-/-}* mice had significantly increased levels of propionate (837.4 mg/L/g feces) compared to the wild type animals (292.4 mg/L/g feces) (**Figure 5B**). While not attaining statistical significance, we also observed trending increases in propionate in the *Nlrp1b^{-/-}* mice and acetate and butyrate in the *Asc^{-/-}* animals compared to the wild type mice (**Figures 5A-C**). In addition to these common SCFA, we also evaluated isobutyrate (iC4), valerate (C5), isovalerate (iC5), which are typically much less abundant (~5-10%) and are associated with protein fermentation. Unlike the SCFAs associated with carbohydrate metabolism, we did not observe any significant differences in levels of isobutyrate, valerate, or isovalerate (**Figures 5D-**

F). Finally, we also evaluated the MCFA heptanoate (C7) (**Figure 5G**). MCFAs have been identified as the most discriminatory metabolites between healthy controls and patients with IBD [38]. Interestingly, we observed a significant increase in heptanoate in the *Asc*^{-/-} mice (997.3 mg/L/g feces) compared to the wild type (387.8 mg/L/g feces) (**Figure 5G**). While not reaching statistical significance, we also observed a trend towards increased heptanoate in the *Nlrp1b*^{-/-} mice (826.5 mg/L/g feces) compared to wild type animals.

To better determine the influence of any specific bacteria within the microbiomes on the SCFA and MCFA abundance, we conducted Canonical correspondence analysis (CCA) between the fatty acids and the top ten most abundant genera from the microbiota profiles of each genotype (**Figure 6**). In *Asc*^{-/-} mice, *Anaerostripes* was ordered in relation to isobutyrate (**Figure 6A**). *Bifidobacterium* was ordered in relation to propionate in the *Nlrp1b*^{-/-} group (**Figure 6B**). In the wild type case, *Oscillospira* and *Anaerotruncus* were ordered in relation to butyrate (**Figure 6C**). Together, these data suggest that the changes in the composition of the microbiome in the *Nlrp1b*^{-/-} and *Asc*^{-/-} mice are sufficient to alter levels of metabolites that reflect an imbalance in GI homeostasis.

Maternal influence not genotype is the biggest factor on microbiome composition between co-housed wild type and *Nlrp1b*^{-/-} mice

Some of the earliest data suggesting a role for the microbiome in the sensitivity of *Nlrp3*^{-/-} and *Nlrp6*^{-/-} mice utilized co-housing studies with wild type animals [11, 14]. These co-housing studies demonstrated that experimental colitis progression could be significantly attenuated in mice lacking NLRP3 or NLRP6 inflammasomes by co-housing with wild type animals [11, 14]. Conversely, the wild type mice demonstrated increased disease progression during co-housing

with either *Nlrp3*^{-/-} or *Nlrp6*^{-/-} mice. Similar to these prior studies, we have also shown that the NLRP1 inflammasome deficient phenotype is partially transmissible between *Nlrp1b*^{-/-} mice to wild type animals, when weaned and co-housed together and evaluated in models of experimental colitis [9]. Wild type mice co-housed with *Nlrp1b*^{-/-} animals displayed increased weight loss patterns compared to non-co-housed wild type mice. However, this increased weight loss did not reach the same level as singly housed *Nlrp1b*^{-/-} animals [9]. Notably, *Nlrp1b*^{-/-} mice housed with wild type animals were not protected from the phenotype during the experimental colitis model; which illustrates that pathogenicity can be transferred, but not protection [9]. To better define this previous observation, we sought to characterize the microbiome in both *Nlrp1b*^{-/-} and wild type mice following co-housing (**Figure 7**). We were interested in two different strategies for co-housing knockout mice with wild type, as both have been used to support previous claims in the field. We postulated that the co-housed wild type mice would develop a microbiome population more consistent with the mice lacking the NLRP1 inflammasome, whereas the microbiome in the co-housed *Nlrp1b*^{-/-} mice would remain relatively unchanged, and that this would remain consistent regardless of co-housing strategy.

We employed two distinct co-housing strategies. In the first, age and gender matched *Nlrp1b*^{-/-} and wild type mice were weaned together (1:1) (Matched Co-Housed) while in the second, *Nlrp1b*^{-/-} and wild type littermates from the offspring of *Nlrp1b*^{+/-} mice were weaned together (Littermate Co-Housed). In both cases, the animals were treated with a standard antibiotic cocktail in their drinking water to ablate the existing bacterial components of their respective microbiomes. After a two-week course of antibiotic treatment, the animals were transitioned back to normal drinking water. At 12 weeks of age (Matched-Co-Housed) and 7 weeks of age (Littermate-Co-Housed), fecal samples were collected following necropsy.

Through 16s sequencing, we found that both Matched-Co-Housed (**Figure 7A**) and Littermate-Co-Housed (**Figure 7B**) animals clustered together mainly based on cage. When comparing the relative abundance at the genus level, we picked the most abundant genera (more than average 0.5% in all samples) and observed significant increases in bacteria from the *Bacteroides* and *Clostridium* genera in Matched-Co-Housed mice (**Table S5**), and no reliable significant differences in Littermate-Co-Housed mice (**Table S6**).

We originally predicted that genotype would be the main contributor of microbiome composition and therefore anticipated the *Nlrp1b*^{-/-} mice and wild type animals would have significantly different microbiome populations following either co-housing strategy, where the *Nlrp1b*^{-/-} microbiome would remain stable and the wild type microbiome would migrate towards the *Nlrp1b*^{-/-} animal's composition. These observations would be consistent with our prior observations following co-housing in the experimental colitis models, which revealed that the *Nlrp1b*^{-/-} phenotype was unchanged whereas the wild type mice became more sensitive to models of experimental colitis [9]. We grouped the microbiomes of Matched-Co-Housed *Nlrp1b*^{-/-} and wild type mice and compared against singly housed *Nlrp1b*^{-/-} and singly housed wild type mice (**Figure 7C**) and saw what appeared to be separation between the three groups. PCoA analysis between the three groups indicated that the microbiome of Matched-Co-Housed *Nlrp1b*^{-/-} and wild type mice are different and unique following co-housing suggesting that even partial transfer of the *Nlrp1b*^{-/-} microbiome is sufficient to skew the GI ecosystem of wild type mice and potentially enhance susceptibility to experimental colitis (**Figure 7E**). However, clustering analysis based on Bray-Curtis distance showed that this separation was dependent on cage rather than genotype (**Figure S2**). Interestingly, the Littermate-Co-Housed cohort separated predominantly based on cage (**Figure 7D**) and not on genotype. This suggests that a matched

knockout and wild type co-housing strategy is not sufficient to determine genetic influences on the microbiome. Taken together, it is evident that the maternal influence in the *Nlrp1b*^{-/-} mice, and not genetic makeup, is the biggest indicator of microbiome composition.

DISCUSSION

Within the NLR field, we are not alone in drawing the conclusion that the microbiome likely plays a role in the phenotype observed in NLR knockout animals. Beyond NLRP1, NLRP3, NLRC4, and NLRP6 have been consistently shown to significantly modulate the progression of experimental colitis and/or colitis associated tumorigenesis in mouse models [9-14]. Likewise, the inflammasome adaptor protein ASC and the relevant caspases, caspase-1 and caspase-11, have also been shown to dramatically modulate inflammation in the gut during IBD and cancer [9-11, 15, 16]. In general, the majority of studies evaluating NLR inflammasomes have found that loss of any specific NLR or inflammasome component results in increased GI inflammation, epithelial cell barrier disruption, and inflammation driven tumorigenesis. It makes logical sense that the next direction in the field is to investigate the microbiome of these animals, especially because cohousing NLR knockout animals with wild type is sufficient to, at least partially, transfer susceptibility to DSS [9-14]. Notably, there has been significant controversy in the PRR field, including both TLRs and NLRs, associated with conflicting results in models of experimental colitis and/or cancer. Despite the consensus data that demonstrates the loss of any specific inflammasome forming NLR results in significantly increased susceptibility in DSS induced experimental colitis models [9-12, 16, 18], there are also counter observations reported that reveal either no differences in phenotype between the NLR deficient animals and wild type

mice, or even opposite results that suggest attenuating NLR inflammasomes actually protect against disease pathogenesis [29]. Unlike the other NLRs, NLRP6 seemed to be exempt from conflicting results in colitis studies and until recently, it has been widely accepted that the main role this NLR was in regulating the intestinal microbiome composition [21]. However, recently this paradigm has also been questioned with results that conclude that NLRP6 and ASC do not actually play a role in influencing the gut microbiome composition [21, 22]. These studies demonstrated that maternal effects and caging have a stronger influence than genotype when different forms of cohousing were employed [21, 22]. These data led us to further investigate our initial conclusions that the NLRP1 inflammasome functions to regulate the intestinal microbiome, and provided the rationale for our cohousing comparisons. In the present study, we report our initial findings that the microbiome composition of singly housed and homozygous bred *Nlrp1b*^{-/-} and *Asc*^{-/-} mice were populated with bacteria that appeared to suggest that the NLRP1 inflammasome regulates microbial ecology, consistent with data on the role of NLRP6 [15, 18, 20]. We investigated and found differences not only in genera of bacteria of our individually bred and housed knockout animals, but also in the abundance of short and medium chain fatty acids.

The preliminary motivation for the data generated in the present manuscript was to identify families and genera of bacteria that flourish in the absence of a functional NLRP1 inflammasome in an attempt to define the driving factor of the increased sensitivity to colitis in knockout animals. The NLRP1 inflammasome senses anthrax LeTx and *Toxoplasma gondii* in mice and muramyl dipeptide in humans [30, 31]. Consistent with the previous *in vitro* data, both *Nlrp1*^{-/-} mouse strains fail to properly process pro-IL-1 β and pro-IL-18 following *in vivo* exposure with these agents [23]. While these data provide significant mechanistic insight into

NLRP1 inflammasome function, recognition of anthrax LeTx and *T. gondii* do not explain its protective effects during experimental colitis and colitis associated cancer. The results from our initial microbiome analysis of our separately and individually bred and housed knockout mice identified several bacteria genera that contain species associated with inflammation and cancer in the GI tract, including *H. pylori*, *H. hepaticus*, *M. schaedleri*, and *C. difficile*, all of which drive colitis and/or tumorigenesis through diverse mechanisms including: degrading the protective mucus layer in the gut, producing barrier degrading toxins and metabolites, restricting the growth of probiotic bacteria, and directly inducing acute inflammation [32-35]. This point is particularly compelling in the initial hypothesis that the composition of the microbiome of these animals is the culprit for the sensitivity to colitis in the absence of NLRP1. For example, we found strong relationships between loss of NLRP1 signaling and the increased abundance of Bacilli, Deferribacteres, and Epsilonproteobacteria classes (**Figure 4**). Thus, these data would support future studies evaluating species that are representative of these classes in an effort to identify specific bacteria species associated with NLRP1 inflammasome formation and function in the gut. Moreover, this concept is reinforced by the finding that *Bacilli* species are overabundant in the absence of NLRP1 inflammasome signaling, which is consistent with the already defined role of NLRP1 sensing *B. anthracis* (a member of the Bacilli class). Thus, it is tempting to speculate that changes in the host microbiome that are directly associated with loss of NLRP1 inflammasome function may underlie many of these disorders.

However, prior to concluding that the NLRP1 inflammasome regulates colonic homeostasis, we compared our work to that of the evolving story and debate surrounding the role of the NLRP6 inflammasome in the regulation of the gut microbiome. Similar to NLRP1, NLRP6 inflammasome deficient mice were also found to be more sensitive to intestinal

inflammation and tumorigenesis in the chemically induced colitis and colitis associated tumorigenesis models [12, 18]. While it is clear that altered processing of pro-IL-18 in the colonic epithelial cells contributes to disease pathogenesis in these animals, these studies and subsequent confirmatory data concluded that altered fecal microbiota during colitis also contributed to intestinal hyperplasia, inflammatory cell recruitment, and exacerbation [18]. Pertinently, antibiotic treatment attenuated colitis progression in the *Nlrp6*^{-/-} mice and co-housing studies demonstrated that the colitogenic activity of the microbiota is transferable to wild type animals [18]. The loss of NLRP6 inflammasome signaling was found to lead to significant expansion of the bacterial phyla Bacteroidetes (*Prevotellaceae*) and reductions in members of the *Lactobacillus* genus and in the Firmicutes phylum [18]. More detailed mechanistic studies reported that the expansion of *Prevotellaceae* was facilitated by attenuated goblet cell mucin production in the *Nlrp6*^{-/-} animals, which established a permissive niche in the GI tract [15]. Our initial data most closely resembles that of Elinav et al. in terms of the homozygous bred and singly housed *Asc*^{-/-} and even some of the changes observed in the *Nlrp1b*^{-/-} mice [18]. This is expected as our matched co-housed experimental design most closely reflected those utilized by these studies and the data shows that separately bred and housed mice lacking NLR inflammasome components have significantly different microbiome compositions under naïve conditions. ASC is a critical adaptor protein for inflammasome formation by functioning as a bridge between NLRs containing PYD domains and caspase-1, as well as enhancing the activity of NLRs containing CARD domains. Due to its role as a pan-inflammasome adaptor protein, the role of ASC in IBD and colitis associated cancer has been well studied. In models based on chemically induced colitis, loss of ASC results in a highly severe phenotype compared to other individual NLR deficient genotypes (reviewed in [8]). The consensus data agrees that mice

lacking functional ASC fail to generate mature IL-1 β and IL-18 in the colon during models of experimental colitis, which results in immune system and epithelial barrier defects [11]. The combination of these defects was suggested to result in enhanced permeability and bacteria translocation in the *Asc*^{-/-} mice [9].

However, subsequent studies utilizing littermate-controlled *Nlrp6*^{-/-} mice and ex-germ-free littermate controlled *Asc*^{-/-} mice revealed that regulation of the gut microbiota was independent of genotype [21]. Here, the authors clearly show that housing and maternal effects contribute to the commensal gut microbiota composition, rather than components of the NLRP6 inflammasome [21]. Indeed, these findings are consistent with our results associated with *Nlrp1b*^{-/-} mice, using a similar experimental design. Thus, similar to NLRP6, the absence of the NLRP1 inflammasome does not appear to significantly influence the microbiome of cohoused homozygous littermates bred from heterozygous parents. The most deterministic factor on the microbial composition in our animals are maternal and housing factors, and not genetic. Because our previous studies evaluating NLRP1 in experimental colitis and colitis associated cancer utilized littermate control animals, we can thus conclude that microbiome differences are likely not a significant component of the phenotypes observed in the *Nlrp1b*^{-/-} mice in these models [9].

The microbiome is consistently cited as a potential factor influencing disease progression in not only IBD and colitis associated cancer, but the gamut of seemingly non-GI related diseases from Alzheimer's disease to cardiovascular and metabolic disorders [39, 40]. Indeed, in the vast majority of studies that produces data that differs from the consensus in any given field, changes in the host microbiome is routinely cited as a possible explanation, but is rarely evaluated. Based on the data presented here, it is certainly possible that differences in the microbiome underlie many of the conflicting results in the NLR field, albeit not in the way typically portrayed. Taken

together with other reports on NLRP6, our data suggests that the NLR inflammasomes likely play less of a role in directly regulating the host microbiome than initially proposed. The consensus data that is building, which is supported by our findings here, indicates that housing and material contributions are stronger variables than genotype in driving microbiome differences. Our data clearly suggest that future studies evaluating NLRs in the context of gastrointestinal inflammation and microbiome interactions should always utilize littermate control animals and proper housing should be a major consideration in experimental design and data analysis.

CONFLICT OF INTEREST STATEMENT:

The authors declare that they have no conflicts of interest.

AUTHORS' CONTRIBUTIONS:

Design and execution of the experiments were conducted by VMRS, YQ, CAT, KEH, DKM, and KE. VMRS and CAT were responsible for mouse breeding, genotyping, and general husbandry. Experimental data interpretation was conducted by VMRS, YQ, CAT, KEH, DKM, KE, PAW, and ICA. All authors, VMRS, YQ, CAT, KEH, DKM, KE, PAW, and ICA, contributed in the writing and revising of the manuscript.

FUNDING:

Grants from the USA National Institutes of Health (ICA (R03 DK105975 and K01 DK092355)); The Via College of Osteopathic Medicine (VCOM) One Health Center Seed Funding (ICA); Virginia Maryland College of Veterinary Medicine Internal Research Competition (ICA), and the Virginia Tech Institute for Critical Technology and Applied Sciences (ICA). Veronica M. Ringel-Scaia was supported through the American Association of Immunologists Careers in Immunology Fellowship Program. This work was supported, in part, by the Intramural Research Program of the National Institute of Environmental Health Sciences (ES101965 to PAW).

ACKNOWLEDGEMENTS:

The authors would like to thank Dr. Beverly H. Koller (The University of North Carolina at Chapel Hill) for generously providing the *Nlrp1b*^{-/-} mice used in this study. We also wish to acknowledge the assistance of the Teaching and Research Animal Care Support Service (TRACSS) at the Virginia Maryland College of Veterinary Medicine, as well as, our technician, graduate students, and undergraduate research students, including Dr. Sheryl Coutermarsh-Ott, Daniel Rothschild, and Bettina Heid. We would also like to especially acknowledge Jody Smiley from the Virginia Tech Sludge Lab for assistance with fecal metabolite analysis. We gratefully acknowledge outstanding technical support in 16s sequencing from the Epigenomics Core Facility at NIEHS.

REFERENCES:

1. Francescone, R., V. Hou, and S.I. Grivennikov, *Cytokines, IBD, and colitis-associated cancer*. *Inflamm Bowel Dis*, 2015. **21**(2): p. 409-18.
2. Alipour, M., et al., *Mucosal Barrier Depletion and Loss of Bacterial Diversity are Primary Abnormalities in Paediatric Ulcerative Colitis*. *J Crohns Colitis*, 2016. **10**(4): p. 462-71.
3. Casen, C., et al., *Deviations in human gut microbiota: a novel diagnostic test for determining dysbiosis in patients with IBS or IBD*. *Aliment Pharmacol Ther*, 2015. **42**(1): p. 71-83.
4. Hedin, C.R., et al., *The gut microbiota of siblings offers insights into microbial pathogenesis of inflammatory bowel disease*. *Gut Microbes*, 2017. **8**(4): p. 359-365.
5. Li, Q., et al., *Dysbiosis of gut fungal microbiota is associated with mucosal inflammation in Crohn's disease*. *J Clin Gastroenterol*, 2014. **48**(6): p. 513-23.
6. Mottawea, W., et al., *Altered intestinal microbiota-host mitochondria crosstalk in new onset Crohn's disease*. *Nat Commun*, 2016. **7**: p. 13419.
7. Putignani, L., et al., *Gut Microbiota Dysbiosis as Risk and Premorbid Factors of IBD and IBS Along the Childhood-Adulthood Transition*. *Inflamm Bowel Dis*, 2016. **22**(2): p. 487-504.
8. Ringel-Scaia, V.M., D.K. McDaniel, and I.C. Allen, *The Goldilocks Conundrum: NLR Inflammasome Modulation of Gastrointestinal Inflammation during Inflammatory Bowel Disease*. 2016. **36**(4): p. 283-314.
9. Williams, T.M., et al., *The NLRP1 inflammasome attenuates colitis and colitis-associated tumorigenesis*. *J Immunol*, 2015. **194**(7): p. 3369-80.

10. Zaki, M.H., et al., *The NLRP3 inflammasome protects against loss of epithelial integrity and mortality during experimental colitis*. *Immunity*, 2010. **32**(3): p. 379-91.
11. Allen, I.C., et al., *The NLRP3 inflammasome functions as a negative regulator of tumorigenesis during colitis-associated cancer*. *J Exp Med*, 2010. **207**(5): p. 1045-56.
12. Chen, G.Y., et al., *A functional role for Nlrp6 in intestinal inflammation and tumorigenesis*. *J Immunol*, 2011. **186**(12): p. 7187-94.
13. Hu, B., et al., *Inflammation-induced tumorigenesis in the colon is regulated by caspase-1 and NLRC4*. *Proc Natl Acad Sci U S A*, 2010. **107**(50): p. 21635-40.
14. Hu, B., et al., *Microbiota-induced activation of epithelial IL-6 signaling links inflammasome-driven inflammation with transmissible cancer*. *Proc Natl Acad Sci U S A*, 2013. **110**(24): p. 9862-7.
15. Wlodarska, M., et al., *NLRP6 Inflammasome Orchestrates the Colonic Host-Microbial Interface by Regulating Goblet Cell Mucus Secretion*. *Cell*, 2014. **156**(5): p. 1045-59.
16. Dupaul-Chicoine, J., et al., *Control of intestinal homeostasis, colitis, and colitis-associated colorectal cancer by the inflammatory caspases*. *Immunity*, 2010. **32**(3): p. 367-78.
17. Hebel, K., et al., *IL-1beta and TGF-beta act antagonistically in induction and differentially in propagation of human proinflammatory precursor CD4+ T cells*. *J Immunol*, 2011. **187**(11): p. 5627-35.
18. Elinav, E., et al., *NLRP6 inflammasome regulates colonic microbial ecology and risk for colitis*. *Cell*, 2011. **145**(5): p. 745-57.
19. Zaki, M.H., M. Lamkanfi, and T.D. Kanneganti, *The Nlrp3 inflammasome: contributions to intestinal homeostasis*. *Trends Immunol*, 2011. **32**(4): p. 171-9.

20. Levy, M., et al., *Microbiota-Modulated Metabolites Shape the Intestinal Microenvironment by Regulating NLRP6 Inflammasome Signaling*. Cell, 2015. **163**(6): p. 1428-43.
21. Mamantopoulos, M., et al., *Nlrp6- and Asc-Dependent Inflammasomes Do Not Shape the Commensal Gut Microbiota Composition*. Immunity, 2017. **47**(2): p. 339-348 e4.
22. Lemire, P., et al., *The NLR Protein NLRP6 Does Not Impact Gut Microbiota Composition*. Cell Rep, 2017. **21**(13): p. 3653-3661.
23. Kovarova, M., et al., *NLRP1-dependent pyroptosis leads to acute lung injury and morbidity in mice*. J Immunol, 2012. **189**(4): p. 2006-16.
24. Mariathasan, S., et al., *Differential activation of the inflammasome by caspase-1 adaptors ASC and Ipaf*. Nature, 2004. **430**(6996): p. 213-8.
25. Chakravorty, S., et al., *A detailed analysis of 16S ribosomal RNA gene segments for the diagnosis of pathogenic bacteria*. J Microbiol Methods, 2007. **69**(2): p. 330-9.
26. Schloss, P.D., *A high-throughput DNA sequence aligner for microbial ecology studies*. PLoS One, 2009. **4**(12): p. e8230.
27. Lozupone, C., et al., *UniFrac: an effective distance metric for microbial community comparison*. ISME J, 2011. **5**(2): p. 169-72.
28. Segata, N., et al., *Metagenomic biomarker discovery and explanation*. Genome Biol, 2011. **12**(6): p. R60.
29. Bauer, C., et al., *Colitis induced in mice with dextran sulfate sodium (DSS) is mediated by the NLRP3 inflammasome*. Gut, 2010. **59**(9): p. 1192-9.
30. Boyden, E.D. and W.F. Dietrich, *Nalp1b controls mouse macrophage susceptibility to anthrax lethal toxin*. Nat Genet, 2006. **38**(2): p. 240-4.

31. Ewald, S.E., J. Chavarria-Smith, and J.C. Boothroyd, *NLRP1 is an inflammasome sensor for Toxoplasma gondii*. Infect Immun, 2014. **82**(1): p. 460-8.
32. Lee, J.Y., et al., *Helicobacter pylori Infection with Atrophic Gastritis Is an Independent Risk Factor for Advanced Colonic Neoplasm*. Gut Liver, 2016. **10**(6): p. 902-909.
33. Daniel, S.G., et al., *Functional Changes in the Gut Microbiome Contribute to Transforming Growth Factor beta-Deficient Colon Cancer*. mSystems, 2017. **2**(5).
34. Robertson, B.R., et al., *Mucispirillum schaedleri gen. nov., sp. nov., a spiral-shaped bacterium colonizing the mucus layer of the gastrointestinal tract of laboratory rodents*. Int J Syst Evol Microbiol, 2005. **55**(Pt 3): p. 1199-204.
35. Cojocariu, C., et al., *Clostridium difficile infection and inflammatory bowel disease*. Turk J Gastroenterol, 2014. **25**(6): p. 603-10.
36. den Besten, G., et al., *The role of short-chain fatty acids in the interplay between diet, gut microbiota, and host energy metabolism*. J Lipid Res, 2013. **54**(9): p. 2325-40.
37. Cook, S.I. and J.H. Sellin, *Review article: short chain fatty acids in health and disease*. Aliment Pharmacol Ther, 1998. **12**(6): p. 499-507.
38. De Preter, V., et al., *Faecal metabolite profiling identifies medium-chain fatty acids as discriminating compounds in IBD*. Gut, 2015. **64**(3): p. 447-58.
39. de, J.R.D.-P.V., A.S. Forlenza, and O.V. Forlenza, *Relevance of gut microbiota in cognition, behaviour and Alzheimer's disease*. Pharmacol Res, 2018.
40. Brial, F., et al., *Implication of gut microbiota metabolites in cardiovascular and metabolic diseases*. Cell Mol Life Sci, 2018.

FIGURES:

Figure 1: Inflammasome deficient mice have a unique microbiome relative to wild type animals

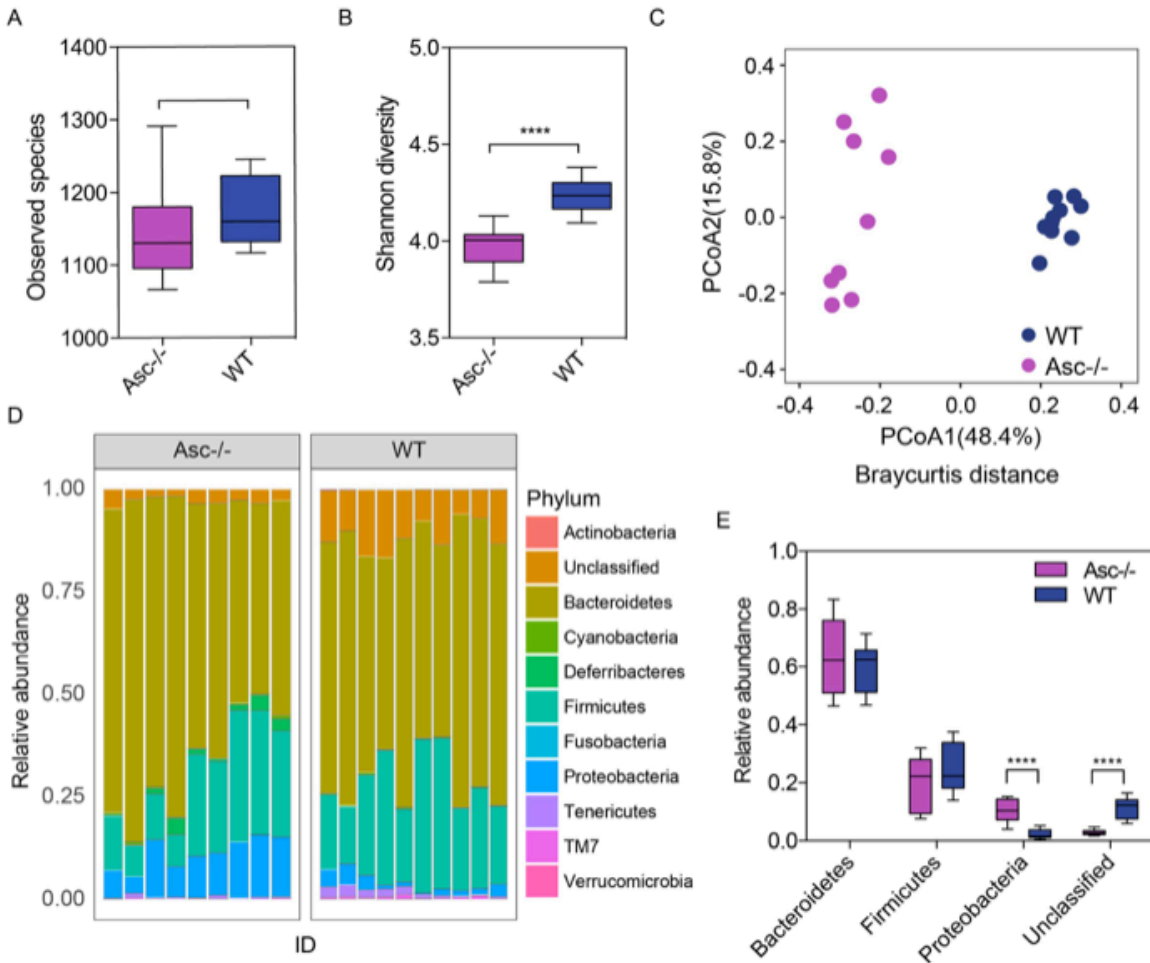


Figure 1: Inflammasome deficient mice have a unique microbiome relative to wild type animals. (A) The observed species number between *Asc^{-/-}* (purple) and wild type (blue) animals. (B) The Shannon diversity index shows *Asc^{-/-}* mice have significantly less diverse populations than wild type mice. (C) PCoA of 16s rRNA sequences using Bray Curtis separation reveals distinct separation and clustering based on genotype. (ANOSIM R=0.9827, P=0.001,999 permutations). (D) Relative abundance of bacteria in *Asc^{-/-}* and wild type animals by phylum. (E) Relative abundance of observed phyla differences between wild type and *Asc^{-/-}* mice reveal that

Asc^{-/-} mice have significantly increased abundance of Proteobacteria and significantly decreased abundance of Unclassified bacteria compared to wild type animals. Wild type (blue), n=10; *Asc*^{-/-} (purple), n=9.

Figure 2: The absence of inflammasome signaling results in dysbiosis and an overabundance of specific bacterial genera

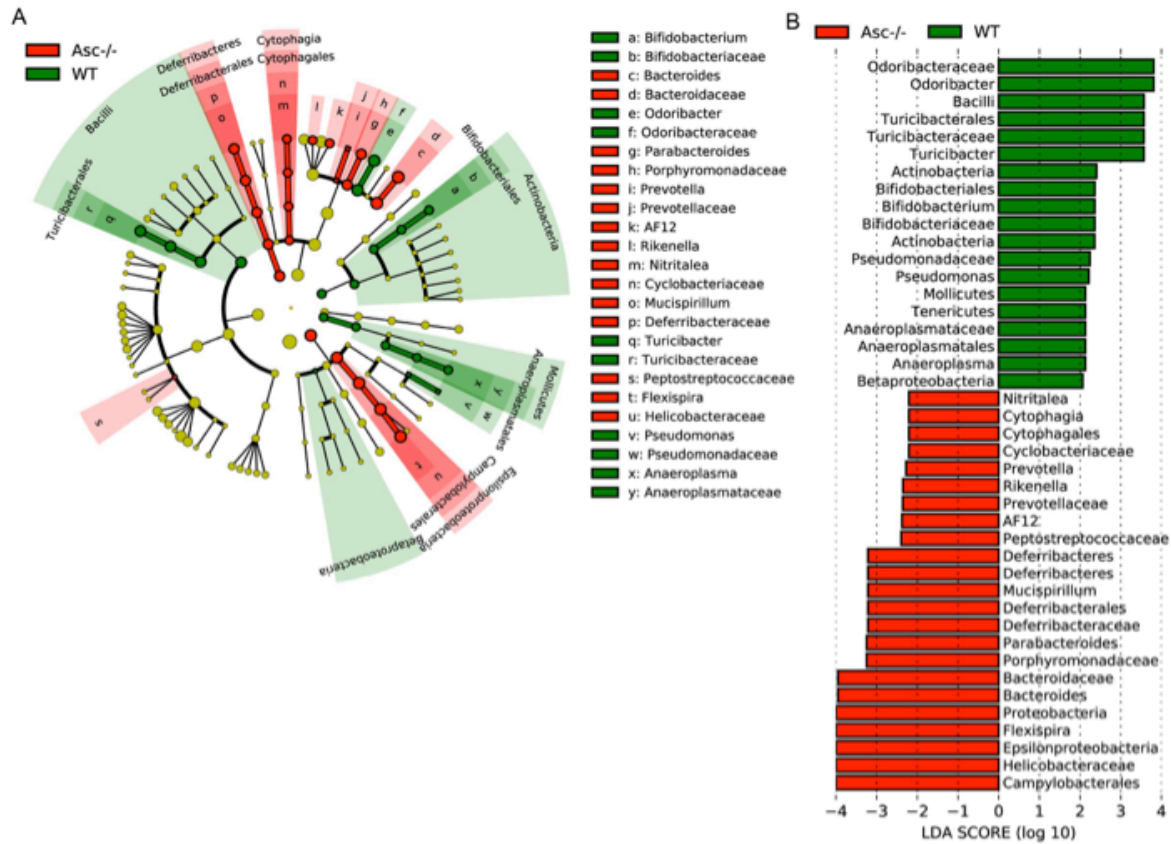


Figure 2: The absence of inflammasome signaling results in dysbiosis and an overabundance of specific bacterial genera. (A) Cladogram display of differential bacterial abundance in *Asc*^{-/-} mice (red) and wild type mice (green). **(B)** LefSe differential analysis displaying bacterial abundance in *Asc*^{-/-} mice and wild type mice reveals that significant differences exist between the microbial populations. The graph was generated using the LefSe program. Wild type (green), n=10; *Asc*^{-/-} (red), n=9.

Figure 3: NLRP1 appears to be essential for maintaining the composition of the host microbiome

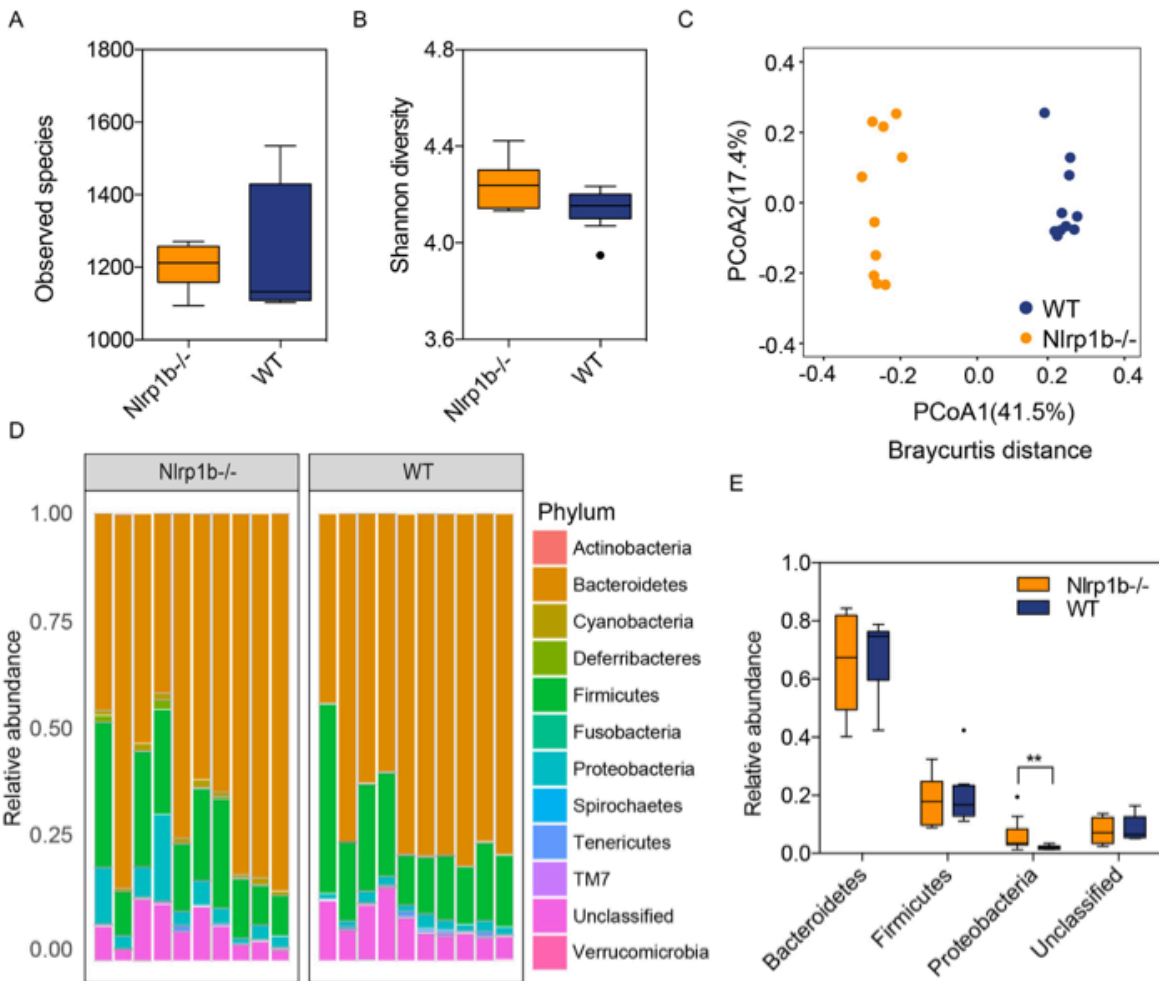


Figure 3: NLRP1 appears to be essential for maintaining the composition of the host microbiome. (A) The observed species number between *Nlrp1b*^{-/-} (orange) and wild type (blue) animals. (B) The Shannon diversity index shows *Nlrp1b*^{-/-} mice have no significant difference in population diversity compared to wild type mice. (C) PCoA of 16S rRNA sequences using Bray Curtis separation reveals distinct separation and clustering based on genotype. (ANOSIM R=0.9851, P=0.001,999 permutations). (D) Relative abundance of bacteria in *Nlrp1b*^{-/-} and wild type animals by phylum. (E) Relative abundance of observed phyla differences between wild

type and *Nlrp1b*^{-/-} mice reveal that *Nlrp1b*^{-/-} mice have significantly increased abundance of Proteobacteria compared to wild type animals. Wild type (blue), n=10; *Nlrp1b*^{-/-} (orange), n=10.

Figure 4: Loss of NLRP1 results in excessive expansion of specific bacteria genera associated with IBD and cancer

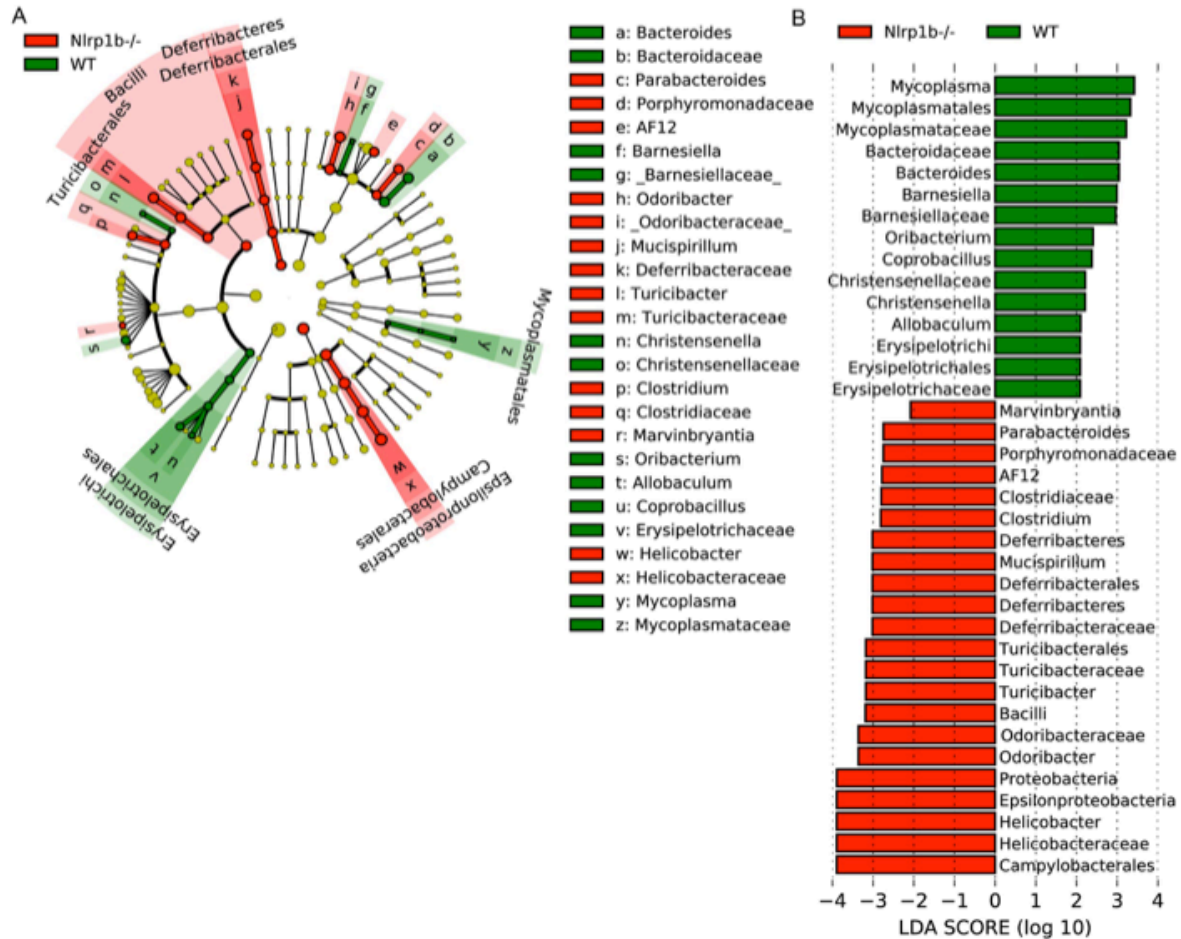


Figure 4: Loss of NLRP1 results in excessive expansion of specific bacteria genera associated with IBD and cancer. (A) Cladogram display of differential bacterial abundance in *Nlrp1b*^{-/-} mice (red) and wild type mice (green). (B) LefSe differential analysis displaying bacterial abundance in *Nlrp1b*^{-/-} mice and wild type mice reveals that significant differences exist between the microbial populations. The graph was generated using the LefSe program. Wild type (green), n=10; *Nlrp1b*^{-/-} (red), n=10.

Figure 5: Short Chain Fatty Acid and Medium Chain Fatty Acid levels significantly differ based on genotype

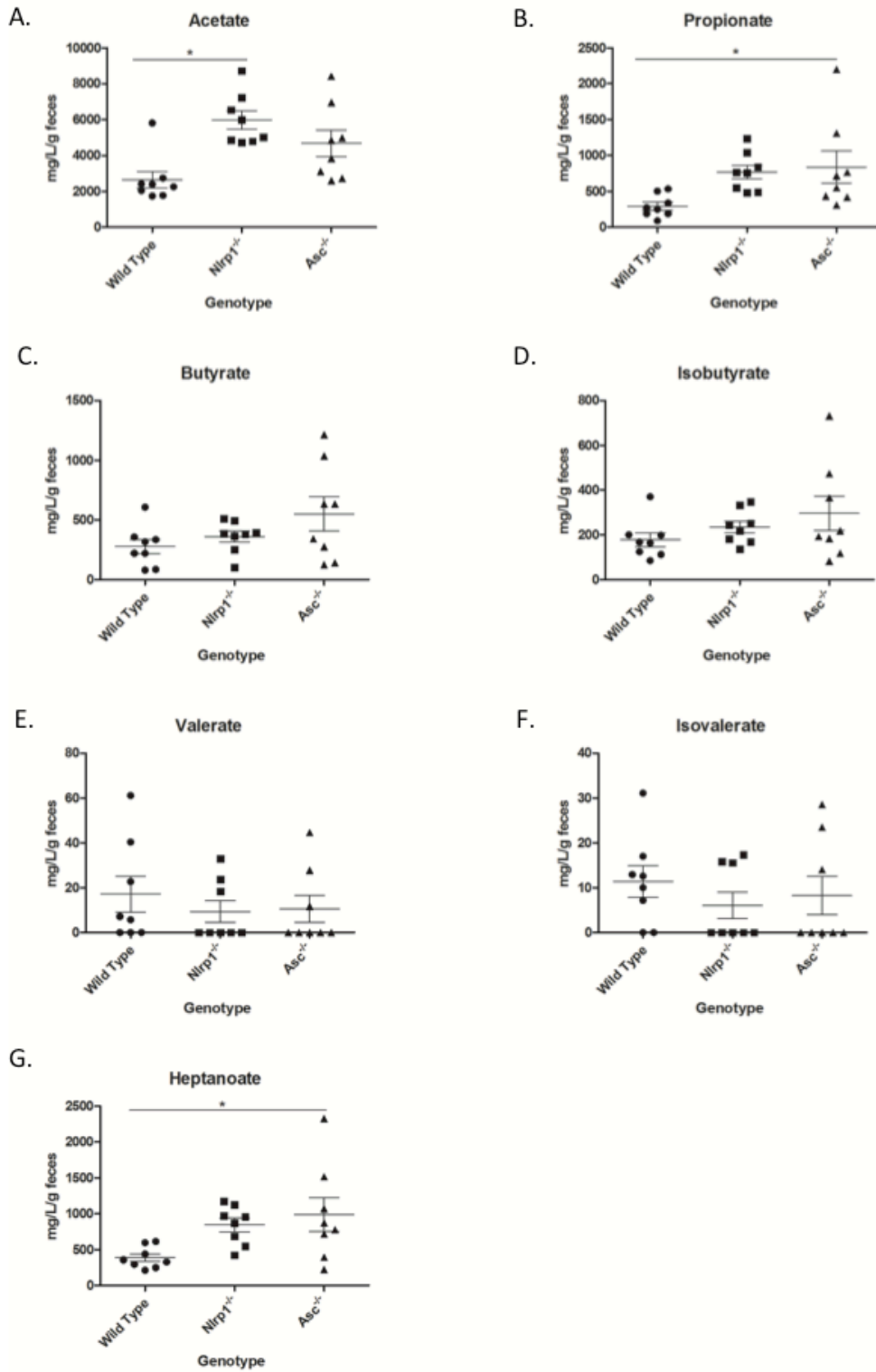


Figure 5: Short Chain Fatty Acid and Medium Chain Fatty Acid levels significantly differ based on genotype. Abundance of the **(A)** acetate (C2), **(B)** propionate (C3), **(C)** butyrate (C4), **(D)** isobutyrate (iC4), **(E)** valerate (C5), **(F)** isovalerate (iC5), and **(G)** heptanoate (C7) in mg/L/g of feces of wild type, *Nlrp1b*^{-/-}, and *Asc*^{-/-} mice. n= 8 mice/genotype. *p<0.05.

Figure 6: Canonical Correspondence Analysis between fatty acids and microbial profiles reveals insight as to metabolic differences in microbiomes

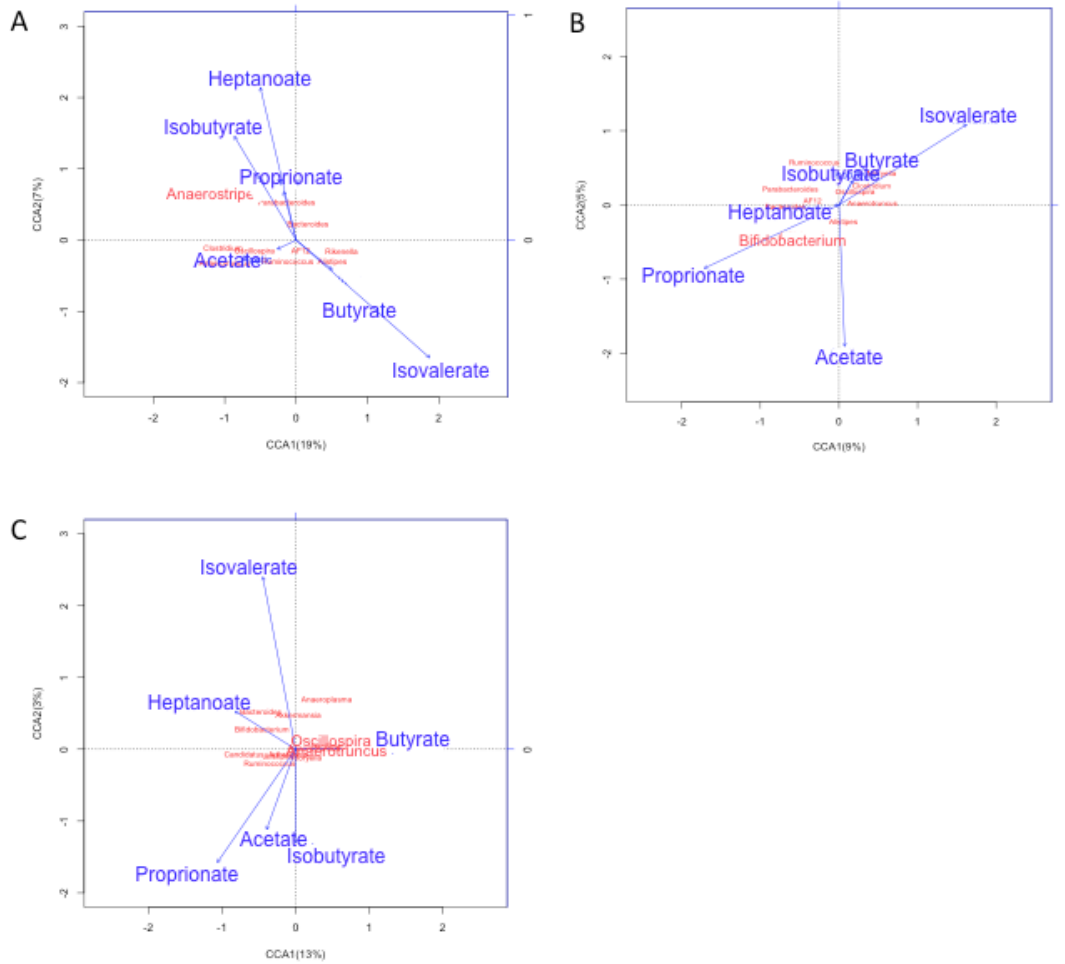


Figure 6: Canonical Correspondence Analysis between fatty acids and microbial profiles reveals insight as to metabolic differences in microbiomes. Ordination diagrams from canonical correspondence analysis (CCA) of genera abundances and SCFAs and MCFAs from (A) *Asc*^{-/-}, (B) *Nlrp1b*^{-/-}, and (C) wild type mice. Blue arrows indicate the direction and magnitude of SCFAs associated with bacterial community structures. Bacterial communities are represented in red.

Figure 7: Co-housing strategy reveals maternal influence is the driving factor in distinct microbiome populations in *Nlrp1b*^{-/-} and wild type animals

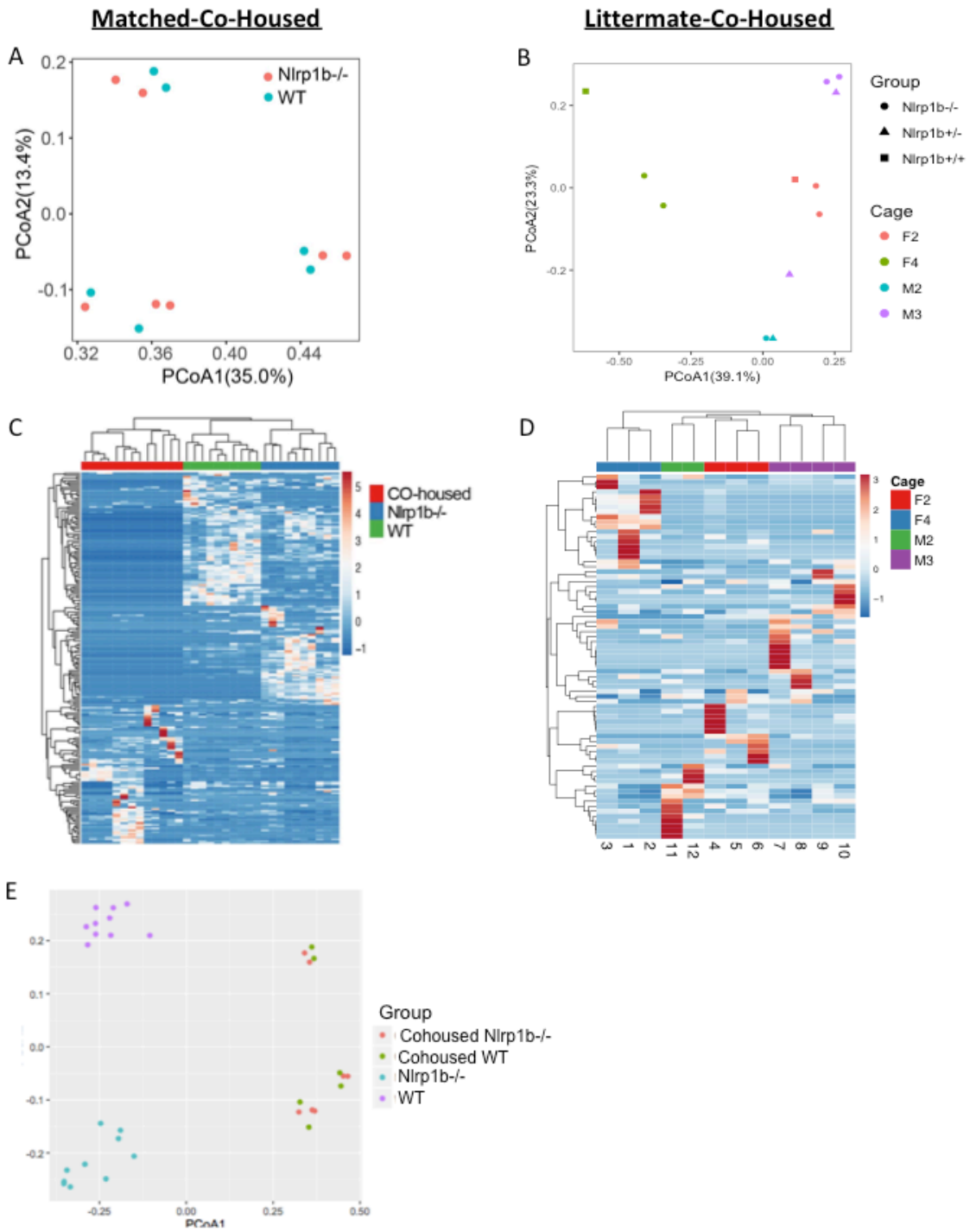


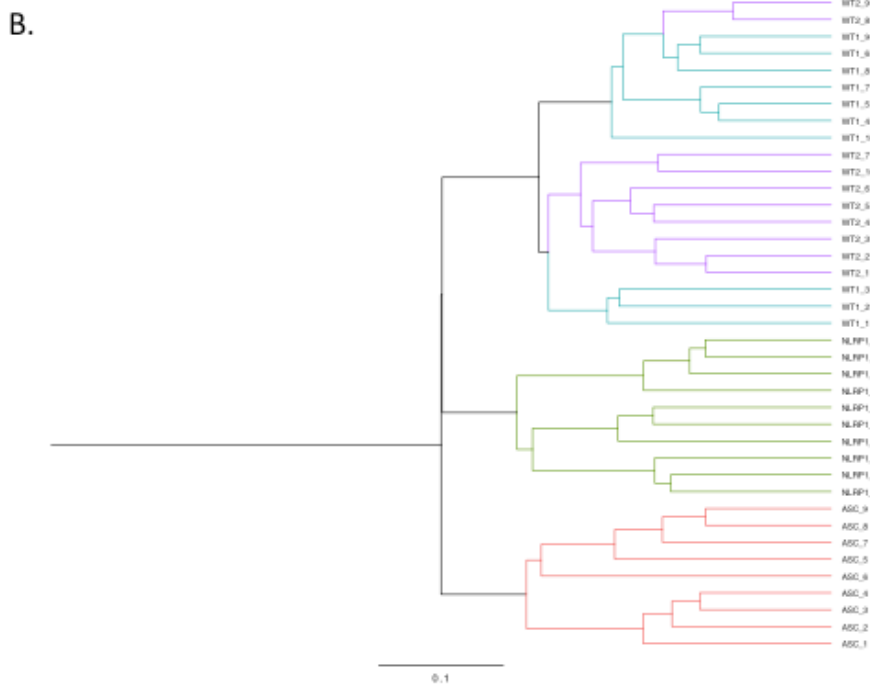
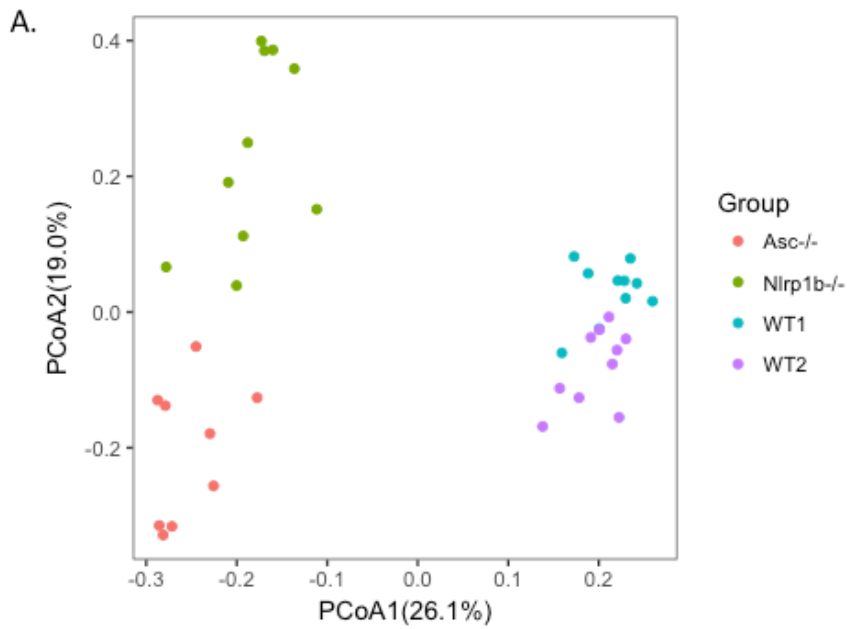
Figure 7: Co-housing strategy reveals maternal influence is the driving factor in distinct microbiome populations in *Nlrp1b*^{-/-} and wild type animals. (A) PCoA of 16s rRNA sequences using Bray-Curtis separation identifies three separate clusters with wild type (blue) and *Nlrp1b*^{-/-} (peach) co-housed with wild type. These clusters correspond to individual housing for each group of mice. (B) PCoA of 16s rRNA sequences using Bray-Curtis separation of littermate-co-housed wild type, heterozygote, and *Nlrp1b*^{-/-} mice shows that cage is the predominant influence on separation. (ANOSIM R=0.7687, P=0.001,999 permutations). (C) The heatmap of > 1000 OTUs reveals differences between the wild type, *Nlrp1b*^{-/-}, and matched-co-housed animals. (D) The heatmap of > 1000 OTUs reveals that the major separations between the littermate-co-housed animals is dependent on cage. (E) PCoA of 16s rRNA sequences using Bray-Curtis separation identifies separate clusters based on cages between wild type individually housed (purple), *Nlrp1b*^{-/-} individually housed (teal), wild type (green) co-housed with *Nlrp1b*^{-/-} or *Nlrp1b*^{-/-} (peach) co-housed with wild type. Wild type, n=10 singly housed; *Nlrp1b*^{-/-}, n=10 singly housed; Matched-Co-Housed, n=13; Littermate-Co-Housed, n=12.

S Table 1: Virginia Maryland College of Veterinary Medicine’s Phase IV Animal Vivarium Excludes Numerous Pathogens

Status	Pathogen	Evaluated by:
-	Mycoplasma pulmonis	Clinical serology
-	Ectromelia	Clinical serology
-	Epizootic Diarrhea of Infant Mice (EDIM)	Clinical serology
-	Lymphocytic choriomeningitis virus (LCMV)	Clinical serology
-	Mouse hepatitis virus (MHV)	Clinical serology
+	Murine norovirus (MNV)	Clinical serology
-	Mouse parvovirus (MPV)	Clinical serology
-	Minute virus of mice (MVM)	Clinical serology
-	Pneumonia Virus of Mice (PVM)	Clinical serology
-	Reovirus (REO3)	Clinical serology
-	Sendai virus (SeV)	Clinical serology
-	Theiler's Murine Encephalomyelitis Virus (TMEV)	Clinical serology
-	Aspicularis tetraptera	PCR on feces
-	Syphacia obvelata	PCR on feces
-	Myocoptes	PCR on skin swab
-	Radfordia/Myobia	PCR on skin swab

S Table 1: Virginia Maryland College of Veterinary Medicine’s Phase IV Animal Vivarium Excludes Numerous Pathogens. The status of the animal housing facility is regularly updated after evaluation for pathogen detection using standard best practices. Pathogens not listed are not routinely screened, and therefore may be present in the colony.

S Figure 1: Wild type cohorts from the *Asc*^{-/-} and *Nlrp1b*^{-/-} evaluations are comparable

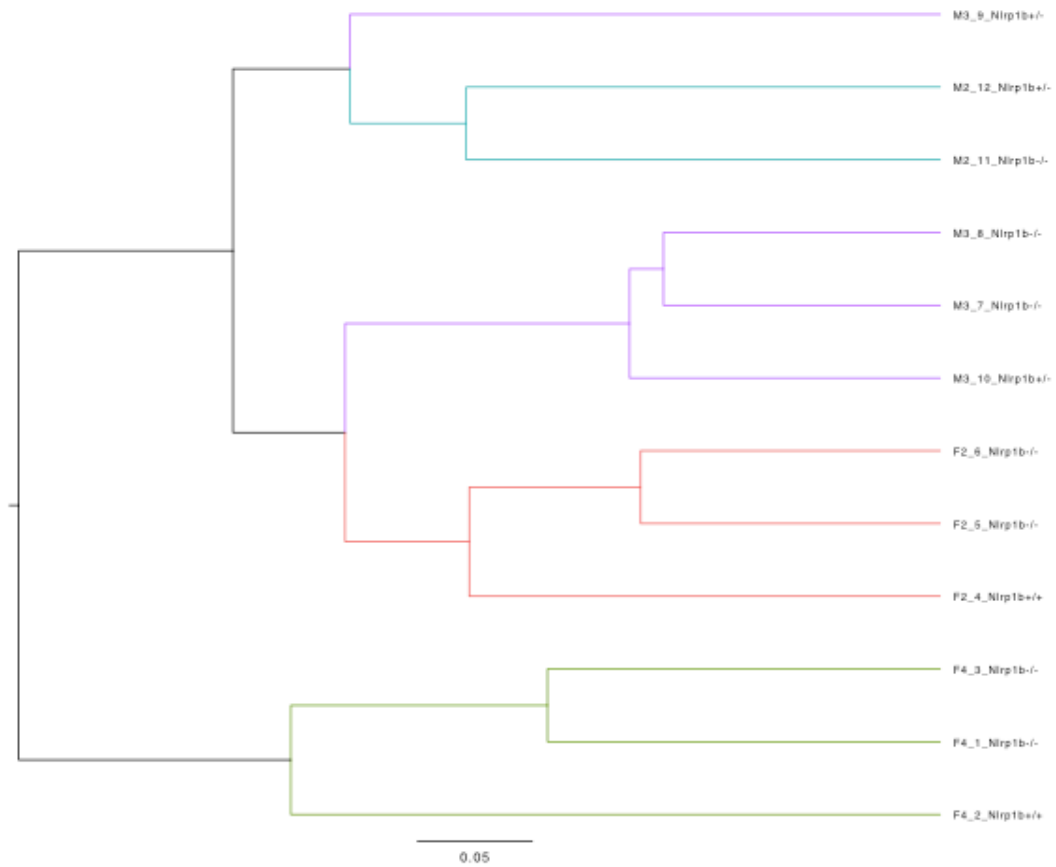


S Figure 1: Wild type cohorts from the *Asc*^{-/-} and *Nlrp1b*^{-/-} evaluations are comparable. (A)

All samples were normalized at the same level (20000 reads) and PCoA analysis of the four

groups show the microbiota composition among these four groups was significantly different (ANOSIM $R=0.8418$, $P=0.001$, 999 permutations). **(B)** Clustering analysis based on Bray-Curtis distance showed that *Nlrp1b*^{-/-} and *Asc*^{-/-} group clustered separately from WT1 and WT2, but WT1 and WT2 clustered together.

S Figure 2: Matched-co-housed animals separate based on cage



S Figure 2: Matched-co-housed animals separate based on cage. Clustering analysis based on Bray-Curtis distance shows that rather than genotype being the predictor for clustering, it is cage-dependent.

Chapter Four

High-Frequency Irreversible Electroporation (H-FIRE) is an Effective Tumor Ablation Strategy that Induces Immunologic Cell Death and Promotes Systemic Anti-Tumor Immunity

Veronica M. Ringel-Scaia, Natalie B. White, Melvin F. Lorenzo, Rebecca M. Brock, Kathleen E. Huie, Sheryl Coutermarsh-Ott, Kristin Eden, Dylan K. McDaniel, Scott S. Verbridge, John H. Rossmeisl Jr, Kenneth J. Oestreich, Rafael V. Davalos, Irving C. Allen

ABSTRACT

Background

Despite promising treatments for breast cancer, mortality rates remain high and treatments for metastatic disease are limited. High-frequency irreversible electroporation (H-FIRE) is a novel and emerging tumor ablation therapeutic approach. This technique utilizes high-frequency bipolar electric pulses to destabilize cancer cell membranes and induce cell death. We predict that H-FIRE induces local inflammatory cell death in mammary tumors, promoting innate and adaptive anti-tumor immunity.

Methods

We utilized the mouse 4T1 mammary tumor model, and evaluated H-FIRE treatment parameters *in vitro* and *in vivo*. We evaluated gene expression via PCR array, infiltrating immune cell populations by flow cytometry, and metastasis through histopathology and selection

plates. Additionally, we performed a modified lysate study to evaluate H-FIRE-triggered neoantigen release.

Findings

Here, we show that H-FIRE effectively ablates the primary tumor and induces a pro-inflammatory shift in the tumor microenvironment. We further show that local treatment with H-FIRE significantly reduces 4T1 metastases. H-FIRE kills 4T1 cells through non-thermal mechanisms associated with necrosis and pyroptosis resulting in damage associated molecular pattern signaling *in vitro* and *in vivo*. Our data indicate that the level of tumor ablation correlates with increased activation of cellular immunity. Likewise, we show that the decrease in metastatic lesions is dependent on the intact immune system and H-FIRE generates 4T1 neoantigens that engage the adaptive immune system to significantly attenuate tumor progression.

Interpretation

Based on these findings, we anticipate that H-FIRE will be an effective complement to conventional breast cancer treatment approaches and improve the efficacy of emerging therapeutic strategies.

RESEARCH IN CONTEXT

Evidence Before This Study

Minimally invasive tumor ablation strategies are being evaluated in a multitude of human cancers, including breast cancer. Breast cancer mortality rates remain high and treatments for

metastatic disease are limited. Irreversible electroporation (IRE) has been successfully used in preclinical and clinical trials for nonthermal tumor ablation, and has been suggested to engage the immune system.

Added Value of this Study

In this study, we demonstrate the effectiveness of high-frequency irreversible electroporation (H-FIRE), the second-generation modality based on IRE that uses high-frequency bipolar electric pulses instead of unipolar pulses. Using a mouse model that closely mimics highly aggressive and metastatic human breast cancer, we show that H-FIRE treatment shifts the local mammary tumor microenvironment to one that favors anti-cancer state and facilitates improved adaptive immune system engagement, resulting in the targeting and elimination of metastatic cells.

Implications of all the Available Evidence

The data presented here suggests that H-FIRE causes localized inflammation and immune cell recruitment, promoting systemic anti-tumor immunity. These would likely improve tumor response to immunotherapies or other targeted treatments. Therefore, H-FIRE may be a valuable tool as a “pre-treatment” to prime the immune system to eliminate metastases.

KEYWORDS: IRE, breast cancer, metastasis, tumor microenvironment, pyroptosis

INTRODUCTION

Breast cancer is the most common malignancy among women, where almost 1.7 million new patients worldwide are diagnosed annually [1]. When coupled with early detection, current treatments are highly effective and have contributed to a decline in mortality over the last three decades. However, the annual death rate remains high. Mortality is typically not associated with breast cancer confined to the breast or draining lymph nodes, rather metastasis to critical organs remains the most significant challenge to patient survival [2].

New therapies for the treatment of breast cancer are emerging including minimally-invasive tumor ablation techniques [3, 4]. One particular ablation technology, irreversible electroporation (IRE), has shown promise in both clinical and pre-clinical cancer studies. IRE is a highly innovative locoregional therapy that delivers short unipolar electric pulses that increase the tumor cell transmembrane potential through non-thermal mechanisms, resulting in cell death while sparing critical structures in the treatment field [5]. IRE is currently being evaluated in a range of veterinary and human clinical trials for malignancies in the liver, pancreas, prostate, kidney, and brain [6-11]. However, there are a few disadvantages of IRE including muscle contractions that require medical paralysis for the procedure and a risk of cardiac arrhythmia that requires cardiac synchronization [5, 12]. Due to these limitations, we have developed a novel, next generation technology that utilizes high-frequency bipolar bursts, which minimizes muscle contraction and cardiac arrhythmia risk [13]. This technique is termed high-frequency irreversible electroporation (H-FIRE).

A major advantage of IRE and H-FIRE is immune system engagement through mechanisms that are not yet fully defined [12, 14, 15]. Previous work by our team demonstrated that *in vitro* IRE treatment of murine 4T1 mammary cancer cells significantly altered expression

of a selection of tumor-associated inflammatory mediators [16]. Likewise, a more recent study utilizing nano-pulse stimulation (NPS) to treat 4T1 tumors *in vivo* demonstrated a reduction in systemic immunosuppressive cells and improved anti-tumor immunity [17]. Similar to IRE and H-FIRE, NPS delivers electric current to permeabilize cell membranes and induce cancer cell death [18]. Here, we investigate the use of H-FIRE in the mouse 4T1 model of mammary tumorigenesis. We demonstrate that H-FIRE is a highly effective tumor ablation strategy that significantly alters the *in situ* anti-inflammatory tumor microenvironment by stimulating the innate immune system through the induction of inflammatory cell death. Local tumor treatment also results in the activation of the adaptive immune system by improving antigen presentation and reducing local immunosuppressive cell populations. Together, our data show that H-FIRE is effective in the induction of a systemic anti-tumor immune response that is capable of eliminating metastases in locations distal to the primary tumor treatment site.

MATERIALS AND METHODS

In Vitro 4T1 H-FIRE Treatment Parameters

The murine 4T1 mammary tumor cell line was acquired from ATCC (Cat#CRL-2539). Cells were sub-cultured to approximately 80% confluence. All experiments were performed within the first 4-8 sub-cultures. At confluence, 4T1 cells were washed and resuspended in a 5.5:1 ratio of low-conductivity sucrose solution (85g sucrose, 3.0g glucose, 7.25ml RPMI, and 992.75ml DI water) to unsupplemented RPMI to 4×10^6 cells/ml. An 800 μ l cell suspension was added to a 4mm electroporation cuvette and H-FIRE was administered using 200 bursts with uniform voltage of 240V, 800V, or 1600V totaling 500, 2000, or 4000V/cm, respectively. Every

experiment was conducted with a 2-5-2 waveform (2 μ s positive pulse, 5 μ s inter-pulse delay, 2 μ s negative pulse), 25 cycles per burst. Temperature was monitored by inserting a fiber optic temperature probe (Lumasense, Inc.) during pulsing. Cells were maintained on ice, and aliquots were immediately removed for staining with acridine orange (AO)/propidium iodide (PI) for automated cell viability counting using a Cellometer Vision CBA Image Cytometer (Nexcelom) and trypan blue for manual cell viability counting via hemocytometer. Remaining cells were divided and plated at a density of approximately 600,000 cells/ml, and maintained in incubators for either 2, 8, or 24hrs before supernatant was isolated for LDH Cytotoxicity Assay (Pierce) following manufacturer's protocol.

Experimental Animals

All experiments were conducted under institutional IACUC approval and in accordance with the NIH Guide for the Care and Use of Laboratory Animals. All experiments utilized 6-10 week-old, female BALB/cJ or NOD scid gamma (NSG) mice (Jackson Labs). 4T1 cells were washed and re-suspended in sterile PBS prior to injection. Mice were anesthetized and 1.2x10⁶ cells were injected into the mammary fat pad. Clinical parameters and tumor measurements were evaluated at least three times/week. Tumor diameter was calculated by the square root of the product of two perpendicular diameters, as previously described[19]. Animals were euthanized when tumors reached 1.6cm of calculated diameter, or if considered clinically moribund.

In Vivo H-FIRE Tumor Treatment

On days 10-11, mice were anesthetized using isoflurane and needle probes were inserted into the tumor. Every experiment was conducted with a 2-5-2 waveform, in 200 bursts. Electrode spacing was adjusted to match tumor diameter using one of the following 3 combinations: 3 mm spacing/750 V; 5 mm spacing/1250 V; or 6 mm spacing/1500 V, ensuring that the same electric field was administered to each tumor (2,500 V/cm). Mice were recovered on room air.

Tissue Collection and Processing

At euthanasia, the primary tumor was dissected, half was flash frozen for RNA isolation, half was fixed in formalin for histopathology. Whole blood was collected via cardiac puncture, washed in HBSS, and resuspended in IMDM supplemented with 10% FBS, 100 units/ml penicillin, 100 µg/ml streptomycin, and 60 µM 6-thioguanine. After 7-12 days incubation, media was removed from the plates, cells were fixed in methanol, stained with 0.03% methylene blue, and counted. The large lobe of the lung was isolated, inflated with formalin, and prepared for histopathology.

Histopathology

Paraffin-embedded formalin-fixed tissues were stained with H&E and independently evaluated by blinded board-certified veterinary pathologists (S.C.O. & K.E.). Pulmonary metastases were quantified per section. Tumor necrosis was graded as a percentage: 0, 0% necrosis; 1, 1-25% necrosis; 2, 26-50% necrosis; 3, 51-75% necrosis; 4, 76-100% necrosis. Tumor leukocyte infiltration was scored on a scale of low, moderate, or high. The skin surrounding the tumor was graded using a binary score for detection of fibrosis.

Flow Cytometry

Tumors were isolated from the animals and mechanically digested. Cells were diluted in complete RPMI. For cell surface marker staining, after an initial 30 minute incubation with anti-CD16/32 (Fc block) in FACS buffer at 4°C, cells were stained for 30 minutes in the dark at 4°C. Cells were washed with PBS and evaluated by FACS Aria (BDBiosciences). The same protocol was followed for surface marker staining, followed by permeabilization with True-Nuclear™ Transcription Factor Buffer Set (BioLegend) following the manufacturer's guidelines for use with FOXP3 staining.

Gene Expression Profiling and Pathway Analysis

For *in vivo* studies, total RNA was harvested from primary tumors using FastRNA Pro Green Kit following manufacturer's protocols (MP Biomedicals). Total RNA was pooled from 3-8 individual mice per group for RT² Profiler PCR Array Platform (QIAGEN) cDNA reaction. For *in vitro* experiments, total RNA was harvested using TRIzol (Invitrogen). Total RNA was pooled from 8-9 samples per treatment for the cDNA reaction. Gene expression was evaluated using PAMM-131Z and PAMM-181Z arrays (*in vivo*), or PAMM-052Z (*in vitro*)(QIAGEN) following manufacturer's protocols. Ingenuity Pathways Analysis (IPA) and the manufacturer's array software (QIAGEN) was used to analyze gene expression data.

Replicates

All studies were repeated at least 3 independent times unless noted.

Statistical Analysis

Data were analyzed using GraphPad Prism, version 7. A Student's two-tailed t-test was utilized for comparisons between two experimental groups. Multiple comparisons were conducted using one-way and two-way ANOVA where appropriate followed by Mann-Whitney or Tukey post-test for multiple pairwise examinations. Statistical significance was defined as $p \leq 0.05$. All data are represented as the mean \pm SEM or SD as appropriate.

RESULTS

H-FIRE is Capable of Delivering High Voltages with Minimal Changes in Temperature

Our team previously defined unipolar IRE pulse parameters that were highly effective in promoting cell death and altering expression of mediators associated with immune system activation in 4T1 cells *in vitro* [16]. Using these studies as our reference, we sought to evaluate similar parameters for H-FIRE in 4T1 cells. 4T1 cell suspensions were exposed to electric field strengths of 0, 500, 2000, and 4000 V/cm while suspended in a cuvette (**Fig. 1A**). The waveform consisted of 25 bipolar pulses with 2 μ s of on-time and 5 μ s delays. In order to determine whether the voltages applied were truly non-thermal, Joule heating was monitored throughout the duration of treatment. A significant increase in temperature was observed at 4000 V/cm, with maximum temperature reaching 62°C, which dissipated away from the electrodes; whereas the maximum temperature was 28.6°C at 2000 V/cm (**Fig. 1B**). The maximum temperature change for the two lower electric field magnitudes remained below 37°C. To detect cell viability, both manual trypan blue and automated AO/PI live/dead exclusion staining was recorded immediately following H-FIRE treatment at each voltage (**Fig. 1C**). At 2000 V/cm, we observed a 29% decrease in cell viability immediately after treatment (**Fig. 1C**). In order to determine whether

cell death was maintained over time following H-FIRE, we chose to use an LDH assay following 2000 V/cm treatment (**Fig. 1C**). Here, we show a steady and consistent increase in cell death over a 24-hour time course (**Fig. 1C**). This is consistent with the unique cell death mechanisms driven by electroporation-based ablation therapy. Unlike other forms of non-thermal tumor ablation, such as histotripsy that causes instant cell rupture [20], the cell death induced by H-FIRE has a delayed initiation and death continues over an extended timeframe.

H-FIRE Promotes Inflammatory Cell Death and Attenuates Local 4T1 Tumor-Promoting Microenvironment

IRE treatment of 4T1 cells results in up-regulation of IL-6 and TNF, and down-regulation of TSLP potentially affecting the tumor microenvironment [16]. To better define the impact of H-FIRE on 4T1 cells, we utilized a broader gene expression profiling strategy coupled with Ingenuity Pathway Analysis (IPA) to profile changes for 162 genes associated with cancer hallmarks and inflammation (**Supplemental Fig. S1**). For this study, we utilized 4T1 cells treated with 2000 V/cm and tracked gene expression changes over 2, 8, and 24-hours (**Fig. 1D-E**). IPA identified several disease and biological functions impacted by H-FIRE treatment based on the expression profiles (**Supplemental Fig. S2A**). This analysis revealed 3 specific biological functions as significantly and differentially impacted by H-FIRE treatment over time: inflammation, injury/repair, and cell death (**Fig. 1E**). H-FIRE induced robust down-regulation of genes associated with immunosuppression and reciprocal increases in pro-inflammatory genes (**Fig. 1E**). We also observed significant decrease in genes associated with cellular injury and an increase in genes associated with regeneration and repair (**Fig. 1E**). This is potentially associated with cells beginning to recover from electroporation.

Consistent with viability studies, we also observed significant increases in expression profiles associated with cell death pathways (**Fig. 1E**). Specifically, we observed a significant increase in pathways associated with inflammatory cell death signaling and necrosis over the 24-hour timecourse (**Fig. 1E**). Prior studies of IRE have suggested that cell death occurs through apoptosis[21-24]. Interestingly, we do observe a gene expression profile that is consistent with apoptosis shortly after H-FIRE (**Fig. 1E**). However, this appears to shift over time towards inflammatory cell death and necrosis (**Fig. 1E**). By 24 hours, we observed up-regulation of genes associated with necrosis and pyroptosis, which are inflammatory forms of cell death associated with NLR inflammasome and caspase-1/11 activation (**Fig. 1F**). IPA identified significant changes in genes associated with *Pycard* signaling following H-FIRE treatment (**Fig. 1F, box**). *Pycard* encodes the essential inflammasome adaptor-protein ASC, critical for inflammation and pyroptosis. Pyroptosis is associated with pattern recognition receptor recognition of damage associated molecular patterns (DAMPs) following pathogen exposure, cellular damage, or stress[25]. Further evaluation of the gene expression data revealed 3 networks associated with DAMP signaling significantly up-regulated post-H-FIRE: (1) ROS signaling, (2) ATP signaling, and (3) high mobility group box 1 (HMGB1) signaling (**Fig. 1G**), which are associated with NLR inflammasome activation and previously shown to be inducers of pyroptosis[26-28].

H-FIRE is a Highly Effective Ablation Therapy in the *In Vivo* 4T1 Mammary Tumor Model

To better define the effectiveness of H-FIRE in mammary tumors, we utilized the *in vivo* murine 4T1 mammary carcinoma model [19]. Animals were injected with 1.2×10^6 4T1 cells into

a single mammary fat pad. We chose to treat the tumors when they reached ~5mm in diameter, which occurs between days 10-11 of our model (**Fig. 2**). Each tumor received 2,500V/cm H-FIRE treatment. The schematic illustrates a pair of 0.4mm electrodes, spaced 4mm apart to deliver H-FIRE (**Fig. 2A**). H-FIRE was administered with 200 bursts in 25 cycles. This dose of H-FIRE was sufficient to ablate the 4T1 mammary tumor (**Fig. 2B**). Representative images of mice showing average tumor sizes on Day 15 (4 days post-treatment) revealed an average 80% reduced tumor diameter post-H-FIRE (**Fig. 2C**). The only H-FIRE side effect noted was superficial scab formation over the treatment area, which resolved within 2 weeks post-treatment (**Fig. 2C**). Similar scabbing was not observed in mice treated with H-FIRE that were not tumor-bearing (**Fig. 2C**). We achieved near-full ablation within the first week following treatment. However, we observed a range of tumor responses to treatment by day 27 with some tumors beginning to exit remission (**Fig. 2B**).

We believe the ability to administer H-FIRE without the muscle contraction side effects is a clinical advantage of this technology over other electroporation approaches, especially for breast cancer applications. Thus, here we compared muscle constriction associated with the monopolar IRE burst and bipolar H-FIRE burst. Animals were fitted with accelerometers on their footpads and contraction was assessed during 2000V/cm of either IRE or H-FIRE. IRE treatment resulted in significant full body muscle spasm (**Fig. 2D; Supplemental Fig. S3A**), while negligible movement was observed during H-FIRE treatment (**Fig. 2E, Supplemental Fig. S3B**). Together, these data show that H-FIRE effectively ablates the 4T1 orthotopic tumor and can be applied with minimal side effects associated with other electroporation-based strategies.

H-FIRE Ablation Results in Increased Cell Death and Inflammation

To determine the extent and mechanisms of mammary tumor ablation following H-FIRE, cell death and inflammation within the tumor were evaluated by histopathology. The 4T1 mammary tumor demonstrates many features of aggressive breast cancer including severe dysplasia, invasive behavior, marked anisocytosis and anisokaryosis, multinucleated cell formation, and high mitotic index (**Fig. 3A**). Previous studies have shown that these tumors characteristically have high levels of necrosis in their core regions and significant 4T1 cell proliferation in the leading edge of the tumor [19]. These tumors are also highly immunosuppressive with low levels of lymphocyte infiltration in the microenvironment [19]. Our histopathology assessments revealed large areas of cell death in the central core of the 4T1 mammary tumors (**Fig. 3B**). Following H-FIRE, we routinely observed large areas of cell death and tumor cell ablation (**Fig. 3C**). By the end of the model, histopathology screening revealed that in 30% of H-FIRE-treated animals, no dysplasia or neoplasia was detected (**Fig. 3D**). Consistent with the *in vitro* data, H-FIRE induced a gene expression profile consistent with necrosis and pyroptosis rather than apoptosis (**Fig. 3D**). Because necrosis and pyroptosis are inflammatory forms of cell death, we next evaluated histopathologic features of inflammation. Following H-FIRE treatment, we observed increases in immune cell infiltration into the treatment zone (**Fig. 3F-H**). However, our histopathology assessments revealed that immune cell infiltration was variable between animals and ranged from none to moderate following H-FIRE treatment (**Fig. 3F-H**). Together, these data support a model whereby H-FIRE alters the tumor microenvironment through the induction of an inflammatory form of cell death.

Tumor Response to H-FIRE Ablation is Correlated with Increased Cellular Immunity

Based on the range of ablation responses to H-FIRE, (**Fig. 2B**), we sought to characterize the microenvironment in animals sub-classified as low-, average-, or high-responders to treatment. At necropsy 15 days post-H-FIRE, tumor specimens were collected and RNA was extracted; data were analyzed based on percentage of ablation post-H-FIRE (low response \leq 84% ablation; average response = 85-94% ablation; high response \geq 95% ablation). When animals were sub-grouped based on their individual tumor response to H-FIRE, we observed a significant correlation between tumor response and expression of genes associated with cellular immunity (**Fig. 4A**). In mice with low response to H-FIRE, the majority of genes associated with cellular immunity were significantly decreased (**Fig. 4A**). Correlation analysis revealed a strong positive correlation ($r=0.70$) between up-regulation of cellular immunity-associated genes and decreased tumor diameter. The biggest shifts in individual gene expression were noted for *Aicda*, *Ccl20*, *Ccl28*, and *Fasl*, which were significantly down-regulated in low-responding tumors and significantly up-regulated in highly responsive tumors (**Fig. 4A**). Analysis of cellular immunity networks most impacted by H-FIRE treatment revealed significant differences in chemokine signaling (**Fig. 4B**). The majority of chemokine-associated gene expression was down-regulated in untreated tumor, with notable exceptions being *Ccr1*, *Ccr2*, *Ccr5*, and *Cxcl6* up-regulated (**Fig. 4B**). However, this pattern was reversed in H-FIRE-treated tumors (here grouped together, not subdivided into responder status) where we observed significant down-regulation of these genes and the vast majority of remaining genes in this network significantly up-regulated (**Fig. 4B**). Together, these data suggest that activation of cellular immunity is associated with the effectiveness of H-FIRE ablation and chemokine signaling networks play a critical role in optimal responses to treatment.

To further evaluate H-FIRE-mediated changes in the *in situ* 4T1 tumor microenvironment, we utilized IPA to identify biological functions and gene networks impacted by treatment. We observed significant down-regulation of breast cancer-associated genes, with lower levels of expression observed in fully ablated tumors compared to the low-responder and untreated tumor groups (**Fig. 4C**). Similar to our findings in the *in vitro* studies, we observed a significant shift in the balance between immunosuppressive and pro-inflammatory-associated gene transcription (**Fig. 4C**). Following treatment, genes associated with immunosuppression were significantly down-regulated, while genes associated with inflammation and pro-inflammatory immune responses were significantly up-regulated (**Fig. 4C**). These responses were increased in average- and high-responder groups, compared to the low-responders and untreated animals (**Fig. 4C**). Signaling networks associated with cytotoxicity were significantly increased in responsive tumors (**Fig. 4C**), likely associated with increased cell death following treatment. Consistent with the chemokine data (**Fig. 4B**), gene networks associated with recruitment of leukocytes were significantly up-regulated in responsive tumors (**Fig. 4C**). Interestingly, IL-17 signaling and antigen presentation networks were up-regulated in average-responder animals compared to the other sub-groups (**Fig. 4C**). We are unsure of the functional significance of the IL-17 findings as this cytokine has been shown to have both pro- and anti-tumor effects in breast cancer, including increased recruitment of tumor-associated neutrophils and promoting cytotoxic T cell responses [29, 30]. However, the data associated with increased antigen presentation signaling is consistent with the pro-inflammatory shift observed in the tumor microenvironment and may suggest that adaptive immune system signaling may benefit from a partial or an incomplete tumor ablation strategy. Together, the data presented here are consistent with those described for the *in vitro* studies (**Fig. 1**) and detail the tumor

microenvironment shifts from one that is favorable for tumor progression to an antitumor microenvironment driven by increased cellular immunity.

H-FIRE Treatment Significantly Alters Local Immune Cell Populations in 4T1 Tumor Microenvironment

Based on the clinical findings and expression profiling data, we next sought to define the impact of H-FIRE on cell populations within the tumor microenvironment to identify mechanism/s associated with increased cellular immunity. Similar to most human breast cancers, the 4T1 microenvironment is characterized as being highly immunosuppressive [19]. While many factors contribute, the recruitment and assimilation of myeloid derived suppressor cells (MDSCs), regulatory T cells (Tregs), tumor-associated macrophages (TAMs), and tumor associated neutrophils (TANs) are potent factors in thwarting anti-tumor immunity[31]. Because these cells are in and around the H-FIRE treatment zone, we evaluated these populations post-treatment using flow cytometry. Tumors were harvested during necropsy two and seven days post-H-FIRE treatment and digested to generate single cell suspensions for labeling and analysis. Common markers were utilized to identify neutrophils, polymorphonuclear-MDSCs (pMDSCs), monocytic-MDSCs (mMDSCs), TAMs, Tregs, and T helper cell populations (**Supplemental Fig. S4A**). Two days after H-FIRE treatment, we observed an 8.7% decrease in CD11b+Ly6G+ neutrophils and no CD11b+Ly6G+Ly6C^{lo}CD45- pMDSCs in the H-FIRE-treated animals (**Fig. 5A**). Although there were trending differences in these populations seven days post-H-FIRE, no significant differences were observed at this later time point (**Supplemental Fig. S4B**). We detected a significant 12.5% decrease in CD4+CD45+ T helper cell populations two days after treatment (**Fig. 5B**). Somewhat counterintuitively, we saw a small but significant increase

(0.15%) in the CD4⁺CD45⁺CD25^{hi}CD127^{lo}Foxp3⁺ Treg population (**Fig. 5B**). While we predicted a reduction in Tregs and an increase in T helper cells, it is possible that depletion of T cells in the microenvironment at these relatively early timepoints post-H-FIRE may negatively impact tumor growth and progression through preventing lymphocyte differentiation into tumor-promoting T cell populations. No significant differences were observed in these lymphocyte populations after seven days (**Supplemental Fig. S4C**). Regarding TAM populations, no significant differences were observed two days after treatment (**Supplemental Fig. S4D**). However, this may suggest the macrophage populations in the treatment zone are resistant to initial death by H-FIRE because at seven days, we observed a significant .45% decrease in CD11b⁺Ly6G⁻Ly6C⁻CD45⁺F4/80⁺ TAMs (**Fig. 5C**). The reduction in TAN, MDSC, and TAM populations and the congruent attenuation of their anti-inflammatory signaling is consistent with the shift to a pro-inflammatory anti-tumor microenvironment observed following H-FIRE.

Local H-FIRE Treatment Promotes a Systemic Anti-Tumor Immune Response

Due to the increase in cellular immunity signaling, we hypothesized we would observe increased adaptive immune system activation. Animals were necropsied 15 days post-H-FIRE, and lungs and blood were evaluated for metastatic lesions. Pulmonary metastatic lesions were characterized using blinded histopathology examination (**Fig. 6A**). We observed 46.7% reduction in the number of lung lesions counted post-H-FIRE (mean = 8.367±1.731) compared to untreated animals (mean = 15.03±2.392) (**Fig. 6B**). IPA expression profiling revealed a significant decrease in metastasis-associated genes in the primary tumor post-H-FIRE (**Fig. 6C**). The extent of down-regulation was consistent with the response to H-FIRE, with the greatest changes in average- or high-responders (**Fig. 6C**). It is possible that the changes in lung

metastases were a direct reflection of the level of tumor ablation and down-regulation of metastatic genes. However, while this is certainly a possibility and likely contributing factor to the data observed, metastasis was already underway at the time of treatment. It is therefore also probable that local ablation effectively activated systemic anti-tumor immunity, resulting in the observed reduction in the metastatic tumor burden.

To evaluate the role of the immune system in controlling metastasis following H-FIRE, we utilized NSG mice that lack T, B, and NK cells. Animals were injected with 1.2×10^6 4T1 cells in the mammary fat pad and treated with identical H-FIRE parameters as wild type BALB/c animals when tumors reached 0.5-0.6cm (**Fig. 6D**). We observed significant ablation in the 4T1 tumors with average diameter decreasing from 0.56cm to 0.30cm post-H-FIRE (**Fig. 6D**). While this decrease was statistically significant compared to untreated NSG animals, tumor diameter remained larger than those of wild type BALB/c mice post-treatment, ablation demonstrated greater variability, and no tumors were completely ablated (**Fig. 6D**). Likewise, the level of ablation steadily decreased until the tumor reached the original size at treatment (0.57 cm) by Day 25 (**Fig. 6D**). In both the untreated and H-FIRE-treated NSG animals, we observed high numbers of metastatic cells in the blood (**Fig. 6E**). In the untreated animals, we counted 4994 ± 2786 colonies and 6806 ± 2842 colonies in H-FIRE-treated NSG animals (**Fig. 6E**). In BALB/c mice we counted 2401 ± 503.7 colonies in the blood from untreated mice and 853.2 ± 437.7 colonies in H-FIRE-treated animals (**Fig. 6E**). The significant decrease in circulating metastatic 4T1 cells following local H-FIRE treatment of the primary tumor was statistically significant and based on the NSG experiment is dependent on an intact immune system.

H-FIRE Ablation Generates Neoantigens Capable of Stimulating the Adaptive Immune System

While the innate immune system and cellular immunity certainly contribute, initiation of systemic anti-tumor immunity relies on robust adaptive immune system activation, largely driven by tumor antigen presentation at the local treatment site. Based on our data, we hypothesized that H-FIRE treatment improves these functions. The non-thermal nature of H-FIRE likely generates novel neoantigens from the 4T1 cells in their native form that are not heat or cold denatured. This is expected to improve antigen recognition and would be consistent with the metastasis data described above. We also anticipate the prolonged cell death associated with H-FIRE allows antigen generation and presentation to occur over an extended period of time, further enhancing APC exposure and sampling. To evaluate this hypothesis, we treated 4T1 cells *in vitro* using 2000 V/cm or treated cells using cryoablation involving 3 rounds of cooling in liquid Nitrogen for 30 seconds followed by rapid recovery at 37°C for 3 minutes (modified from [32]). Following 24-hour recovery, cell suspensions were filtered to remove any remaining 4T1 cells, and the resultant cell-free lysate was i.v.-injected into healthy BALB/c mice. After 10 days, mice were injected with 1.2×10^6 4T1 cells into a single mammary fat pad, tumor progression was monitored, and tumor diameter was reported at day 30 (**Fig. 6F**). Control mice i.v.-injected with lysate that did not receive the 4T1 mammary injection (“lysate only”), did not show any clinical signs of local or systemic tumor progression (**Fig. 6F**). As expected, mice that received sham treated lysate and 4T1 mammary injection (“tumor only”) demonstrated typical tumor progression (**Fig. 6F**). Mice that received the 4T1 lysate following cryoablation demonstrated more variability in tumor progression, but primary tumor size at harvest did not significantly differ from the tumor only group (0.91 ± 0.02 cm vs. 0.89 ± 0.06 cm, respectively) (**Fig. 6F**).

Whereas, mice that received lysate from H-FIRE-treated cells demonstrated a statistically significant reduction in tumor size ($0.74\pm 0.04\text{cm}$) compared to both the tumor only and the cryoablation lysate groups (**Fig. 6F**). Tumors from mice treated with H-FIRE lysate were 19% reduced compared to tumor only animals and 17% reduced compared to cryoablation lysate (**Fig. 6F**). In addition to the improvement in primary tumor progression, mice treated with either cryoablation lysate or H-FIRE lysate demonstrated a significant decrease in circulating blood metastatic cells compared to the tumor only group (**Fig. 6G**). Together, these data indicate that H-FIRE treatment is effective in generating neoantigens that can stimulate the immune system, which contributes to attenuated mammary tumor progression.

DISCUSSION

In previous studies by our research team utilizing IRE to treat mouse 4T1 cells or human MDA-MB-231 cancerous mammary cells, the effects of varying pulse parameters were evaluated on a selection of cell signaling mediators and general assessments of cell death [16, 33]. The current work expands these data to a more comprehensive assessment of the tumor microenvironment and hallmarks of tumorigenesis following electroporation. Here, we show that H-FIRE initiates inflammatory cell death signaling and a shift in the tumor microenvironment from anti-inflammatory to pro-inflammatory *in vitro* and *in vivo*. Defining the mechanism of cell death as necrosis and pyroptosis is an important distinction, as previous studies have associated electroporation with apoptosis [21-24], considered a non-inflammatory form of cell death. Although we observed expression consistent with apoptosis within the first hours post-H-FIRE treatment, cell death shifted to necrosis and pyroptosis over time (**Fig. 1**). We identified the

production of DAMPs ROS, ATP, and HMGB1 as likely contributors to both the shift towards a pro-inflammatory microenvironment and the related shift towards necrosis/pyroptosis (**Fig. 1**). HMGB1 and ATP, along with calreticulin, were also implicated in electroporation-mediated cell death following NPS in 4T1 cells [17]. Similar to our present study, NPS detected high levels of inflammatory cell death, ultimately resulting in increased activation of dendritic cells [17]. All four mediators (ATP, HMGB1, ROS, and calreticulin) function as DAMPs and activate the NLRP3 inflammasome [34-37], which is a likely mechanism underlying these observations.

As with previous electroporation-based tumor ablation studies in other cancer types, H-FIRE was effective in ablating murine mammary tumors. However, we observed a range of responses we classified as low, average, and high responses. In clinical applications of IRE, computational modeling is used to map and plan treatment for each individual patient, leading to improved ablation [38, 39]. We did not model electrode placement in the mouse studies, likely resulting in partial coverage in some animals. However, this variability also allowed us to evaluate immune system activation in animals with different levels of treatment response. Our data reveal a significant correlation between activation of the innate immune system and cellular immunity with ablation responses (**Fig. 4**). It is interesting to speculate that identification of specific cellular immunity genes correlated with favorable treatment response could be further developed and leveraged as biomarker/s of H-FIRE responsiveness in human patients.

Early studies evaluating IRE and related electroporation techniques used human cancer cell lines implanted into immunocompromised mice [40-42]. These studies were critical to explore tumor ablation in human-relevant cancers, but the lack of a functional immune system missed key elements of the host response to treatment. In one of the few studies directly comparing immunocompetent (BALB/c) versus immunodeficient (nude) mice, IRE treatment of

subcutaneous renal tumors was more effective in BALB/c mice, requiring 60% less voltage for complete regression compared to nude animals [43]. These findings are similar to ours, where H-FIRE treatment was more effective in ablating the primary tumor in BALB/c mice compared to NSG animals (**Fig. 2&6**). Interestingly, Neal et al., re-injected animals with the same renal cell line 18 days post-IRE treatment and found attenuation of secondary tumor growth in immunocompetent mice [43]. Similar findings were also reported for animals following NPS in the 4T1 model [17]. Together, these data suggest engagement of the adaptive immune system that is consistent with our findings following the pre-treatment of animals with the lysate from H-FIRE treated 4T1 cells (**Fig. 6**). Based on these data, we believe that non-thermal ablation modalities, such as H-FIRE, have negligible effects on protein structure and folding, improving antigen presentation and recognition. We believe these data illustrate the potential for H-FIRE to engage the adaptive immune system and promote immunological memory that could be harnessed to minimize tumor progression and prevent recurrence.

One of the most striking findings from these studies reveals that local treatment with H-FIRE can significantly impact metastasis (**Fig. 6**). We observed reduced lung and blood metastases in H-FIRE-treated animals. These findings are complementary to recent NPS studies, which induced similar levels of anti-tumor immunity and reduced distant organ metastases in the 4T1 model [17]. Following NPS, the authors focused on assessments of systemic leukocytes, and found that NPS induced long-term memory T cells and reduced circulating Tregs [17]. We evaluated the cell populations as described in this study, but did not observe these changes post-H-FIRE (**data not shown**). However, this is not surprising as our study focused on earlier timepoints and changes in the local tumor microenvironment. We detected the biggest differences in local cell populations, and observed reduced TANs, MDSCs, and TAMs. NPS and

H-FIRE are fundamentally different electroporation techniques, but despite mechanistic differences, the same overall clinical and phenotypic results of tumor ablation and systemic anti-tumor immune system activation were observed, emphasizing the utility of electroporation-based therapeutics.

Overall, our data support a model whereby the inflammatory cell death mechanism following H-FIRE increases cellular immune responses and leukocyte recruitment, improving antigen processing and promoting systemic anti-tumor immunity. The removal of anti-inflammatory components of the tumor microenvironment, including TAN, MDSC, and TAM populations, should make the microenvironment more favorable for combination therapies. Additionally, improved antigen presentation and greater lymphocyte accessibility to the tumor should improve responses to immunotherapeutics, such as checkpoint inhibitors. This is expected to improve ablation of the primary breast tumor, eliminate metastases, and prevent recurrence. Using H-FIRE as a pre-treatment to improve immune system activation and surveillance, even in tumors that will ultimately be surgically removed in a treat and resect strategy, may also improve long-term prognosis.

ACKNOWLEDGEMENTS

We would like to acknowledge Dr. Robert C.G. Martin II for providing clinical insight related to this manuscript. We would also like to acknowledge undergraduate students that assisted with aspects of this manuscript, including Cassidy Thomas, Maia Tatum, and Jenna Coulturi. Dr. Daniel Rothschild assisted with live animal images. Dr. Catharine Cowan and Melissa Makris of our Flow Cytometry Core provided technical assistance with this aspect of the

study. We would also like to acknowledge the staff and personnel related to our Teaching and Research Animal Care Support Service (TRACSS). Center support was provided by the Virginia Tech Center for Engineered Health and the Virginia Tech Institute for Critical Technology and Applied Science.

FUNDING SOURCES

This work was supported by the Virginia-Maryland College of Veterinary Medicine (I.C.A.), the Virginia Tech Institute for Critical Technology and Applied Science Center for Engineered Health (I.C.A.), the Virginia Biosciences Health Research Corporation (VBHRC) Catalyst (R.V.D.), and the National Institutes of Health R01CA213423 (R.V.D. and S.S.V.), P01CA207206 (R.V.D and R.V.D.), R56AI127800 (K.J.O.), and R01AI134972 (K.J.O.). Student work on this publication was supported by the National Institute of Allergy and Infectious Diseases Animal Model Research for Veterinarians (AMRV) training grant (T32-OD010430) (S.C.O. and K.E.) and the American Association of Immunologist Careers in Immunology Fellowship Program (V.M.R.S.). The content is solely the responsibility of the authors and does not necessarily represent the official views of the NIH or any other funding agency.

DECLARATION OF INTERESTS

I.C.A., S.S.V., J.H.R., and R.V.D. are inventors on pending and issued patents related to the work. Authors declare no other conflicts of interest.

AUTHOR CONTRIBUTIONS

V.M.R.-S. designed, performed the *in vitro* and *in vivo* experiments, analyzed and interpreted the data, prepared the figures, and wrote the paper. N.B.W., M.F.L., and R.V.D. were responsible for designing the H-FIRE treatment parameters. N.B.W. performed the *in vitro* H-FIRE experiments. M.F.L. performed the *in vivo* H-FIRE experiments. R.M.B. performed the *in vitro* cell viability studies. R.M.B., K.E.H., D.K.M., and K.E. assisted with live animal monitoring and necropsy. S.C.-O. and K.E. read all the H&E slides and provided scoring and expertise on the methods and results. S.S.V., J.H.R., K.J.O., R.V.D., and I.C.A. provided expertise on the design of the studies, interpretation of results, and revisions to the manuscript. I.C.A. provided overall direction, generated the IPA figures, and wrote the manuscript. All authors have read and approved the manuscript.

REFERENCES

1. DeSantis, C., et al., *Breast cancer statistics, 2013*. CA Cancer J Clin, 2014. **64**(1): p. 52-62.
2. Xiao, W., et al., *Breast cancer subtypes and the risk of distant metastasis at initial diagnosis: a population-based study*. Cancer Manag Res, 2018. **10**: p. 5329-5338.
3. Vikas, P., N. Borcherding, and W. Zhang, *The clinical promise of immunotherapy in triple-negative breast cancer*. Cancer Manag Res, 2018. **10**: p. 6823-6833.
4. Garcia-Tejedor, A., et al., *Radiofrequency Ablation Followed by Surgical Excision versus Lumpectomy for Early Stage Breast Cancer: A Randomized Phase II Clinical Trial*. Radiology, 2018. **289**(2): p. 317-324.
5. Thomson, K.R., H. Kavnoudias, and R.E. Neal, 2nd, *Introduction to Irreversible Electroporation--Principles and Techniques*. Tech Vasc Interv Radiol, 2015. **18**(3): p. 128-34.
6. Garcia, P.A., et al., *Non-thermal irreversible electroporation (N-TIRE) and adjuvant fractionated radiotherapeutic multimodal therapy for intracranial malignant glioma in a canine patient*. Technol Cancer Res Treat, 2011. **10**(1): p. 73-83.
7. Rossmeisl, J.H., Jr., et al., *Safety and feasibility of the NanoKnife system for irreversible electroporation ablative treatment of canine spontaneous intracranial gliomas*. J Neurosurg, 2015. **123**(4): p. 1008-25.
8. Ruarus, A.H., et al., *Irreversible Electroporation in Hepatopancreaticobiliary Tumours*. Can Assoc Radiol J, 2018. **69**(1): p. 38-50.

9. Tarantino, L., et al., *Irreversible electroporation of locally advanced solid pseudopapillary carcinoma of the pancreas: A case report*. *Ann Med Surg (Lond)*, 2018. **28**: p. 11-15.
10. Hong, Y., et al., *The use of IRE in multi-modality treatment for oligometastatic pancreatic cancer*. *Am J Surg*, 2018. **216**(1): p. 106-110.
11. Rodriguez, A., S.B. Tatter, and W. Debinski, *Neurosurgical Techniques for Disruption of the Blood-Brain Barrier for Glioblastoma Treatment*. *Pharmaceutics*, 2015. **7**(3): p. 175-87.
12. Sanchez, K., D. Page, and H.L. McArthur, *Immunotherapy in breast cancer: An overview of modern checkpoint blockade strategies and vaccines*. *Curr Probl Cancer*, 2016. **40**(2-4): p. 151-162.
13. Arena, C.B., et al., *High-frequency irreversible electroporation (H-FIRE) for non-thermal ablation without muscle contraction*. *Biomed Eng Online*, 2011. **10**: p. 102.
14. Lee, E.W., S. Thai, and S.T. Kee, *Irreversible electroporation: a novel image-guided cancer therapy*. *Gut Liver*, 2010. **4 Suppl 1**: p. S99-S104.
15. Lencioni, R. and L. Crocetti, *Image-guided ablation for hepatocellular carcinoma*. *Recent Results Cancer Res*, 2013. **190**: p. 181-94.
16. Goswami, I., et al., *Irreversible electroporation inhibits pro-cancer inflammatory signaling in triple negative breast cancer cells*. *Bioelectrochemistry*, 2017. **113**: p. 42-50.
17. Guo, S., et al., *Nano-pulse stimulation induces potent immune responses, eradicating local breast cancer while reducing distant metastases*. *Int J Cancer*, 2018. **142**(3): p. 629-640.

18. Kolb, J.F., S. Kono, and K.H. Schoenbach, *Nanosecond pulsed electric field generators for the study of subcellular effects*. *Bioelectromagnetics*, 2006. **27**(3): p. 172-87.
19. Pulaski, B.A. and S. Ostrand-Rosenberg, *Mouse 4T1 breast tumor model*. *Curr Protoc Immunol*, 2001. **Chapter 20**: p. Unit 20 2.
20. Lundt, J.E., et al., *Non-invasive, Rapid Ablation of Tissue Volume Using Histotripsy*. *Ultrasound Med Biol*, 2017. **43**(12): p. 2834-2847.
21. Zhang, H., et al., *High-voltage pulsed electric field plus photodynamic therapy kills breast cancer cells by triggering apoptosis*. *Am J Transl Res*, 2018. **10**(2): p. 334-351.
22. Kim, H.B., et al., *Changes of apoptosis in tumor tissues with time after irreversible electroporation*. *Biochem Biophys Res Commun*, 2013. **435**(4): p. 651-6.
23. Long, G., et al., *Histological and finite element analysis of cell death due to irreversible electroporation*. *Technol Cancer Res Treat*, 2014. **13**(6): p. 561-9.
24. Zhang, Z., et al., *Rapid dramatic alterations to the tumor microstructure in pancreatic cancer following irreversible electroporation ablation*. *Nanomedicine (Lond)*, 2014. **9**(8): p. 1181-92.
25. Man, S.M., R. Karki, and T.D. Kanneganti, *Molecular mechanisms and functions of pyroptosis, inflammatory caspases and inflammasomes in infectious diseases*. *Immunol Rev*, 2017. **277**(1): p. 61-75.
26. Deng, M., et al., *The Endotoxin Delivery Protein HMGB1 Mediates Caspase-11-Dependent Lethality in Sepsis*. *Immunity*, 2018. **49**(4): p. 740-753 e7.
27. Zhou, B., et al., *Tom20 senses iron-activated ROS signaling to promote melanoma cell pyroptosis*. *Cell Res*, 2018. **28**(12): p. 1171-1185.

28. Zha, Q.B., et al., *ATP-Induced Inflammasome Activation and Pyroptosis Is Regulated by AMP-Activated Protein Kinase in Macrophages*. *Front Immunol*, 2016. **7**: p. 597.
29. Benevides, L., et al., *IL17 Promotes Mammary Tumor Progression by Changing the Behavior of Tumor Cells and Eliciting Tumorigenic Neutrophils Recruitment*. *Cancer Res*, 2015. **75**(18): p. 3788-99.
30. Murugaiyan, G. and B. Saha, *Protumor vs antitumor functions of IL-17*. *J Immunol*, 2009. **183**(7): p. 4169-75.
31. Kim, K., et al., *Eradication of metastatic mouse cancers resistant to immune checkpoint blockade by suppression of myeloid-derived cells*. *Proc Natl Acad Sci U S A*, 2014. **111**(32): p. 11774-9.
32. Alaniz, L., M.M. Rizzo, and G. Mazzolini, *Pulsing dendritic cells with whole tumor cell lysates*. *Methods Mol Biol*, 2014. **1139**: p. 27-31.
33. Neal, R.E., 2nd and R.V. Davalos, *The feasibility of irreversible electroporation for the treatment of breast cancer and other heterogeneous systems*. *Ann Biomed Eng*, 2009. **37**(12): p. 2615-25.
34. Allen, I.C., et al., *The NLRP3 inflammasome mediates in vivo innate immunity to influenza A virus through recognition of viral RNA*. *Immunity*, 2009. **30**(4): p. 556-65.
35. Mariathasan, S., et al., *Cryopyrin activates the inflammasome in response to toxins and ATP*. *Nature*, 2006. **440**(7081): p. 228-32.
36. Willingham, S.B., et al., *NLRP3 (NALP3, Cryopyrin) facilitates in vivo caspase-1 activation, necrosis, and HMGB1 release via inflammasome-dependent and -independent pathways*. *J Immunol*, 2009. **183**(3): p. 2008-15.

37. Fang, L., et al., *Involvement of endoplasmic reticulum stress in albuminuria induced inflammasome activation in renal proximal tubular cells*. PLoS One, 2013. **8**(8): p. e72344.
38. van den Bos, W., et al., *The correlation between the electrode configuration and histopathology of irreversible electroporation ablations in prostate cancer patients*. World J Urol, 2016. **34**(5): p. 657-64.
39. Scheltema, M.J., et al., *Irreversible electroporation for the treatment of localized prostate cancer: a summary of imaging findings and treatment feedback*. Diagn Interv Radiol, 2017. **23**(5): p. 365-370.
40. Neal, R.E., 2nd, et al., *Treatment of breast cancer through the application of irreversible electroporation using a novel minimally invasive single needle electrode*. Breast Cancer Res Treat, 2010. **123**(1): p. 295-301.
41. Jose, A., et al., *Irreversible electroporation shows efficacy against pancreatic carcinoma without systemic toxicity in mouse models*. Cancer Lett, 2012. **317**(1): p. 16-23.
42. Su, J.J., et al., *Histological analysis of human pancreatic carcinoma following irreversible electroporation in a nude mouse model*. World J Gastrointest Oncol, 2018. **10**(12): p. 476-486.
43. Neal, R.E., 2nd, et al., *Improved local and systemic anti-tumor efficacy for irreversible electroporation in immunocompetent versus immunodeficient mice*. PLoS One, 2013. **8**(5): p. e64559.

FIGURES

Figure 1: High Frequency Irreversible Electroporation (H-FIRE) Induces Inflammatory Cell Death and Effectively Attenuates the Tumor Promoting Microenvironment *In Vitro*

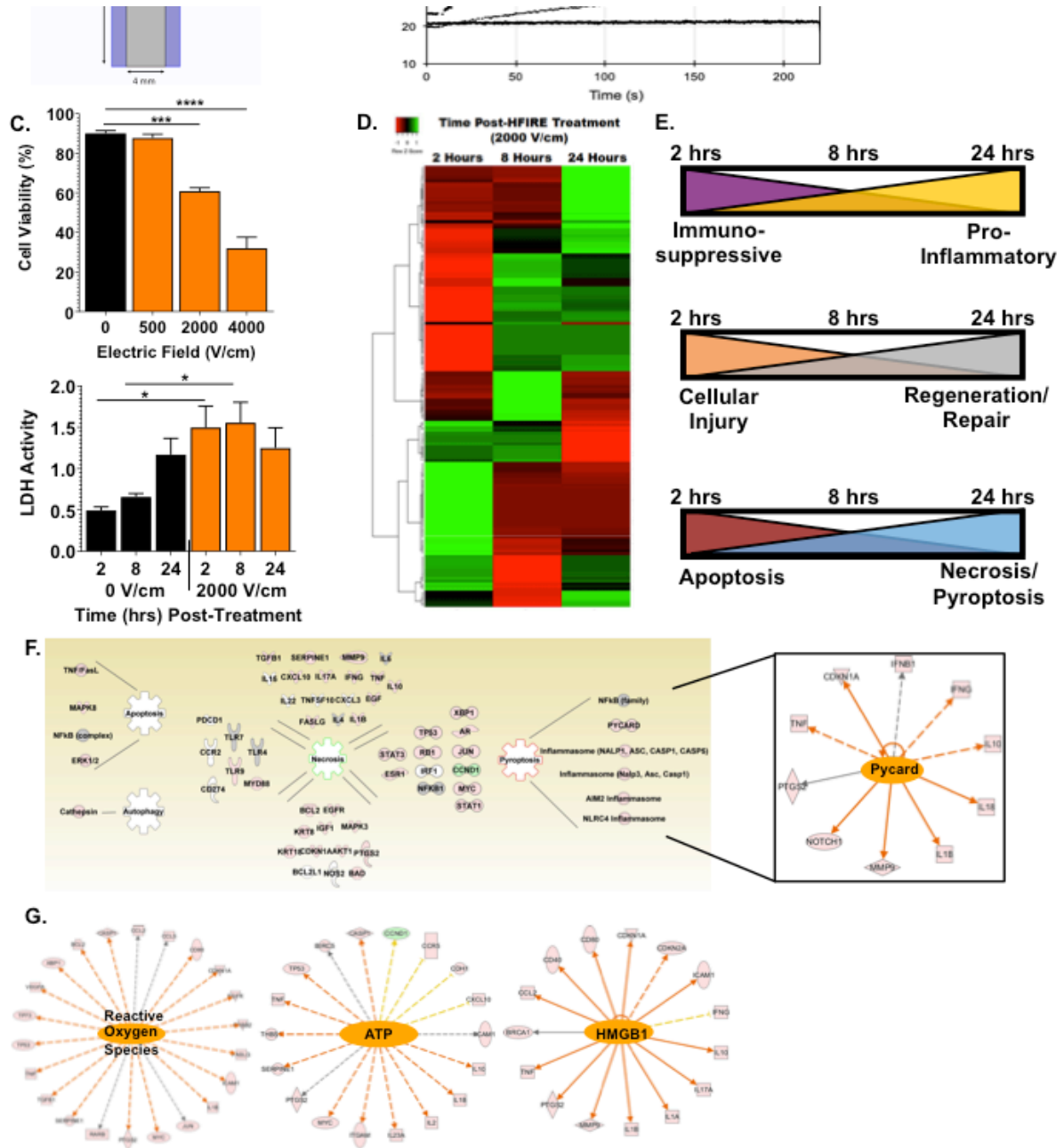


Figure 1. High Frequency Irreversible Electroporation (H-FIRE) Induces Inflammatory Cell Death and Effectively Attenuates the Tumor Promoting Microenvironment *In Vitro*.

H-FIRE was administered using 200 bursts, in a 2-5-2 waveform, and with a uniform voltage of either 240 V, 800 V, or 1600 V across the 4 mm cuvette totaling 500, 2000, or 4000 V/cm, respectively. **A.** Schematic of H-FIRE delivery to 4T1 cells in a 4mm cuvette. **B.** Temperature during *in vitro* H-FIRE treatment. At 2000V/cm, cell suspension temperature remains below 30°C. **C.** Influence of electric pulse parameters on cell viability. Cell viability was determined via trypan blue (manual) and AO/PI staining (automated); the average percent viability shown. LDH Activity was utilized to evaluate cell death at 2000 V/cm over time. **D-H.** Real time PCR-based gene expression arrays were utilized to evaluate the expression of 162 genes associated with cancer and inflammation. **D.** Heat map of gene expression changes at 2, 8, and 24 hours following H-FIRE treatment with 2000 V/cm. **E.** Ingenuity Pathway Analysis (IPA) of gene expression data revealed significant shifts in pathways associated with inflammation, injury/repair, and cell death. **F.** Gene expression analysis further indicates that necrosis and pyroptosis are the dominant forms of cell death 24 hours post-H-FIRE treatment. **G.** IPA identified significant changes in pathways associated with reactive oxygen species, adenosine triphosphate, and HMGB1 signaling. All studies were repeated at least 3 times. *p<0.05.

Figure 2: H-FIRE Treatment Results in Significant Tumor Ablation in the *In Vivo* 4T1 Mammary Tumor Model

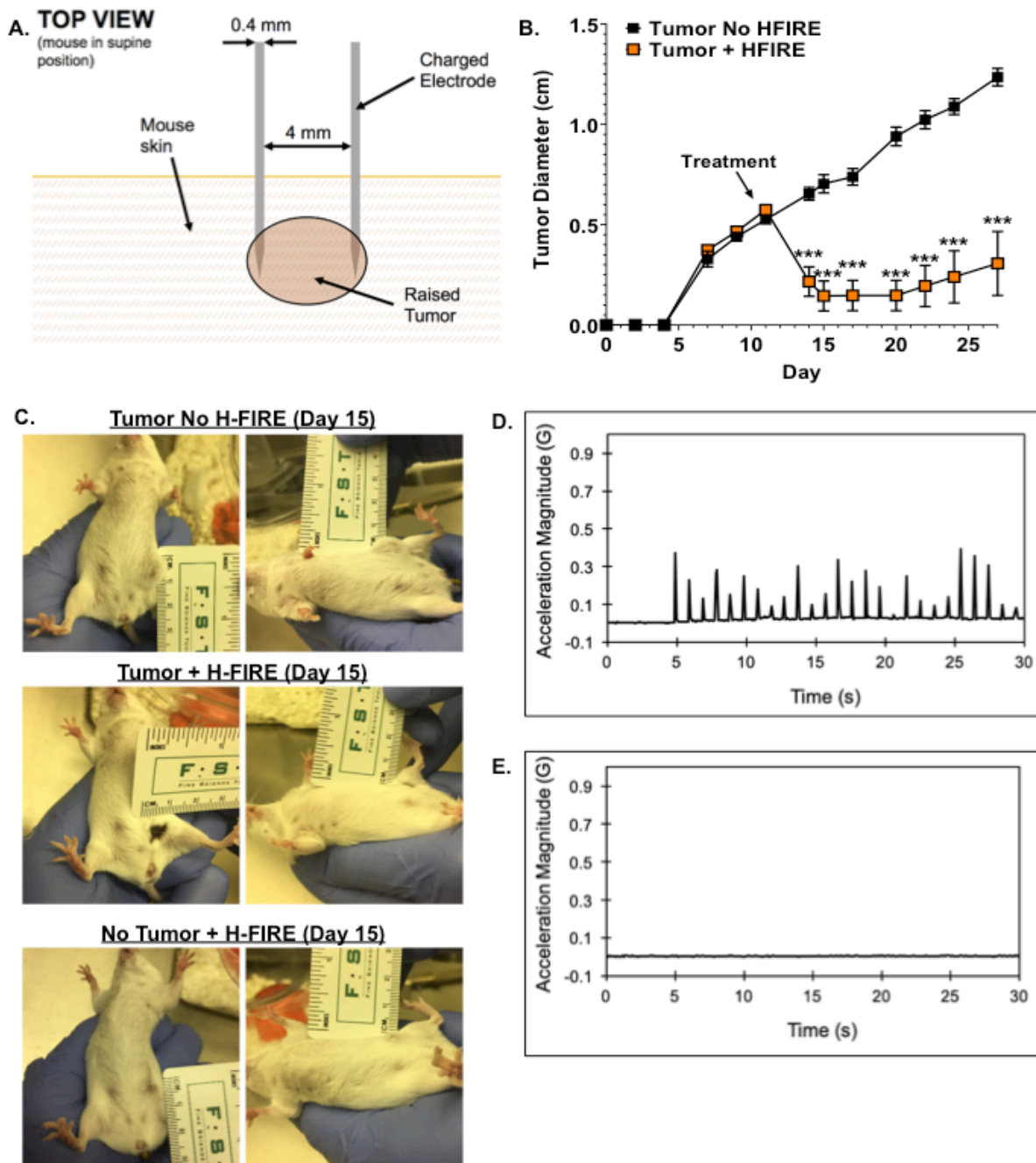


Figure 2. H-FIRE Treatment Results in Significant Tumor Ablation in the *In Vivo* 4T1 Mammary Tumor Model. Mice were injected with 1.2×10^6 4T1 cells into the mammary fat pad of wild type BALB/c mice. On day 11, mice were anesthetized and needle probes were

inserted into the tumor to deliver 2,500 V/cm H-FIRE with a 2-5-2 waveform for 25 cycles per burst, totaling 200 bursts. Animals were monitored a least 3 times/week for clinical parameters and tumor progression. **A.** Schematic illustrating treatment strategy and probe placement. **B.** Tumor diameter changes following H-FIRE reveals significant decreases in tumor diameter and progression. **C.** Images of tumors from representative animals 15 days post-H-FIRE treatment. 4T1 tumor/H-FIRE sham treatment (top panels); 4T1 tumors and H-FIRE treatment (middle panels); no tumor/no H-FIRE treatment (bottom panels). **D.** Accelerometer output at 2000V/cm IRE. **E.** Accelerometer output at 2000V/cm H-FIRE. n = 3-10 mice in each experimental group. *** $p \leq 0.001$.

Figure 3: H-FIRE Ablation Results in Significant Cell Death and Inflammation

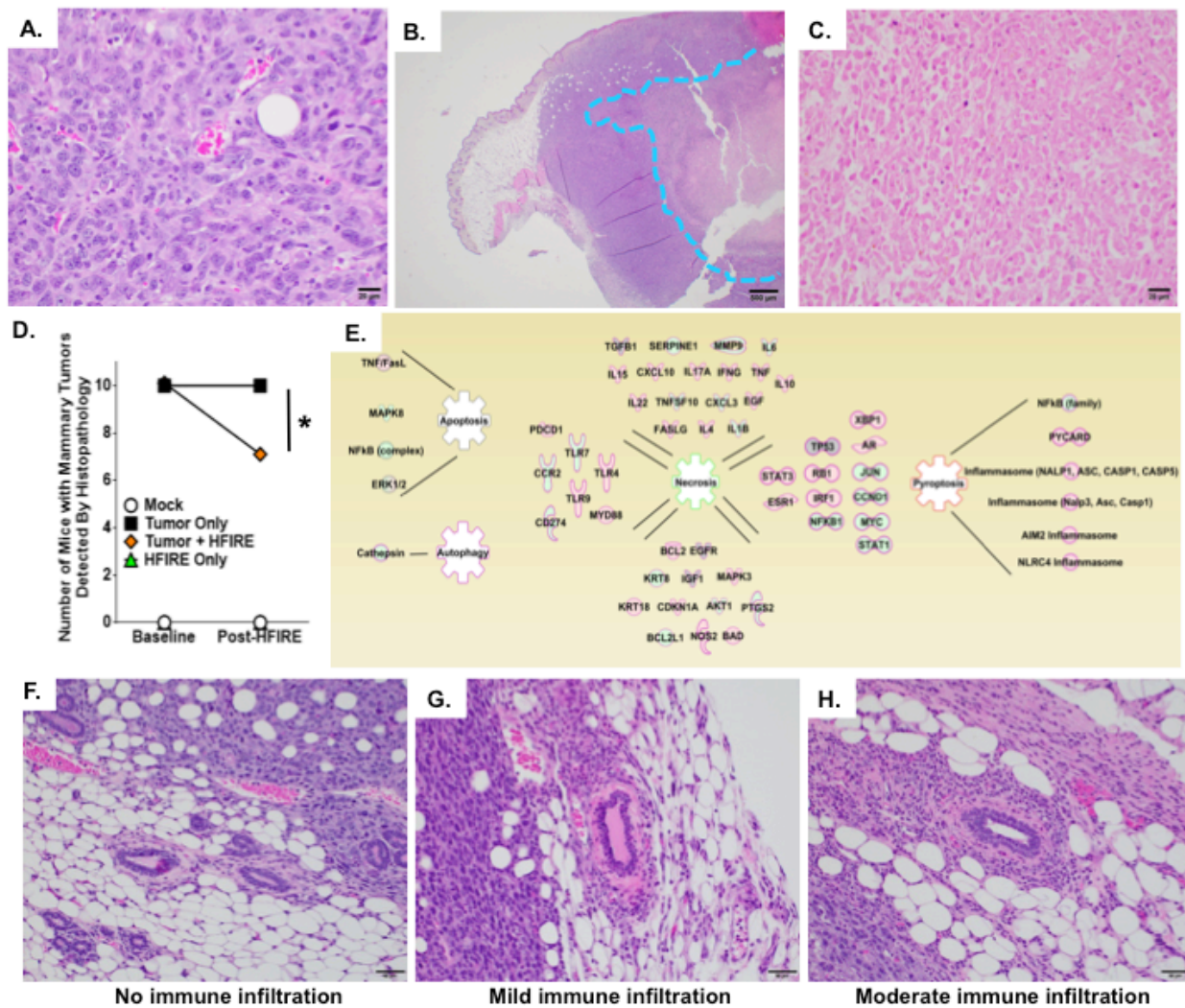


Figure 3. H-FIRE Ablation Results in Significant Cell Death and Inflammation.

Histopathology evaluation revealed significant signs of cell death in the 4T1 mammary tumor that was increased following H-FIRE. **A.** The architecture of the untreated 4T1 tumors remains intact, with aggressively proliferating neoplastic cells obliterating normal subcutaneous structures. **B.** The central core of these large tumors often contains abundant necrosis, and can be visually distinguished from the rest of the neoplasm (blue line). **C.** Following H-FIRE application, neoplastic cells in the treatment zone undergo cell death as evidenced by nuclear

pyknosis and loss, cytoplasmic blanching, and disintegration of cellular architecture. **D.** Pathology assessments of the H-FIRE treated areas revealed a significant decrease in histologically identifiable mammary tumors. **E.** Gene expression arrays were utilized to evaluate 156 genes associated with cancer and inflammation. IPA analysis revealed that necrosis and pyroptosis are significantly increased and are the dominant pathways associated with cell death following H-FIRE treatment compared to the untreated 4T1 tumors *in vivo*. **F.** Typical 4T1 tumors are relatively immunosuppressive with minimal immune cell infiltration. **G-H.** Following H-FIRE, histopathology revealed increased inflammation. This inflammation could be further sub-classified as either **(G)** mild or **(H)** moderate. n = 3-10 mice in each group. *p_≤0.05.

Figure 4: Tumor Response to H-FIRE Ablation is Correlated with Increased Cellular Immunity

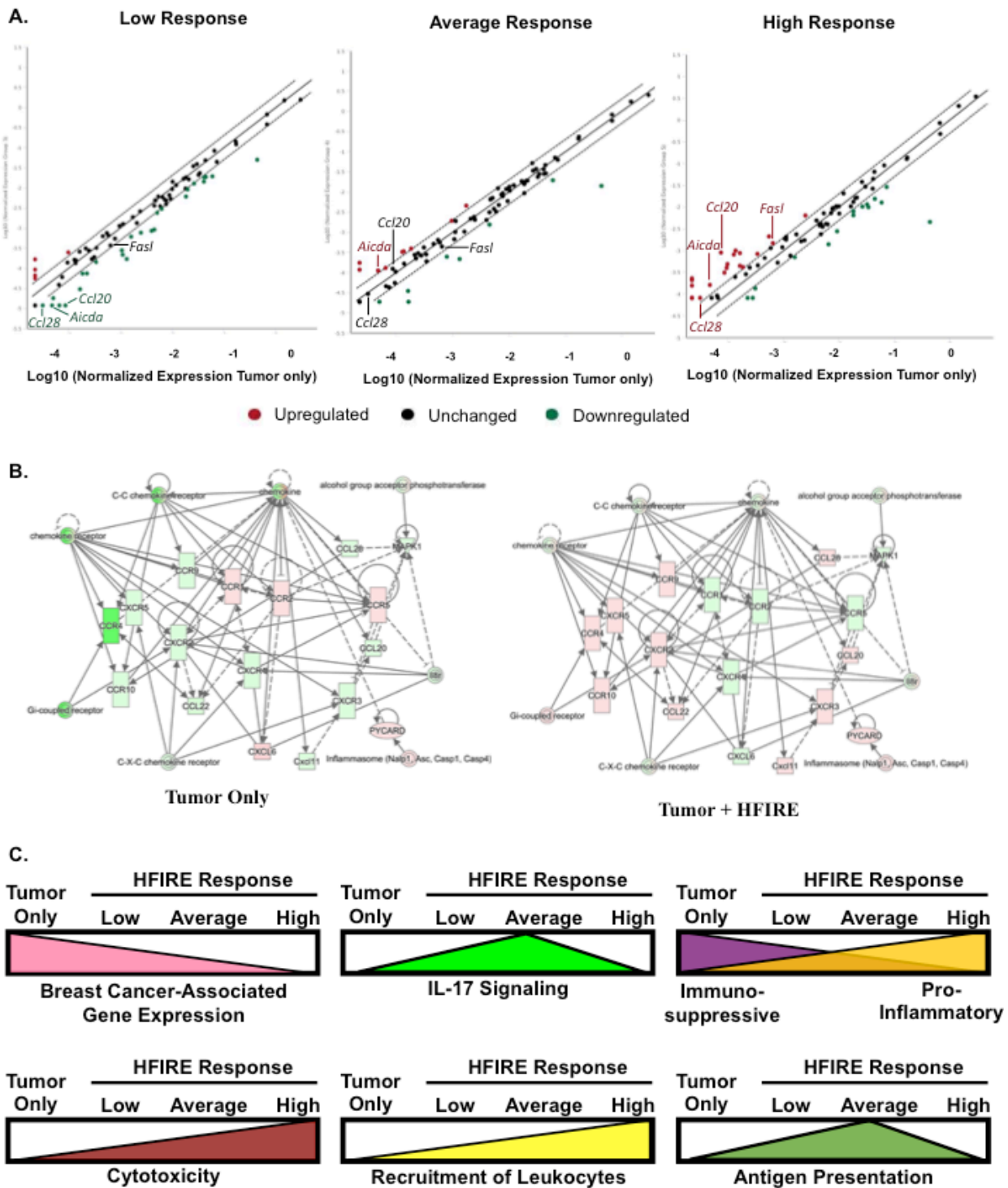


Figure 4. Tumor Response to H-FIRE Ablation is Correlated with Increased Cellular Immunity. At necropsy 15 days post H-FIRE, tumor specimens were collected and total RNA was extracted for gene expression profiling. Data were analyzed based on the % of tumor ablation following H-FIRE (low response $\leq 85\%$ ablation; average response = 85% - 94% ablation; high response $\geq 95\%$ ablation). **A.** The up-regulation of genes associated with cellular immunity are strongly correlated with tumor ablation. In tumors classified in the low-responder group, a significant number of genes associated with cellular immunity were down-regulated. Conversely, a significant number of genes were up-regulated in the animals that saw the highest levels of tumor ablation. **B.** Chemokine signaling networks were the most impacted by H-FIRE treatment, with highly responsive tumors demonstrating a significant up-regulation compared to the other groups. **C.** Further pathway analysis identified 6 additional signaling networks that were significantly impacted by H-FIRE treatment response. We observed a significant decrease in breast cancer-associated gene expression and immunosuppression from untreated to high therapeutic response. Conversely, we observed a significant increase in gene expression associated with inflammation, cytotoxicity, and recruitment of leukocytes over the same treatment scale. We also observed a significant increase in IL-17 signaling and antigen presentation that was highest in the animals with average responses. $n = 3-10$ mice in each group.

Figure 5: H-FIRE Treatment Significantly Alters Local Immune Cell Populations in the 4T1 Tumor Microenvironment

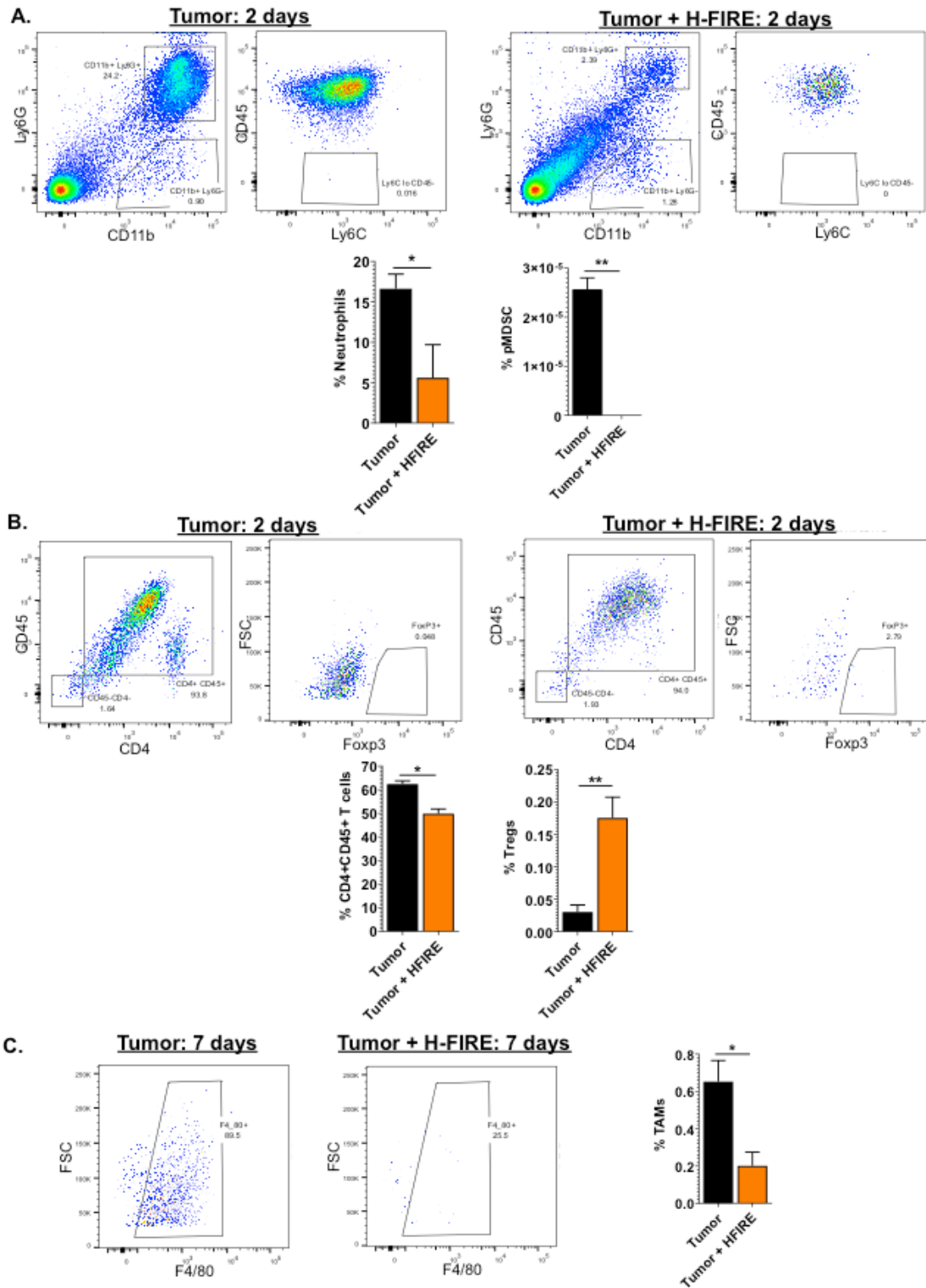


Figure 5. H-FIRE Treatment Significantly Alters Local Immune Cell Populations in the 4T1 Tumor Microenvironment. Mice were treated with H-FIRE and tumors were harvested at 2 and 7 days post-treatment. Single cell suspensions were generated from each tumor and labeled for flow cytometry. **A.** 2 days after H-FIRE, the treated groups showed significant reduction in CD11b⁺LY6G⁺ cells, representing neutrophil populations, and CD11b⁺LY6G⁺Ly6C^{lo}CD45⁻ cells, representing pMDSC populations. **B.** Significant decreases were observed in CD4⁺CD45⁺ T helper cells, while significant increases were observed in CD4⁺CD45⁺CD25^{hi}CD127^{lo}Foxp3⁺ Treg population. **C.** CD11b⁺Ly6G⁻Ly6C⁻CD45⁺F4/80⁺ Tumor Associated Macrophage populations were significantly decreased 7 days post-treatment. n=4 mice in each group. *p≤0.05; **p≤0.01.

Figure 6: Local H-FIRE Treatment Attenuates Metastatic Lesions in Immunocompetent mice

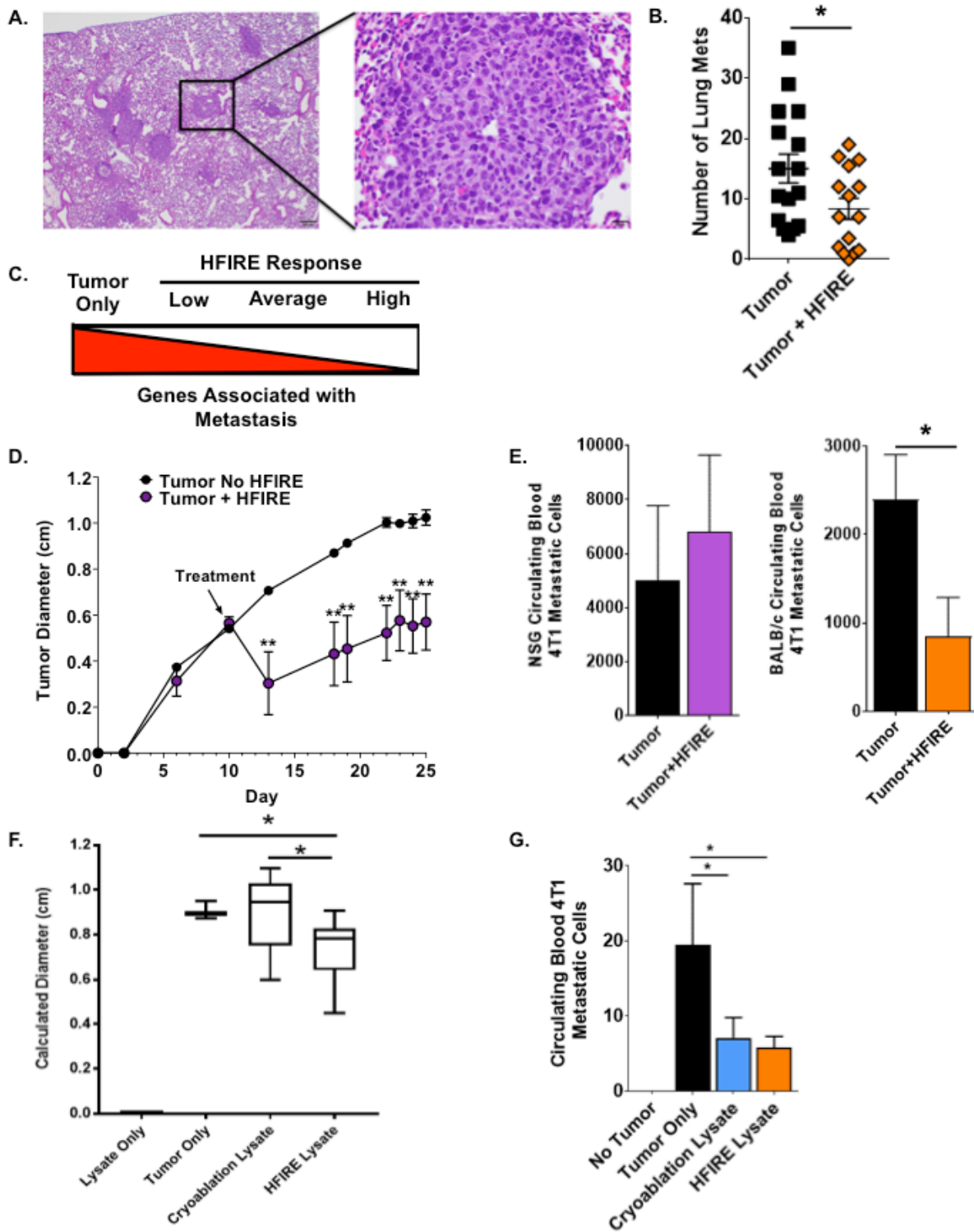


Figure 6. Local H-FIRE Treatment Attenuates Metastatic Lesions in Immunocompetent mice. Lung and blood metastasis is typical in the 4T1 tumor model. **A.** Histopathology evaluation of the lungs revealed 4T1 metastatic lesions in all of the animals that were not treated with H-FIRE. **B.** Pathologic enumeration of metastatic lesions revealed a significant decrease in lung metastases in animals 15 days post-H-FIRE treatment compared to untreated animals. **C.** Gene expression in the primary tumor post-H-FIRE revealed a significant decrease in signaling pathways associated with tumor metastasis in animals with tumors that were highly responsive to H-FIRE ablation. **D-E.** Metastasis attenuation depends on an intact immune system. Nod Scid Gamma (NSG) mice were injected with 1.2×10^6 4T1 cells into the mammary fat pad, treated with H-FIRE (2-5-2 waveform, 2500V/cm), and tumor progression was monitored. **D.** A significant attenuation in tumor progression was observed in the NSG mice; however, no tumors reached complete ablation. **E.** Whole blood was collected from both NSG and BALB/c mice and plated under 6-thioguanine selection. A significant number of metastatic cells were observed in the NSG mice, regardless of H-FIRE treatment. In the BALB/c mice, a significant reduction in average circulating 4T1 metastatic cells was observed in animals treated with H-FIRE. **F-G.** 4T1 cells were treated with either H-FIRE (2-5-2 waveform, 2000 V/cm) or cryoablation (liquid Nitrogen to 37°C , 3 freeze-thaw cycles). Cell-free lysates were generated and injected (i.v.) into wild type BALB/c mice. Mice were injected with 1.2×10^6 4T1 cells into the mammary fat pad 10 days post-injection of cell-free lysate. **F.** At necropsy, the calculated tumor diameter of mice treated with the H-FIRE lysate was significantly decreased compared to both untreated tumor only (19% reduction) and cryoablation lysate (17% reduction). **G.** Circulating blood 4T1 metastatic cells were quantified at necropsy. Both cyroablation lysate and H-FIRE lysate

treatment significantly attenuated 4T1 metastasis. n = 3-10 mice in each group. * $p \leq 0.05$;
** $p \leq 0.01$.

SUPPLEMENTAL DATA

Supplemental Table S1

A. List of Genes Profiled *In Vitro* and Evaluated Using Ingenuity Pathway Analysis

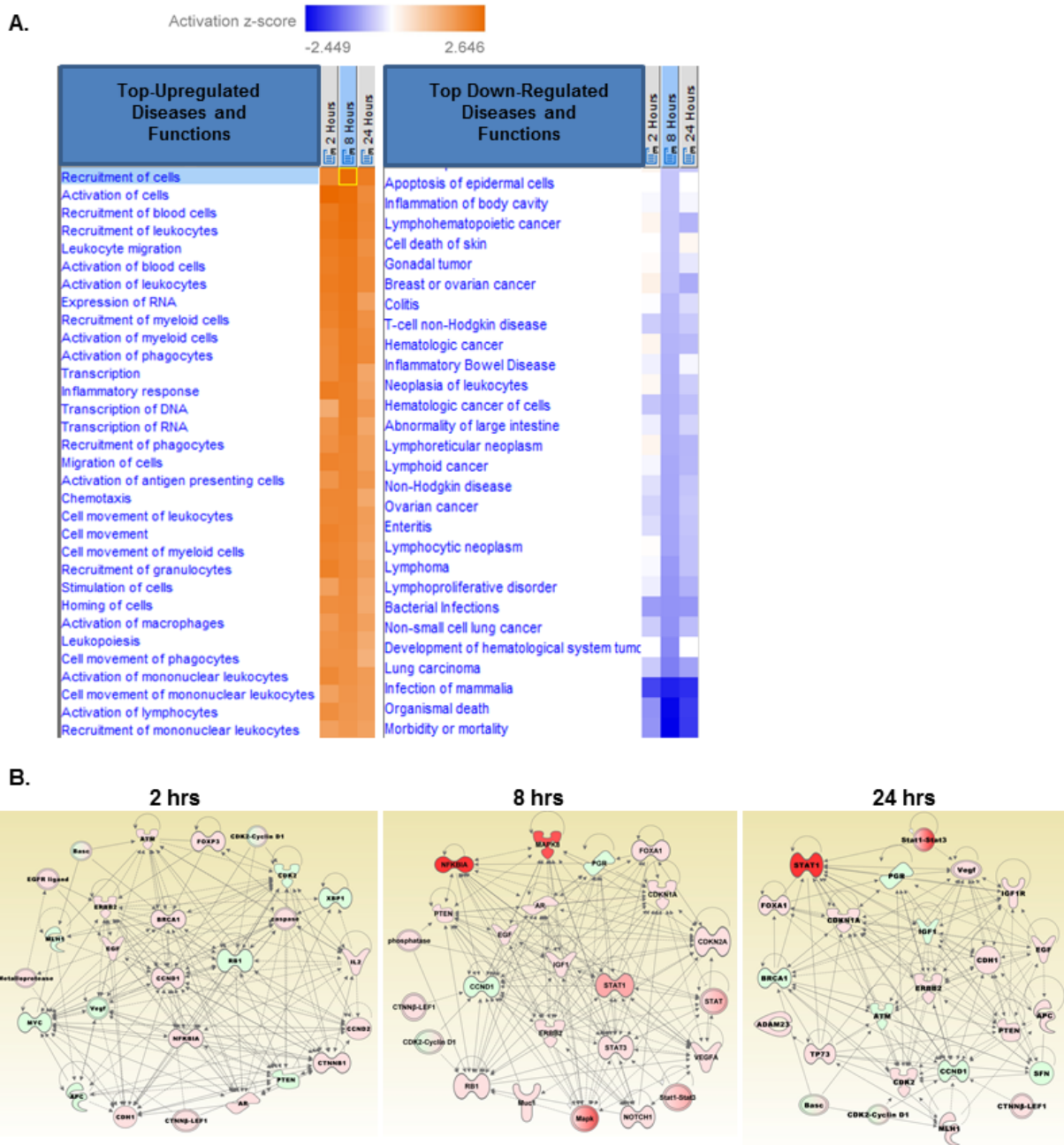
<i>Abcb1a</i>	<i>Csf1</i>	<i>Krt5</i>	<i>Rb1</i>	<i>Ccr4</i>	<i>Ifnar1</i>	<i>Mbl2</i>	<i>Tlr5</i>
<i>Abcg2</i>	<i>Cst6</i>	<i>Krt8</i>	<i>Serpine1</i>	<i>Ccr5</i>	<i>Ifnb1</i>	<i>Mpo</i>	<i>Tlr6</i>
<i>Adam23</i>	<i>Ctnnb1</i>	<i>Mapk3</i>	<i>Sfn</i>	<i>Ccr6</i>	<i>Ifng</i>	<i>Mx1</i>	<i>Tlr7</i>
<i>Akt1</i>	<i>Ctsd</i>	<i>Mapk8</i>	<i>Sfrp1</i>	<i>Ccr8</i>	<i>Ifngr1</i>	<i>Myd88</i>	<i>Tlr8</i>
<i>Apc</i>	<i>Egf</i>	<i>Mgmt</i>	<i>Slc39a6</i>	<i>Cd14</i>	<i>Il10</i>	<i>Nfkb1</i>	<i>Tlr9</i>
<i>Ar</i>	<i>Egfr</i>	<i>Mki67</i>	<i>Slit2</i>	<i>Cd4</i>	<i>Il13</i>	<i>Nfkbia</i>	<i>Tnf</i>
<i>Atm</i>	<i>Erb2</i>	<i>Mlh1</i>	<i>Snai2</i>	<i>Cd40</i>	<i>Il17a</i>	<i>Nlrp3</i>	<i>Traf6</i>
<i>Bad</i>	<i>Esr1</i>	<i>Mmp2</i>	<i>Src</i>	<i>Cd40lg</i>	<i>Il18</i>	<i>Nod1</i>	<i>Tyk2</i>
<i>Bcl2</i>	<i>Esr2</i>	<i>Mmp9</i>	<i>Tff3</i>	<i>Cd80</i>	<i>Il1a</i>	<i>Nod2</i>	
<i>Birc5</i>	<i>Foxa1</i>	<i>Muc1</i>	<i>Tgfb1</i>	<i>Cd86</i>	<i>Il1b</i>	<i>Rag1</i>	
<i>Brca1</i>	<i>Gli1</i>	<i>Myc</i>	<i>Thbs1</i>	<i>Cd8a</i>	<i>Il1r1</i>	<i>Rorc</i>	
<i>Brca2</i>	<i>Grb7</i>	<i>Nme1</i>	<i>Trp53</i>	<i>Crp</i>	<i>Il2</i>	<i>Slc11a1</i>	
<i>Ccna1</i>	<i>Gstp1</i>	<i>Notch1</i>	<i>Trp73</i>	<i>Csf2</i>	<i>Il23a</i>	<i>Stat1</i>	
<i>Ccnd1</i>	<i>Hic1</i>	<i>Nr3c1</i>	<i>Twist1</i>	<i>Cxcl10</i>	<i>Il4</i>	<i>Stat3</i>	
<i>Ccnd2</i>	<i>Id1</i>	<i>Pgr</i>	<i>Vegfa</i>	<i>Cxcr3</i>	<i>Il5</i>	<i>Stat4</i>	
<i>Ccne1</i>	<i>Igf1</i>	<i>Plau</i>	<i>Xbp1</i>	<i>Ddx58</i>	<i>Irak1</i>	<i>Stat6</i>	
<i>Cdh1</i>	<i>Igf1r</i>	<i>Prdm2</i>	<i>Apcs</i>	<i>Fasl</i>	<i>Irf3</i>	<i>Tbx21</i>	
<i>Cdh13</i>	<i>Igfbp3</i>	<i>Pten</i>	<i>C3</i>	<i>Foxp3</i>	<i>Irf7</i>	<i>Ticam1</i>	
<i>Cdk2</i>	<i>Il6</i>	<i>Ptgs2</i>	<i>C5ar1</i>	<i>H2-Q10</i>	<i>Iltgam</i>	<i>Tlr1</i>	
<i>Cdkn1a</i>	<i>Jun</i>	<i>Pycard</i>	<i>Casp1</i>	<i>H2-T23</i>	<i>Jak2</i>	<i>Tlr2</i>	
<i>Cdkn1c</i>	<i>Krt18</i>	<i>Rarb</i>	<i>Ccl12</i>	<i>Icam1</i>	<i>Ly96</i>	<i>Tlr3</i>	
<i>Cdkn2a</i>	<i>Krt19</i>	<i>Rassf1</i>	<i>Ccl5</i>	<i>Ifna2</i>	<i>Ly22</i>	<i>Tlr4</i>	

B. List of Genes Profiled *In Vivo* and Evaluated Using Ingenuity Pathway Analysis

<i>Aicda</i>	<i>Cxcl11</i>	<i>Il10</i>	<i>Ptgs2</i>	<i>Brca2</i>	<i>Id1</i>	<i>Prdm2</i>	
<i>Bcl2</i>	<i>Cxcl12</i>	<i>Il12a</i>	<i>Spp1</i>	<i>Ccna1</i>	<i>Igf1</i>	<i>Pten</i>	
<i>Bcl2l1</i>	<i>Cxcl2</i>	<i>Il12b</i>	<i>Stat1</i>	<i>Ccnd1</i>	<i>Igf1r</i>	<i>Pycard</i>	
<i>Ccl2</i>	<i>Cxcl5</i>	<i>Il13</i>	<i>Stat3</i>	<i>Ccnd2</i>	<i>Igfbp3</i>	<i>Rarb</i>	
<i>Ccl20</i>	<i>Cxcl9</i>	<i>Il15</i>	<i>Tgfb1</i>	<i>Ccne1</i>	<i>Jun</i>	<i>Rassf1</i>	
<i>Ccl22</i>	<i>Cxcr1</i>	<i>Il17a</i>	<i>Tlr2</i>	<i>Cdh1</i>	<i>Krt18</i>	<i>Rb1</i>	
<i>Ccl28</i>	<i>Cxcr2</i>	<i>Il1a</i>	<i>Tlr3</i>	<i>Cdh13</i>	<i>Krt19</i>	<i>Serpine1</i>	
<i>Ccl4</i>	<i>Cxcr3</i>	<i>Il1b</i>	<i>Tlr4</i>	<i>Cdk2</i>	<i>Krt5</i>	<i>Sfn</i>	
<i>Ccl5</i>	<i>Cxcr4</i>	<i>Il1r1</i>	<i>Tlr7</i>	<i>Cdkn1a</i>	<i>Krt8</i>	<i>Sfrp1</i>	
<i>Ccr1</i>	<i>Cxcr5</i>	<i>Il2</i>	<i>Tlr9</i>	<i>Cdkn1c</i>	<i>Mapk1</i>	<i>Slc39a6</i>	
<i>Ccr10</i>	<i>Egf</i>	<i>Il22</i>	<i>Tnf</i>	<i>Cdkn2a</i>	<i>Mapk3</i>	<i>Slit2</i>	
<i>Ccr2</i>	<i>Egfr</i>	<i>Il23a</i>	<i>Tnfsf10</i>	<i>Cst6</i>	<i>Mapk8</i>	<i>Snai2</i>	
<i>Ccr4</i>	<i>Fasl</i>	<i>Il4</i>	<i>Trp53</i>	<i>Ctnnb1</i>	<i>Mgmt</i>	<i>Src</i>	
<i>Ccr5</i>	<i>Foxp3</i>	<i>Il5</i>	<i>Vegfa</i>	<i>Ctsd</i>	<i>Mki67</i>	<i>Tff3</i>	
<i>Ccr7</i>	<i>Gbp2b</i>	<i>Il6</i>	<i>Abcg2</i>	<i>Erb2</i>	<i>Mlh1</i>	<i>Thbs1</i>	
<i>Ccr9</i>	<i>Gzma</i>	<i>Irf1</i>	<i>Adam23</i>	<i>Esr1</i>	<i>Mmp2</i>	<i>Trp73</i>	
<i>Cd274</i>	<i>Gzmb</i>	<i>Kitl</i>	<i>Akt1</i>	<i>Esr2</i>	<i>Mmp9</i>	<i>Twist1</i>	
<i>Csf1</i>	<i>H2-D1</i>	<i>Mif</i>	<i>Apc</i>	<i>Foxa1</i>	<i>Muc1</i>	<i>Xbp1</i>	
<i>Csf2</i>	<i>H2-K1</i>	<i>Myc</i>	<i>Ar</i>	<i>Gata3</i>	<i>Nme1</i>		
<i>Csf3</i>	<i>Hif1a</i>	<i>Myd88</i>	<i>Atm</i>	<i>Gli1</i>	<i>Notch1</i>		
<i>Ctla4</i>	<i>Ido1</i>	<i>Nfkb1</i>	<i>Bad</i>	<i>Grb7</i>	<i>Nr3c1</i>		
<i>Cxcl1</i>	<i>Ifng</i>	<i>Nos2</i>	<i>Birc5</i>	<i>Gstp1</i>	<i>Pgr</i>		
<i>Cxcl10</i>	<i>Igf1</i>	<i>Pdcd1</i>	<i>Brca1</i>	<i>Hic1</i>	<i>Plau</i>		

Supplemental Table S1. Real time PCR based gene expression arrays were utilized to evaluate gene expression and modeled using Ingenuity Pathway Analysis software and RT² Profiler online tools. **A.** Table of 162 genes evaluated in *in vitro* 4T1 studies. **B.** Table of 156 genes evaluated in *in vivo* mammary tumor studies.

Supplemental Figure S2: IPA identified multiple diseases and biological functions significantly altered following H-FIRE treatment of 4T1 cells



Supplemental Figure S2. IPA identified multiple diseases and biological functions significantly altered following H-FIRE treatment of 4T1 cells. A. Top 20 diseases and biological functions predicted to be either up-regulated or down-regulated by H-FIRE treatment,

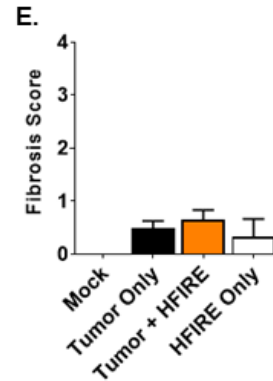
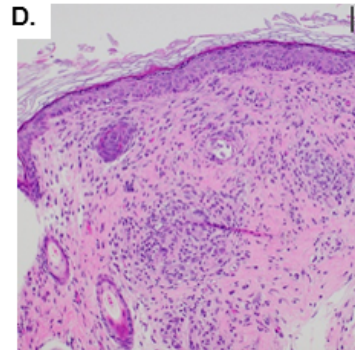
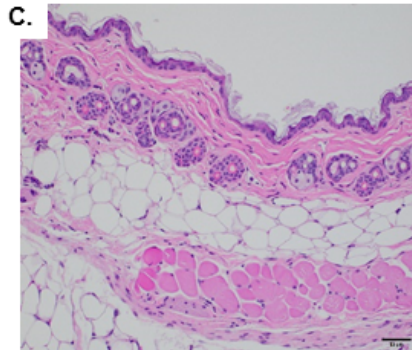
based on gene expression data. **B.** Relationships between the top genes altered following H-FIRE treatment at 2, 8, 24 hours post-treatment.

Supplemental Figure S3: Minimum muscle contraction and movement associated with H-FIRE treatment

A. Movie: IRE 2000 V/cm² to mammary tumor



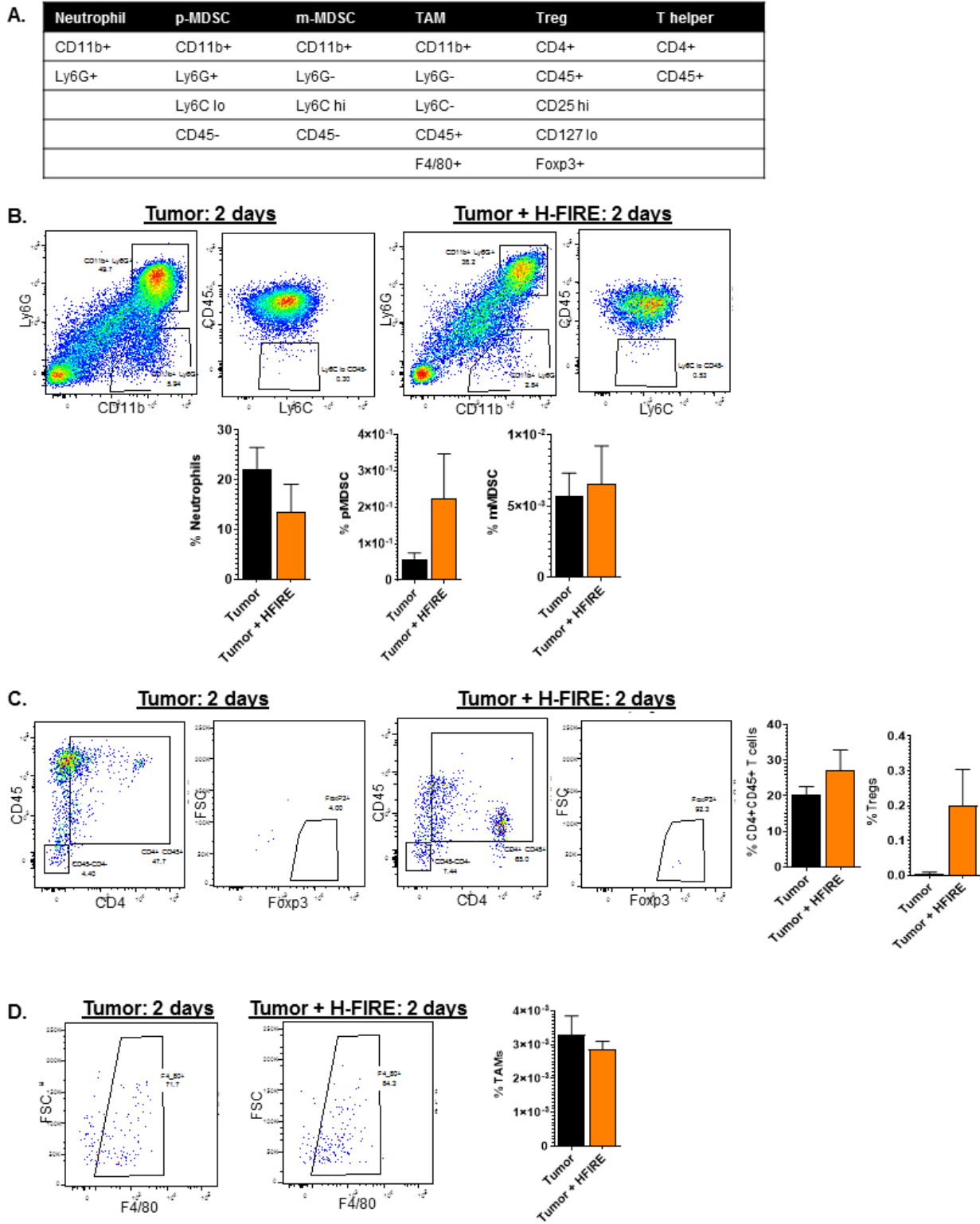
B. Movie: H-FIRE 2000 V/cm² to mammary tumor



Supplemental Figure S3. Minimum muscle contraction and movement associated with H-FIRE treatment. Mice were injected with 1.2×10^6 4T1 cells into the mammary fat pad of wild type BALB/c mice. Control mice (No Tumor) received the same volume of sterile PBS. On days 10-11, mice were anesthetized and maintained on isoflurane anesthesia during electroporation treatment, and needle probes were inserted into the tumor. **A.** Significant muscle contraction occurring during IRE treatment of 4T1 mammary tumor with 2000 V/cm. **B.** Minimal muscle

contraction occurring during H-FIRE treatment of 4T1 mammary tumor with 2000 V/cm. **C-D.** Scab formation following treatment is superficial and limited to the skin. **E.** Histopathology assessments and scoring revealed low levels of fibrin deposition, graded on a binary score detecting fibrosis.

Supplemental Figure S4: Immune cell populations in the microenvironment after H-FIRE ablation return over time



Supplemental Figure S4. Immune cell populations in the microenvironment after H-FIRE ablation return over time. A. Gating strategy for cells isolated from the 4T1 tumors. **B.** H-FIRE resulted in no significant changes in $CD11b^+Ly6G^+$ cells (neutrophils), $CD11b^+Ly6G^+Ly6C^{lo}CD45^-$ cells (pMDSCs), $CD11b^+Ly6G^+Ly6C^{hi}CD45^-$ cells (mMDSCs), at 7 days. **C.** $CD4^+CD45^+$ T helper cells, and $CD4^+CD45^+CD25^{hi}CD127^{lo}Foxp3^+$ cells (Tregs) 7 days post-treatment in the tumor. **D.** $CD11b^+Ly6G^-Ly6C^-CD45^+F4/80^+$ cells (TAMs) were not different 2 days post-treatment. n=4 for all groups.

Chapter Five

The Role of Nanotechnology in Detection and Treatment in Gastrointestinal Cancers

Veronica M. Ringel, Irving C. Allen

Reprinted from Gastrointestinal Cancers: Prevention, Detection and Treatment, Volume 2, VM Ringel, IC Allen, "The Role of Nanotechnology in Detection and Treatment in Gastrointestinal Cancers," pp. 271-290, (2016), with permission from Nova Science Publishers Inc., under license number 4534231394446. Full citation: VM Ringel, IC Allen. (2016). The Role of Nanotechnology in Detection and Treatment in Gastrointestinal Cancers. *In Gastrointestinal Cancers: Prevention, Detection and Treatment, Volume 2.* Amit Tyagi and Sahdeo Prasad, eds. New York: NOVA Science Publishers, pp. 271-290.

ABSTRACT

Gastrointestinal (GI) cancers include some of the most relevant malignancies worldwide. The poor prognoses associated with many GI cancers are motivation to develop more specific therapeutic and diagnostic options. Over the last decade, significant progress has been made in the application of nanotechnology to address the highly complex clinical needs of diverse GI cancers. Specifically, targeted drug delivery, controlled release and biodistribution remain the three most challenging aspects of therapeutic effectiveness in the gut. Likewise, imaging of the

GI tract and cancer diagnostics have made significant advances over the last decade, but are still sub-optimal in many respects. Recent developments in nanotechnology specifically address these issues and have begun to yield a plethora of newly approved products for use in GI cancers. Here, we review a variety of the most promising applications of nanotechnology in the context of GI cancer, with a focus on nanocarriers and nanoparticles. Nanotechnology provides clinicians with opportunities for improved care of patients with devastating malignancies in the GI tract. Ongoing and future research are constantly improving our approach to treating GI cancer and providing opportunities for cancer care that did not exist several years ago. Although there is still significant progress to be made in the field, the application of nanotechnology to GI cancers is likely to dramatically improve disease pathogenesis.

INTRODUCTION

Nanotechnology is a comprehensive term, referring to a wide range of technology that operates on the nanoscale. The term “nanotechnology” was first used by Norio Taniguchi in 1974 in a conference for the Society of Precision Engineering [1]. Although it has its origins in a lecture given by Richard Feynman (Nobel Prize in Physics, 1965) at a meeting of the American Physical Society in 1959 [2]. In this theoretical lecture, Feynman imagined the possibility of working and manufacturing on the atomic level, acknowledging that working with atoms at this level would result in different properties and laws. Feynman envisioned that “maneuvering things atom by atom” could be applicable to both chemistry and biology, expressing the possibility of an object with the capability to function on the scale of a biological cell. However, a limiting factor cited by Feynman was the lack of an adequate tool to visualize such particles, and he called for improvements to the microscope [2]. Therefore, the discovery and development of improved microscopy, including scanning tunneling microscopes (STM), transmission electron microscopes (TEM) and atomic force microscopes (AFM) was a crucial step in the history of nanotechnology. The application of nanotechnology to the field of medicine is termed “nanomedicine.”

The use of nanotechnology for cancer applications has gained significant interest in the past few decades. This chapter will introduce nanotechnology and give a brief description of several relevant forms of nanomedicine before delving into the current status of nanotechnology in the detection and treatment of gastrointestinal (GI) cancers. GI cancer is one of the most devastating malignancies worldwide [3]. The poor prognosis associated with GI cancer is motivation to find novel, more specific therapeutic and diagnostic options. The application of nanotechnology for the treatment and/or diagnosis of GI cancer is ever growing, whether

specifically designed for GI tumors or initially developed for use with a different tumor type [4]. Over the last decade, research and usage of nanotechnology targeting GI cancer has significantly expanded from the bench to the clinic. For example, a recent search of the National Institutes of Health database of clinical trials (clinicaltrials.gov) revealed 211 trials currently on-going involving nanoparticles and GI cancer. A selection of these studies is shown in **Table 1**.

NANOPARTICLES

The definition of a “nanoparticle” is relatively broad: a particle that exists in the nanoscale, with at least one dimension smaller than 100 nm. Nanoparticles can be composed of a variety of materials, allowing for alterations and a diversity of functions. On the nanoscale, molecules exhibit different properties, which allows for valuable and unique opportunities for medicinal uses. Nanoparticles have the potential to revolutionize the way that GI cancers are treated and diagnosed. There are several distinct types of nanoparticles, categorized by fabrication method and material. The application of nanotechnology to cancer is primarily based on the principle of enhanced permeability of tumor-associated vessels. The relative leakiness of newly formed blood vessels that develop in tumors, known as the enhanced permeability and retention (EPR) effect [19, 20], together with the poor lymphatic drainage that is characteristic of tumors, allows for many options for specific targeting of tumors with nanoparticles (**Figure 1**). In general, nanoparticles with a size less than 100 nm exhibit excellent tumor targeting because they are capable of infiltrating into the surrounding vascular endothelium [21, 22]. The ultimate goal of all cancer research is to improve therapeutics and reduce toxicity to normal healthy tissues and cells. Therapeutic uses of nanotechnology include utilizing nanocarriers for enhanced

delivery of a payload, using metallic nanoparticles for imaging and diagnostic purposes and incorporating both for what is termed “theranostics.” Theranostics is a recent term combining “therapeutics” and “diagnostics”.

All of the possible usages of nanotechnology for cancer application are dependent upon the delivery of nanoparticles to cancerous cells with specificity and precision and can be divided into two categories: active and passive targeting. The objective of active targeting is to coat the nanoparticles in order to promote homing and specific binding to cancerous cells. Active targeting is achieved by attaching a particular ligand to the surface of the nanoparticle in order to selectively bind to receptors or antigens that are overexpressed in certain cancer cells. In theory, this would allow for highly specific tumor cell targeting while ensuring the avoidance of healthy cells. The idea behind passive targeting is to take advantage of the abnormal blood flow to tumors to enhance delivery without any “homing” additions to the nanoparticles. Passive targeting utilizes the EPR effect of the tumor vasculature, including the irregular tumor capillaries and porous endothelium that permit the entry of nanoparticles while normal tissue and vasculature would likely prevent entry (**Figure 1**). Inefficient lymphatic drainage associated with tumors also leads to increased accumulation of nanoparticles within the tumor, regardless of how the particle was targeted to the tissue [23, 24].

Both actively and passively targeted nanoparticles have the capability to be loaded with small molecular weight drugs or macromolecules, such as genes or proteins, increasing the bioavailability of these anticancer agents. The increased bioavailability is partly due to nanoparticle avoidance of the mononuclear phagocyte system (MPS), occasionally referred to as the reticuloendothelial system (RES) [25]. The MPS is composed of mononuclear phagocytes, such as macrophages and dendritic cells, and poses significant challenges to drug delivery

systems. In the case of nanoparticles, they can be readily recognized and destroyed by the MPS before being able to reach the desired target and release their payloads [26].

In order for a nanoparticle to enact its desired effects, the particle itself must possess a circulation half-life long enough to reach the tumor microenvironment while additionally avoiding the MPS and RES [19, 27]. One easily controlled parameter to aid in this evasion is size; particles smaller than 400 nm are more likely to escape recognition and phagocytosis by the MPS, while diameters smaller than 200 nm are more likely to have improved extravasation into tumors via the EPR effect [23, 28-30]. An additional modification to escape or delay the macrophage attack of circulating nanoparticles is to modify the surface, which should be hydrophilic and neutral or slightly anionic to avoid plasma proteins (opsonins) and the MPS [31]. This is achieved through the addition of hydrophilic polymers like polyethylene glycol (PEG) [32] or amphiphilic polymers like synthetic copolymers polyethylene oxide (hydrophilic block) and propylene oxide (hydrophobic block) to the surface of the particles [33, 34]. This modification of the surface with the addition of polymers, termed “stealth polymers,” is commonly used when the target treatment site is beyond the MPS.

Occasionally, macrophages and/or dendritic cells within the tumor microenvironment are the cell type targeted by the nanoparticles. In these cases it is not necessary to modify the surface or the size of the particle. Liposomes (discussed in the next section on nanocarriers) are a model example of this strategy. Unmodified liposomal formulations can be used to effectively target macrophages and other phagocytic cells [35, 36] or to increase the half-life of a drug in circulation in order to reach a target beyond the MPS [37].

NANOCARRIERS

Nanocarriers are nanosized molecular structures that provide enhanced delivery of therapeutic anticancer agents to a tumor site by physically shielding the drug from both the environment and phagocytic cells or by stabilizing the payload [23]. Nanocarriers can be used for transport of existing therapeutics, small molecule drugs and macromolecules such as genes or proteins. A schematic of the different types of nanocarriers to be discussed, including average sizes of each, can be found in **Figure 2**. Potential exists for nanocarriers to overcome traditional limitations to GI system delivery. For example, oral drug delivery, one of the most commonly used and preferred forms of drug administration, poses several problems to GI tract delivery including: instability in the gastric acidic environment, low bioavailability and prevention of drug absorption by the mucus barrier [38]. Formulation of a drug to a nanocarrier is a common strategy to circumvent some of these issues and in many cases can even take advantage of these unique features. For example, it is possible to promote controlled release at varying levels of the GI tract based on pH.

Many anti-cancer drugs have low bioavailability, which is due to inadequate solubility and permeability, as well as vulnerability to metabolism. Nanocarriers can affect bioavailability by making water insoluble drugs more soluble and increasing circulation time of these drugs via physical protection from degrading enzymes or phagocytic cells. An example of such a modification to a therapeutic target is the addition of nanocarrier encapsulation or conjugation to curcumin (diferuloylmethane), which is an agent known to have natural anti-cancer properties. However, its use in GI cancers has been limited because the drug is water insoluble, has low absorption, is rapidly metabolized and systemic curcumin is quickly eliminated [39]. Recent

studies have significantly improved the bioavailability of curcumin by conjugating it to, and encapsulating it within, various types of nanoparticles and nanocarriers (reviewed in [40]).

The prevention of absorption due to the mucus barrier is another significant obstacle to drug delivery in the GI tract [38]. Mucus functions to trap pathogens and foreign particles for excretion, which is a unique problem for nanoparticles and nanocarriers. This non-specific mucoadhesion of foreign particles is well characterized in the context of nanocarriers and typically leads to rapid excretion and limited payload absorption [38]. However, targeting mucoadhesion can also be an effective strategy to prolong nanocarrier persistence in the GI tract if the nanocarrier is modified through polymer addition. Polymers, such as poly(lactic acid) (PLA), poly(sebacic acid) (PSA), poly(lactic-co-glycolic acid) (PLGA) and poly(acrylic acid) (PAA) can be used to promote mucoadhesion via hydrogen bonding, polymer entanglements with mucins, or hydrophobic interactions [41]. If the mucus barrier remains intact, then payload delivery can effectively be maximized, especially in areas of increased mucus adherence.

Counter to this mucoadhesion strategy, mucus-penetrating particles (MPP) are also an area of significant interest in targeting GI cancers. Yuan *et al.* recently reported modifying the surface of lipid nanoparticles in an attempt to improve transport and absorption through the GI tract via the addition of the polymer polyethelene glycol (PEG) [42]. The addition of inert polymers was found to increase bioavailability and improve mucus penetration [43, 44]. The group concluded that the modified particles demonstrated improved absorption efficiency and prolonged blood circulation times with a 1.99-fold higher relative circulation time compared with unmodified particles after oral administration and penetration through mucus [42].

An outline of the advantages and disadvantages of each of the unique nanotechnology that will be summarized in this paper is outlined in **Table 2**.

Liposomes

Liposomes are biocompatible colloidal vesicles made of an amphiphilic lipid bilayer membrane capable of forming single (unilamellar) or more (multilamellar) hydrophobic bilayers, surrounding a hydrophilic center [45, 46] (**Figure 2**). In aqueous solutions, liposomes form enclosed spheres with the polar hydrophilic membrane components oriented towards the interior and exterior aqueous environment, with an average diameter between 50-300 nm [46]. Due to the amphipathic composition of liposomes, they can be used to encapsulate hydrophilic agents in their aqueous interior or to carry hydrophobic moieties in their hydrophobic membrane, making them valuable drug nanocarriers [23]. Unique to nanoscale liposomes, the parameters which control and affect the formation of conventional lipid bilayers including molecular shape, temperature, environmental and preparation conditions, do not influence or limit the assembly of liposomal bilayers [47].

The formulation of a liposome requires energy because they are not thermodynamically stable and therefore will not spontaneously form in aqueous media [48]. Several distinct methods exist for liposome preparation; however, each involves the general steps of drying down lipids from an organic solvent, dispersing the lipid in an aqueous media and purifying and analyzing the liposome [47]. Unmodified, or “conventional” liposomes, were initially used to entrap drugs for delivery *in vivo*, but over time were shown to be inefficient transporters as the drugs were degrading within the liposome or dispersing through uncontrolled release [49]. These initial “naked” conventional liposomes without additional modification [36, 50] evolved to give rise to stealth liposomes and actively targeted liposomes that could be further modified through the addition of different lipid components or via unique activation mechanisms. Liposome

nanocarriers can be manipulated to release their payload at particular destination sites or in specific environments. This is achieved by fabrication of liposomes that are sensitive to physiological changes, in which a specific change in pH or temperature of the physiologic “destination” for the therapeutic target leads to the breakdown of the liposome and the subsequent release of the payload [47, 48, 51]. Despite the fact that liposomes are biocompatible, they are recognized as foreign by the immune system and are targeted by the MPS and RES. Liposomes with specific pH-sensitivity provide an advantageous strategy because of the well characterized acidic environment within the lysosome, which can be manipulated to trigger the controlled release of the payload [51]. Similarly, temperature-sensitive liposomes can be engineered to respond to external manipulations of temperature.

Stealth liposomes were some of the first FDA-approved nanocarriers. Stealth liposomes arise from the addition of hydrophilic polymers to the surface of conventional liposomes [47, 51]. Stealth liposomes are often conjugated with the widely used polymer, PEG, historically proven safe in humans with Generally Regarded as Safe (GRAS) classification by the FDA [52]. The combination of a stealth polymer to a standard liposome acts to dramatically increase the circulation time of the nanocarrier in the blood stream by avoiding MPS and RES recognition. Doxil, a PEGylated hydrochloride liposome conjugated with doxorubicin is an excellent example of a stealth liposome and was approved for use in breast and ovarian cancer in 1995 [53]. A generic version of a liposomal-doxorubicin, Lipodox, was rapidly approved in 2013 due to a shortage of Doxil in the United States [54]. Ongoing research is evaluating liposomal-doxorubicin for use in other malignancies besides breast and ovarian cancer, including GI cancers such as colorectal cancer [55, 56], esophageal cancer [56] and pancreatic cancer [57]. Further clinical research is exploring the coupling of multiple drugs to treatment with liposomal-

doxorubicin for advanced and unresectable gastric cancer [17], which seems to suggest safe and encouraging efficacy of combination treatment with liposomal-doxorubicin, 5-Fluorouracil and cisplatin. Other drugs have also shown to have increased efficacy when encapsulated in a liposome. One such example is BikDD, a phosphorylation-mimic mutant of pro-apoptotic protein Bik, which elicits a strong apoptosis response in cancer cells [58].

Altering the liposome to respond to a specific pH, to be sensitive to temperature changes, or to contain polymers that effectively disguise the nanocarrier are all forms of passive targeting. However, liposome nanocarriers can also be modified in line with the classification of active targeting. This is achieved by attaching specific ligands to the surface of the liposome that should bind with specificity to tumor cells. For example, immunoliposomes are conjugated with antibodies or antibody fragments with the goal of maximizing specific and targeted delivery of the nanocarrier to the tumor [51, 59]. This represents an area of significant emerging interest, especially in the context of GI cancers.

Carbon Nanotubes

Carbon nanotubes (CNTs) are tubular networks of carbon atoms with a diameter between 1- 4 nm and a length between 1 to 100 μm (**Figure 2**). The tubular structure of CNTs is made up of rolled graphene carbon hexagons in either single or multi wall arrangements [60]. CNTs have unique structural, electronic, optical and mechanical properties with a highly hydrophobic surface [61, 62]. Different payloads can be conjugated either to the surface of the nanotubes or within the inner cavity at a high payload percentage because of their ultrahigh surface area [23].

CNTs have the potential to be used therapeutically despite being insoluble in all solvents. Modifications to the CNT composition and structure can improve cellular uptake and resolve

toxicity issues. Specific modifications to improve the physiochemical and surface properties of CNTs include surface modifications or functionalization, with the overall objective to increase the solubility of the payload in aqueous biocompatible media, while simultaneously reducing toxicity [61]. Functionalization of CNTs involves attaching amphipathic ligands such as oligonucleotides, biomolecules, surfactants and polymers to the surface of the nanotubes [61, 63, 64]. Although there are no clinical trials involving CNTs, there is promising preclinical data that suggests the feasibility for their use. For example, CNTs can be loaded with high concentrations of anti-cancer drugs in their inner cavity [65, 66] or on their surface [67]. Sobhani *et al.* demonstrated one such promising preclinical feasibility study, in which CNTs were conjugated to paclitaxel that increased cytotoxicity selectively in cancer cells [68].

One method of cellular uptake of CNTs involves “nanoneedle” entry into the membrane [63, 64, 69, 70]. The sequence of needlelike entry into the cellular lipid bilayer involves landing of the nanotube, penetration of the lipid headgroup and entry into the membrane [69]. CNTs can also enter cells via endocytosis, which seems to be size-dependent, as larger nanotubes do not seem to enter cells when under endocytosis-restricted conditions [70]. Subcellular localization of CNTs is also size-dependent. In general, the trend holds that smaller diameter and shorter length CNTs are much more likely to enter a cell and once in the cell, they will have a wider range of intracellular dispersion. This includes very small CNTs that even have the ability to shuttle into the nucleus [71]. The nanoneedle entry of CNTs into the cell was debated for some time until key studies were replicated with two different CNT formulations and a variety of cell types (reviewed in [72]).

Beyond treatment, carbon nanoparticles have proven highly useful in imaging and tumor visualization. For example, traditional treatment of GI cancer solid tumors is surgical resection,

followed by adjuvant chemotherapy and radiation [73]. A study conducted by the Japan Clinical Oncology Group utilized carbon nanoparticles (average size of 150 nm) that were injected into the subserosa of the stomach of patients around the gastric tumor to improve gastrectomy [74-76]. This study revealed that nanoparticles selectively traffic into the lymphatics and draining regional lymph nodes resulting in nanoparticle accumulation and the tissue taking on a black color. This allowed the surgeon to better visualize these regions during lymph node dissection and surgery [77, 78]. The initial trials concluded that the use of the carbon nanoparticles was an effective, easy and safe procedure to guide gastric cancer lymphadenectomy.

Polymer Nanocarriers

Polymeric nanocarriers are a general category of nanosized vesicles composed of any water-soluble polymers. Polymer nanocarriers can be divided into subclasses: polymeric micelles, polymeric dendrimers and polymer nanoparticles [23, 79]. The polymers used to generate nanocarriers can be either synthetic or natural and conjugated to a drug or agent via different methods so as to alter the delivery [80]. Coupling a polymer to a drug is a strategy to increase bioavailability and biodistribution, while also allowing for the delivery of a hydrophobic payload [81].

Polymeric micelles are self-assembled biocompatible nanosized spherical structures composed of amphiphilic di-(hydrophilic-hydrophobic) or tri-(hydrophilic-hydrophobic-hydrophilic) block copolymers [81, 82] (**Figure 2**). The average diameter of micelles is between 10-100 nm [83]. Micelles were first explored for theoretical use in drug delivery thirty years ago, but many initial formulations were not constructed from biocompatible polymers [82]. Construction of micelles from biocompatible polymers led to advances in potential delivery of

therapeutic agents that are poorly soluble in water and the bloodstream. Micelles spontaneously form spheres in aqueous solutions, orienting with their hydrophobic components shielded in the interior core with the hydrophilic components on the exterior. One of the most commonly used hydrophilic blocks in the fabrication of micelles is PEG, which provides high stability due to the presence of multiple sites for hydrophobic interaction [81].

Polymeric micelles make excellent drug nanocarriers due to the high loading capacity of the hydrophobic core and the additional solubility of the drugs provided by the hydrophilic exterior can drastically reduce the toxicity of many anti-cancer drugs. Both the hydrophobic core and the hydrophilic exterior of the micelle can be modified to provide additional specificity of the micelle as a drug nanocarrier, offering versatility, reducing the toxicity of the payload and improving the circulation time of anti-cancer agents. In most cases, the amphiphilic nature of the composition of the molecule increases circulation time, while simultaneously increasing anti-tumor effects because of the capability to be loaded with a higher concentration of drug. For example, Gao *et al.* combined paclitaxel and curcumin in polymeric micelles [84]. Using both *in vitro* and *in vivo* mouse models of colon cancer, the micelle nanocarrier induced apoptosis, inhibited angiogenesis and repressed tumor growth [84]. Similarly, another study by Abouzeid *et al.* loaded both paclitaxel and curcumin into polymeric micelles coated with transferrin-targeting moieties [85]. This study demonstrated that active targeted polymeric micelles could be used to overcome chemotherapy-resistant tumors, as the targeted and dually loaded micelles selectively killed cancer cells more efficiently compared to non-targeted or individually loaded micelles [85].

Dendrimers are nanosized highly branched three-dimensional synthetic globular polymeric macromolecules [23, 86] (**Figure 2**). Unlike linear polymers, dendrimers can be more

closely regulated at every step of the synthesis process, resulting in nearly monodisperse macromolecules [87]. Dendrimers can be fabricated in one of two methods: either starting from the central core growing outwards to the branching periphery, introduced by Tomalia and Newkome and referred to as the “divergent method” [88, 89], or from the periphery inward to the central core, introduced by Freché and called the “convergent method” [90]. Anti-cancer drugs or agents can be non-covalently encapsulated in the dendrimer core or covalently conjugated to the surface of the dendrimer [23, 87, 91]. With the addition of polymeric branches termed dendrimer “generations,” the hydrophobic core remains unaltered while the outreaching hydrophilic branches become more densely packed together [92]. For this reason, the diameter of the average ten generations dendrimer is approximately 10 nm [92].

Encapsulation of drugs in dendrimers with a hydrophobic core surrounded by hydrophilic branches is only feasible for use in local treatments because, despite solubilizing the hydrophobic drugs and leaving the drug unaltered in its original condition, it results in uncontrolled drug release [23, 87, 91, 93]. Despite promising applications of dendrimers *in vitro*, there are no current clinical trials involving dendrimers, likely due to toxicity issues [93]. In one of the early *in vivo* experiments with dendrimers, a polyamidoamine (PAMAM) dendrimer with a sodium carboxylate surface was conjugated to cisplatin [94]. Although the conjugation of cisplatin to the dendrimer led to a tenfold increase in solubility of the drug, there was significant cross-linking that resulted in dendrimer aggregation, which led to the formation of complexes with diameters of 30-40 nm [92, 94].

Polymeric nanoparticles are biodegradable colloidal systems with the capability to form either nanospheres or nanocapsules when conjugated with a therapeutic agent. A nanosphere is a system in which the drug or agent is dispersed equally throughout the body of the particle, while

a nanocapsule is a system in which the drug or agent is confined to a specific cavity surrounded by a single polymeric membrane [80] (**Figure 2**). The average size of a polymeric nanoparticle is between 10-1000 nm diameter [81]. CRLX-101 (formally IT-101) is an example from this class of nanoparticle. CRLX-101 is a cyclodextrin-polyethylene glycol (CD-PEG) co-polymer nanoparticle covalently linked to the drug camptothecin [95]. Camptothecin is a water insoluble and highly toxic drug that functions to inhibit type I DNA topoisomerase [96], but encapsulation with the CD-PEG nanocarrier solubilizes and reduces toxicity of the agent. It is under investigation for use in rectal cancer, among other malignancies, currently recruiting Phase Ib/II clinical trials [97].

METALLIC NANOPARTICLES

Metal nanoparticles allow for unique and diverse nanomedicine applications for cancer treatment, imaging and diagnostics and theranostics. The unique physical and chemical properties of various metals make them suitable as nanocarriers [98]. Certain metals also possess anti-cancer properties that make them sufficient for cancer treatment directly. Additionally, the chemical properties of metals render many suitable for the fabrication of nanoparticles to be used for imaging purposes. Metals at the nanoscale exhibit different properties than the typical bulk metals used in other therapeutic and imaging applications.

Metal Nanocarriers

Similar to the previously mentioned types of nanocarriers, metal nanoparticles can encapsulate or be conjugated to therapeutic agents or drugs [98]. Also, similar to other

nanocarriers, the strategy behind targeting tumors with a high degree of specificity is based on either active or passive targeting. Metal nanoparticles have a very high surface area to volume ratio, which is advantageous because the surface of the particles can be modified with specific cancer cell-targeting ligands [99] and additional attachment of imaging agents such as dyes, radioisotopes and optical imaging agents to the surface [98, 100]. Metals that are frequently used for nanomedicine include gold, iron, silver and zinc. Although these metals are inert and biocompatible, a significant portion of the metal is retained in the body after exposure to the nanoparticles [21].

Properties of gold render it an excellent nanocarrier due to the ease with which the surface of a gold nanoparticle (AuNP) can be manipulated [98]. Indeed, gold is one of the most commonly used metals for biomedical applications and more specifically in nanotechnology applications associated with cancer treatments and imaging owing to the inert and nontoxic nature of the molecule [22]. For example, AuNPs have proven highly useful for photothermal therapy (PTT) or hyperthermic applications. During PTT, the surface plasmon resonance of the AuNP is excited with a specific wavelength, creating heat as electrons on the surface of the particle oscillate. These particles put off very high oscillatory energy, causing localized tissue and cancer cell death [22, 101-103].

Iron is also commonly used in nanomedicine. The superparamagnetic properties of iron make it an ideal choice for imaging. However, therapeutic agents can also be conjugated to its surface [98]. Superparamagnetic iron oxide nanoparticles (SPIONs) contain a superparamagnetic iron core, surrounded by a biodegradable and biocompatible polymer coating [100]. The polymer coating surrounding a SPION is typically the site of drug conjugation, either encapsulating the drug into the matrix or through covalent coupling of the drug to the polymer. These particles can

also function in drug delivery. For example, anti-cancer agents can be directly loaded into hollow SPIONs via physical absorption [104].

Metal Nanoparticles in Imaging

As discussed earlier, the high surface area of metallic nanoparticles and the inherent properties of metals enable their use for theranostics. Not only can dyes or imaging agents be conjugated to these particles along with a drug, but additionally, the core metal is often a contrast agent itself. These metallic nanoparticles can provide clearer and more specific images. For example, the distinct pattern of light scattering properties of AuNPs can be exploited to allow for single molecule imaging [103]. Likewise, SPIONs make excellent contrast agents and drug nanocarriers. The superparamagnetic iron core is made of either magnetite (Fe_3O_4) or maghemite (Fe_2O_3), which acts as a contrast agent for imaging [100]. Superparamagnetic iron oxide particles are currently under investigation for use in magnetic resonance imaging (MRI), so termed “ultrasmall superparamagnetic iron oxide magnetic resonance imaging” (USPIO MRI). The particles are conjugated to an FDA-approved therapeutic agent, Feraheme. USPIO MRI has been evaluated and tested for preoperative diagnostic and staging purposes in liver cancer [105, 106], colorectal metastases of liver cancer [107], esophageal cancer [108] and is currently being explored for use in imaging and diagnosing pancreatic cancer.

CONCLUSIONS

Part of what makes not only GI cancer, but all cancer, so difficult to treat is a lack of effective delivery of therapeutics to the target cancer cells. Recent developments in

nanotechnology specifically address challenges associated with traditional treatment of GI cancers. Specific impediments to delivery of therapeutics to GI tumors include: toxicity issues associated with delivering a sufficient concentration of drugs; insolubility of anti-cancer small molecular weight macromolecules, such as genes or proteins; impenetrable mucus; uncontrolled release of therapeutics; and a lack of specific targeting of tumors. Nanomedicine provides the opportunity for novel approaches to overcome all of these obstacles through the employment of biocompatible nanocarriers to solubilize, stabilize and control release of drugs and other anti-cancer agents. These nanocarriers are also able to increase penetration of acidic or otherwise incompatible gastric environments and in many cases, can even specifically target tumor cells. This chapter reviewed a selection of the literature involving the application of nanotechnology to GI cancer, but the volume of new papers and research that includes the same topics is increasing daily. Before the novel nanotechnological approaches to GI cancer fully infiltrate the medical field and become routine, there is still noteworthy progress to be made. However, there is no argument that we are rapidly progressing in the incorporation of these advances into general practice. The number of pre-clinical data suggesting the efficacy of nanotechnology for cancer treatment, combined with the number of active clinical trials involving GI cancer and nanotechnology, is promising. Together, these observations would indicate that the routine employment of nanomedicine for the treatment, detection and diagnosis of GI cancer should be anticipated in the near future. It is our opinion that nanotechnology holds the exciting potential to revolutionize the diagnosis of GI cancer and redefine current therapeutic paradigms.

REFERENCES

1. Taniguchi, N. *On the basic concept of 'nano-technology'*. in *The International Conference of Production Engineering*. 1974. Tokyo, Japan: Society of Precision Engineering.
2. Feynman, R., *There's plenty of room at the bottom, An invitation to enter a new field of physics*, in *Engineering and Science*. 1959, CalTech. p. 7.
3. Torre, L.A., et al., *Global cancer statistics, 2012*. CA Cancer J Clin, 2015. **65**(2): p. 87-108.
4. Prados, J., et al., *Application of nanotechnology in the treatment and diagnosis of gastrointestinal cancers: review of recent patents*. Recent Pat Anticancer Drug Discov, 2014. **9**(1): p. 21-34.
5. ClinicalTrials.gov.
6. Gradishar, W.J., *Albumin-bound paclitaxel: a next-generation taxane*. Expert Opin Pharmacother, 2006. **7**(8): p. 1041-53.
7. Borazanci, E. and D.D. Von Hoff, *Nab-paclitaxel and gemcitabine for the treatment of patients with metastatic pancreatic cancer*. Expert Rev Gastroenterol Hepatol, 2014. **8**(7): p. 739-47.
8. Goldstein, D., et al., *nab-Paclitaxel plus gemcitabine for metastatic pancreatic cancer: long-term survival from a phase III trial*. J Natl Cancer Inst, 2015. **107**(2): p. 10.
9. Von Hoff, D.D., et al., *Increased survival in pancreatic cancer with nab-paclitaxel plus gemcitabine*. N Engl J Med, 2013. **369**(18): p. 1691-703.
10. Li, L.Y., et al., *Targeted hepatocellular carcinoma proapoptotic BikDD gene therapy*. Oncogene, 2011. **30**(15): p. 1773-83.

11. Mao, C., et al., *Cell-specific expression of artificial microRNAs targeting essential genes exhibit potent antitumor effect on hepatocellular carcinoma cells*. *Oncotarget*, 2015. **6**(8): p. 5707-19.
12. Marill, J., et al., *Hafnium oxide nanoparticles: toward an in vitro predictive biological effect?* *Radiat Oncol*, 2014. **9**: p. 150.
13. Liu, X., *Targeting Polo-Like Kinases: A Promising Therapeutic Approach for Cancer Treatment*. *Transl Oncol*, 2015. **8**(3): p. 185-95.
14. Northfelt, D.W., et al., *A phase I dose-escalation study of TKM-080301, a RNAi therapeutic directed against polo-like kinase 1 (PLK1), in patients with advanced solid tumors: Expansion cohort evaluation of biopsy samples for evidence of pharmacodynamic effects of PLK1 inhibition*. *Journal of Clinical Oncology*, 2013. **31**(15): p. [Abstract TPS2621].
15. Tolcher, A.W., et al., *Safety and activity of DCR-MYC, a first-in-class Dicer-substrate small interfering RNA (DsiRNA) targeting MYC, in a phase I study in patients with advanced solid tumors*. *Journal of Clinical Oncology*, 2015. **33**(15): p. [Abstract 11006].
16. Rakowski, J.A., S. Ahmad, and R.W. Holloway, *Use of pegylated liposomal doxorubicin in the management of platinum-sensitive recurrent ovarian cancer: current concepts*. *Expert Rev Anticancer Ther*, 2012. **12**(1): p. 31-40.
17. Cascinu, S., et al., *Pegylated liposomal doxorubicin, 5-fluorouracil and cisplatin versus mitomycin-C, 5-fluorouracil and cisplatin for advanced gastric cancer: a randomized phase II trial*. *Cancer Chemother Pharmacol*, 2011. **68**(1): p. 37-43.
18. El-Rayes, B.F., et al., *Phase I study of liposomal doxorubicin (Doxil) and cyclophosphamide in solid tumors*. *Invest New Drugs*, 2005. **23**(1): p. 57-62.

19. Maeda, H., *The enhanced permeability and retention (EPR) effect in tumor vasculature: the key role of tumor-selective macromolecular drug targeting*. Adv Enzyme Regul, 2001. **41**: p. 189-207.
20. Matsumura, Y. and H. Maeda, *A new concept for macromolecular therapeutics in cancer chemotherapy: mechanism of tumor-tropic accumulation of proteins and the antitumor agent smancs*. Cancer Res, 1986. **46**(12 Pt 1): p. 6387-92.
21. Wang, A.Z., R. Langer, and O.C. Farokhzad, *Nanoparticle delivery of cancer drugs*. Annu Rev Med, 2012. **63**: p. 185-98.
22. Singh, M., et al., *Application of gold nanoparticles for gastrointestinal cancer theranostics: A systematic review*. Nanomedicine, 2015. **11**(8): p. 2083-98.
23. Perez-Herrero, E. and A. Fernandez-Medarde, *Advanced targeted therapies in cancer: Drug nanocarriers, the future of chemotherapy*. Eur J Pharm Biopharm, 2015. **93**: p. 52-79.
24. Maeda, H., G.Y. Bharate, and J. Daruwalla, *Polymeric drugs for efficient tumor-targeted drug delivery based on EPR-effect*. Eur J Pharm Biopharm, 2009. **71**(3): p. 409-19.
25. Danhier, F., O. Feron, and V. Preat, *To exploit the tumor microenvironment: Passive and active tumor targeting of nanocarriers for anti-cancer drug delivery*. J Control Release, 2010. **148**(2): p. 135-46.
26. Malam, Y., M. Loizidou, and A.M. Seifalian, *Liposomes and nanoparticles: nanosized vehicles for drug delivery in cancer*. Trends Pharmacol Sci, 2009. **30**(11): p. 592-9.
27. Moghimi, S.M., A.C. Hunter, and J.C. Murray, *Long-circulating and target-specific nanoparticles: theory to practice*. Pharmacol Rev, 2001. **53**(2): p. 283-318.

28. Yuan, F., et al., *Vascular permeability in a human tumor xenograft: molecular size dependence and cutoff size*. *Cancer Res*, 1995. **55**(17): p. 3752-6.
29. Maeda, H., *Macromolecular therapeutics in cancer treatment: the EPR effect and beyond*. *J Control Release*, 2012. **164**(2): p. 138-44.
30. Maruyama, K., *Intracellular targeting delivery of liposomal drugs to solid tumors based on EPR effects*. *Adv Drug Deliv Rev*, 2011. **63**(3): p. 161-9.
31. Owens, D.E., 3rd and N.A. Peppas, *Opsonization, biodistribution, and pharmacokinetics of polymeric nanoparticles*. *Int J Pharm*, 2006. **307**(1): p. 93-102.
32. Shan, X., et al., *Influence of PEG chain on the complement activation suppression and longevity in vivo prolongation of the PCL biomedical nanoparticles*. *Biomed Microdevices*, 2009. **11**(6): p. 1187-94.
33. Li, F., et al., *The internalization of fluorescence-labeled PLA nanoparticles by macrophages*. *Int J Pharm*, 2013. **453**(2): p. 506-13.
34. Duan, X. and Y. Li, *Physicochemical characteristics of nanoparticles affect circulation, biodistribution, cellular internalization, and trafficking*. *Small*, 2013. **9**(9-10): p. 1521-32.
35. Kelly, C., C. Jefferies, and S.A. Cryan, *Targeted liposomal drug delivery to monocytes and macrophages*. *J Drug Deliv*, 2011. **2011**: p. 727241.
36. Cattel, L., M. Ceruti, and F. Dosio, *From conventional to stealth liposomes: a new frontier in cancer chemotherapy*. *Tumori*, 2003. **89**(3): p. 237-49.
37. Feeney, O.M., et al., *'Stealth' lipid-based formulations: poly(ethylene glycol)-mediated digestion inhibition improves oral bioavailability of a model poorly water soluble drug*. *J Control Release*, 2014. **192**: p. 219-27.

38. Ensign, L.M., R. Cone, and J. Hanes, *Oral drug delivery with polymeric nanoparticles: the gastrointestinal mucus barriers*. *Adv Drug Deliv Rev*, 2012. **64**(6): p. 557-70.
39. Mohanty, C., M. Das, and S.K. Sahoo, *Emerging role of nanocarriers to increase the solubility and bioavailability of curcumin*. *Expert Opin Drug Deliv*, 2012. **9**(11): p. 1347-64.
40. Yallapu, M.M., et al., *Therapeutic Applications of Curcumin Nanoformulations*. *AAPS J*, 2015. **17**(6): p. 1341-56.
41. Lai, S.K., Y.Y. Wang, and J. Hanes, *Mucus-penetrating nanoparticles for drug and gene delivery to mucosal tissues*. *Adv Drug Deliv Rev*, 2009. **61**(2): p. 158-71.
42. Yuan, H., et al., *Improved transport and absorption through gastrointestinal tract by PEGylated solid lipid nanoparticles*. *Mol Pharm*, 2013. **10**(5): p. 1865-73.
43. Suk, J.S., et al., *Rapid transport of muco-inert nanoparticles in cystic fibrosis sputum treated with N-acetyl cysteine*. *Nanomedicine (Lond)*, 2011. **6**(2): p. 365-75.
44. Yang, M., et al., *Biodegradable nanoparticles composed entirely of safe materials that rapidly penetrate human mucus*. *Angew Chem Int Ed Engl*, 2011. **50**(11): p. 2597-600.
45. Roberto Solaro, F.C., Antonella Battisti, *Targeted Delivery of Protein Drugs by Nanocarriers*. *Materials*, 2010. **3**: p. 1928-1980.
46. Kraft, J.C., et al., *Emerging research and clinical development trends of liposome and lipid nanoparticle drug delivery systems*. *J Pharm Sci*, 2014. **103**(1): p. 29-52.
47. Akbarzadeh, A., et al., *Liposome: classification, preparation, and applications*. *Nanoscale Res Lett*, 2013. **8**(1): p. 102.
48. Taylor, T.M., et al., *Liposomal nanocapsules in food science and agriculture*. *Crit Rev Food Sci Nutr*, 2005. **45**(7-8): p. 587-605.

49. Allen, T.M. and P.R. Cullis, *Liposomal drug delivery systems: from concept to clinical applications*. Adv Drug Deliv Rev, 2013. **65**(1): p. 36-48.
50. Zhang, J.X., et al., *Application of liposomes in drug development--focus on gastroenterological targets*. Int J Nanomedicine, 2013. **8**: p. 1325-34.
51. Mallick, S. and J.S. Choi, *Liposomes: versatile and biocompatible nanovesicles for efficient biomolecules delivery*. J Nanosci Nanotechnol, 2014. **14**(1): p. 755-65.
52. Suk, J.S., et al., *PEGylation as a strategy for improving nanoparticle-based drug and gene delivery*. Adv Drug Deliv Rev, 2015. **99**: p. 24.
53. Immordino, M.L., F. Dosio, and L. Cattel, *Stealth liposomes: review of the basic science, rationale, and clinical applications, existing and potential*. Int J Nanomedicine, 2006. **1**(3): p. 297-315.
54. Mamidi, R.N., et al., *Pharmacokinetics, efficacy and toxicity of different pegylated liposomal doxorubicin formulations in preclinical models: is a conventional bioequivalence approach sufficient to ensure therapeutic equivalence of pegylated liposomal doxorubicin products?* Cancer Chemother Pharmacol, 2010. **66**(6): p. 1173-84.
55. Shields, A.F., L.M. Lange, and M.M. Zalupski, *Phase II study of liposomal doxorubicin in patients with advanced colorectal cancer*. Am J Clin Oncol, 2001. **24**(1): p. 96-8.
56. Wang-Gillam, A., et al., *A phase I study of pegylated liposomal doxorubicin and temsirolimus in patients with refractory solid malignancies*. Cancer Chemother Pharmacol, 2014. **74**(2): p. 419-26.
57. Falchook, G.S., et al., *Age-stratified phase I trial of a combination of bortezomib, gemcitabine, and liposomal doxorubicin in patients with advanced malignancies*. Cancer Chemother Pharmacol, 2012. **69**(5): p. 1117-26.

58. Sun, Y., et al., *Proteasome inhibition enhances the killing effect of BikDD gene therapy*. Am J Transl Res, 2015. **7**(2): p. 319-27.
59. Manjappa, A.S., et al., *Antibody derivatization and conjugation strategies: application in preparation of stealth immunoliposome to target chemotherapeutics to tumor*. J Control Release, 2011. **150**(1): p. 2-22.
60. Kumar, R., et al., *Carbon nanotubes: a potential concept for drug delivery applications*. Recent Pat Drug Deliv Formul, 2014. **8**(1): p. 12-26.
61. Vardharajula, S., et al., *Functionalized carbon nanotubes: biomedical applications*. Int J Nanomedicine, 2012. **7**: p. 5361-74.
62. Sinha, N. and J.T. Yeow, *Carbon nanotubes for biomedical applications*. IEEE Trans Nanobioscience, 2005. **4**(2): p. 180-95.
63. Ali-Boucetta, H., et al., *Cellular uptake and cytotoxic impact of chemically functionalized and polymer-coated carbon nanotubes*. Small, 2011. **7**(22): p. 3230-8.
64. Bianco, A., K. Kostarelos, and M. Prato, *Making carbon nanotubes biocompatible and biodegradable*. Chem Commun (Camb), 2011. **47**(37): p. 10182-8.
65. Ajima, K., et al., *Enhancement of in vivo anticancer effects of cisplatin by incorporation inside single-wall carbon nanohorns*. ACS Nano, 2008. **2**(10): p. 2057-64.
66. Hampel, S., et al., *Carbon nanotubes filled with a chemotherapeutic agent: a nanocarrier mediates inhibition of tumor cell growth*. Nanomedicine (Lond), 2008. **3**(2): p. 175-82.
67. Wu, W., et al., *Covalently combining carbon nanotubes with anticancer agent: preparation and antitumor activity*. ACS Nano, 2009. **3**(9): p. 2740-50.
68. Sobhani, Z., et al., *Increased paclitaxel cytotoxicity against cancer cell lines using a novel functionalized carbon nanotube*. Int J Nanomedicine, 2011. **6**: p. 705-19.

69. Kraszewski, S., et al., *Insertion of short amino-functionalized single-walled carbon nanotubes into phospholipid bilayer occurs by passive diffusion*. PLoS One, 2012. **7**(7): p. e40703.
70. Kostarelos, K., et al., *Cellular uptake of functionalized carbon nanotubes is independent of functional group and cell type*. Nat Nanotechnol, 2007. **2**(2): p. 108-13.
71. Kang, B., et al., *Cell response to carbon nanotubes: size-dependent intracellular uptake mechanism and subcellular fate*. Small, 2010. **6**(21): p. 2362-6.
72. Lacerda, L., et al., *Cell-penetrating CNTs for delivery of therapeutics*. Nano Today, 2007. **2**(6): p. 38-43.
73. Lordick, F., et al., *Unmet needs and challenges in gastric cancer: the way forward*. Cancer Treat Rev, 2014. **40**(6): p. 692-700.
74. Catarci, M., et al., *Prospective randomized evaluation of preoperative endoscopic vital staining using CH-40 for lymph node dissection in gastric cancer*. Ann Surg Oncol, 1998. **5**(7): p. 580-4.
75. Siewert, J.R., et al., *Benefits of D2 lymph node dissection for patients with gastric cancer and pN0 and pN1 lymph node metastases*. Br J Surg, 1996. **83**(8): p. 1144-7.
76. Okamoto, K., et al., *Number and anatomical extent of lymph node metastases in gastric cancer: analysis using intra-lymph node injection of activated carbon particles (CH40)*. Jpn J Clin Oncol, 1999. **29**(2): p. 74-7.
77. Huang, G.J., et al., *[Effect of injecting activated carbon ultramicroparticles around the gastric tumor on staining lymph node]*. Zhonghua Yi Xue Za Zhi, 2004. **84**(24): p. 2070-2.

78. Sasako, M., et al., *D2 lymphadenectomy alone or with para-aortic nodal dissection for gastric cancer*. N Engl J Med, 2008. **359**(5): p. 453-62.
79. Duncan, R., *The dawning era of polymer therapeutics*. Nat Rev Drug Discov, 2003. **2**(5): p. 347-60.
80. Prabhu, R.H., V.B. Patravale, and M.D. Joshi, *Polymeric nanoparticles for targeted treatment in oncology: current insights*. Int J Nanomedicine, 2015. **10**: p. 1001-18.
81. Gupta, M., G.P. Agrawal, and S.P. Vyas, *Polymeric nanomedicines as a promising vehicle for solid tumor therapy and targeting*. Curr Mol Med, 2013. **13**(1): p. 179-204.
82. Owen, S.C., Chan, D.P.Y., Shoichet, M.S., *Polymeric micelle stability*. NanoToday, 2012. **7**(1): p. 53-65.
83. Rapoport, N., *Physical stimuli-responsive polymeric micelles for anti-cancer drug delivery*. Progress in polymer science, 2007. **32**(8): p. 962-990.
84. Gao, X., et al., *Combined Delivery and Anti-Cancer Activity of Paclitaxel and Curcumin Using Polymeric Micelles*. J Biomed Nanotechnol, 2015. **11**(4): p. 578-89.
85. Abouzeid, A.H., et al., *Transferrin-targeted polymeric micelles co-loaded with curcumin and paclitaxel: efficient killing of paclitaxel-resistant cancer cells*. Pharm Res, 2014. **31**(8): p. 1938-45.
86. Kesharwani, P., Jain, K., Jain, N. K., *Dendrimer as nanocarrier for drug delivery*. Progress in Polymer Science, 2014. **39**(2): p. 268-307.
87. Wolinsky, J.B. and M.W. Grinstaff, *Therapeutic and diagnostic applications of dendrimers for cancer treatment*. Adv Drug Deliv Rev, 2008. **60**(9): p. 1037-55.

88. D.A. Tomalia, H.B., J. Dewald, M. Hall, G. Kallos, S. Martin, J. Roeck, J. Ryder, P. Smith, *A New Class of Polymers: Starburst-Dendritic Macromolecules*. *Polymer Journal*, 1985. **17**(1): p. 117-132.
89. G.R. Newkome, Z.Y., G.R. Baker, V.K. Gupta, *Cascade molecules: a new approach to micelles. A [27]-arborol*. *J. Org Chem.*, 1985. **50**(11): p. 2.
90. Hawker, C.J., Freché J.M.J., *Preparation of polymers with controlled molecular architecture. A new convergent approach to dendritic macromolecules*. *J. Am. Chem. Soc.*, 1990. **112**: p. 7638-7647.
91. Kesharwani, P. and A.K. Iyer, *Recent advances in dendrimer-based nanovectors for tumor-targeted drug and gene delivery*. *Drug Discov Today*, 2015. **20**(5): p. 536-47.
92. Lee, C.C., et al., *Designing dendrimers for biological applications*. *Nat Biotechnol*, 2005. **23**(12): p. 1517-26.
93. Morgan, M.T., et al., *Dendritic molecular capsules for hydrophobic compounds*. *J Am Chem Soc*, 2003. **125**(50): p. 15485-9.
94. Malik, N., E.G. Evagorou, and R. Duncan, *Dendrimer-platinate: a novel approach to cancer chemotherapy*. *Anticancer Drugs*, 1999. **10**(8): p. 767-76.
95. Young, C., et al., *CRLX101 (formerly IT-101)-A Novel Nanopharmaceutical of Camptothecin in Clinical Development*. *Curr Bioact Compd*, 2011. **7**(1): p. 8-14.
96. Numbenjapon, T., et al., *Preclinical results of camptothecin-polymer conjugate (IT-101) in multiple human lymphoma xenograft models*. *Clin Cancer Res*, 2009. **15**(13): p. 4365-73.

97. Weiss, G.J., et al., *First-in-human phase 1/2a trial of CRLX101, a cyclodextrin-containing polymer-camptothecin nanopharmaceutical in patients with advanced solid tumor malignancies*. Invest New Drugs, 2013. **31**(4): p. 986-1000.
98. Sharma, H., et al., *Metal nanoparticles: a theranostic nanotool against cancer*. Drug Discov Today, 2015. **20**(9): p. 1143-51.
99. Gautier, J., et al., *Recent advances in theranostic nanocarriers of doxorubicin based on iron oxide and gold nanoparticles*. J Control Release, 2013. **169**(1-2): p. 48-61.
100. Thomas, R., I.K. Park, and Y.Y. Jeong, *Magnetic iron oxide nanoparticles for multimodal imaging and therapy of cancer*. Int J Mol Sci, 2013. **14**(8): p. 15910-30.
101. Akhter, S., et al., *Gold nanoparticles in theranostic oncology: current state-of-the-art*. Expert Opin Drug Deliv, 2012. **9**(10): p. 1225-43.
102. Rai, P., et al., *Development and applications of photo-triggered theranostic agents*. Adv Drug Deliv Rev, 2010. **62**(11): p. 1094-124.
103. Khan, M.S., G.D. Vishakante, and H. Siddaramaiah, *Gold nanoparticles: a paradigm shift in biomedical applications*. Adv Colloid Interface Sci, 2013. **199-200**: p. 44-58.
104. Liu, G., et al., *Applications and potential toxicity of magnetic iron oxide nanoparticles*. Small, 2013. **9**(9-10): p. 1533-45.
105. Bashir, M.R., et al., *Retrospective assessment of the utility of an iron-based agent for contrast-enhanced magnetic resonance venography in patients with endstage renal diseases*. J Magn Reson Imaging, 2014. **40**(1): p. 113-8.
106. Savranoglu, P., et al., *The role of SPIO-enhanced MRI in the detection of malignant liver lesions*. Clin Imaging, 2006. **30**(6): p. 377-81.

107. Strotzer, M., et al., *Diagnosis of liver metastases from colorectal adenocarcinoma. Comparison of spiral-CTAP combined with intravenous contrast-enhanced spiral-CT and SPIO-enhanced MR combined with plain MR imaging.* Acta Radiol, 1997. **38**(6): p. 986-92.
108. Mack, M.G., et al., *Superparamagnetic iron oxide-enhanced MR imaging of head and neck lymph nodes.* Radiology, 2002. **222**(1): p. 239-44.

TABLES AND FIGURES

Table 1

Product Name	Composition	Status	Therapeutic Indication	Ref.
FOLFIRABAX*	Paclitaxel albumin-stabilized nanoparticle formulation + fluorouracil + leucovorin calcium + irinotecan hydrochloride	Phase I/II	Advanced and/or metastatic gastric cancer	[5]
Nab Paclitaxel	Nanoparticle albumin-bound Paclitaxel	Approved	Pancreatic cancer	[6-9]
C-VISA BikDD**	Cholesterol liposome with Bik siRNA	Phase I	Advanced pancreatic cancer	[5, 10, 11]
PEP503 (NBTXR3)*	Halfnium oxide radio-enhancer + 5-fluorouracil or oral capecitabine	Phase Ib/II	Unresectable rectal cancer	[5, 12]
TKM 080301	Lipid nanoparticles with PLK1 siRNA	Phase I	Colorectal, pancreas, gastric, or esophageal, (breast, ovarian) cancer with hepatic metastases	[5, 13, 14]
DCR-MYC*	Lipid nanoparticles with siRNA targeting MYC	Phase Ib/II	Hepatocellular carcinoma	[5, 15]
Doxil	PEGylated hydrochloride liposomal doxorubicin	Approved Phase I/II	Breast, ovarian cancers Pancreas, gastric, or esophageal cancer (small cell lung, head and neck cancer)	[16] [5, 17, 18]

* Denotes recruiting.

** Denotes withdrawn.

Table 1: Selected nanoparticle-drug formulations in clinical trials and/or approved for use in a variety of GI cancers.

Figure 1: Schematic Illustrating the Enhanced Permeability and Retention (EPR) Effect

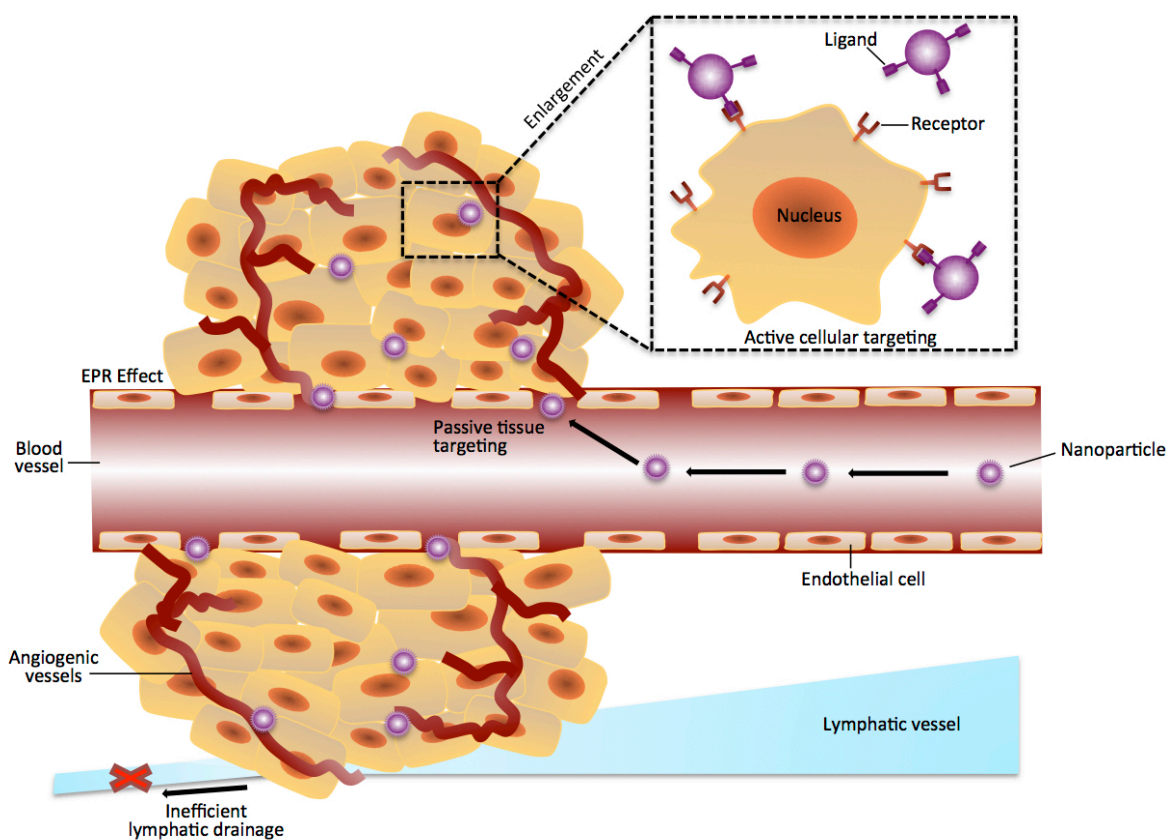


Figure 1. Schematic Illustrating the Enhanced Permeability and Retention (EPR) Effect: “Passive tissue targeting” of nanoparticles carrying therapeutic drugs or contrast agents to tumors is based on the leaky epithelium of tumor vasculature and the poor lymphatic drainage of tumors (EPR effect). Nanoparticles can additionally be directed to cancer cells via the attachment of a ligand or some targeting moiety to the surface of nanoparticles facilitate homing to a receptor or antigen present on the tumor cells, which is referred to as “active cellular targeting.”

Figure 2: Schematic Depicting Different Nanocarriers

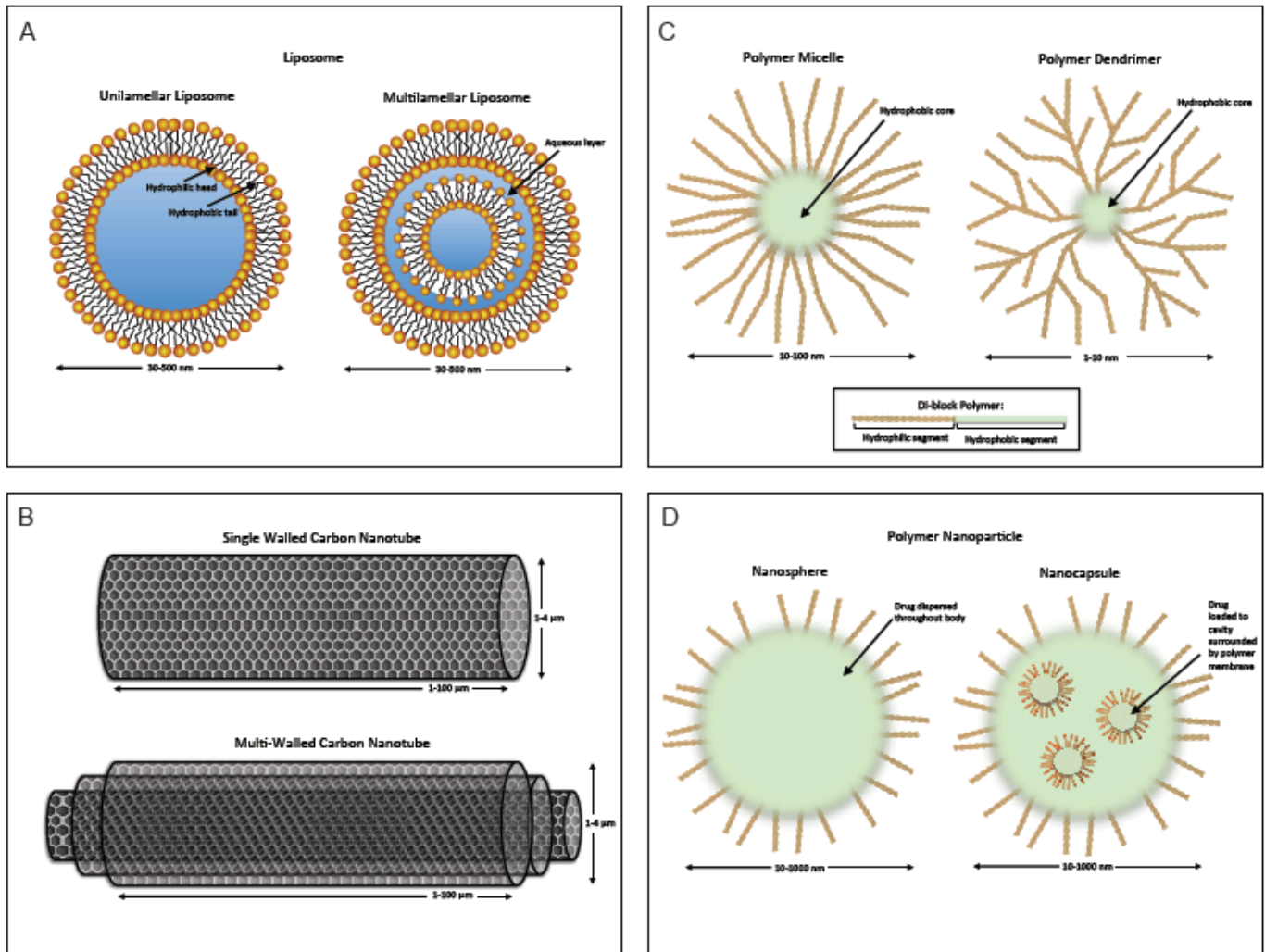


Figure 2. Schematic Depicting Different Nanocarriers: A) Liposomal nanocarriers can be synthesized as either unilamellar or multilamellar liposomes, with their defining feature including a lipid bilayer resulting in an internal hydrophilic environment when in an aqueous environment. B) Carbon nanotubes are composed of rolled graphene carbon hexagons in either single or multi wall arrangements. C) Polymer micelles, dendrimers and D) nanoparticles are composed of di-block amphiphilic copolymers. Upon conjugation with a drug (or other anti-cancer agent), polymer nanoparticles will form either a nanosphere in which the drug is

dispersed equally throughout the body of the nanoparticle, or a nanocapsule in which the drug is limited to a cavity surrounded by an additional polymer membrane.

Table 2: Advantages and Disadvantages for Therapeutic Application by Nanotechnology

Nanotechnology	Application	Advantages/ Disadvantages
Liposomes	Drug delivery/ Imaging	<p><u>Advantages:</u></p> <ul style="list-style-type: none"> • Increase solubility of drug(s); • Payload release upon specific physiologic triggers; • Biocompatible; • Surface modifications: form stealth liposomes or attaching cancer-specific ligands or receptors (“immunoliposomes”) <p><u>Disadvantages:</u></p> <ul style="list-style-type: none"> • Recognized by MPS/RES
Carbon nanotubes (single-walled or multi-walled)	Drug delivery/ Imaging	<p><u>Advantages:</u></p> <ul style="list-style-type: none"> • Ultrahigh surface area allows for conjugation of high concentration of drug(s) and/or dye(s); • Surface modifications increase solubility <p><u>Disadvantages:</u></p> <ul style="list-style-type: none"> • Highly hydrophobic surface; • Insoluble in all solvents (unless modified); • Toxicity concerns; • Size limited
Polymeric Micelles	Drug delivery/ Imaging	<p><u>Advantages:</u></p> <ul style="list-style-type: none"> • Increase solubility of drug(s) and/or dye(s); • High loading capacity of hydrophobic core; • Decrease cytotoxicity of drugs; • Biocompatible; • Surface modifications to decrease immune recognition/clearance <p><u>Disadvantages:</u></p> <ul style="list-style-type: none"> • Recognized by MPS/RES
Polymeric Dendrimers	Drug delivery/ Imaging	<p><u>Advantages:</u></p> <ul style="list-style-type: none"> • Increase solubility of drug(s) and/or dye(s); • More closely regulated synthesis; • Highly branched structure allows for loading high concentration of drug(s) and/or dye(s);

		<ul style="list-style-type: none"> • Biocompatible; • Surface modifications to decrease immune recognition/clearance <u>Disadvantages:</u> <ul style="list-style-type: none"> • Uncontrolled release of payload; • Possible aggregation in bloodstream; • Recognized by MPS/RES
Polymeric Nanoparticles (nanospheres or nanocapsules)	Drug delivery/ Imaging	<u>Advantages:</u> <ul style="list-style-type: none"> • Increase solubility of drug(s) and/or dye(s); • Reduce toxicity of drug(s) and/or dye(s); • Biocompatible; • Surface modifications to decrease immune recognition/clearance <u>Disadvantages:</u> <ul style="list-style-type: none"> • Recognized by MPS/RES
Metal Nanocarriers	Drug delivery/ Imaging	<u>Advantages:</u> <ul style="list-style-type: none"> • Increase solubility of drug(s) and/or dye(s); • High surface area to volume ratio; • PTT applications; • Inert and biocompatible; • Theranostic applications: metal core as a contrast agent in addition to being loaded with drug(s) and/or dye(s) <u>Disadvantages:</u> <ul style="list-style-type: none"> • Some metal retained in body post-exposure

Table 2. Advantages and Disadvantages for Therapeutic Application by Nanotechnology:

The theoretical medicinal use of each of the unique types of nanoparticle discussed in this paper is dependent upon the specific advantages and disadvantages. This table summarizes each of the different types of nanotechnology and the advantages and disadvantages associated with each for the application to nanomedicine.

MPS: mononuclear phagocyte system; RES: reticuloendothelial system; PTT: photothermal therapy.

Chapter Six

Fabrication and characterization of PLGA nanoparticles encapsulating large CRISPR-Cas9 plasmid

Ami Jo*, Veronica M. Ringel-Scaia*, Dylan K. McDaniel, Cassidy A. Thomas, Rui Zhang, Judy S. Riffle, Irving C. Allen, Richey M. Davis

ABSTRACT

Background

The Clustered Regularly Interspaced Short Palindromic Repeats (CRISPR) and Cas9 protein system is a revolutionary tool for gene therapy. Despite promising reports of the utility of CRISPR-Cas9 for *in vivo* gene editing, a principal problem in implementing this new process is delivery of high molecular weight DNA into cells.

Results

Using poly(lactic-co-glycolic acid) (PLGA), a nanoparticle carrier was designed to deliver a model CRISPR-Cas9 plasmid into primary bone marrow derived macrophages. The engineered PLGA-based carriers were approximately 160 nm and fluorescently labeled by encapsulation of the fluorophore 6,13-bis(triisopropylsilylethynyl) pentacene (TIPS pentacene). An amine-end capped PLGA encapsulated 1.6 wt% DNA, with an encapsulation efficiency of 80%. Release studies revealed that most of the DNA was released within the first 24 hours and corresponded to ~2-3 plasmid copies released per nanoparticle. *In vitro* experiments conducted

with murine bone marrow derived macrophages demonstrated that after 24 hours of treatment with the PLGA-encapsulated CRISPR plasmids, the majority of cells were positive for TIPS pentacene and the protein Cas9 was detectable within the cells.

Conclusions

Taken together, these data suggest successful nanoparticle-based delivery of high molecular weight plasmid and suggests that the process described here will be effective for future *in vivo* applications.

Keywords: nanoprecipitation, transfection, TLR4

BACKGROUND

The Clustered Regularly Interspaced Short Palindromic Repeats (CRISPR)-Cas9 system has received much attention recently due to its potential for revolutionizing targeted genome editing with unprecedented precision and control. CRISPR was discovered in bacteria and function as a defense mechanism against invading viral DNA¹. Over the last two decades, CRISPR-Cas9 based systems have revolutionized our ability to rapidly and effectively target genes in eukaryotic cells for genetic modification. In biomedical research applications, CRISPR-Cas9 is now routinely utilized to generate novel genetically modified animal models and is being aggressively pursued in gene therapy applications. Indeed, a series of high profile proof-of-concept studies recently demonstrated that the CRISPR-Cas9 system could be harnessed to modify the mouse genome in adult animals and modulate disease phenotypes.²⁻⁴

The CRISPR-Cas9 system is typically delivered to cells as a single large plasmid or multiple smaller plasmids that encode a target sequence, a CRISPR guide, and Cas9. However, efficient transfection of DNA or RNA into the cell for transcription is a significant hurdle. Both chemically- and mechanically-based transfection methods have been successfully utilized *in vitro*, but effective, clinically relevant, *in vivo* transfection methods are significantly lacking. Lipofectamine is a cationic lipid-based transfection agent often used to increase permeability of the cell membrane, but it can destabilize the membrane and result in unacceptable toxicity, especially in test animals.⁵ Electroporation and sonoporation have also been examined *in vivo*.^{6,7} However, these approaches are not always feasible when attempting to transfect animals or humans due to accessibility limitations and invasiveness of the treatments. Finally, adenoviral vectors are also being studied as potential carriers for the CRISPR-Cas9 system and have shown great success *in vitro*,^{8,9} yet the relatively large size of the CRISPR-Cas9 system and potential immunogenicity of adenoviral vectors have, for the moment, limited *in vivo* applications.

The lack of an efficient and clinically relevant delivery system is a major hurdle in advancing CRISPR-Cas9 from proof-of-principle to *in vivo* clinical application. Specifically, the delivery system must be clinically relevant, capable of being targeted to specific cells of interest and minimize immune system stimulation. After considering a range of delivery approaches, we believe that polymeric nanoparticles offer a promising solution to this limitation. For example, Cohen et al. studied sustained marker gene expression using plasmid DNA in PLGA nanoparticles and liposomes, which concluded that while nanoparticles resulted in a much lower level of gene transfection *in vitro*, it produced almost two orders of magnitude more successful transfection *in vivo* than with liposomes.¹⁰ By using a polymeric nanocarrier, the bioavailability of the therapy is increased by reducing the premature clearance of these biomaterials from the body. In theory, a nanoparticle can be designed to enter the cell by endocytosis and release the plasmid directly into the cytoplasm. Poly(lactic-co-glycolic acid) (PLGA) has proven very useful for drug delivery given its biocompatibility, biodegradability, and toxicologically safe degradation products.¹¹ PLGA has been approved by the FDA for human use in nanomedicine formulations.^{12,13} Proteins, peptides, genes, vaccines, antigens, and human growth factors have been successfully incorporated into PLGA or PLGA-based particles.¹¹ However, to our knowledge, the use of biodegradable polymer nanoparticles to deliver plasmid DNA for implementing CRISPR-Cas9 gene editing has not previously been demonstrated.

This study explores the engineering and processing steps to fabricate high molecular weight plasmid DNA-encapsulated fluorescently-labeled PLGA nanoparticles. The particles themselves are internalized by the cell and tracking is enabled by a novel fluorescent dye. The most relevant study prior to this work was that of Niu et al. who used a modified slow nanoprecipitation method to encapsulate plasmid DNA into PLGA particles for enhanced

expression of green fluorescent protein (GFP) in cells.¹⁴ They tested loading, structural integrity, DNA protection from enzymes when in the particles, and functionality in cell studies. This nanoprecipitation method became the starting point for the work presented here for encapsulating CRISPR-Cas9 plasmid. The main differences between the work by Niu et al. and this work was the size of the CRISPR-Cas9 plasmid (~8500 bp), which is approximately twice the size of their GFP plasmid (~4000 bp), and the need for fluorescently labeled particles to track the NP for future *in vitro* and *in vivo* applications. Because high molecular weight plasmid DNA tends to be susceptible to shear degradation, we used this low-shear nanoprecipitation method to address these particle design constraints. Nanoprecipitation forms particles by adding a water-miscible organic solution of a polymer and therapeutic drop-wise into an aqueous solution containing a polymeric surfactant which, in the work of Niu et al was the triblock copolymer Pluronic F127™.¹⁴ Using this modified nanoprecipitation method, we characterized fluorescently labeled PLGA nanoparticles encapsulating a high molecular weight CRISPR-Cas9 plasmid DNA and investigated their transfection *in vitro* in murine bone-marrow derived macrophages.

RESULTS

Solvent mixture used in particle formation

Since 6,13-bis(triisopropylsilylethynyl) pentacene (TIPS pentacene), DNA, and PLGA have very different solubility characteristics, a solvent mixture was needed to solubilize all 3 components and form well-defined nanoparticles when mixed with the aqueous Pluronic F-127 solution. TIPS pentacene is highly nonpolar and therefore readily soluble in THF while only partially soluble in DMF (**Figure 1a-b**). In contrast to TIPS pentacene, PLGA was more soluble

in DMF than THF. However, DNA was not soluble in this purely organic mixture and thus a mixed aqueous-organic mixture was sought. Ke et al. used a mixture of 5 vol% TE buffer and 95 vol% DMF and showed that plasmid DNA was stable in this mixture at room temperature.¹⁵ Therefore, to solubilize the DNA, some TE buffer was added to the mixture of DMF and THF but the concentration was kept low to prevent the TIPS pentacene from precipitating. Because the CRISPR plasmid used in this work was about twice the size as that used by Ke et al., 5 vol% was not sufficient to solubilize the DNA and was found experimentally to leave a small visible pellet of DNA that was not loaded into the syringe for particle formation. The final solvent mixture solubilizing TIPS pentacene, DNA, and PLGA consisted of 10 vol% TE buffer, 45 vol% DMF, and 45 vol% THF and was used in the nanoprecipitation process to form nanoparticles.

Evaluation of nanoparticles made with different PLGA end groups show main difference to be in DNA loading

For particles made with the ester-end capped PLGA, the intensity-average hydrodynamic diameters (D_i) were ~ 160 nm while the diameters of particles made with the amine-end capped PLGA were slightly larger, D_i ~ 180 nm with no significant change when DNA was encapsulated (**Table 1**). Because PLGA degrades by hydrolysis, the particles were freeze dried for extended storage which greatly simplified the subsequent cell-based experiments. Since PLGA aggregates irreversibly during freeze-drying, trehalose was used as a cryoprotectant. A mass ratio of NP to trehalose ranging from 1:25 to 1:42 - determined by experiments described in the SI – resulted in particles redispersed in DI water that were somewhat aggregated during freeze drying with D_i ~ 210-350 nm but still small enough to be useful for cell uptake. The trehalose:NP ratio varied slightly from batch to batch as the exact concentration of the final suspension after the

centrifugal wash during particle fabrication varied and was calculated after the freeze-drying process. The zeta potentials of the particles showed little variation, ranging from -29 to -35 mV, due most likely to carboxylate groups on the particles formed due to hydrolysis of the PLGA.

Proton NMR analysis can be used to estimate Pluronic F127 versus PLGA mass ratio in nanoparticles

Because Pluronic F127 was added in excess and any material not physisorbed to the surfaces of the nanoparticles during formation was removed during the centrifugation step, it was important to determine the polymer composition of the final nanoparticle product. By determining the mass content of F127 and PLGA in the nanoparticles, the encapsulation efficiency can also be more accurately calculated. Using proton NMR, solutions of the PLGA and F127 in deuterated chloroform (CDCl₃) separately were first analyzed.

In the ¹H NMR spectrum of Pluronic F127, the methyl protons have a chemical shift around 1 ppm (**Figure 2a**). All other peaks from both PEO and PPO blocks are integrated into one peak, between 3.2-3.8 ppm, due to the presence of adjacent oxygen atoms. Based on the NMR, the composition of the F127 is PEO₁₀₈-*b*-PPO₆₅-*b*-PEO₁₀₈ which is close to the theoretical values of PEO₁₀₀-*b*-PPO₆₅-*b*-PEO₁₀₀.¹⁶ Alternatively, if the integrals of the methyl protons on the PPO segment are set to be 100, then there would be 100/3 = 33.3 repeating units of PO. The PEO methylene proton peaks then have an integral of 544.2 – 100 = 444.2, after subtracting the methylene and methine protons from the PO. It means there are 444.2/4 = 111 repeating units of EO, per 33.3 units of PO. The molar ratios of the EO over PO are then:

$$\frac{\text{mole of EO}}{\text{mole of PO}} = \frac{3.33}{1}$$

Another important value was the percent of the integrals in the overlapped chemical shift region that contributed to the EO mass. The % value becomes important when calculating the PPO ratios in case overlapping occurs when mixed with the PLGA components. The PPO proton wt% can be calculated as follows.

$$\%A_{3.25-3.8\text{ppmPPO}} = \frac{444.2}{544.2} = 81.2\%$$

The PLGA spectra show two distinctive peaks around 4.5-5.5 ppm (**Figure 2b-c**). Specifically, the methine protons (g peak) from the poly(lactide) segment have a chemical shift of ~5-5.5 ppm, while the value for the methylene protons (f peak) from the poly(glycolide) segment was 4.5-5 ppm. The molar ratios of the poly(lactide) segment over poly(glycolide) can be determined by comparing the integral of g to the integral of f divided by two, as there are two protons in peak f compared to only one in peak g. The results indicated the molar ratios are ~1:1, close to the values provided by the manufacturer.

Because the F127 and the poly(lactide) and poly(glycolide) have distinctive, non-overlapping peaks, the PLGA to F127 ratios in the TIPS loaded NPs could be calculated. For example, using the ester end cap PLGA case (**Figure 3a**):

$$\frac{\text{mole of EO}}{\text{mole of PO}} = \frac{3.3}{1}; \quad \frac{\text{mole of GA}}{\text{mole of LA}} = \frac{\frac{253.3}{2}}{\frac{100}{1}} = \frac{1.27}{1}; \quad \%A_{3.25-3.8\text{ppmPPO}} = 81.2\%$$

$$\frac{\text{mole of EO}}{\text{mole of LA}} = \frac{\frac{96.3 * 81.2\%}{4}}{100} = \frac{1}{5.11} = \frac{3.33 \text{ EO}}{17.0 \text{ LA}}$$

The result means that in the mixed systems, per 3.33 mole of EO, there would be 1 mole of PO, 17 moles of LA, and 17*1.27 mole of GA. With all these ratios, we can use the MW of the repeat units to find the mass ratio of F127 to PLGA and from there the wt% of each:

$$\frac{m_{F127}}{m_{PLGA}} = \frac{3.33 * (44.04) + 58.06}{17.0 * (1.27 * (58.02) + 72.04)} = \frac{204.7}{2477.3} \rightarrow \mathbf{91.7\% PLGA/8.3\% F127}$$

This same method can be used for the amine end cap case (**Figure 3b**), yielding similar results of 92.4% PLGA. Given the approximate 5% error in the NMR spectra integration, the uncertainty of these calculations is $\pm 6-7\%$ and therefore both of these compositions are statistically identical and assumed to be $\sim 92\%$ PLGA for all future loading calculations.

DNA release profiles differ between NP formulations and pH conditions

From an analysis of the DNA content of the supernatant after centrifugation during the fabrication process, the DNA loading was determined to be 0.7 and 1.6 wt% for the ester and amine endcap PLGA cases, respectively (**Table 1**). The difference between the two formulations may be due to charge and hydrophobic interactions from the different PLGA end groups. We hypothesized that an amine end group would provide additional electrostatic attraction with the negatively charged DNA which would enhance loading. By contrast, the PLGA with the ester end cap contained a 9-carbon chain as the end group and thus the lower DNA loading with this polymer could be due to a combination of the lack of attractive charge interactions and the increased hydrophobicity of the chain ends which could interact unfavorably with the hydrophilic DNA. Based on the particle sizes and DNA loadings of the samples in **Table 1**, the estimated number of plasmids per NP ranged from ~ 2 to 5 copies (eq. (S4)).

DNA release measurements were performed at 3 different pH values (pH 7, 6, 4.5) to mimic the different pH environments that the particles would experience during incubation in the media (pH 7.4) outside the cell, through early (pH 6.8-6.1) and late endocytosis (pH 6.0-4.8), and in lysosomes (pH 4.5) inside the cell.¹⁷ The amine end-capped PLGA case shows a higher release at all 3 pHs, with the highest release being DNA equivalent to 0.8 wt% loading with

respect to PLGA (eq. (S5)) at pH 7 after 3 days (**Figure 4**). By contrast, the corresponding release for the ester end-capped case after 3 days at pH 7 was 0.4 wt% with somewhat lower values at pH 4.5 and 6.0. Because the amine end-capped case had over 2X higher overall loading, it is reasonable that it would release more DNA relative to the ester end-capped case.

From 1-3 days, release at pH 7.0 appeared to be systematically higher by ~ 30-60% than for the pH 4.5 case. However, it is possible that pH may affect the concentration of DNA detected by the PicoGreen assay. The first step to depurination and β -elimination during dsDNA degradation in aqueous media is catalyzed by acidic conditions.¹⁸ Evans et al. showed in their accelerated stability studies that even at a pH 6, significant difference in degradation could be seen for supercoiled plasmid DNA when compared to pH 7.¹⁸ The formation of acid groups due to hydrolysis is probably why lower DNA release was measured for the lower pH cases. Hydrolysis of PLGA is catalyzed by acidic conditions and, as the PLGA breaks down to form more acid groups, the local pH inside the core decreases.¹⁹ This positive feedback loop accelerates the further breakdown of PLGA.²⁰ When the pH of the surrounding media was already lower as in the pH 4.5 and 6.0 cases, the acid-catalyzed hydrolysis happens more rapidly and thus could have degraded more DNA than in the more neutral pH 7 case. If the DNA is exposed to these highly acidic conditions for a long period of time, it could degrade quickly and fall below the detection limit of the assay. Balmert et al. estimated the intraparticle pH of ester endcapped PLGA microparticles (MW = 15 kDa) as ~ 3-4 within 1-3 days in neutral pH media conditions.¹⁹ This may account for the relatively rapid release of the DNA. The particles are rapidly being hydrolyzed which, in turn, forms more acid groups that further catalyze hydrolysis, leading to formation of pores that lead to faster diffusion of DNA out of the particle into the aqueous media. However, at lower pH values, especially at pH 4.5, the acidic environment in the

nanoparticles may lead to early DNA degradation, thus lowering the apparent release levels. This is supported by the decline in DNA release for the pH 4.5 case after 3 days.

The apparently anomalous points in the release profile at the $t=0$ time point at all 3 pH values occurred when the buffer was initially added to the NPs, followed by immediate centrifugation to obtain the supernatant for the PicoGreen assay. The DNA content at this time point was found to be higher than the subsequent 1-hour time point for all 6 of the DNA-containing conditions tested. We believe this was due to surface-bound or partially encapsulated DNA that may have been partly degraded during processing due to its exposure to the environment. Because that DNA was close to the surface, it was quickly released. Although all processing steps were done carefully to minimize degradation, between mixing, centrifugation, freeze drying, and reconstitution in buffers, it is possible that some of the surface-bound DNA had degraded. We hypothesize that, at $t=0$, this surface-bound DNA was released rapidly and detected by the assay. If this DNA had already been partially degraded to form relatively short linear DNA fragments due to the effects of the handling steps, it may have degraded faster once in the media with its chain length eventually falling below the detection limit of PicoGreen (<200 bp) as specified by the manufacturer. Other sources have shown experimentally that PicoGreen could accurately detect DNA chains as short as 150 bp.^{21,22} Regardless of the cutoff length for detection, the hypothesis of partially degraded DNA chains on the surface undergoing rapid burst release and degradation to lengths below detection by PicoGreen still applies.

This degraded DNA can also show up as a stronger signal for the same amount of DNA than when in plasmid form given the nature of the PicoGreen assay. The assay involves intercalation of the reagents into the DNA and therefore will not have access to the entire chain when the plasmid is supercoiled. Holden et al. reported that, for their plasmid, the PicoGreen

assay showed the supercoiled plasmid to be 60% the mass of the same plasmid that had been linearized.²³ The discrepancy between the supercoiled and linearized forms will depend on the sequence and conformation of the plasmid but, in all cases, the supercoiled case may show a lower signal due to inaccessibility of parts of the chain. The DNA concentration for the stock solution was measured by NanoDrop 2000 (ThermoFisher) which is a UV absorption method and thought to be more accurate than the assay for plasmids. This measurement was taken to be accurate and used to concentrate the stock for a targeted 2 wt% DNA loading with respect to mass of PLGA. Under the assumption that the added DNA was enough for exactly 2 wt% DNA loading, the unincorporated DNA and encapsulated DNA should add up to that total mass added. However, given the lowered detection by picoGreen, the mass of unincorporated DNA as measured from the supernatant using PicoGreen would be an underestimate. Similarly, the DNA released over the 5 days was ~ 50% of what was loaded. These measurements are also underestimates and could be a main factor in accounting for the missing mass in the mass balance.

More important than the actual estimated loading is the DNA released as shown by the release study. The amount of measured DNA released for the amine case after 5 days at pH 7.0 was equivalent to a DNA loading of 0.8 wt% with respect to PLGA or approximately half of the total 1.6 wt% loading. This corresponds to ~2-3 plasmid copies released per NP and is a rough underestimate as mentioned above. An underestimated plasmid release is better than an overestimate in this application because the chances of successful delivery of the plasmid to the nucleus for transcription increases with the number of plasmid copies released. Therefore, the particles may be more effective for the apparent DNA added. To test this, cell studies were

conducted to investigate the expression of the Cas9 protein and to explore any changes to the mouse DNA after NP treatments.

Bacterial *S. pyogenes* Cas9 protein is successfully translated inside murine macrophages

To further test the successful encapsulation of CRISPR plasmid into the amine end-capped PLGA nanoparticles, we next wanted to determine whether the plasmid remained functional, defined by its ability to transcribe and translate *S. pyogenes* Cas9 protein. To do so, we harvested wild type mouse bone marrow derived macrophages (BMDMs), replated at a density of 500,000 cells/mL, and challenged the macrophages with either blank nanoparticles (100 µg/ml), CRISPR plasmid-loaded nanoparticles (100 µg/ml), CRISPR plasmid with Lipofectamine 3000 transfection (2 µg/ml DNA), CRISPR plasmid only (2 µg/ml), or PBS for 24 hours. The total remaining cells were removed from the plates, lysed, and Western blot was performed for Cas9 using a *S. pyogenes* specific monoclonal antibody (**Figure 5**).

The nanoparticle concentrations were chosen to keep the DNA concentration constant between the samples under the assumption of 2 wt% targeted DNA loading. However, the measured loading was 1.6 wt% with respect to the PLGA, and with the presence of F127 included in the total NP mass, the nominal DNA concentration of the plasmid NP case was approximately 1.5 µg/ml. In order to control for suboptimal nanoparticle delivery of CRISPR plasmids, we used Lipofectamine 300 (Invitrogen) in order to transfect approximately the same total DNA that was encapsulated in the particles. Due to the phagocytic nature of the BMDM primary cells that we used for this study, we also treated the cells with the free plasmid DNA. Cas9 was detectable in the cells transfected with Lipofectamine (lanes 1 and 2) as well as the cells treated with CRISPR plasmid only (lanes 3 and 4) and CRISPR-loaded nanoparticle (lane

6), while the cells treated with blank nanoparticle (lane 7) and PBS only (lane 5) were not (**Figure 5**). Qualitatively, the band intensities between all 3 CRISPR-containing samples were comparable. Again, given the phagocytic nature of these cells, the BMDMs internalized the plasmid only control with no additional carrier or transfection needed. From release studies shown earlier, we showed that most of the plasmid was released from the particles within the first 24 hours in suspension, and more specifically within the first 8 hours. From imaging cytometry, we found ~ 95% of the macrophages exhibited red fluorescence from the TIPS pentacene indicating internalization after 24 hours (**Figure 1d**). McDaniel et al. showed similar statistics using TIPS pentacene loaded poly(lactic acid)-based nanoparticles. That study also showed that within the first 2 hours ~ 30% of cells showed particle uptake increasing to ~40% at 4 hours but not reaching the 90+% until after 8 hours of incubation.²⁴ Assuming similar DNA release kinetics in cell culture media, and similar particle uptake behaviors with these PLGA particles, it is difficult to discern whether the entire nanoparticle was internalized by the macrophages before releasing the plasmid into the cytosol as intended, the plasmid in the particles were released outside the cell and the free plasmids phagocytosed, or a combination of the two. We hypothesize this will become more clear in future *in vivo* studies. Cohen et al. found that nanoparticles performed better than liposomes for *in vivo* delivery of plasmid DNA for gene editing applications, although it did not do as well in *in vitro* cell studies.¹⁰ Even though we cannot see a clear advantage in using transfecting agents from this particular study, what this result does show is that the encapsulated high molecular weight plasmids in the nanoparticles were intact enough to express the Cas9 protein and can therefore be considered functional. In the current set of studies, we cloned a test gRNA targeting the Lps-d allele in the mouse *Tlr4* gene

into our pX330 CRISPR plasmid.²⁵ Future studies will include functional and validated CRISPR gRNAs that target a range of murine genes of interest both *in vitro* and *in vivo*.

DISCUSSION

CRISPR-Cas9 is an extremely valuable tool towards an effective therapy for a vast range of genetic diseases. Successful delivery of high molecular weight plasmid DNA into cells is a significant hurdle in the application of CRISPR-Cas9 based therapeutic strategies. With most of the current methods for transfection being *ex vivo*, there is a clear need for investigations into other delivery methods. By using polymer nanoparticles, the CRISPR-Cas9 tool can be translated to *in vivo* therapies without the immunogenicity concerns of viral vectors or cationic liposomes. This proof-of-concept study has shown a method of fabricating versatile particles made from biocompatible materials that can be applied to multiple CRISPR-Cas9 systems and beyond to other plasmid-based treatments. The particles were shown to release 2-3 plasmid copies per particle with loadings as high as 1.6 wt% with respect to PLGA when previous studies using this method of fabrication have encapsulated plasmids half the size at only 1 wt%.¹⁴

Previous studies have shown promising results using adenoviral vectors but historically, viral vectors have had low success rates in FDA approval.²⁶ However, there have been major recent steps in the development of liposomes and lipid nanoparticles to deliver CRISPR-Cas9. Researchers have used gold nanoparticles coated with lipid layers to passivate the surface and also to encapsulate the Cas9-gRNA ribonucleoprotein and donor DNA. Lee et al. used gold nanoparticles due to the ability to coat a thick layer of DNA on the surface and their tendency to be internalized by many different cell types.²⁷ Wang et al. used gold nanoparticles as a thermally

triggered release mechanism for plasmid-loaded gold nanoparticle and lipid complexes.²⁸ Finn et al. used lipid nanoparticles to encapsulate mRNA/gRNA complexes and demonstrated delivery *in vivo*.²⁹ There are advantages and disadvantages to using the different forms of CRISPR-Cas9 and different delivery vehicles.

By using plasmid DNA, we are able to deliver a high Cas9 dosage with indefinite production by the cells, but there are higher risks for off-target effects.³⁰ One disadvantage of liposomal and lipid nanoparticle formulations is that the product is difficult to characterize and store. The liposomes are made in solution so the product yield and encapsulation are characterized solely on the payload concentration. The initial molar ratios of the different lipids and components are given under the assumption that the end product has the exact same ratios. It is difficult to determine the absolute loading of the payload and long-term storage can be an obstacle. By using polymeric nanoparticles, the particles can be freeze-dried to increase shelf-life, the material composition of the particles can be characterized to determine loading so that dosages can be identified by product mass concentrations, and the particles are dispersible at desired concentrations. Without much literature on the direct comparison of liposomal delivery versus polymer nanoparticle delivery *in vivo*, it is difficult to give a clear functional advantage of one over the other. However, future work in this work will include a comparison especially given the larger number of studies showing successful implementation of liposomal/lipid nanoparticle CRISPR-Cas9.

Several studies that have successfully employed nanoparticle delivery of CRISPR-Cas9 plasmids have done so using immortalized cell lines.³¹⁻³³ In this way, our study is unique as we utilize primary cells. There has been a previous study by Jin et al. using a magnetic nanoparticle delivery system to transfect rat primary cortical neurons with a CRISPR plasmid, but delivery to

these primary cells were found to be at a much lesser degree relative to studies done in immortalized HEK cells.³³ Therefore, delivery in primary cell systems is an needed area of investigation in this field. With the ultimate goal of applying this method of CRISPR-loaded nanoparticles *in vivo*, primary cells are advantageous as they more accurately represent physiological conditions.

Here, we have chosen to validate the CRISPR-Cas9 plasmid functionality via detection of the *S. pyogenes* Cas9 protein within the murine macrophages. In future work, this can be taken a step further to confirm genetic changes within the target gene to verify CRISPR plasmid delivery and functionality. Due to the nature of the double-stranded break created by the Cas9 enzyme, it should be expected that the genetic changes would not be uniform or even predictable. As the interest of this work was to create a base pair substitution within the Lps-d allele in the mouse *Tlr4* gene, sufficient number of cells must be utilized to account for all the possible outcomes after a double stranded break: insertions or deletions of a few base pairs (less than 20),³⁴ to up to several hundred,³⁵ and resultant complex rearrangements.³⁶

With multiple plasmid copies per particle, the nanoparticle-based carrier described here successfully delivered the high molecular weight CRISPR-Cas9 plasmid into primary mouse derived macrophages. The relative expression and translation of the bacterial Cas9 protein in macrophages treated with NP-encapsulated plasmids was comparable to cells transfected using more traditional transfection approach of Lipofectamine (**Figure 5**). This may not mean that the NP delivery is directly comparable to this method, as this can be attributed to the 80% encapsulation efficiency of the DNA. Previous studies have shown that polymer carrier systems can be much more effective at delivering genetic material *in vivo* even when levels of transfection are less than levels observed in cell studies.¹⁰ Thus, given the successes of this

formulation *in vitro*, future work involving transfer of this technology into *in vivo* animal studies for comparison to current methods of delivery looks promising. It is our hope the procedures described here will ultimately improve genome editing as a whole to move us towards an effective treatment for a range of genetic diseases.

METHODS

Materials

PLGA AP063 (15,000-25,000 M_w advertised (31,700 M_w by GPC), PDI=1.86, 50:50 lactic acid:glycolic acid, ester end-capped), and PLGA AI063 (10,000-20,000 M_w advertised (16,000 M_w by GPC), PDI=1.41, 50:50 lactic acid:glycolic acid, diamine end-capped) from Akina Inc. PolySciTech was used as purchased. Pluronic® F127 copolymer (PEO(~4.3 kDa)-PPO(~3.9 kDa)-PEO(~4.3 kDa)), D-(+)- Trehalose dehydrate, uninhibited tetrahydrofuran (THF) (anhydrous $\geq 99.9\%$), dimethyl sulfoxide (DMSO) ($\geq 99.9\%$) and 6,13-bis(triisopropylsilylethynyl)pentacene (TIPS pentacene) were purchased from Sigma Aldrich and used as received. Dimethylformamide (DMF) (spectrophotometric grade), and chloroform (HPLC grade) was purchased and used as received from Spectrum Chemical. Deuterated chloroform ($CDCl_3$) (D, 99.9%) was purchased from Cambridge Isotope Laboratories, Inc. and used as received. GE Hyclone Phosphate Buffered Saline (1X, 0.0067M PO_4 , without Calcium and Magnesium) (PBS), Tris-Ethylenediaminetetraacetic acid (Tris-EDTA or TE) buffer, and PicoGreen Assay Kit were purchased from Fisher Scientific and used as received. CRISPR Cas-9 DNA (~8500 bp; MW $\sim 5.5 \times 10^6$ g/mol) was cultured using *Escherichia coli* (described below) and purified using the Qiagen plasmid purification maxi prep kit. Autoclaved Milli-Q deionized

water (resistivity ~ 18 MΩ-cm produced from a Millipore Synergy Ultrapure Water system) was used in all experiments.

CRISPR plasmid design

The CRISPR plasmid pX330-U6-Chimeric_BB-CBh-hSpCas9 was a gift from Feng Zheng (Addgene plasmid # 42230).³⁷ The plasmid was digested with the restriction enzyme BbsI, and a murine *Tlr4*- specific gRNA was cloned into the vector. The goal with the design of the gRNA was to specifically target site 2342 in the *Mus musculus Lps-d* allele. The oligos were designed based on this target sequence, self-complimentary, and with overhang specified in order to be successfully cloned into the pX330 plasmid once digested with BbsI restriction enzyme. The sequences of the oligos in the 5' to 3' direction: CACCCCTGGTG TAGCCATTGCTGCCAA and AAAGTTGGCAGCAATGGCTACACCAGG. (**Figure S1**).

Competent *E. coli* cells (Sigma Aldrich) were transformed with cloned pX330 containing *Tlr4* gRNA and amplified in Ampicillin-containing selection media according to standard transformation protocols. Plasmid DNA was isolated from competent cells via plasmid MaxiPrep kit (QIAGEN) following the manufacturer's protocol, and the concentration was verified by a NanoDrop 2000 (ThermoFisher).

Fabrication of DNA loaded PLGA nanoparticles by nanoprecipitation

The method used for nanoprecipitation of PLGA nanoparticles was modified from that previously described by Niu et al.¹⁴ PLGA with two different end groups (ester and amine groups) were used to test the hypothesis that the positively charged amine end caps could increase the encapsulation efficiency and loading due to the charge interactions between it and

the negatively charged backbone of the DNA. In a 50 mL polypropylene conical centrifuge tube, 100 mg Pluronic F127 was dissolved in 20 mL autoclaved DI water by vortex mixing followed by 30 minutes of sonication (Fisherbrand CPXH Series Heated Ultrasonic Cleaning Bath; 110 W, 40 kHz). An autoclaved magnetic stirring bar was added and the solution was mixed at 600 RPM for 30 minutes while the other solutions were made. Plastic labware was used instead of glassware throughout to minimize nonspecific adsorption of DNA. Solutions of PLGA dissolved in DMF (44.48 mg/mL) and TIPS pentacene dissolved in THF (0.667 mg/mL) were made separately. The PLGA was left quiescently to wet in DMF for 30 minutes before being sonicated for 30 minutes but the TIPS pentacene was only vortex mixed and not sonicated to avoid degradation from heat and sonication. Next, 400 μ L of a 1.41 mg/mL stock solution of plasmid DNA in TE buffer were placed in an Amicon 100 kDa MWCO Ultra 0.5 centrifugal filter and spun at 11k RPM (11,498 x g) (Fisher Scientific accuSpinTM Micro; PCR-Rotor 7500 3243) for 10 minutes to concentrate the solution. The filter was then inverted into a clean tube and spun at 3k RPM (855 x g) for 3 minutes to recover the now-concentrated DNA (~8.14 mg/mL). Next, 63 μ L of the concentrated DNA solution was diluted with 63 μ L TE buffer. To make the final solution, 562 μ L of PLGA stock, 562 μ L TIPS pentacene stock, 126 μ L TE (with or without DNA) were combined in a 1.5 mL centrifuge tube with gentle pipetting until visually homogenous. This solution had a volume of ~ 1.25 mL and contained 25 mg PLGA, 0.513 mg DNA, and 0.375 g TIPS corresponding to a 2 wt% DNA and 1.5 wt% TIPS loading with respect to the PLGA. The mixture was then loaded into a 3 mL plastic syringe fitted with a 21-gauge beveled needle. Using a syringe pump (New Era Pump Systems, Farmingdale, NY), the organic solution was added drop-wise (30 mL/hr) to the aqueous Pluronic F-127 solution magnetically stirred at 600 rpm. The combined solution was left stirring for 5 hours on ice and covered to

minimize light exposure for the TIPS pentacene before being centrifuged at 4°C and 22,789 xg for 30 minutes (Thermo Scientific, Sorvall Legend X1R, FIBERLite™ F15-8x50c rotor). The supernatant was decanted and saved for assaying the unincorporated DNA by PicoGreen. The pellet was re-suspended in 20 mL of DI water by 30 minutes of sonication and then filtered through a 0.45 µm nitrocellulose membrane to make the “reserve” suspension. Meanwhile, 200 mg of trehalose were dissolved in 1 mL of DI water. Next, 1.5 mL of the reserve suspension was split into three 1.5 mL tubes (0.5 mL per tube) to freeze dry without a cryoprotectant to determine the concentration of the reserve suspension. The remaining ~16-18 ml was added to the trehalose mixture for a targeted NP:trehalose mass ratio of 1:25. All samples were frozen in a -70°C freezer and then lyophilized (FreeZone6, LABCONCO) for at least 5 days at <0.09 mBar and ~ -50°C.

Size and zeta potential characterization

Size distributions were measured by dynamic light scattering (Zetasizer NanoZS, Malvern Instruments, software version 7.12) at 25°C unless otherwise noted. The sizes reported are averages of 5 measurements of the intensity peak corresponding to the bulk of the mass in the system. Each measurement consisted of 12-16 subruns averaged by the software and all solutions had a NP concentration of ~0.2 mg/mL. For the measurement of reserve suspensions, 50 µL of sample were diluted with 1 mL of DI water. For solutions made with freeze-dried samples, the powdered samples were left quiescently to wet for 15 minutes followed by vortex mixing and then sonication for 1 minute. Zeta potentials were also measured using the same suspensions used for DLS (Zetasizer NanoZS) which were loading into pre-wetted folded capillary tubes.

Five measurements were conducted per sample with each measurement consisting of an average from 42 subruns.

Determining PLGA and Pluronic content per nanoparticle by proton NMR

Proton NMR was used in order to find the mass ratio of PLGA to Pluronic content in nanoparticles. PLGA, Pluronic, and TIPS pentacene loaded nanoparticles were dissolved separately in CDCl₃ at concentrations of ~1-2 mg/mL, and placed in standard 5 mm o.d. tubes. The ¹H NMR spectra were obtained using a Bruker Avance 500 spectrometer operating at 500 MHz and 25°C with 32 scans per sample.

Measurement and calculation of TIPS pentacene encapsulation

The targeted TIPS pentacene loading of 1.5 wt% was based on the mass of TIPS pentacene and PLGA dissolved in the solvent mixture used for fabrication. As with the NMR measurements, NPs for the TIPS pentacene composition measurements were freeze dried without trehalose cryoprotectant. The particles were dissolved in THF at specific mass concentrations to liberate the TIPS pentacene and the absorbances were measured at 641 nm to calculate the concentration from (**Figure 3b**) where the absorbance was related to the concentration by:

$$Absorbance = 29.084 * C_{TIPS\ pentacene} + 0.0021 \quad (S1)$$

The calculated TIPS concentration was subtracted from the known NP concentration to obtain the polymer concentration in solution and then, using the PLGA/F127 mass ratio of 92/8 determined by NMR (described below), the PLGA concentration was calculated which permitted a calculation of the TIPS pentacene loading relative to the PLGA content. For example, a 0.2 mg/mL concentration of NP dissolved in THF had an absorbance of 0.075 so that:

$$\text{TIPS pentacene concentration} = \frac{\text{Absorbance} + 0.0021}{29.084} = \frac{0.075 + 0.0021}{29.084} = 0.0025 \frac{\text{mg}}{\text{mL}}$$

The TIPS pentacene loading, defined as (TIPS mass/PLGA mass) is given by:

$$\text{TIPS pentacene loading} = \frac{0.0025}{(0.2 - 0.0025) * 92\% \text{ PLGA}} \times 100\% = 1.38 \pm 0.11 \text{ wt\%}$$

and the TIPS encapsulation efficiency, EE, is:

$$\text{EE} = \frac{\text{wt\% TIPS pentacene calculated}}{\text{wt\% TIPS pentacene targeted during fabrication}} = \frac{1.38 \text{ wt\%}}{1.5 \text{ wt\%}} = 92\% \text{ EE}$$

The major source of uncertainty comes from the propagation of uncertainty in the PLGA composition given the NMR measurements. This analysis shows that almost all of the TIPS pentacene was encapsulated which is consistent with the highly hydrophobic nature of the small molecule fluorophore.

Determination of fluorophore loading and encapsulation efficiency

To determine fluorophore loading and encapsulation efficiency, the particles were freeze-dried as mentioned above without any cryoprotectant. The freeze-dried nanoparticles were then dissolved in THF at concentrations of 0.2 and 0.5 mg/mL with vortex mixing and no sonication, again to protect TIPS pentacene from thermal degradation. TIPS exhibits a local absorbance maximum at 641 nm (**Figure 4a**) where PLGA and Pluronic F127 do not absorb at all and so the absorbance at this wavelength was used to quantify TIPS pentacene loading. The absorbances of these solutions were compared to an absorbance vs. TIPS pentacene concentration calibration curve (**Figure 4b**) to determine the TIPS pentacene concentration in the NP solution and therefore the TIPS pentacene loading. The loading was then used to back calculate the encapsulation efficiency defined as:

$$EE = \frac{\text{wt\% TIPS pentacene determined by absorbance measurement}}{\text{wt\% TIPS pentacene targeted during fabrication}} \quad (\text{S2})$$

Determining NP:trehalose ratio using TIPS pentacene

From the 3 tubes of 0.5 mL reserve suspension that were freeze dried without trehalose, the NP concentration of the reserve suspension (eq. (S3)) was determined using the TIPS pentacene calibration curve and the calculated TIPS pentacene loading.

$$C_{NP;reserve} = \frac{C_{TIPS;tube}}{\text{wt\%}_{TIPS(\text{wrtNP})}} * 100 \quad (\text{S3})$$

where $C_{NP;reserve}$ is the NP concentration in the reserve suspension, $C_{TIP;tube}$ is the concentration of TIPS pentacene in the dissolved NP samples from the freeze dried tubes, and $\text{wt\%}_{TIPS(\text{wrtNP})}$ is the wt% TIPS pentacene with respect to the entire NP as measured from UV-Vis spectrophotometry of a known mass of NP (not to be confused with the wt% TIPS calculated with respect to PLGA as done during the EE calculations) ($\text{wt\%}_{TIPS(\text{wrtNP})} = 1.25$). Eq. (S3) also assumes the freeze-dried particles were dissolved in the same volume of THF as volume of reserve suspension added to the tube (0.5 mL).

From the reserve concentration, the concentration was multiplied by the volume of suspension added to the trehalose tube to get the mass of NPs added and compared to the 200 mg trehalose added per batch to determine the final NP:trehalose mass ratio which ranged from 1:25 to 1:42.

Measuring DNA loading by PicoGreen assay

To determine the DNA loading of the particles, the free DNA concentration in the supernatant that was not encapsulated into the particles was measured using the PicoGreen

dsDNA assay. After the particles were centrifuged during fabrication, the supernatants were decanted into new 50 mL centrifuge tubes. The supernatant was diluted 10-fold into 1 mL aliquots for the measurement. The samples were measured as per instruction of the assay and compared to a set of lambda DNA solutions ranging 0-2000 ng/mL. The assay was read on black 96-well plates using a plate reader (BioTek, SynergyMx) with the sensitivity adjusted so that the 2000 ng/mL signal was below the saturation level of the detector. The DNA concentration of the supernatant was back calculated assuming 21 mL volume (20 mL F127 solution + 1 mL organic solution) and 0.41 mg DNA added in the 1 mL organic during particle formation.

Estimation of the number of plasmid copies per particle

Estimating the number of plasmid copies per particle starts with the hydrodynamic diameter as measured by DLS. The PEG chains from the Pluronic F127 that coat the surface of the particles are assumed to be ~15 nm as assumed by Pansare et al. in their own fluorescence per nanoparticle calculations.³⁸ With the known wt% DNA with respect to PLGA as measured by picoGreen and NMR, we can calculate the approximate plasmid copies per particle with the following equation:

$$\frac{\#plasmids}{NP} = \frac{\pi(d_{core})^3 \rho_{PLGA} * wt\%_{DNA} * N_A}{MW_{DNA}} \quad (S4)$$

where d_{core} is the estimated diameter of the hydrophobic PLGA core [cm], ρ_{PLGA} is the density of bulk PLGA [1.34 g/cm³],³⁹ $wt\%_{DNA}$ is the measured loading of DNA with respect to PLGA, N_A is Avogadro's number, and MW_{DNA} is the molecular mass of the 8500 bp plasmid [g/mol] assuming 650 g/mol base pair.

Calculations of DNA loading with respect to PLGA

The wt% DNA with respect to PLGA values that make up the y-axis for **Figure 5** in the main text was calculated from picoGreen assays of the DNA concentrations in the supernatant during the release studies at known NP concentrations.

$$\text{wt\%}_{\text{DNA}} = \frac{C_{\text{DNA;picoGreen}}}{C_{\text{NP}} * \text{wt\%}_{\text{PLGA}}} \quad (\text{S5})$$

where $C_{\text{DNA;picoGreen}}$ is the DNA concentration as measured by the picoGreen assay, C_{NP} is the known NP concentration in the suspension, and $\text{wt\%}_{\text{PLGA}}$ is the percent PLGA that makes up the polymer carrier as determined by NMR analysis. The mass of DNA is not accounted for in the total mass calculation of the denominator because the DNA loadings with respect to the entire nanoparticle is less than 1 wt% and considered negligible.

DNA release profile

Using the approximate ratio of trehalose:NP as described, ~9-10 mg of NPs were weighed into three separate 15 mL tubes for each of the 4 cases, i.e. the ester and the amine end-capped PLGA types with and without DNA for a total of 12 samples. The 3 tubes of each NP case were resuspended in PBS at 3 different pHs (4.5, 6.0, 7.0) at a final nanoparticle concentration of 1 mg/mL. The buffers started from 1x PBS and were titrated to the target pHs using HCl measured using a pH meter (Denver Instrument UB-5 with ThermoScientific OrionTM 9156DJWP Double Junction Electrode). The samples were left to equilibrate overnight and titrated again back to the target pH. The buffers were then autoclaved for sterility and aliquots were tested a final time for correct pH to keep the stock sterile. The 15 mL tubes of suspensions were vortexed and sonicated for 1 minute before being aliquoted to 9 separate 2 mL centrifuge tubes for each of the time points. The tubes were stored in a 37°C incubator on a nutating mixer (Fisher Scientific Nutating Mixer Variable Speed 3D Platform Rotator Model # 88861043) at 15

RPM and removed at specified time points for analysis. At each time point, the particles were spun down at 16,060 x g for 20 minutes at room temperature and 500 μ L of the supernatant were used for the PicoGreen assay. A stock volume (1 mL per time point) of each dilution for the lambda DNA standard calibration was made to keep the standard concentrations consistent across all times points.

Macrophage Nanoparticle and CRISPR Challenge

Bone marrow derived macrophages (BMDMs) were isolated from wild type mice following standard procedures.⁴⁰ Briefly, bone marrow isolated from the femur and tibia from C57Bl/6 female mice aged 8-12 weeks was incubated for 6 days with Dulbecco Modified Eagle Media (DMEM) supplemented with 10% fetal bovine serum, 1x penicillin/streptomycin, and 20% L929-conditioned media. On day 6, total cell numbers were counted and replated at a cell density of 500,000 cells/mL. After overnight incubation with complete DMEM supplemented with 10% fetal bovine serum and 1x penicillin/streptomycin, the macrophages were resuspended with plain DMEM and either blank nanoparticles (100 μ g/ml), CRISPR plasmid-loaded nanoparticles (100 μ g/ml), CRISPR plasmid with Lipofectamine 3000 (2 μ g/ml DNA), CRISPR plasmid only (2 μ g/ml), PBS for 24 hours.

LIST OF ABBREVIATIONS

CRISPR	clustered regularly interspaced palindromic repeats
PLGA	poly(lactic-co-glycolic acid)
TIPS	6,13-bis(triisopropylsilylethynyl)
BMDM	bone marrow derived macrophages
THF	tetrahydrofuran
DMSO	dimethyl sulfoxide

DMF dimethylformamide
TE Tris-Ethylenediaminetetraacetic acid

DECLARATIONS

Ethics Approval

Animals were housed and maintained, prior to humane euthanasia for the generation of bone marrow derived macrophages, with institutional IACUC approval and in accordance with the NIH Guide for the Care and Use of Laboratory Animals.

Availability of Data and Materials

All data generated or analyzed during this study are included in this article and in the Supplemental files.

Competing Interests

The authors declare no competing interests.

Funding

Financial support for this work was provided by the American Association of Immunologist (I.C.A. and V.M.R.-S.), the Virginia Tech Center for Engineered Health (I.C.A. and R.M.D.), the Institute for Critical Technology and Applied Sciences (D.K.M., I.C.A. and R.M.D.), and the Virginia Maryland College of Veterinary Medicine (I.C.A.).

Authors' Contribution

A.J. and V.M.R.-S. contributed equally to this work. A.J. conducted the fabrication and characterization experiments of the nanoparticles and analyzed the results with help from R.Z. for the NMR work. D.K.M. and V.M.R.-S conducted and analyzed the cell studies. V.M.R.-S. also purified the biologic of interest with additional help from C.T. All authors analyzed the results and reviewed the manuscript.

Acknowledgements

The authors would like to thank Dr. Kiho Lee for generously providing plasmids and vectors used in this research study. We would also like to thank Melissa Makris for providing flow cytometry support.

REFERENCES

- 1 Horvath, P. & Barrangou, R. CRISPR/Cas, the immune system of bacteria and archaea. *Science* **327**, 167-170, doi:10.1126/science.1179555 (2010).
- 2 Long, C. *et al.* Prevention of muscular dystrophy in mice by CRISPR/Cas9-mediated editing of germline DNA. *Science* **345**, 1184-1188, doi:10.1126/science.1254445 (2014).
- 3 Xue, W. *et al.* CRISPR-mediated direct mutation of cancer genes in the mouse liver. *Nature* **514**, 380-384, doi:10.1038/nature13589 (2014).
- 4 Yin, H. *et al.* Genome editing with Cas9 in adult mice corrects a disease mutation and phenotype. *Nature biotechnology* **32**, 551-553, doi:10.1038/nbt.2884 (2014).
- 5 Bauer, M. *et al.* Toxic effects of lipid-mediated gene transfer in ventral mesencephalic explant cultures. *Basic Clin Pharmacol* **98**, 395-400, doi:DOI 10.1111/j.1742-7843.2006.pto_310.x (2006).
- 6 Murakami, T. & Sunada, Y. Plasmid DNA Gene Therapy by Electroporation: Principles and Recent Advances. *Current Gene Therapy* **11**, 447-456 (2011).
- 7 Zolochavska, O. *et al.* Sonoporation Delivery of Interleukin-27 Gene Therapy Efficiently Reduces Prostate Tumor Cell Growth In Vivo. *Hum Gene Ther* **22**, 1537-1550, doi:10.1089/hum.2011.076 (2011).
- 8 Maggio, I., Holkers, M., Liu, J., Janssen, J. M. & Goncalves, M. A. Adenoviral Vector Delivery of RNA-Guided CRISPR/Cas9 Nuclease Complexes Induces Targeted Mutagenesis in a Diverse Array of Human Cells. *Mol Ther* **22**, S190-S190 (2014).
- 9 Ehrke-Schulz, E. *et al.* CRISPR/Cas9 delivery with one single adenoviral vector devoid of all viral genes. *Sci Rep* **7**, doi:ARTN 17113 10.1038/s41598-017-17180-w (2017).

- 10 Cohen, H. *et al.* Sustained delivery and expression of DNA encapsulated in polymeric nanoparticles. *Gene Ther* **7**, 1896-1905, doi:DOI 10.1038/sj.gt.3301318 (2000).
- 11 Acharya, S. & Sahoo, S. K. PLGA nanoparticles containing various anticancer agents and tumour delivery by EPR effect. *Adv Drug Deliver Rev* **63**, 170-183, doi:10.1016/j.addr.2010.10.008 (2011).
- 12 Danhier, F. *et al.* PLGA-based nanoparticles: An overview of biomedical applications. *J Control Release* **161**, 505-522, doi:10.1016/j.jconrel.2012.01.043 (2012).
- 13 Cun, D. M. *et al.* High loading efficiency and sustained release of siRNA encapsulated in PLGA nanoparticles: Quality by design optimization and characterization. *European Journal of Pharmaceutics and Biopharmaceutics* **77**, 26-35, doi:10.1016/j.ejpb.2010.11.008 (2011).
- 14 Niu, X. M., Zou, W. W., Liu, C. X., Zhang, N. & Fu, C. H. Modified nanoprecipitation method to fabricate DNA-loaded PLGA nanoparticles. *Drug Dev Ind Pharm* **35**, 1375-1383, doi:10.3109/03639040902939221 (2009).
- 15 Ke, F., Luu, Y. K., Hadjiargyrou, M. & Liang, D. Characterizing DNA Condensation and Conformational Changes in Organic Solvents. *PLoS ONE* **5**, e13308, doi:doi:10.1371/journal.pone.0013308 (2010).
- 16 Oh, K. T., Bronich, T. K. & Kabanov, A. V. Micellar formulations for drug delivery based on mixtures of hydrophobic and hydrophilic Pluronic block copolymers. *J Control Release* **94**, 411-422 (2004).
- 17 Huotari, J. & Helenius, A. Endosome maturation. *Embo J* **30**, 3481-3500, doi:10.1038/emboj.2011.286 (2011).

- 18 Evans, R. K. *et al.* Evaluation of degradation pathways for plasmid DNA in pharmaceutical formulations via accelerated stability studies. *Journal of Pharmaceutical Sciences* **89**, 76-87, doi:Doi 10.1002/(Sici)1520-6017(200001)89:1<76::Aid-Jps8>3.0.Co;2-U (2000).
- 19 Balmert, S. C. *et al.* Positive charge of "sticky" peptides and proteins impedes release from negatively charged PLGA matrices. *Journal of Materials Chemistry B* **3**, 4723-4734, doi:10.1039/c5tb00515a (2015).
- 20 Croll, T. I., O'Connor, A. J., Stevens, G. W. & Cooper-White, J. J. Controllable surface modification of poly(lactic-co-glycolic acid) (PLGA) by hydrolysis or aminolysis I: physical, chemical, and theoretical aspects. *Biomacromolecules* **5**, 463-473, doi:10.1021/bm0343040 (2004).
- 21 Sedlackova, T., Repiska, G., Celec, P., Szemes, T. & Minarik, G. Fragmentation of DNA affects the accuracy of the DNA quantitation by the commonly used methods. *Biol Proced Online* **15**, doi:Artn 5 10.1186/1480-9222-15-5 (2013).
- 22 Ahn, S. J., Costa, J. & Emanuel, J. R. PicoGreen quantitation of DNA: Effective evaluation of samples pre- or post-PCR (vol 24, pg 2623, 1996). *Nucleic Acids Res* **24**, 3282-3282 (1996).
- 23 Holden, M. J. *et al.* Factors Affecting Quantification of Total DNA by UV Spectroscopy and PicoGreen Fluorescence. *J Agr Food Chem* **57**, 7221-7226, doi:10.1021/jf901165h (2009).
- 24 McDaniel, D. K. *et al.* TIPS pentacene loaded PEO-PDLLA core-shell nanoparticles have similar cellular uptake dynamics in M1 and M2 macrophages and in corresponding

- in vivo microenvironments. *Nanomedicine: Nanotechnology, Biology and Medicine* **13**, 1255-1266, doi:http://doi.org/10.1016/j.nano.2016.12.015 (2017).
- 25 Poltorak, A. *et al.* Defective LPS signaling in C3H/HeJ and C57BL/10ScCr mice: Mutations in Tlr4 gene. *Science* **282**, 2085-2088, doi:DOI 10.1126/science.282.5396.2085 (1998).
- 26 Glass, Z., Li, Y. M. & Xu, Q. B. Nanoparticles for CRISPR-Cas9 delivery. *Nat Biomed Eng* **1**, 854-855, doi:10.1038/s41551-017-0158-x (2017).
- 27 Lee, K. *et al.* Nanoparticle delivery of Cas9 ribonucleoprotein and donor DNA in vivo induces homology-directed DNA repair. *Nat Biomed Eng* **1**, 889-901, doi:10.1038/s41551-017-0137-2 (2017).
- 28 Wang, P. *et al.* Thermo-triggered Release of CRISPR-Cas9 System by Lipid-Encapsulated Gold Nanoparticles for Tumor Therapy. *Angewandte Chemie-International Edition* **57**, 1491-1496, doi:10.1002/anie.201708689 (2018).
- 29 Finn, J. D. *et al.* A Single Administration of CRISPR/Cas9 Lipid Nanoparticles Achieves Robust and Persistent In Vivo Genome Editing. *Cell Rep* **22**, 2227-2235, doi:10.1016/j.celrep.2018.02.014 (2018).
- 30 Cross, R. CRISPR's breakthrough problem. *Chem Eng News* **95**, 28-33 (2017).
- 31 Zhou, W., Cui, H., Ying, L. & Yu, X. F. Enhanced Cytosolic Delivery and Release of CRISPR/Cas9 by Black Phosphorus Nanosheets for Genome Editing. *Angew Chem Int Ed Engl*, doi:10.1002/anie.201806941 (2018).
- 32 Lin, Y. *et al.* Exosome-Liposome Hybrid Nanoparticles Deliver CRISPR/Cas9 System in MSCs. *Adv Sci* **5**, doi:ARTN 1700611 10.1002/advs.201700611 (2018).

- 33 Jin, W. *et al.* Transfection of Difficult-to-Transfect Rat Primary Cortical Neurons with Magnetic Nanoparticles. *J Biomed Nanotechnol* **14**, 1654-1664, doi:10.1166/jbn.2018.2604 (2018).
- 34 van Overbeek, M. *et al.* DNA Repair Profiling Reveals Nonrandom Outcomes at Cas9-Mediated Breaks. *Mol Cell* **63**, 633-646, doi:10.1016/j.molcel.2016.06.037 (2016).
- 35 Ghezraoui, H. *et al.* Chromosomal translocations in human cells are generated by canonical nonhomologous end-joining. *Mol Cell* **55**, 829-842, doi:10.1016/j.molcel.2014.08.002 (2014).
- 36 Kosicki, M., Tomberg, K. & Bradley, A. Repair of double-strand breaks induced by CRISPR-Cas9 leads to large deletions and complex rearrangements. *Nat Biotechnol* **36**, 765-771, doi:10.1038/nbt.4192 (2018).
- 37 Ran, F. A. *et al.* Genome engineering using the CRISPR-Cas9 system. *Nat Protoc* **8**, 2281-2308, doi:10.1038/nprot.2013.143 (2013).
- 38 Pansare, V. J., Bruzek, M. J., Adamson, D. H., Anthony, J. & Prud'homme, R. K. Composite Fluorescent Nanoparticles for Biomedical Imaging. *Mol. Imaging. Biol.* **16**, 180-188, doi:10.1007/s11307-013-0689-9 (2014).
- 39 Arnold, M. M., Gorman, E. M., Schieber, L. J., Munson, E. J. & Berkland, C. NanoCipro encapsulation in monodisperse large porous PLGA microparticles. *J Control Release* **121**, 100-109, doi:10.1016/j.jconrel.2007.05.039 (2007).
- 40 Pineda-Torra, I., Gage, M., de Juan, A. & Pello, O. M. Isolation, Culture, and Polarization of Murine Bone Marrow-Derived and Peritoneal Macrophages. *Methods Mol Biol* **1339**, 101-109, doi:10.1007/978-1-4939-2929-0_6 (2015).

FIGURES

Figure 1: TIPS pentacene can be used as a fluorescent marker for cell internalization

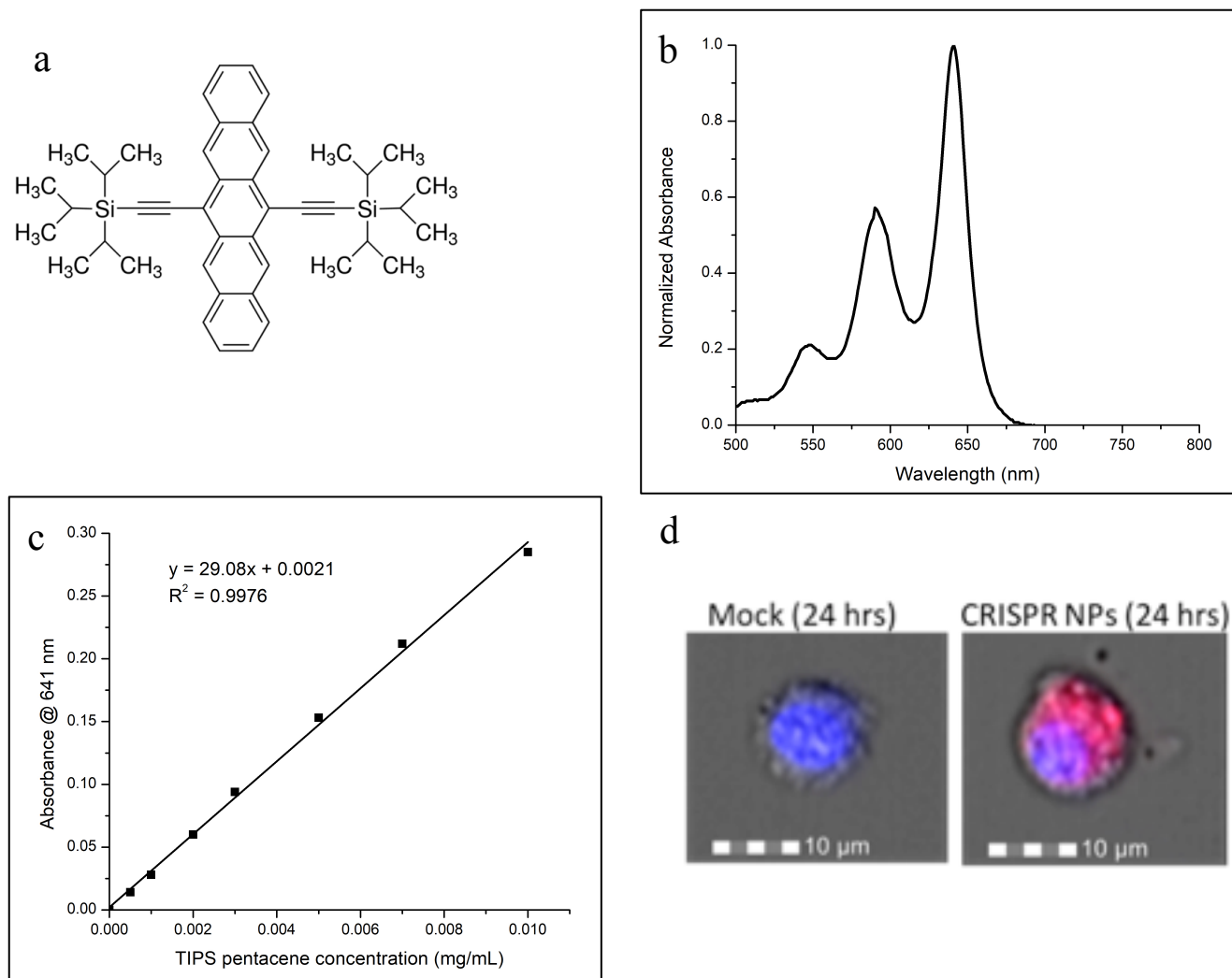


Figure 1. TIPS pentacene can be used as a fluorescent marker for cell internalization. (a) TIPS structure, (b) Normalized absorbance spectrum of TIPS pentacene in THF (v/v), (c) Calibration curve of absorbance vs. TIPS pentacene concentration in THF by volume, (d) Imaging cytometer images of BMDM cells treated with either mock or TIPS loaded NPs demonstrates internalization of particles into the cell as indicated by red fluorescence signal.

Figure 2: Analysis of F127 and PLGA proton NMR spectra show distinct peaks that can be used to determine polymer composition of resulting nanoparticles

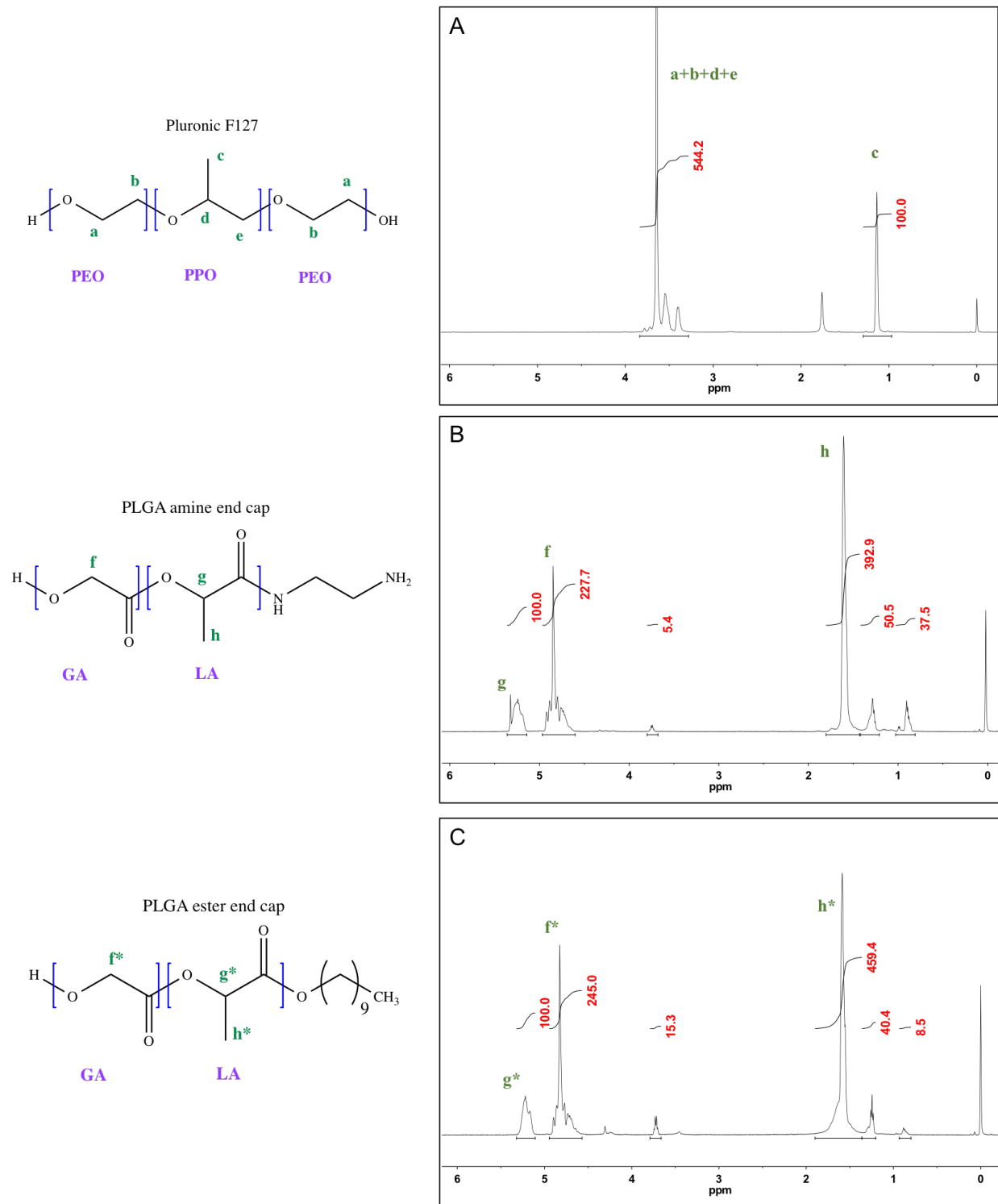


Figure 2. Analysis of F127 and PLGA proton NMR spectra show distinct peaks that can be used to determine polymer composition of resulting nanoparticles. ^1H NMR spectra of (a) Pluronic F127 and (b) ester end capped PLGA (c) amine end capped PLGA in CDCl_3 .

Figure 3: Mass ratio of Pluronic F127 and PLGA in the nanoparticles determined by proton NMR allows for more accurate calculations of encapsulation efficiency

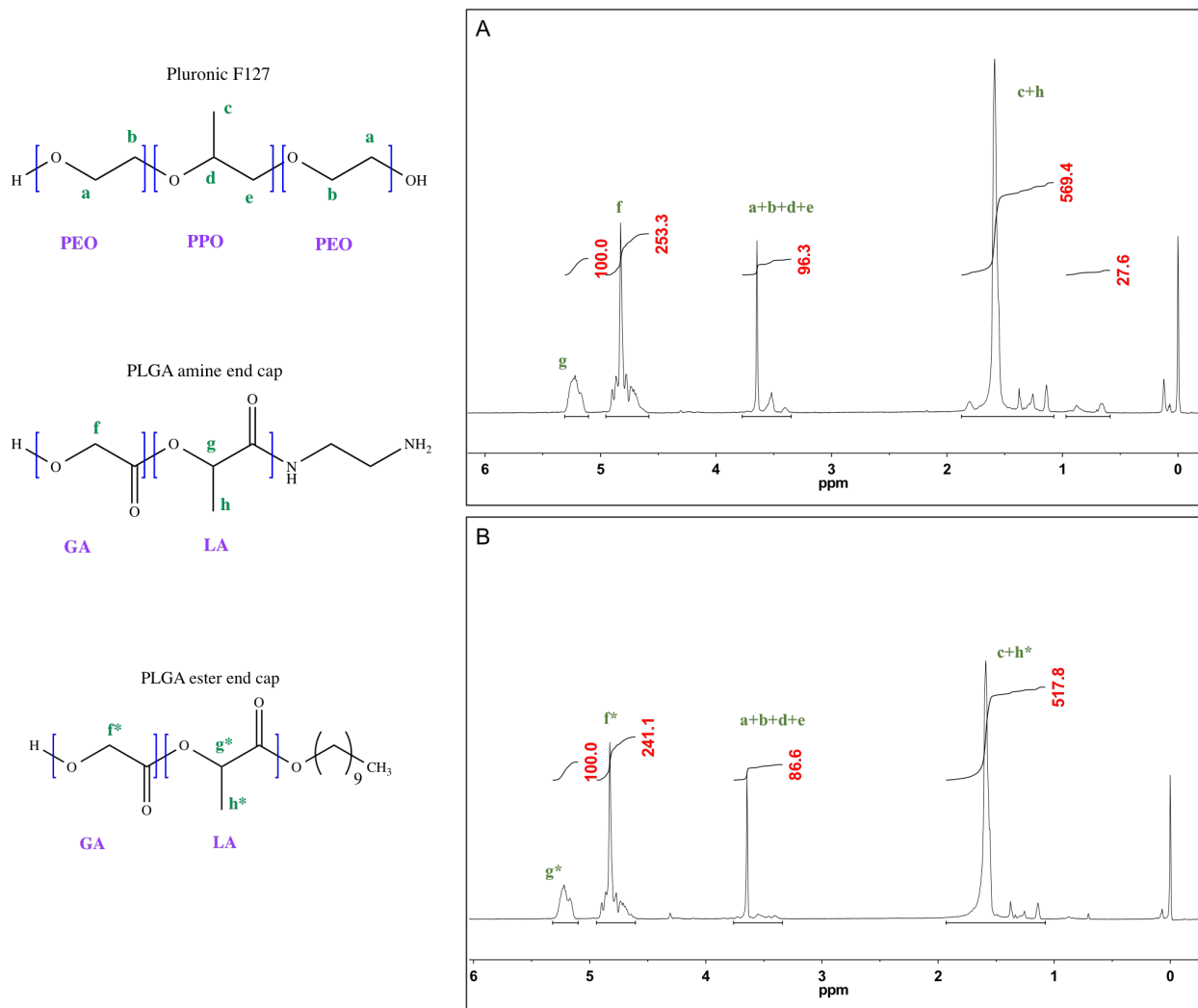


Figure 3. Mass ratio of Pluronic F127 and PLGA in the nanoparticles determined by proton NMR allows for more accurate calculations of encapsulation efficiency. ^1H NMR of NPs made with (a) ester end cap PLGA and (b) amine end cap PLGA.

Figure 4: Majority of DNA released within the first 24 hours with NPs made from amine endcaps at pH 7 showing the highest level of release

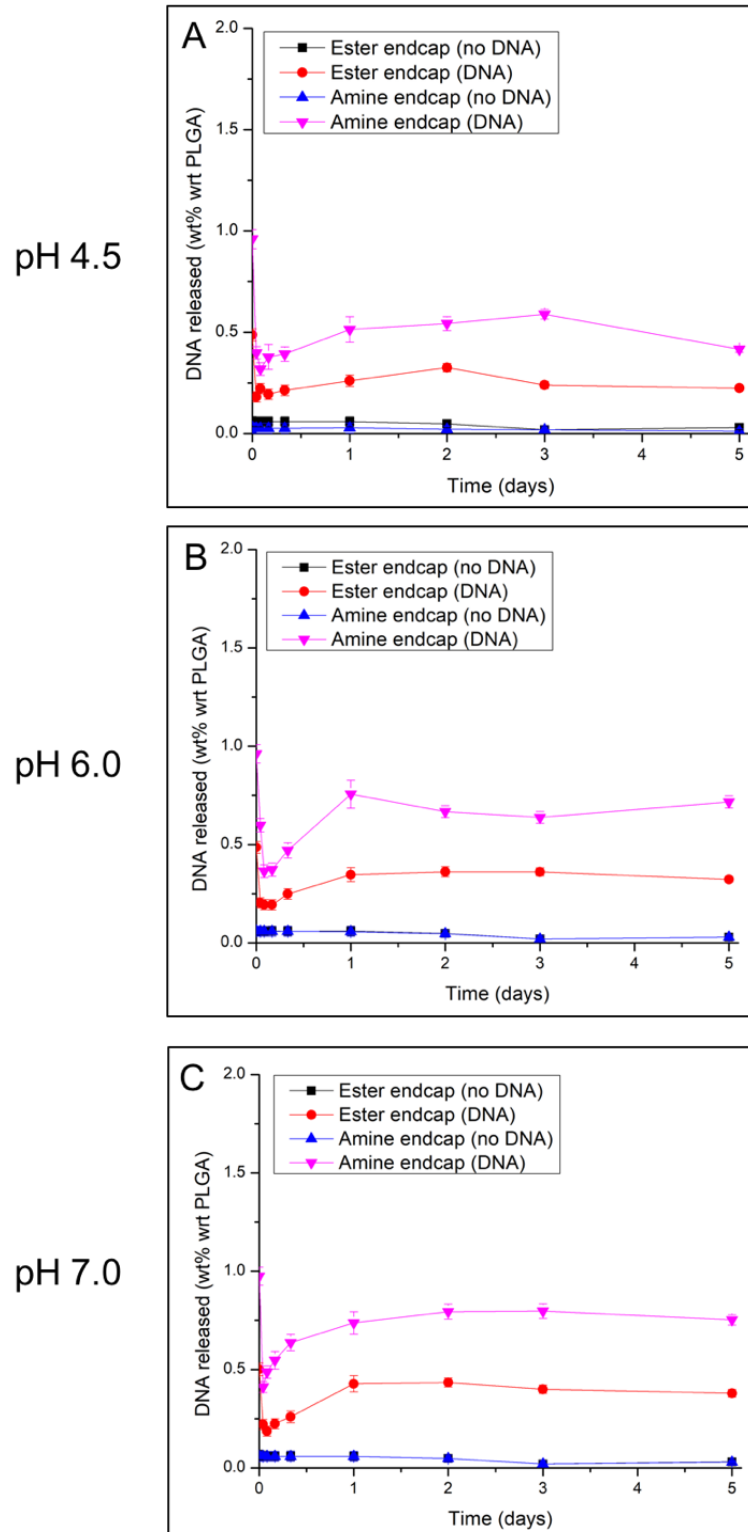


Figure 4. Majority of DNA released within the first 24 hours with NPs made from amine endcaps at pH 7 showing the highest level of release. DNA release profile from the particles with respect to time at pH (a) 7.0, (b) 6.0 (c) 4.5.

Figure 5: Bacterial *S. pyogenes* Cas9 protein is successfully translated inside murine macrophages

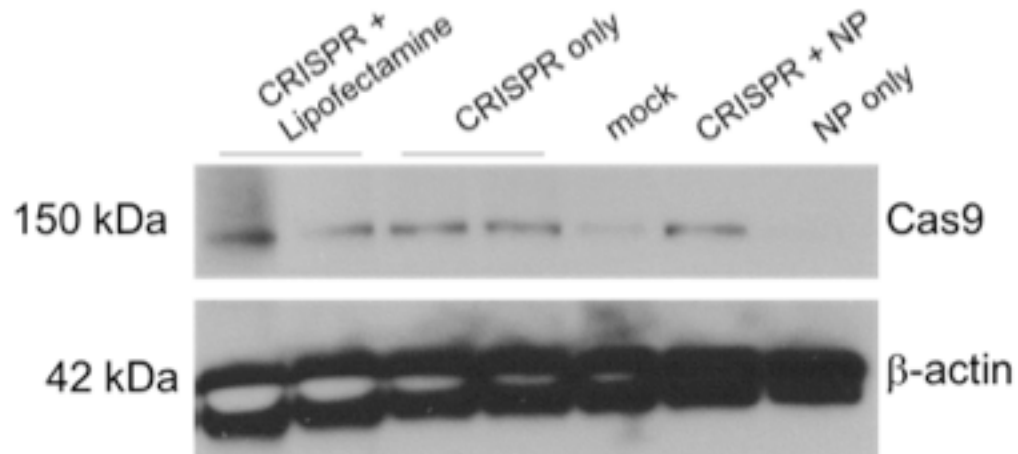


Figure 5. Bacterial *S. pyogenes* Cas9 protein is successfully translated inside murine macrophages. After 24 hours incubation with CRISPR+ Lipofectamine (lanes 1 and 2), CRISPR plasmid only (lanes 3 and 4), PBS only (lane 5), CRISPR loaded nanoparticle (lane 6), and blank nanoparticle (lane 7), *S. pyogenes* Cas9 protein was detectable by Western Blot.

Table 1

Sample	PLGA end cap	Target DNA loading (wt% based on PLGA)	Actual DNA loading (wt% based on PLGA)	Before freeze drying			Freeze dried 1:~25 NP:trehalose (w:w)		
				D ₁ (nm)	PDI	ZP (mV)	D ₁ (nm)	PDI	ZP (mV)
A	Ester (neutral)	-	-	157	0.06	-31	344	0.42	-29
B		2	0.7	160	0.11	-33	213	0.23	-35
C	Amine (+)	-	-	177	0.11	-24	290	0.37	-27
D		2	1.6	182	0.08	-26	260	0.21	-30

Table 1. Size and zeta potential of NPs in DI water made with different end-capped PLGA before and after lyophilization.

SUPPLEMENTAL FIGURE

Figure S1: Designed target sequence for gRNA in CRISPR-Cas9 plasmid, targeting *Tlr4*

<p><u>gRNA target sequence:</u></p> <p>CACC CCT GGT GTA GCC ATT GCT GCC AA GGA CCA CAT CGG TAA CGA CGG TT CAAA</p>

Figure S1. Designed target sequence for gRNA in CRISPR-Cas9 plasmid, targeting *Tlr4*.

Chapter Seven

Discussion and Conclusions

Veronica M. Ringel-Scaia

Cancer affects millions of people worldwide, and is the second leading cause of death in the United States.¹ Despite improvements to the overall average survival rate, the most updated estimates predict that over 600,000 American patients will die from cancer in 2019, equating to nearly 1,700 deaths per day.¹ Awareness of preventable lifestyle-related risks²⁻⁵ has not led to significant improvements in prevention, and cancer rates continue to rise. Combatting the ever-increasing exposure to cancer risks within the world population may not be feasible on a meaningful scale; to refine treatments and outcomes for the millions of cancer patients, novel ways of thinking about the disease is necessary. The focus of this work was to provide unique insight for understanding, treating, and targeting cancer from the perspective of a family of cellular receptors of the innate immune system. By focusing on Pattern Recognition Receptors (PRRs), this work provides context for improving overall understanding of cancer. The goal of the work presented here is to provide evidence of the advantages of considering PRRs as a tool for understanding cancer, in order to ultimately lead to improved treatments for patients.

Attempts to pinpoint specific causes of cancer have oftentimes fallen short due to the complexity and heterogeneity of the disease. Conclusions drawn from laboratory techniques that isolate and utilize a single cancer cell type, while useful, oftentimes fail or cannot be reproduced *in situ* or *in vivo*. The cunning nature of cancer is to usurp normal and crucial biological

processes of the body to the advantage of the tumor and ultimate detriment to the healthy tissue. We have since accepted that the immune system is often one such process that is hijacked by cancer. The “immune surveillance” concept and hypothesis has evolved in the years since its inception; after initially being abandoned due to lack of experimental evidence, it is now considered a means for understanding cancer and the immune system.⁶ Dunn et al. described an updated theory of immunological regulation of cancer, “cancer immunoediting,” in three parts: the elimination phase where cancerous cells are destroyed by the immune system, the equilibrium phase between the immune system and malignant cells, and the escape phase where the immune system fails to destroy the tumor and it is now clinically detectable as a tumor.⁷ It is now clear that both the innate and adaptive arms of the immune system play a role in the regulation of cancer,⁶ and advances in cancer treatments founded in the role of the immune system have been successful when exploiting this. The current status of cancer therapy that relies on activating the host immune system to produce antitumor effects, or cancer immunotherapy, can be grouped into three main categories: tumor vaccinations, adoptive cell transfer, and checkpoint inhibitors.^{8,9} In order to improve the outcomes of not only immunotherapies, but all therapies, clearer understanding of the biological causes for both the prevention and promotion of cancer development is crucial.

NLRs and Understanding Cancer

No two tumors are exactly alike. Few targets remain consistent between tumor types and tissue of origin, patients and risk factors, metastatic and localized disease. Reaffirming this point, we have described a phenomenon associated with a particular group of PRRs whose role in regulating gastrointestinal inflammation we have coined “The Goldilocks Conundrum.”¹⁰ The

particular PRRs of interest are nucleotide-binding oligomerization domain and leucine-rich repeat containing (NOD-like) receptors (NLRs), which can further be classified based on how they respond when activated and their predominant role as either regulatory, reproductive, or inflammasome-forming. As described in chapter two, inflammasome-forming NLRs play a dual role in gastrointestinal homeostasis and disease: both hyper- and hypo-activity can lead to the development of disease.¹⁰ This insight is noteworthy, as it implies that the mechanism of inflammasome activation is likely more closely regulated and controlled than perhaps initially thought. It is interesting to speculate that there may be an as of yet unknown drug-targetable mechanism responsible for regulating the activity of inflammasome-forming NLRs within the gastrointestinal tract and beyond.

Indeed, the role of NLRs within the gastrointestinal tract is complex and intricate, as we see in chapter three. As previously described, animals that lack a specific inflammasome-forming NLR, NLRP1, are predisposed to worsened disease phenotype of experimentally induced colitis-associated cancer.¹¹ We initially anticipated that the communities within the gut microbiome of these *Nlrp1*^{-/-} animals would be characterized by dysbiosis and an overabundance of bacteria that should be regulated and controlled by the NLRP1 receptor. However, after carefully controlling for all potential influencing factors, we saw that caging and maternal influence were far greater predictors of microbiota composition rather than genotype in our *Nlrp1*^{-/-} animals.¹² This work has major implications for all future work involving NLR knockout animals, as we clearly see that the housing strategy significantly alters the microbiome composition. It also calls into question all previous studies that used NLR-deficient animals that were not bred as littermates to equilibrate microbiomes prior to being subjected to the model.

Pyroptosis and Treating Cancer

Beyond immunotherapy, additional treatment approaches are showing significant promise in both pre-clinical and clinical breast cancer studies,^{13,14} the most commonly diagnosed cancer in woman. These therapeutic approaches include cryotherapy, laser irradiation, microwave irradiation, radiofrequency ablation, high-intensity focused ultrasound ablation, and irreversible electroporation (IRE). IRE delivers short electric pulses through electrodes inserted directly into the targeted tumors, and induces cell death by increasing the transmembrane potential and disrupting cancer cell homeostasis. This technique is being evaluated in clinical trials for a range of cancers including liver, pancreas, prostate, kidney, and brain.¹⁵⁻²⁰ The second-generation adaptation of this technology, high-frequency irreversible electroporation (H-FIRE), utilizes high-frequency bipolar bursts.

Effective tumor ablation does not depend on or require a functioning immune system. However, as observed in chapter four, a functioning immune system results in a significantly improved reduction in both primary tumor size and metastases in animals treated with H-FIRE. In the murine 4T1 model of triple negative breast cancer, we saw evidence of a shift in the immunosuppressive tumor microenvironment to one that is pro-inflammatory, significant decreases in infiltrating immunosuppressive cells within the tumor microenvironment, and significant increase in inflammatory cell death within the treatment field. The predominant form of cell death induced via H-FIRE was mechanistically consistent with pyroptosis, a pathway downstream of NLR activation.²¹ Localized H-FIRE tumor ablation leads to the activation of the innate immune system via increased damage signals associated with pyroptosis in the treatment zone. The damage signals, coupled with the shift to a pro-inflammatory tumor microenvironment, are sufficient to ultimately engage the adaptive immune system and increase

systemic antitumor immunity. H-FIRE is a promising new modality with the potential to revolutionize cancer treatment options for metastatic disease, if a localized ablation is sufficient to stimulate systemic antitumor effects at any and all metastatic tumors. It is within reason to hypothesize that H-FIRE could be clinically administered prior to surgical resection to “prime” the immune system and increase the odds of minimizing metastases.

TLRs and Targeting Cancer

Despite best efforts to develop drugs and technology with high specificity for tumors, physical limitations associated with tumor configuration and location impede successful delivery. Malignancies associated with the gastrointestinal tract epitomize a difficult to target tumor location. Specifically, several impediments to drug delivery to gastrointestinal tumors include: toxicity associated with delivering a sufficient concentration of drugs, insolubility of anti-cancer small molecular weight macromolecules such as genes or proteins, impenetrable mucus, uncontrolled release of therapeutics, and a lack of specific targeting of tumors. As reviewed in chapter five, advances in nanoparticle-coupled drug delivery systems, or nanocarriers, have addressed some of the numerous challenges associated with traditional treatment of gastrointestinal cancers through the employment of biocompatible nanocarriers to solubilize, stabilize, and control release of drugs and other anti-cancer agents.²²

Oftentimes, nanoparticle delivery to tumors relies on the relative leakiness of the blood vessels and poor lymphatic drainage that is characteristic of tumors, known as the enhanced permeability and retention (EPR) effect.²² However, this form of passive targeting to tumors can be hindered by the high interstitial pressure within solid tumors which prevents adequate uptake of the nanoparticle within a tumor and homogenous distribution of the nanoparticle.²³ To combat

this, strategies known as active targeting, whereby the surfaces of nanoparticles can be coated with highly specific ligands for markers on or within the cancerous cells of interest, such as antibodies, proteins, or aptamers,²⁴ can be employed. In theory, active targeting would lead to the “homing” of a nanoparticle to the tumor of interest, while sparing the surrounding healthy tissue. Nanoparticle drug encapsulation and subsequent nanocarrier delivery is essentially limitless; the most significant challenge is efficient and successful encapsulation of the drug or therapeutic within uniform and nanoscale particles.

Nanoparticle delivery actively or passively targeting PRRs could open the door for a variety of new therapeutic outcomes in any disease associated with increased or decreased PRR activation. As a proof of principle, one such example of PRR-targeting via nanoparticles is highlighted in chapter six, in which a very large CRISPR-Cas9 plasmid targeting a murine PRR gene, *Tlr4*, was loaded into polymer nanoparticles. TLR4 is a PRR responsible for sensing the endotoxin or lipopolysaccharide (LPS) from gram-negative bacteria.²⁵ Both hypoactive and hyperactive LPS responsiveness have been linked to detrimental inflammatory responses and disease.²⁶ As we see from the work presented in chapter six, the nanoprecipitation fabrication method can be employed to successfully encapsulate large genetic material and importantly conserves plasmid functionality. The technique developed in chapter six has broad implications for drug encapsulation and delivery in a multitude of cancers and diseases. It is certainly interesting to speculate that nanocarriers could be developed in the future that actively target ligands expressed on or within a tumor, while passively targeting aberrant PRRs within the tumor.

CONCLUSIONS

Each of the studies included in this work have attempted to address gaps in the literature surrounding PRRs and cancer in different ways. There has been debate within the NLR field as to the role of NLRs in regulating the microbiome and how this may potentially translate to cancer risk; dysbiosis within the microbiome is often cited as a hypothetical contribution to gastrointestinal disease development. As we clearly demonstrate in chapter three, the function of a specific NLR, NLRP1, in the attenuation of colitis-associated cancer is not due to regulation of microbial communities within the gut microbiome. Contrary to the assumed importance of NLRs in the microbiome, other PRR-dependent mechanisms in cancer can frequently be overlooked. An example of such unnoticed system is the influence of the innate immune system following tumor ablation with H-FIRE. After the initial development of the technology, it was assumed that the mechanical destruction of the tumors themselves was sufficient. As we have clearly shown in chapter four, the mechanism of cell death following H-FIRE ablation has the capability to activate the innate immune system, leading to improved overall outcomes of treatment and long term survival. PRRs are important and significant in the prevention of and/or predisposition to cancer, as well as the success or failure of a therapeutic treatment. As such, it was our goal to develop a technology whereby a specific PRR, TLR4, could be targeted with nanoparticles in chapter six. We have proved that we can encapsulate a plasmid specific for *Tlr4* in a nanocarrier, opening numerous possibilities for modifications to target other PRRs with nanotechnology. This collection of work merely begins to explore the role of PRRs on a variety of key components of cancer and undoubtedly demonstrates that PRRs are vital to understanding, treating, and targeting cancer.

REFERENCES

- 1 Siegel, R. L., Miller, K. D. & Jemal, A. Cancer statistics, 2019. *CA Cancer J Clin* **69**, 7-34, doi:10.3322/caac.21551 (2019).
- 2 Grosso, G. *et al.* Possible role of diet in cancer: systematic review and multiple meta-analyses of dietary patterns, lifestyle factors, and cancer risk. *Nutr Rev* **75**, 405-419, doi:10.1093/nutrit/nux012 (2017).
- 3 Peisch, S. F., Van Blarigan, E. L., Chan, J. M., Stampfer, M. J. & Kenfield, S. A. Prostate cancer progression and mortality: a review of diet and lifestyle factors. *World J Urol* **35**, 867-874, doi:10.1007/s00345-016-1914-3 (2017).
- 4 Pischon, T. & Nimptsch, K. Obesity and Risk of Cancer: An Introductory Overview. *Recent Results Cancer Res* **208**, 1-15, doi:10.1007/978-3-319-42542-9_1 (2016).
- 5 Yamagiwa, Y. *et al.* Fruit and vegetable intake and pancreatic cancer risk in a population-based cohort study in Japan. *Int J Cancer* **144**, 1858-1866, doi:10.1002/ijc.31894 (2019).
- 6 Ribatti, D. The concept of immune surveillance against tumors. The first theories. *Oncotarget* **8**, 7175-7180, doi:10.18632/oncotarget.12739 (2017).
- 7 Dunn, G. P., Bruce, A. T., Ikeda, H., Old, L. J. & Schreiber, R. D. Cancer immunoediting: from immunosurveillance to tumor escape. *Nat Immunol* **3**, 991-998, doi:10.1038/ni1102-991 (2002).
- 8 Yousefi, H., Yuan, J., Keshavarz-Fathi, M., Murphy, J. F. & Rezaei, N. Immunotherapy of cancers comes of age. *Expert Rev Clin Immunol* **13**, 1001-1015, doi:10.1080/1744666X.2017.1366315 (2017).

- 9 Yu, Y. & Cui, J. Present and future of cancer immunotherapy: A tumor microenvironmental perspective. *Oncol Lett* **16**, 4105-4113, doi:10.3892/ol.2018.9219 (2018).
- 10 Ringel-Scaia, V. M., McDaniel, D. K. & Allen, I. C. The Goldilocks Conundrum: NLR Inflammasome Modulation of Gastrointestinal Inflammation during Inflammatory Bowel Disease. *Crit Rev Immunol* **36**, 283-314, doi:10.1615/CritRevImmunol.2017019158 (2016).
- 11 Williams, T. M. *et al.* The NLRP1 inflammasome attenuates colitis and colitis-associated tumorigenesis. *J Immunol* **194**, 3369-3380, doi:10.4049/jimmunol.1402098 (2015).
- 12 Ringel-Scaia, V. M. *et al.* Maternal Influence and Murine Housing Confound Impact of NLRP1 Inflammasome on Microbiome Composition. *J Innate Immun*, 1-16, doi:10.1159/000495850 (2019).
- 13 Vikas, P., Borcherdig, N. & Zhang, W. The clinical promise of immunotherapy in triple-negative breast cancer. *Cancer Manag Res* **10**, 6823-6833, doi:10.2147/CMAR.S185176 (2018).
- 14 Garcia-Tejedor, A. *et al.* Radiofrequency Ablation Followed by Surgical Excision versus Lumpectomy for Early Stage Breast Cancer: A Randomized Phase II Clinical Trial. *Radiology* **289**, 317-324, doi:10.1148/radiol.2018180235 (2018).
- 15 Garcia, P. A. *et al.* Non-thermal irreversible electroporation (N-TIRE) and adjuvant fractionated radiotherapeutic multimodal therapy for intracranial malignant glioma in a canine patient. *Technol Cancer Res Treat* **10**, 73-83, doi:10.7785/tcrt.2012.500181 (2011).

- 16 Rossmeisl, J. H., Jr. *et al.* Safety and feasibility of the NanoKnife system for irreversible electroporation ablative treatment of canine spontaneous intracranial gliomas. *J Neurosurg* **123**, 1008-1025, doi:10.3171/2014.12.JNS141768 (2015).
- 17 Ruarus, A. H. *et al.* Irreversible Electroporation in Hepatopancreaticobiliary Tumours. *Can Assoc Radiol J* **69**, 38-50, doi:10.1016/j.carj.2017.10.005 (2018).
- 18 Tarantino, L. *et al.* Irreversible electroporation of locally advanced solid pseudopapillary carcinoma of the pancreas: A case report. *Ann Med Surg (Lond)* **28**, 11-15, doi:10.1016/j.amsu.2018.01.009 (2018).
- 19 Hong, Y., Rice, J., Sharma, D. & Martin, R. C. G., 2nd. The use of IRE in multi-modality treatment for oligometastatic pancreatic cancer. *Am J Surg* **216**, 106-110, doi:10.1016/j.amjsurg.2018.01.037 (2018).
- 20 Rodriguez, A., Tatter, S. B. & Debinski, W. Neurosurgical Techniques for Disruption of the Blood-Brain Barrier for Glioblastoma Treatment. *Pharmaceutics* **7**, 175-187, doi:10.3390/pharmaceutics7030175 (2015).
- 21 Karki, R. & Kanneganti, T. D. Diverging inflammasome signals in tumorigenesis and potential targeting. *Nat Rev Cancer* **19**, 197-214, doi:10.1038/s41568-019-0123-y (2019).
- 22 Ringel, V. M. A., I. C. in *Gastrointestinal Cancers: Prevention, Detection, and Treatment* Vol. 2 (ed A.; Prasad Tyagi, S.) 271-290 (NOVA Science Publishers, 2016).
- 23 Mohammadi, M. & Chen, P. Effect of microvascular distribution and its density on interstitial fluid pressure in solid tumors: A computational model. *Microvasc Res* **101**, 26-32, doi:10.1016/j.mvr.2015.06.001 (2015).

- 24 Zhang, M. *et al.* Edible Ginger-derived Nano-lipids Loaded with Doxorubicin as a Novel Drug-delivery Approach for Colon Cancer Therapy. *Mol Ther* **24**, 1783-1796, doi:10.1038/mt.2016.159 (2016).
- 25 Poltorak, A. *et al.* Defective LPS signaling in C3H/HeJ and C57BL/10ScCr mice: mutations in Tlr4 gene. *Science* **282**, 2085-2088 (1998).
- 26 Opal, S. M. The host response to endotoxin, antilipopolysaccharide strategies, and the management of severe sepsis. *Int J Med Microbiol* **297**, 365-377, doi:10.1016/j.ijmm.2007.03.006 (2007).

Appendix A

Complete List of Published Works

1. **VM Ringel-Scaia**, MD Powell, KA Read, IC Allen, KJ Oestreich. (2019). Systemic *Listeria monocytogenes* Infection as a Model to Study T Helper Cell Immune Responses. In: Allen, I. (eds) *Mouse Models of Innate Immunity. Methods in Molecular Biology*, vol 1960. Humana Press, New York, NY. 2019;1960:149-160. PMID: 30798529.
2. **VM Ringel-Scaia***, Y Qin*, CA Thomas, KE Huie, DK McDaniel, K Eden, PA Wade, IC Allen. (2019). Maternal Influence and Murine Housing Confound Impact of NLRP1 Inflammasome on Microbiome. *Journal of Innate Immunity*. 2019 Feb 13:1-16. PMID: 30759441.
3. SB Suh, A Jo, MA Traore, S Coutermarsh-Ott, **VM Ringel-Scaia**, Ying Zhan, IC Allen, RM Davis, B Behkam. (2018). Bacteria-Enabled Autonomous Drug Delivery System (NanoBEADS) Enhances Intratumoral Transport of Nanomedicine. *Advanced Science*. 2018 Dec 5;6(3):1801309. PMID: 30775227.
4. Y Lebovitz, **VM Ringel-Scaia**, IC Allen, MH Theus. (2018). Emerging Developments in Microbiome and Microglia Research: Implications for Neurodevelopmental Disorders. *Frontiers in Immunology*. Sep 3;9:1993. PMID: 30233586.

5. DE Rothschild*, DK McDaniel*, **VM Ringel-Scaia***, IC Allen. (2018). Modulating Inflammation through the Negative Regulation of NF- κ B Signaling. *Journal of Leukocyte Biology*. 2018;103:1131-1150. PMID: 29389019.
6. KA Read, MD Powell, CE Baker, B Sreekumar, **VM Ringel-Scaia**, H Bachus, RE Martin, ID Cooley, IC Allen, A Ballesteros-Tato, KJ Oestreich. (2017). Integrated STAT3 and Ikaros Zinc Finger transcription factor activities regulate Bcl-6 expression in CD4⁺ T cells. *Journal of Immunology*. Oct 1;199(7):2377-2387. PMID: 28848064.
7. DK McDaniel, **VM Ringel-Scaia**, S Coutermarsh-Ott, IC Allen. (2017). Utilizing the Lung as a Model to Study Nanoparticle Based Drug Delivery Systems. In: Sirianni, R. and Behkam, B. (eds) *Targeted Drug Delivery: Methods and Protocols. Methods in Molecular Biology*, vol 1831. Humana Press, New York, NY. 2018;1831:179-190. PMID: 30051432.
8. **VM Ringel-Scaia**, DK McDaniel, IC Allen. (2016). The Goldilocks Conundrum: NLR Inflammasome Modulation of Gastrointestinal Inflammation during Inflammatory Bowel Disease. *Critical Reviews in Immunology*. 2016;36(4):283-314. PMID: 28322135.
9. DK McDaniel, A Jo, **VM Ringel-Scaia**, S Coutermarsh-Ott, DE Rothschild, M Powell, R Zhang, TE Long, K Oestreich, JS Riffle, RM Davis, IC Allen. (2016). TIPS Pentacene Loaded PEO-PDLLA Core-Shell Nanoparticles have Similar Cellular Uptake Dynamics in M1 and M2 Macrophages and In Corresponding *In Vivo* Microenvironments. *Nanomedicine*. Apr;13(3):1255-1266. PMID: 28040495.

10. DK McDaniel*, K Eden*, **VM Ringel***, Irving C. Allen. (2016). Emerging Roles for Noncanonical NF- κ B Signaling in the Modulation of Inflammatory Bowel Disease. *Inflammatory Bowel Diseases*. Sep;22(9):2265-79. PMID: 27508514.
11. **VM Ringel**, IC Allen. (2016). The Role of Nanotechnology in Detection and Treatment in Gastrointestinal Cancers. In: Tyagi, A. and Prasad, S. (eds) *Gastrointestinal Cancers: Prevention, Detection and Treatment*, vol 2. NOVA Science Publishers, New York, NY, pp. 271-290.

**denotes co-first author*

